

ISTANBUL TECHNICAL UNIVERSITY ★ GRADUATE SCHOOL

**COMPOSITE NANOFIBER PATCHES FOR TOPICAL DRUG DELIVERY
SYSTEMS**



Ph.D. THESIS

Zarife BARBAK

Department of Textile Engineering

Textile Engineering Programme

APRIL 2021

ISTANBUL TECHNICAL UNIVERSITY ★ GRADUATE SCHOOL

**COMPOSITE NANOFIBER PATCHES FOR TOPICAL DRUG DELIVERY
SYSTEMS**



Ph.D. THESIS

**Zarife BARBAK
(503122805)**

Department of Textile Engineering

Textile Engineering Programme

Thesis Advisor: Prof. Dr. Hale KARAKAS

APRIL 2021

İSTANBUL TEKNİK ÜNİVERSİTESİ ★ LİSANSÜSTÜ EĞİTİM ENSTİTÜSÜ

**KOMPOZİT NANOLİFLERİN TOPIKAL İLAÇ SALIM SİSTEMLERİNDE
KULLANIMI**

DOKTORA TEZİ

**Zarife BARBAK
(503122805)**

Tekstil Mühendisliği Anabilim Dalı

Tekstil Mühendisliği Programı

Tez Danışmanı: Prof. Dr. Hale KARAKAŞ

NİSAN 2021

Zarife BARBAK, a Ph.D. student of ITU Graduate School student ID 503122805, successfully defended the thesis entitled “COMPOSITE NANOFIBER PATCHES FOR TOPICAL DRUG DELIVERY SYSTEMS”, which she prepared after fulfilling the requirements specified in the associated legislations, before the jury whose signatures are below.

Thesis Advisor : **Prof. Dr. Hale KARAKAŞ**
Istanbul Technical University

Jury Members : **Prof. Dr. Ali DEMİR**
Istanbul Technical University

Assoc. Prof. Dr. Meryem Sedef ERDAL
Istanbul University

Prof. Dr. Ayşe Merih SARIŞIK
Dokuz Eylul University

Prof. Dr. Burçak Karagüzel KAYAOĞLU
Istanbul Technical University

Date of Submission : 10 March 2021

Date of Defense : 19 April 2021





To my family,



FOREWORD

Firstly, I would like to express my sincere gratitude to my advisor Prof. Dr. Hale KARAKAS for her valuable guidance, support, motivation and patience during the all period of my PhD. She always encouraged me to study on subject of the thesis.

I would like to thank to the members of my thesis committee, Prof. Dr. Ali DEMIR and Assoc. Prof. Dr. Meryem Sedef ERDAL for their insightful comments and sparing their valuable time during the thesis study. I would also like to thank to the members of my thesis juries, Prof. Dr. Ayse Merih SARIISIK and Prof. Dr. Burcak Karaguzel KAYA OGLU for their time and insightful comments to complete the thesis. I wish to thank to Prof. Dr. A. Sezai SARAC for share me his deep knowledge, advices and experiences during my thesis work.

I would like to heartily thank to Prof. Dr. İsmail KOYUNCU for allowing the use of MEMTEK laboratory equipment and facilities. I want to thank to Dr. Serkan GUCLU, Burcu SAYINLI and Sevde KORKUT for their helps in MEMTEK laboratories. I would like to thank to Prof. Dr. Mehmet Kerim RAMAZANOGLU for permission to use of his laboratory facilities and also for carrying out the AFM analysis of my thesis.

I wish to give specials thanks to Dr. Imren ESENTURK for sharing me her time, knowledge on drug delivery systems and also valuable friendship.

I would like to thank to Prof. Dr. Mustafa Tahsin YILMAZ to open me his Microbiology laboratory at Yıldız Technical University. I owe a special thanks to Dr. Azime YILMAZ and Canan Yagmur KARAKAS for their collaboration and efforts in antibacterial activity studies.

Finally, I would like to express my special thanks to my dear parents Sahnizer and Durhasan DOGAN, my husband Akif BARBAK and my lovely son Omer Talha BARBAK for their love, support and patience. Without them, I could not complete the PhD studies.

This work was supported financially by Istanbul Technical University Scientific Research Projects Coordination Unit (ITU-BAP Project number: 39605). I wish to thank to Istanbul Technical University for financial supporting of the thesis studies.

April 2021

Zarife BARBAK
(Textile Engineer)

TABLE OF CONTENTS

| | <u>Page</u> |
|--|-------------|
| FOREWORD | ix |
| TABLE OF CONTENTS | xi |
| ABBREVIATIONS | xv |
| SYMBOLS | xvii |
| LIST OF TABLES | xix |
| LIST OF FIGURES | xxi |
| SUMMARY | xxv |
| ÖZET | xxix |
| 1. INTRODUCTION | 1 |
| 2. THEORETICAL BACKGROUND | 5 |
| 2.1 Nanofibers | 5 |
| 2.2 Electrospinning Process | 7 |
| 2.2.1 Parameters of electrospinning | 8 |
| 2.3 Biopolymers in Electrospinning | 9 |
| 2.3.1 Polysaccharides | 9 |
| 2.3.1.1 Cellulose and derivatives | 10 |
| 2.3.1.2 Alginates | 11 |
| 2.3.1.3 Chitin and chitosan..... | 11 |
| 2.3.1.4 Hyaluronic acid | 12 |
| 2.3.2 Proteins..... | 12 |
| 2.3.2.1 Collagen | 12 |
| 2.3.2.2 Gelatine | 12 |
| 2.3.2.3 Fibrin | 13 |
| 2.3.3 Poly (ϵ -caprolactone) (PCL) | 13 |
| 2.3.4 Poly (lactic acid) (PLA) | 14 |
| 2.3.5 Poly (ethylene oxide) (PEO) | 16 |
| 2.4 Nanofibers in Medical Applications | 17 |
| 2.4.1 Wound dressings | 19 |
| 2.4.2 Artificial blood vessels..... | 20 |
| 2.4.3 Tissue scaffolds..... | 20 |
| 2.5 Drug Delivery Systems | 21 |
| 2.5.1 Structure of the skin | 21 |
| 2.5.2 The skin and drug delivery..... | 22 |
| 2.5.3 Topical drug delivery systems | 23 |
| 2.6 Nanofiber Based Drug Delivery Systems | 24 |
| 2.7 Silver Sulfadiazine | 31 |
| 2.7.1 Antibacterial activity mechanism..... | 33 |
| 2.7.2 SSD based drug delivery systems | 33 |
| 2.7.3 Silver Sulfadiazine in nanofiber drug delivery applications..... | 37 |
| 3. EXPERIMENTAL STUDIES | 43 |
| 3.1 Materials..... | 43 |

| | |
|---|-----------|
| 3.2 Electrospinning Process..... | 43 |
| 3.3 Tape Casting Method (Doctor Blade) | 44 |
| 3.4 Preparation of the Polymer Solutions..... | 45 |
| 3.4.1 Preparation of the PEO, PCL, PCL/PEO and PCL/(PEO+SSD) | 45 |
| 3.4.2 Preparation of the PEO, PLA, PLA/PEO and PLA/(PEO+SSD)..... | 46 |
| 3.5 Fabrication of Electrospun Nanofibers..... | 46 |
| 3.6 Fabrication of Casting Films | 48 |
| 3.7 <i>In vitro</i> Release Studies of SSD with UV Method..... | 48 |
| 3.7.1 Solubility studies of SSD | 49 |
| 3.7.2 Preparation of calibration curve | 50 |
| 3.7.3 UV method validation | 51 |
| 3.7.3.1 Specificity..... | 52 |
| 3.7.3.2 Linearity | 52 |
| 3.7.3.3 Precision..... | 52 |
| 3.7.3.4 Accuracy..... | 52 |
| 3.7.4 <i>In Vitro</i> drug release studies (Dialysis bag method) | 53 |
| 3.7.5 Controlling the drug release with conductivity | 54 |
| 3.7.6 Drug release kinetics | 54 |
| 3.7.6.1 Zero Order kinetic model | 54 |
| 3.7.6.2 First Order kinetic model | 55 |
| 3.7.6.3 Higuchi square root kinetic model | 55 |
| 3.7.6.4 Hixson-Crowell kinetic model | 55 |
| 3.7.6.5 Korsmeyer-Peppas kinetics model | 56 |
| 3.7.7 Drug loading efficiency..... | 56 |
| 3.8 Characterizations and Measurements | 57 |
| 3.8.1 SEM analysis..... | 57 |
| 3.8.2 SEM-EDS and EDS-Mapping analysis..... | 57 |
| 3.8.3 Water uptake measurement | 57 |
| 3.8.4 Optical Profilometer..... | 58 |
| 3.8.5 Viscosity measurement | 58 |
| 3.8.6 Attenuated Total Reflectance Infrared (FTIR-ATR) spectroscopy analysis | 58 |
| 3.8.7 X-Ray diffraction (XRD) analysis | 58 |
| 3.8.8 Contact angle measurements | 58 |
| 3.8.9 Atomic Force Microscope (AFM) studies | 58 |
| 3.8.10 Antibacterial activity test | 59 |
| 3.8.10.1 Disc diffusion method | 59 |
| 3.8.10.2 Minimum Inhibition Concentration (MIC) and Minimum Bactericidal Concentration (MBC) methods..... | 60 |
| 3.8.11 Stability studies of formulations | 61 |
| 3.8.11.1 Stability testing with SEM analysis | 61 |
| 3.8.11.2 Stability testing with calculating the drug loading efficiency..... | 61 |
| 3.8.11.3 Stability testing with cumulative drug release | 61 |
| 3.8.12 Cytotoxicity..... | 61 |
| 4. RESULTS AND DISCUSSION..... | 63 |
| 4.1 Preparation of the Polymer Solutions | 63 |
| 4.1.1 Viscosity measurements of the solutions | 64 |
| 4.2 Electrospinning Process..... | 65 |
| 4.3 Doctor Blading Process | 66 |
| 4.4 UV Method Validation | 67 |

| | |
|--|-----|
| 4.4.1 Specificity | 67 |
| 4.4.2 Linearity | 67 |
| 4.4.3 Precision | 67 |
| 4.4.4 Accuracy | 68 |
| 4.5 Measurement and Characterization Studies of Silver Sulfadiazine (SSD) | 69 |
| 4.5.1 FT-IR ATR spectrum of Silver Sulfadiazine | 69 |
| 4.5.2 XRD spectrum of Silver Sulfadiazine | 70 |
| 4.6 Measurements and Characterization Studies of PCL/(PEO+SSD) Nanofiber Formulations..... | 71 |
| 4.6.1 SEM analysis..... | 71 |
| 4.6.1.1 SEM analysis of PEO and PEO+SSD nanofiber | 72 |
| 4.6.1.2 SEM analysis of PCL, PCL/PEO and PCL/(PEO+SSD) nanofibers . | 73 |
| 4.6.1.3 Effect of viscosity on nanofiber morphology..... | 76 |
| 4.6.1.4 Water uptake | 77 |
| 4.6.2 Elemental analyses of SSD loaded composite nanofibers | 78 |
| 4.6.3 Atomic Force Microscopy (AFM) | 80 |
| 4.6.4 Wettability-Contact angle measurements | 81 |
| 4.6.5 X-ray diffraction (XRD) study..... | 84 |
| 4.6.6 Attenuated Total Reflectance Infrared (FTIR-ATR) spectroscopy analysis | 85 |
| 4.6.7 Loading efficiency, drug release profile and kinetics | 88 |
| 4.6.8 Controlling the drug release with conductivity..... | 91 |
| 4.7 Measurements and Characterization Studies of PCL/(PEO+SSD) Film Casting Formulations..... | 91 |
| 4.7.1 SEM Analysis of the PEO, PEO+SSD, PCL, PCL/ PEO, PCL/(PEO+SSD) casting films | 92 |
| 4.7.2 Elemental analysis of PCL/(PEO+SSD) casting film | 93 |
| 4.7.3 Optical Profilometer analysis..... | 95 |
| 4.7.4 Wettability-Contact angle measurements | 97 |
| 4.7.5 Loading efficiency, drug release profile and kinetics | 98 |
| 4.8 Measurements and Characterization Studies of PLA/(PEO+SSD) Nanofiber Formulations..... | 100 |
| 4.8.1 SEM analysis..... | 100 |
| 4.8.1.1 SEM analysis of PEO and PEO+SSD nanofibers | 101 |
| 4.8.1.2 SEM analysis of PLA, PLA+PEO and PLA/(PEO+SSD) nanofibers | 102 |
| 4.8.1.3 Effect of viscosity on nanofiber morphology..... | 106 |
| 4.8.1.4 Water uptake | 106 |
| 4.8.2 Elemental analyses of SSD loaded composite nanofibers | 107 |
| 4.8.3 Atomic Force Microscopy (AFM) | 109 |
| 4.8.4 Wettability-Contact angle measurements | 110 |
| 4.8.5 X-ray diffraction (XRD) study..... | 113 |
| 4.8.6 Attenuated Total Reflectance Infrared (FTIR-ATR) spectroscopy analysis | 115 |
| 4.8.7 Loading efficiency, drug release profile and kinetics | 118 |
| 4.8.8 Controlling the drug release with conductivity..... | 124 |
| 4.9 Results of Antibacterial Activity Studies | 125 |
| 4.9.1 Results of disc diffusion tests..... | 125 |
| 4.9.2 Results of Minimum Inhibition Concentration (MIC) and Minimum Bactericidal Concentration (MBC) | 127 |

| | |
|---|------------|
| 4.10 Results of Stability Studies..... | 129 |
| 4.10.1 Results of stability testing with SEM analysis | 129 |
| 4.10.2 Results of stability testing with calculating the drug loading amount .. | 135 |
| 4.10.3 Results of stability testing with cumulative drug release | 136 |
| 4.11 Results of Cytotoxicity Test | 138 |
| 5. CONCLUSIONS..... | 139 |
| REFERENCES | 149 |
| CURRICULUM VITAE | 161 |



ABBREVIATIONS

| | |
|----------------------|---|
| AD | : Average Diameter |
| AFM | : Atomic Force Microscope |
| ATCC | : American Type of Culture Collection |
| CFU | : Colony Forming Units |
| DDS | : Drug Delivery Systems |
| DMEM | : Dulbecco's Minimal Eagle Medium |
| DMSO | : Dimethyl Sulfoxide |
| ECM | : Extracellular Matrix |
| <i>E. coli</i> | : <i>Escherichia Coli</i> |
| EDS | : Energy-Dispersive Spectroscopy |
| EtOH | : Ethanol |
| FBS | : Fetal Bovine Serum |
| FTIR | : Fourier Transform Infrared Spectroscopy |
| FTIR-ATR | : Attenuated Total Reflectance Infrared Spectroscopy |
| NA | : Nutrient Agar |
| NB | : Nutrient Broth |
| MBC | : Minimum Bactericidal Concentration |
| MIC | : Minimum Inhibition Concentration |
| MTT | : 3-(4,5- dimethyl-2-thiazolyl)-2,5-diphenyltetrazolium bromide |
| <i>P. aeruginosa</i> | : <i>Pseudomonas Aeruginosa</i> |
| PCL | : Poly (ϵ -caprolactone) |
| PEO | : Poly (ethylene oxide) |
| PLA | : Poly (lactic acid) |
| PBS | : Phosphate Buffer Saline |
| PTFE | : Polytetrafluoroethylene |
| RSD | : Relative Standard Deviation |
| <i>S. aureus</i> | : <i>Staphylococcus Aureus</i> |
| SC | : Stratum Corneum |
| SD | : Standard Deviation |
| SEM | : Scanning Electron Microscopy |
| SSD | : Silver sulfadiazine |
| UV-vis | : Ultraviolet-visible |
| XRD | : X-ray Diffraction |



SYMBOLS

| | |
|------------------------|----------------------------------|
| A_{act} | : Amount of actual drug loading |
| A_{int} | : Amount of initial drug loading |
| Ag | : Silver |
| Au | : Gold |
| N | : Nitrogen |
| OD | : Optical Density |
| R² | : Regression Coefficient |
| S | : Sulphur |
| W_w | : Wet weight |
| W_d | : Dry weight |
| w/w | : Weight/weight |
| v/v | : Volume/volume |



LIST OF TABLES

| | <u>Page</u> |
|--|-------------|
| Table 2.1 : Biological molecules loaded nanofiber based polymer matrices..... | 26 |
| Table 2.2 : SSD loaded polymer matrices..... | 34 |
| Table 2.3 : SSD loaded nanofibers..... | 38 |
| Table 3.1 : Solubility study of SSD in different buffers (+ soluble, - insoluble).. | 50 |
| Table 4.1 : Viscosity values of the solutions..... | 65 |
| Table 4.2 : Optimized electrospinning parameters for PCL/(PEO+SSD) formulations. | 66 |
| Table 4.3 : Optimized electrospinning parameters for PLA/(PEO+SSD) formulations. | 66 |
| Table 4.4 : Evaluation data of precision study. | 68 |
| Table 4.5 : Evaluation data of accuracy study. | 69 |
| Table 4.6 : Viscosity values of electrospinning solutions..... | 77 |
| Table 4.7 : Elemental distribution of Ag, S and N on EDS Mapping image. | 80 |
| Table 4.8 : Drug release kinetics models for PCL/(PEO+SSD) nanofibers with regression coefficient (R^2)..... | 90 |
| Table 4.9 : Elemental distribution of Ag, S and N on EDS Mapping image. | 95 |
| Table 4.10 : Roughness values of the casting films. | 96 |
| Table 4.11 : Drug release kinetics models for PCL/(PEO+SSD) nanofibers with regression coefficient (R^2)..... | 99 |
| Table 4.12 : Viscosity values of the electrospinning solutions. | 106 |
| Table 4.13 : Elemental distribution of Ag, S and N on EDS Mapping image. | 109 |
| Table 4.14 : Drug loading efficiencies (%) of SSD loaded formulations in the literature. | 119 |
| Table 4.15 : Cumulative release of SSD loaded formulations in the literature..... | 123 |
| Table 4.16 : Drug release kinetics models for PLA/(PEO+SSD) nanofibers with regression coefficient (R^2)..... | 124 |
| Table 4.17 : Disc diffusion test results..... | 126 |
| Table 4.18 : MIC and MBC results of PLA/(PEO+SSD) and PCL/(PEO+SSD) formulations. | 128 |
| Table 4.19 : Drug loading amount of SSD loaded and SSD free nanofiber formulations which were waited for 3 and 6 months at $25 \pm 2^\circ\text{C}$ and $+4^\circ\text{C}$ refrigerator conditions..... | 135 |
| Table 4.20 : Cytotoxicity test results..... | 138 |



LIST OF FIGURES

| | <u>Page</u> |
|---|-------------|
| Figure 2.1 : Nanofiber scale (human hair, pollen grain, nanofiber mat)..... | 5 |
| Figure 2.2 : Relationship between specific surface area and diameter of different fibers..... | 6 |
| Figure 2.3 : Basic electrospinning equipment..... | 8 |
| Figure 2.4 : Collector types using in electrospinning set up: (A) solid collector, (B) guidewire collector, (C) rotating mandrel, (D) rotating wire drum, (E) rotating disk, (F) liquid bath collector. | 9 |
| Figure 2.5 : Chemical structure of Cellulose. | 10 |
| Figure 2.6 : Chemical structure of Chitin. | 11 |
| Figure 2.7 : Chemical structure of Poly (ϵ -caprolactone). | 13 |
| Figure 2.8 : Isomeric of lactides; L-lactide (a dimer of L-lactic acid), D-lactide (a dimer of D-lactic acid) and <i>meso</i> -lactide (a dimer of D- and L- lactic acid)... | 15 |
| Figure 2.9 : Polymerization of Lactic Acid..... | 16 |
| Figure 2.10 : Chemical structure of PEG and PEO. | 17 |
| Figure 2.11 : Publication numbers of nanofiber researches in the biomedical field. | 18 |
| Figure 2.12 : Illustration of nanofibers in biomedical field. | 18 |
| Figure 2.13 : Structure of the human skin..... | 22 |
| Figure 2.14 : Representation of the skin cross-section showing the difference of drug penetration levels between transdermal drug delivery and topical drug delivery. | 23 |
| Figure 2.15 : Schematic illustration of RGD functionalized nanofibers (PCL/P3ANA-RGD) on Saos-2 cells..... | 27 |
| Figure 2.16 : SEM Images of sandwiched structure of PCL (poly- ϵ -caprolactone)/PLLA (poly-L-lactic acid) composite nanofibers (bottom layer) and PCL/Gelatine composite nanofibers (upper layer). | 28 |
| Figure 2.17 : Schematic illustration of Ag ⁺ reduction mechanism. | 29 |
| Figure 2.18 : a) Drug release profile of the only niclosamide loaded and the nic@Ag NP loaded composite nanofibers. (b) Ag NP release profile of only Ag NPs loaded and nic@Ag NP loaded composite nanofibers..... | 30 |
| Figure 2.19 : Cumulative drug release profile of vitamin B ₁₂ with plasma treatment. | 31 |
| Figure 2.20 : Chemical structure of SSD. | 32 |
| Figure 2.21 : Percentage of unreacted silver compounds in human serum..... | 33 |
| Figure 2.22 : Formation of Ag-SD/PVA nanorods. | 35 |
| Figure 2.23 : Antibacterial activity studies of BC and BC-AgSD composites: <i>S. aureus</i> (A) and <i>C. albicans</i> (B). (In all plates, a is BC as the control, b-f are BC 1, BC 2, BC 3, BC 4 and BC 5). | 36 |
| Figure 2.24 : Accumulated drug release (%) of AgSD from AgSD/NS gel, commercial AgSD cream, AgSD bulk, and AgSD NS solution. | 37 |
| Figure 2.25 : Photos of wounds that treated with Ag-based wound dressings at 3, 7 and 14 days after wounding | 39 |

| | |
|---|----|
| Figure 2.26 : Cyclodextrin SSD inclusion complex loaded PVA nanofibers..... | 40 |
| Figure 2.27 : SSD release amount..... | 41 |
| Figure 2.28 : Antibacterial activity evaluation of SSD Cyclodextrin complex loaded PCL nanofibers..... | 41 |
| Figure 2.29 : A) Photos of burn healing process B) Comparison of wound closure rates of Gauze, PU/ Gelatine nanofiber without SSD (NF), different amount SSD loaded PU/ Gelatine nanofibers (NFSSD-1 and NFSSD-2) during the healing period..... | 42 |
| Figure 3.1 : Photograph of the electrospinning set up. | 44 |
| Figure 3.2 : Schematic illustration of PCL/(PEO+SSD) and PLA/(PEO+SSD) composite nanofiber fabrication..... | 47 |
| Figure 3.3 : Schematic illustration of doctor blade technique. | 48 |
| Figure 3.4 : Calibration curve of SSD..... | 51 |
| Figure 3.5 : Photographs of <i>in vitro</i> drug release studies..... | 54 |
| Figure 4.1 : Photograph of PEO, PEO+SSD, PCL, PCL/PEO and PCL/(PEO+SSD) solutions. | 63 |
| Figure 4.2 : Photograph of PEO, PEO+SSD, PLA, PLA+PEO and PLA/(PEO+SSD) electrospinning solutions..... | 64 |
| Figure 4.3 : Photograph of the electrospinning process..... | 66 |
| Figure 4.4 : Fabrication of casting films with Doctor Blade..... | 67 |
| Figure 4.5 : FT-IR ATR Spectrum of SSD. | 70 |
| Figure 4.6 : XRD Spectrum of SSD..... | 71 |
| Figure 4.7 : General surface images of a) PEO and b) PEO+SSD (at X 2000 magnification). | 72 |
| Figure 4.8 : SEM Images and corresponding diameter distribution histograms of a) Pure PEO and b) PEO+SSD nanofibers..... | 73 |
| Figure 4.9 : General surface images of a) PCL and b) PCL/PEO c) PCL/(PEO+SSD) (at X 2000 magnification). | 75 |
| Figure 4.10 : SEM images and corresponding diameter distribution histograms of a) Pure PCL, b) PCL+PEO, c) PCL/(PEO+SSD) nanofibers. | 76 |
| Figure 4.11 : SEM Images of PCL/(PEO+SSD) a) before and b) after immersing in buffer solution. | 78 |
| Figure 4.12 : EDS Mapping image (a,b) and spectra (c) of PCL/(PEO+SSD)..... | 79 |
| Figure 4.13 : Representation of elemental distribution of S, N and Ag atoms on formulation with SEM-EDS Mapping image..... | 80 |
| Figure 4.14 : AFM images of pure PCL/ PEO nanofibers..... | 81 |
| Figure 4.15 : AFM images of SSD loaded PCL/ PEO nanofibers..... | 81 |
| Figure 4.16 : Contact angle photographs of nanofibers..... | 83 |
| Figure 4.17 : Contact Angle values of nanofibers..... | 84 |
| Figure 4.18 : XRD pattern of SSD, PEO+SSD, PEO+PCL and PCL (PEO+SSD) nanofibers..... | 84 |
| Figure 4.19 : FTIR -ATR Spectra of a) SSD, PCL, PEO and b) PEO+SSD, PCL/PEO, PCL/(PEO+SSD) nanofibers..... | 86 |
| Figure 4.20 : Interaction between PCL, PEO and SSD..... | 87 |
| Figure 4.21 : Cumulative release % of SSD from PCL/(PEO+SSD) nanofibers..... | 89 |
| Figure 4.22 : Conductivity measurement of the released aliquots versus time..... | 91 |
| Figure 4.23 : SEM Images of a) PEO, b) PEO+SSD, c) PCL, d) PCL/PEO, e) PCL/(PEO+SSD) casting films (at X500 magnification). | 92 |
| Figure 4.24 : SEM Images of a) PEO, b) PEO+SSD, c) PCL, d) PCL/PEO, e) PCL/(PEO+SSD) casting films (at X5000 magnification). | 93 |

| | |
|--|-----|
| Figure 4.25 : EDS Mapping image (a) and Spectra (b) of PCL/(PEO+SSD) casting film. | 94 |
| Figure 4.26 : Representation of elemental distribution of S, N and Ag atoms on formulation with SEM-EDS Mapping image. | 95 |
| Figure 4.27 : Optical profilometer images of PEO, PEO+SSD, PCL, PCL/PEO and PCL/(PEO+SSD) casting films. | 96 |
| Figure 4.28 : Contact angle photographs of casting films. | 97 |
| Figure 4.29 : Contact angle values of casting films. | 98 |
| Figure 4.30 : Cumulative release % of SSD from PCL/(PEO+SSD) casting film. .. | 99 |
| Figure 4.31 : General surface images of a) PEO and b) PEO+SSD nanofibers (X 2000 magnification). | 101 |
| Figure 4.32 : SEM images and corresponding the diameter distribution histograms of a) Pure PEO b) PEO+SSD nanofibers. | 102 |
| Figure 4.33 : General surface images of a) PLA b) PLA+PEO c) PLA/(PEO+SSD) (at X 2000 magnification). | 104 |
| Figure 4.34 : SEM Images and corresponding diameter distribution histograms of a) Pure PLA b) Pure PEO c) PLA/PEO (7:3) and d) SSD loaded PLA/PEO composite nanofibers. | 105 |
| Figure 4.35 : SEM Images of PLA/(PEO+SSD) a) Before and b) After immersing in buffer solution c) Schematic illustration of before and after immersing in buffer solution for 24 hours. | 107 |
| Figure 4.36 : EDS Mapping image (a) and spectra (b) of PLA(PEO+SSD). | 108 |
| Figure 4.37 : Representation of elemental distribution of S, N and Ag atoms on formulation with SEM-EDS Mapping image. | 109 |
| Figure 4.38 : AFM Images of pure PLA/ PEO nanofibers. | 110 |
| Figure 4.39 : AFM images of SSD loaded PLA/ PEO nanofibers. | 110 |
| Figure 4.40 : Contact angle photographs of nanofibers. | 111 |
| Figure 4.41 : Contact angle values of nanofibers. | 112 |
| Figure 4.42 : Contact angle values of PCL/(PEO+SSD) casting film, PCL/(PEO+SSD) and PLA/(PEO+SSD) nanofiber formulations. | 113 |
| Figure 4.43 : XRD pattern of SSD, PEO+SSD, PEO+PLA and PLA/(PEO+SSD) nanofibers. | 114 |
| Figure 4.44 : FTIR -ATR spectra of a) SSD, PLA, PEO and b) PEO+SSD, PLA/PEO, PLA/(PEO+SSD) nanofibers. | 116 |
| Figure 4.45 : Interaction between PLA, PEO and SSD. | 117 |
| Figure 4.46 : Cumulative release % of SSD of PLA/(PEO+SSD) nanofibers. | 120 |
| Figure 4.47 : Cumulative SSD release of PCL/(PEO+SSD) casting film, PCL/(PEO+SSD) nanofibers and PLA/(PEO+SSD) nanofibers. | 121 |
| Figure 4.48 : Amount of SSD release from PCL/(PEO+SSD) and PLA/(PEO+SSD) formulations. | 122 |
| Figure 4.49 : Conductivity of released aliquots versus time. | 125 |
| Figure 4.50 : Antibacterial activity photographs of SSD loaded a) PCL/PEO and b) PLA/PEO composite nanofiber mats c) Commercial SSD cream. | 127 |
| Figure 4.51 : Photograph from MIC and MBC tests. | 128 |
| Figure 4.52 : SEM images of PCL/PEO a) Initial a1) Storage at +4°C; a2) Storage at 25°C after 3 months. | 131 |
| Figure 4.53 : SEM images of PCL/(PEO+SSD) composite nanofibers a) Initial, a1- Storage at +4°C after 3 months, a2) Storage at 25°C after 3 months. | 132 |
| Figure 4.54 : SEM Images of a) PLA/PEO composite nanofibers a) Initial a1) Storage at +4°C; a2) storage at 25°C after 3 months. | 133 |

Figure 4.55 : SEM images of PLA/(PEO+SSD) composite nanofibers a) Initial a1) Storage at +4°C after 3 months; a2) Storage at 25°C after 3 months..... 134

Figure 4.56 : *In vitro* drug release profiles for a) PLA(PEO+SSD) nanofibers b) PCL(PEO+SSD) after 3 and 6 months of storage, protecting from light at +4°C refrigerator conditions. 137



COMPOSITE NANOFIBER PATCHES FOR TOPICAL DRUG DELIVERY

SUMMARY

Nanofibers are ultrafine, continuous, solid state textile fibers that have diameters less than 1 micrometre. Nanofibers possess remarkable properties such as high interconnected porosity, specific surface area, ability to imitate the Extra Cellular Matrix (ECM) and potential carrier for drug delivery. Due to these fascinating properties, nanofibers are attractive candidates for medical applications for instance wound dressings, tissue scaffolds and artificial blood vessels.

Electrospinning is the simplest and most practical among all methods to produce fine fibers with diameters ranging from micrometres to nanometres. Basic electrospinning equipment includes a high voltage source, a solution feeding unit, a syringe with a tip and a collector. At first, high voltage is applied to the polymer solution to produce an electrical field between the tip and the collector to shape the droplet on the tip as Taylor Cone. When the electrostatic force is higher than the surface tension of the polymer solution, polymer jet is ejected from the tip to the collector. Then, polymer jet reaches to collector following a spiral way by getting longer and thinner. Finally, nanoscale fibers are obtained on the collector.

Topical drug delivery systems are composed of a formulation that applied to the skin directly to heal disorders or disease of the skin which guide/target pharmacological effect of the drug to the skin surface. Different pharmaceutical dosage forms can be used in topical drug delivery such as gels, creams, ointment, liquid preparation, sprays and solid powders.

Electrospun nanofibers are excellent materials for drug delivery systems due to high interconnected porosity, high surface area, ability to imitate the Extra Cellular Matrix (ECM), potential carrier for drug delivery. Utilization of nanofibers in drug delivery systems is based on the principle that the high surface area of the nanofibrous formulation increases the dissolution rate of the drug. Compared with other dosage forms such as; liposomes, micelles and hydrogels, major advantages of nanofibers are increment in drug loading efficiency and loading capacity, low systemic toxicity and excellent stability. Furthermore, several drugs can be carried within nanofibers with high local drug concentration due to their excellent targeting and drug transportation ability in a safe way. Electrospinning offers the opportunity for direct loading of drugs or biological agents for instance antibacterial molecules, antibiotics, enzymes, growth factors, proteins, peptides, vitamins, DNA into the electrospun nanofibers.

Poly (ϵ -caprolactone) (PCL), Poly Lactic Acid (PLA) and Poly (ethylene oxide) (PEO) were used as carrier polymers for drug delivery. PEO is a highly aqueous soluble polymer, that interacts with the body fluid quickly due to its hydrophilicity resulting in dissolution. PEO is widely used in the polymer matrix to enhance bioavailability and solubility of drugs because of its high aqueous solubility and unique properties in drug delivery applications. The compatibility of PCL and PLA with different types of drugs enables uniform drug distribution in the polymer matrix and the slow

degradation rate makes them favourable for prolonged drug delivery systems. In recent years, various studies were reported on the fabrication of drug delivery systems, generated by electrospinning of PCL, PEO, PLA and their blends. PCL, PEO, PLA nanofibers or their blends were loaded with different drugs and biological agents such as; Niclosamide, Silver nanoparticles, Vitamin B₁₂, Curcumin, Lysozyme, AgNO₃, Metronidazole (MNA).

Polymer blending is an effective approach to prepare functional nanofibers by incorporating the favourable properties of the component polymers. Furthermore, polymer blending facilitates the manipulation of physical, mechanical or biochemical properties of nanofibers. Hydrophilic/hydrophobic polymer blends have been electrospun into nanofibers to fabricate controlled DDS. The hydrophobic polymer forms the backbone structure and it degrades slowly, creating a long term but steady-state drug release. On the other hand, the hydrophilic polymer degrades with a more rapid process, faster than hydrophobic, which accelerates the drug release. In this study, hydrophilic water-soluble PEO was selected for the polymer matrix to enhance the solubility and bioavailability of insoluble SSD. The hydrophobic character of PCL and PLA offers a long period SSD release therefore hydrophilic PEO was blended with hydrophobic PCL and PLA. Thus, PCL/ PEO and PLA/PEO composite polymer matrix was used to provide both increased solubility and controlled release of SSD.

Silver sulfadiazine (SSD) is a non-ionized, water-insoluble, topical agent with a wide range of antimicrobial activity that is affected both on bacteria and fungi. SSD is a sulfonamide based drug that is formed by the reaction of sulfadiazine with silver nitrate to form complex silver salt. SSD is used extensively in the topical treatment of infected burns. Silver sulfadiazine provides a long-term release of silver ions, whereas in the case of other silver salts, such as silver nitrate, large amounts of silver ions are released all at once. Thus, the use of SSD decreases the need for frequent application. This makes SSD a desirable and favourable agent since the frequent application is not always practical or possible for patients. However, the low aqueous solubility (3.4 mg/l at pH = 6.8) restricts the drug efficiency, bioavailability and potential antimicrobial activity of SSD thus its applications are limited. Drug solubility is an important issue since efficient drug release and antimicrobial efficiency is contributed just by decomposition of SSD to sulfadiazine and silver ions. Also, the solubility problem of SSD makes it difficult to be stabilized and incorporated into the polymer matrix.

The aim of the thesis is to produce a novel SSD loaded topical drug delivery system by using advantages of electrospun nanofibers. Also, a new buffer, Water/Propylene Glycol/ Phosphoric Acid (82:16:2) was utilized to investigate the dissolution and release behaviour of SSD. Thereby SSD containing PCL/PEO and PLA/PEO composite nanofiber carriers were electrospun to achieve the enhancement in solubility, effective drug release and efficient drug loading of SSD. For this purpose, initially, the water-insoluble SSD was incorporated into highly aqueous soluble PEO to increase the solubility. Afterwards, the PEO+SSD solution was blended with PCL and PLA solution to produce composite PCL/(PEO+SSD) and PLA/(PEO+SSD) nanofibers and PCL/(PEO+SSD) casting films for topical drug delivery.

SEM method was used to enable the observations of fiber defects and irregularities in the nanofibers structures and to measure the average fiber diameters of the nanofibers. The morphological characterization of the casting films was carried out by SEM and Optical Profilometer. Energy dispersive spectra (EDS) analysis was performed to confirm that the composite nanofibers and casting film which contain SSD, by

detecting the Silver (Ag), Nitrogen (N), Sulphur (S) content of the nanofibers. Moreover, EDS-Mapping was carried out to show the distributions of these elements in the composite nanofibers and casting films.

The stability of SSD in the fiber structure and the molecular interactions in the drug-free and drug loaded nanofibers were examined by Attenuated Total Reflectance Infrared (FTIR-ATR) Spectroscopy. The crystalline structure of the SSD loaded composite electrospun nanofibers were investigated with X-ray diffraction (XRD) analysis.

Atomic Force Microscopy (AFM) was used to determine the surface roughness of the composite nanofibers. 3D AFM Images show the roughness structure of nanofibers. Water contact angle measurements were performed to evaluate the wettability properties of the fabricated nanofibers and casting films surfaces.

In vitro drug release media and release conditions were optimized and the controlled drug release profile was obtained for 24 hours. Drug loading efficiency of the nanofiber formulations and casting film were calculated. To understand the SSD drug release mechanisms from SSD loaded formulations; Zero Order, First Order, Higuchi, Hixon Crowell and Korsmeyer-Peppas kinetics models were applied in the drug release profiles of the formulations. Drug release studies were also verified with conductivity measurement due to the conductive nature of SSD.

Antibacterial activities of the composite nanofibers against gram-positive *Staphylococcus aureus* (S. aureus) and gram negative *Pseudomonas Aeruginosa* (P. aeruginosa) *Escherichia coli* (E. Coli) bacteria were performed for the period of 24, 48 and 72 hours according to disc diffusion test method. Also, the antibacterial activity of commercial SSD cream was tested for comparison with nanofiber formulations. Furthermore, antibacterial activity of the SSD loaded PCL/PEO and PLA/PEO nanofibers were examined with determining MIC and MBC values.

Stability studies of the composite nanofibers were done for 3 and 6 months periods. Nanofiber samples were kept both at refrigerator conditions (+4°C) and room conditions (25°C ±2 and 65 % ±2°C relative humidity) to evaluate stability of nanofiber patches. Stability tests were performed with calculating drug loading amount, cumulative drug release by UV absorption measurements and analysing surface morphology by SEM analysis.

Finally, the cytotoxicity studies of the drug loaded and drug-free PCL/PEO and PLA/PEO nanofiber patches were done with using the cell viability assay (MTT assay).



KOMPOZİT NANOLİFLERİN TOPIKAL İLAÇ SALIM SİSTEMLERİNDE KULLANIMI

ÖZET

Nanolifler, çapı 1 mikronun altında olan ince uzun tekstil lifleri olarak tanımlanır. Sahip oldukları, yüksek porozite, düşük por çapları, yüksek yüzey alanı, doğal hücre dışı matris (Extra Cellular Matrix; ECM) özelliklerini taklit edebilirlik, biyoaktif molekül/ilaç taşıyabilirlik gibi özelliklerden ötürü ilaç salım sistemleri, yara örtüleri, doku iskeleleri gibi pek çok biyomedikal alanda kullanılmaktadır.

Elektroüretim yöntemi nanometre düzeyinde lif üretimi için en yaygın, kolay ve düşük maliyetli lif üretim tekniğidir. Temel elektroüretim düzeneği yüksek güç kaynağı, çözelti besleme ünitesi (pompa), şırınga, iğne/düze ucu ve toplayıcıdan oluşur. Bu yöntemde çözelti formuna getirilmiş polimerik malzeme polimer besleme ünitesi tarafından iğne veya düze ucuna beslenir. Daha sonra polimer çözeltisinin beslendiği iğne ucuna yüksek voltaj (5-80kV) uygulanır ve iğne ucu - toplayıcı arasında elektrik alan oluşturulur. Elektrik alanın oluşturduğu yüzey gerilimi etkisiyle, iğne ucunda asılı durumda duran polimer damlası önce Taylor konisi formunu alır ve belli bir voltaj değerine ulaşıldığında, üzerine uygulanan yüzey gerilim kuvvetlerini yenerek, toplayıcı ünitesine doğru hızlı ve spiral bir yol çizerek hareket eder. Bu hareket esnasında, polimer çözeltisi toplayıcıya ulaşınca kadar çözücü buharlaşır. Nihayetinde toplayıcı üzerinde nano boyutta ve uzun lif üretimi gerçekleştirilmiş olur. Elektroüretim prosesinde çözelti konsantrasyonu, çözücü tipi, voltaj, besleme hızı, iğne ucu toplayıcı arası mesafe gibi pek çok parametre değiştirilerek istenen lif çapında nanolifler elde edilebilir. Ayrıca yüksek hızda dönen toplayıcı kullanımı ile lif oryantasyonu artırılabilir.

Topikal ilaç salım sistemleri ilacın farmakolojik etkisini deri yüzeyinde hedefleyen ve doğrudan cilde uygulanan bir formülasyondan oluşan sistemlere denilir. Genel bir hastalığın (örneğin, sedef hastalığı) kutanöz bozuklukları (örneğin akne) veya kutanöz belirtilerini tedavi etmek için kullanılırlar.

Nanoliflerin ilaç salımında kullanımı, nanolif taşıyıcının yüksek yüzey alanlarının ilacın çözünme oranını artırması ilkesine dayanmaktadır. Nanolifler; lipozomlar, miseller ve hidrojeller gibi diğer dozaj formları ile karşılaştırıldığında en belirgin avantajları; ilaç yükleme verimliliği, ilaç yükleme kapasitesindeki artış, düşük sistemik toksisite ve mükemmel stabiledir. Ayrıca, nanoliflerin mükemmel ilaç taşıma kabiliyetleri sayesinde pek çok ilaç yüksek lokal konsantrasyonunda güvenli bir şekilde hedef bölgeye taşınabilir.

Elektroüretim yöntemi ile üretilen ilaç salım sistemlerinde, Polikaprolakton (PCL), Polilaktik asit (PLA) ve Polietilen oksit (PEO) biyopolimerleri taşıyıcı matriks olarak tercih edilmiştir. Kullanılan biyopolimerlerden PEO hidrofilik, PCL ve PLA ise hidrofobik karakterdedir.

PEO suda çözünürlüğü yüksek olan ve hidrofil yapıda olduğu için vücut sıvısı ile hızlıca etkileşime giren bir polimerdir. PEO, yüksek çözünürlüğünden ötürü ilaçların çözünürlüğünü ve biyoyararlanımını artırmak için ilaç salım uygulamalarında polimer matriksi olarak sıkça kullanılır. PCL ve PLA'nın ise farklı tip ilaçlarla kombine edilebilirliği, ilacın polimer matriksinde homojen bir şekilde dağılımına olanak sağlar. Ayrıca, PCL ve PLA yavaş degradasyon hızına sahip oldukları için bu iki polimer uzun süreli ilaç salımında tercih edilir. Son yıllarda yapılan bilimsel çalışmalarda; PCL, PLA ve PEO'nun, hem ayrı ayrı hem de karışım olarak elektroüretiminin gerçekleştirildiği ve ilaç salım sistemlerinde kullanıldığı bildirilmiştir. PCL, PEO, PLA nanoliflerine veya bunların karışımlarına farklı ilaçlar ve biyolojik ajanlar ilave edilmiştir. Bunlardan bazıları, niklosamid, gümüş nanopartikülleri, B₁₂ Vitamini, Kurkumin, Lizozim, AgNO₃, metronidazole (MNA) olarak sıralanabilir.

Polimerlerin karışım olarak elektroüretimi, bileşimde kullanılan her bir polimerin olumlu özelliklerini birleştirerek fonksiyonel nanolif matriksleri hazırlamak için etkili bir yaklaşımdır. Ayrıca bu sayede; nanoliflerin fiziksel, mekanik veya biyokimyasal özelliklerinin manipülasyonu kolaylaştırılır. Kontrollü ilaç salım sistemi üretmek için hidrofilik / hidrofobik polimer karışımlarının elektroüretimi ile kompozit nanolifler elde edilmiştir. Hidrofobik polimer sistemin omurgasını oluşturur ve yavaşça bozunarak uzun vadeli ve kararlı bir ilaç salımı sağlar. Öte yandan, ilaç salımını hızlandıran hidrofilik polimer ise, hidrofobikten daha hızlı bir süreçle bozunmaktadır. Bu çalışmada, çözünürlüğü çok düşük olan GSD'nin çözünürlüğünü ve biyoyararlanımını artırmak için hidrofilik PEO polimeri seçilmiştir. PCL ve PLA'nın hidrofobik karakteri, uzun süreli bir GSD salımı sağladığı için hidrofilik PEO, hidrofobik PCL ve PLA ile harmanlanmıştır. Bu çalışmada, PCL / PEO ve PLA / PEO kompozit polimer matrisleri hem GSD'nin çözünürlüğünü artırmak hem de kontrollü ilaç salımını sağlamak için kullanılmıştır.

Gümüş sülfadiazin (GSD), erime noktası 285°C ve moleküler ağırlığı 357,14 g / mol olan, iyonize olmayan ve suda çözünmeyen topikal bir ajandır. Hem bakteriler hem de mantarlar üzerinde etkili geniş bir antimikrobiyal aktiviteye sahiptir. GSD, sülfadiazinin gümüş nitrat ile reaksiyona girerek kompleks gümüş tuzu oluşturması sonucu oluşan sülfonamid bazlı bir ilaçtır ve enfekte yanıkların topikal tedavisinde yaygın olarak kullanılmaktadır. Gümüş nitrat gibi gümüş tuzları büyük miktarlarda gümüş iyonlarını aynı anda salarken, GSD diğer gümüş tuzlarının aksine iyonlarının uzun süreli salımını sağlar. Bu sebeple, GSD'nin hastalara uygulama sıklığı daha azdır. Sık uygulama ihtiyacı hastalar açısından her zaman pratik veya mümkün olmaması GSD'yi arzu edilen ve uygun bir biyolojik ajan yapar. Bununla birlikte, GSD'nin sudaki düşük çözünürlüğü (pH = 6.8'de 3.4 mg/l) GSD'nin ilaç verimini, biyoyararlanımını ve potansiyel antimikrobiyal aktivitesini kısıtlamaktadır, bu nedenle GSD uygulamaları sınırlı kalmaktadır. Etkin ilaç salımı ve antimikrobiyal aktivite GSD'nin gümüş iyonlarına ve sülfadiazine ayrışmasıyla sağlandığından, ilaç çözünürlüğü hayati öneme sahiptir. Ayrıca, GSD'nin çözünürlük problemi, stabilize edilmesini ve polimer matrisi içine ilave edilmesini de zorlaştırır. Bu nedenle araştırmacılar GSD'nin çözünürlüğünün, biyoyararlanımının ve antibakteriyel etkinliğinin artırılması üzerine çalışmalar yapmaktadırlar. Bu amaçla GSD; nanopartikül, nanorod, nano süspansiyon formunda veya farklı polimer sistemlere yüklenerek film, hidrojel, kompozit ve fiber bazlı ilaç taşıyıcı sistemleri şeklinde üretilmiştir.

Bu tezin amacı, elektroüretim yöntemi ile elde edilmiş nanoliflerin avantajlarını kullanarak yeni bir GSD yüklü topikal ilaç salım sistemi elde etmektir. Bununla

birlikte, GSD'nin çözünme ve salım davranışını araştırmak için daha önce başka bir çalışmada kullanılmamış olan Su / Propilen Glikol / Fosforik Asit (82: 16: 2) tampon çözeltisi kullanılmıştır. Dolayısıyla, GSD'nin çözünürlüğünde, etkin ilaç salımında ve ilaç yükleme veriminde artış sağlamak için GSD içeren PCL/PEO ve PLA/PEO kompozit nanolif taşıyıcıları elektroüretim yöntemi ile üretilmiştir. Bu amaç doğrultusunda öncelikle GSD'nin çözünürlüğünü artırmak için, GSD suda çözünürlüğü yüksek olan PEO polimer yapısına dahil edilmiştir. Daha sonra ise PEO+GSD çözeltisi, ilaç salım sistemi olarak kullanılacak PCL/(PEO+GSD) ve (PLA/PEO+GSD) kompozit nanoliflerini ve film yüzeylerini elde etmek için PCL ve PLA çözeltileri ile karışım yapılmıştır.

Çalışmada öncelikle elektroüretim ve film üretim parametreleri optimize edilip nanolif ve film yüzeylerinin üretimi gerçekleştirilmiştir. Sonrasında ise üretilen PCL/(PEO+GSD) ve PLA/(PEO+GSD) nanolif ve PCL/(PEO+GSD) film formundaki ilaç salım sistemlerinin karakterizasyon çalışmaları yapılmıştır. Karakterizasyon çalışmaları kapsamında; elektroüretim yöntemi ile oluşturulan nanoliflerin yüzey özelliklerinin incelenmesi ve ortalama lif çaplarının hesaplanması için Taramalı Elektron Mikroskobu (SEM) yöntemi kullanılmıştır. Üretilen film yüzeylerinin morfolojik karakterizasyonu ise SEM ve Optik Profilometre ile yapılmıştır. GSD içeren nanolif ve film yapısındaki formülasyonların Gümüş (Ag), Azot (N), Kükürt (S) içeriklerini tespit etmek için Enerji Dağılım Spektroskopisi (EDS) analizi yapılmıştır. Ayrıca bu elementlerin kompozit nanolif ve film yapısındaki homojen dağılımlarını göstermek için EDS-Mapping (haritalama) analizi gerçekleştirilmiştir.

GSD'nin nanolif yapısındaki stabilitesi, ilaçsız ve ilaç yüklü nanoliflerdeki moleküler etkileşimler, Zayıflatılmış toplam yansımali Fourier dönüşümlü kızılötesi (FTIR-ATR) Spektroskopisi ile incelenmiştir. GSD yüklü kompozit nanoliflerinin kristal yapısını incelemek için ise X-ışını kırınımı (XRD) çalışması yapılmıştır.

Kompozit nanoliflerin yüzey pürüzlülüğünü belirlemek için Atomik Kuvvet Mikroskobu (AFM) kullanılmıştır. Üretilen nanoliflerin filmlerin yüzey ıslanabilirliğini incelemek için temas açısı ölçümleri yapılmıştır.

In vitro ilaç salım ortamı ve salım koşulları optimize edilmiş ve kontrollü ilaç salım çalışmaları gerçekleştirilmiştir. Nanolif ve film formülasyonlarının ilaç yükleme verimliliği hesaplanmıştır. GSD yüklü formülasyonlarının GSD ilaç salım mekanizmalarını incelemek için; *in vitro* salım neticesinde elde edilen ilaç salım profillerine Zero Order, First Order, Higuchi, Hixon Crowell ve Korsmeyer-Peppas kinetik modelleri uygulanmış ve her bir formülasyon için uygun olan kinetik model belirlenmiştir. Ayrıca ilaç salım çalışmaları, GSD'nin bilinen iletken yapısı nedeniyle iletkenlik ölçümüyle de doğrulanmıştır.

Kompozit nanoliflerin gram pozitif *Staphylococcus aureus* (S. aureus) ve gram negatif *Pseudomonas Aeruginosa* (P. aeruginosa) *Escherichia coli* (E.Coli) bakterilerine karşı antibakteriyel aktiviteleri disk difüzyon test methoduna göre araştırılmış ve ticari GSD kremin antibakteriyel etkinliği ile karşılaştırılmıştır. Ayrıca, GSD yüklü PCL / PEO ve PLA / PEO nanoliflerinin antibakteriyel aktivitesi kantitatif duyarlık testleri ile MIC ve MBC değerleri belirlenerek de incelenmiştir.

Kompozit nanoliflerin stabilite çalışmaları 3 ve 6 aylık periyotlarla yapılmıştır. Nanolif örnekleri, nanolif formülasyonlarının stabilitesini değerlendirmek için hem buzdolabı koşullarında (+4°C) hem de oda koşullarında (25°C ±2 ve% 65 ±2°C bağıl nem) muhafaza edilmiştir. Stabilite testleri; ilaç yükleme miktarının hesaplanması, UV

absorpsiyon ölçümleri ile kümülatif ilaç salımının belirlenmesi ve SEM analizi ile yüzey morfolojisinin analiz edilmesi yöntemleri ile gerçekleştirilmiştir.

Son olarak, ilaç içeren ve içermeyen PCL / PEO ve PLA / PEO nanoliflerin sitotoksosite çalışmaları, hücre canlılık testi (MTT testi) kullanılarak yapılmıştır.



1. INTRODUCTION

Textile materials are commonly used in medical applications. The usage of textile materials in medical field ranges from simple gauze or bandage materials to tissue scaffolds and artificial blood vessels. Due to the variety of facilities of medical textiles for end-use performance, textile materials can be fabricated in the form of fibre, yarn, knitted, woven, nonwoven fabrics in healthcare applications. The major requirements for medical textiles are softness, lightness, flexibility, biocompatibility O₂ permeability, porosity, absorption and filtering etc.

Medical textile applications can be classified as followings; Barrier materials (for infection control), Bandaging & pressure garments, Wound dressing materials, Antimicrobial textiles, Hygiene materials and Implantable materials (Ahmed et al., 2014)

Nowadays advanced medical textiles are significantly enhancing with development in polymer and fiber technologies. Especially, nanofiber based materials represent innovations in medical applications. Nanofibers possess remarkable properties such as high interconnected porosity, specific surface area, ability to imitate the Extra Cellular Matrix (ECM) and potential carrier for drug delivery. Due to these fascinating properties, nanofibers are attractive candidates for medical applications for instance wound dressings, tissue scaffolds and artificial blood vessels (Wen et al., 2005; Huang et al., 2003).

Silver sulfadiazine (SSD) is a non-ionized, water-insoluble, topical antibacterial agent that is formed by the reaction of sulfadiazine with silver nitrate to form complex silver salt. SSD is used extensively in the topical treatment of infected burns (White & Cooper, 2005). Silver sulfadiazine provides a long-term release of silver ions, whereas in the case of other silver salts, such as silver nitrate, large amounts of silver ions are released all at once. Thus, the use of SSD decreases the need for frequent application. This makes SSD a desirable and favourable agent since frequent application is not

always practical or possible for patients. Because of these reasons, SSD is more effective than the other silver salts (Fox & Modak, 1974).

SSD is a poorly aqueous soluble drug (3.4 mg/l at pH = 6.8). The low solubility restricts the drug efficiency, bioavailability and potential antibacterial activity of SSD thus its applications are limited. Drug solubility is an important issue since efficient drug release is contributed just by decomposition of SSD to sulfadiazine and silver ions. Also, the solubility problem of SSD makes it difficult to be stabilized and incorporated into the polymer matrix. Water insolubility of SSD is a challenge, therefore researchers have focused on the enhancement of its solubility and bioavailability. To this end, SSD was formed as nanoparticles, nanorods, nanosuspensions or loaded into different types of polymeric carriers by formulating as film, hydrogel, composite and fiber-based drug delivery systems (Szegeedi et al., 2014; Li et al., 2015). However, although SSD is usually used to heal burns, there are a limited number of researches on SSD loading into nanofibers, its solubility and drug release behaviour. However, in the literature, there are few studies related to loading SSD in electrospun nanofibers.

Utilization of nanofibers in drug delivery systems is based on the principle that the high surface area of the nanofibrous formulation increases the dissolution rate of the drug. Compared with other dosage forms such as; liposomes, micelles and hydrogels, major advantages of nanofibers are increment in drug loading efficiency and loading capacity, low systemic toxicity and excellent stability (Hu et al., 2014). Furthermore, several drugs can be carried within nanofibers with high local drug concentration due to their excellent targeting and drug transportation ability in a safe way (Morie et al., 2016).

Electrospinning is one of the simplest among all methods to fabricate nanoscaled fibers and it offers the opportunity for direct loading of drug into the electrospun nanofibers (Taylor, 1964; Sarac, 2017). Many drugs and bioactive molecules are loaded into nanofibers such as rifampin, paclitaxel, tetracycline hydrochloride, doxorubicin hydrochloride, proteins, and DNA to improve bioavailability, bioactivity and control delivery (Zamani et al., 2013). Different polymers have been electrospun into nanofiber such as gelatine, chitosan, silk fibroin, hyaluronic acid (HA), hydroxypropyl cellulose (HPC), polyurethane (PU), polyvinyl alcohol (PVA), poly (lactic acid) (PLA), poly (ϵ -caprolactone) (PCL), poly (ethylene oxide) (PEO) and poly (lactic-co-

glycolic acid) (PLGA), to fabricate patches for drug-delivery applications (Hu et al., 2014; Gunn & Zhang, 2010; Esenturk et al., 2016; Sarac, 2017).

Poly (ϵ -caprolactone) (PCL), Poly (lactic acid) (PLA) and Poly (ethylene oxide) (PEO) were used as carrier polymers for drug delivery. PEO is a highly aqueous soluble polymer, that interacts with the body fluid quickly due to its hydrophilicity resulting in dissolution. PEO is widely used in the polymer matrix to enhance bioavailability and solubility of drugs because of its high aqueous solubility and unique properties in drug delivery applications (Gunn & Zhang, 2010; Kohsari et al., 2016; Wang et al. 2016; Cheng et al., 2015; Dubey & Gopinath, 2016). The compatibility of PCL and PLA with different types of drugs enables uniform drug distribution in the polymer matrix and the slow degradation rate makes them favourable for prolonged drug delivery systems. In recent years, various studies were reported on the fabrication of drug delivery systems, generated by electrospinning of PCL, PEO, PLA and their blends. PCL, PEO, PLA nanofibers or their blends were loaded with different drugs and biological agents such as, Niclosamide, Silver nanoparticles, Vitamin B₁₂, Curcumin, Lysozyme, AgNO₃, Metronidazole (MNA) (Dubey & Gopinath, 2016; Dubey et al., 2015; Xue et al., 2014; Madhaiyan et al., 2013; Khan et al., 2009; Merrell et al., 2009; Li et al., 2008; Kim et al, 2007).

Polymer blending is an effective approach to prepare functional nanofibers by incorporating the favourable properties of the component polymers. Furthermore, polymer blending facilitates the manipulation of physical, mechanical or biochemical properties of nanofibers. Hydrophilic/hydrophobic polymer blends have been electrospun into nanofibers to fabricate controlled DDS. The hydrophobic polymer forms the backbone structure and it degrades slowly, creating a long term but steady-state drug release. On the other hand, the hydrophilic polymer degrades with a more rapid process, faster than hydrophobic, which accelerates the drug release (Heunis & Dicks, 2010; Hanumantharao et al., 2019).

In this study, hydrophilic water-soluble PEO was selected for the polymer matrix to enhance the solubility and bioavailability of insoluble SSD. The hydrophobic character of PCL and PLA offers a long period SSD release therefore hydrophilic PEO was blended with hydrophobic PCL and PLA. Thus, PCL/ PEO and PLA/PEO composite polymer matrix was used to provide both increased solubility and controlled release of SSD.

In literature, few authors focused on dissolution and release studies in detail due to the insoluble nature of SSD. Although SSD is usually utilized in burn treatment, there are limited researches on SSD loading into nanofibers. In this thesis, taking the advantages of nanofibers such as high interconnected porosity and specific surface area SSD was loaded into PCL/PEO and PLA/PEO nanofibers for the first time. Moreover, for comparison with nanofibers PCL/PEO casting films were fabricated.

Also, a new buffer, Water/Propylene Glycol/ Phosphoric Acid (82:16:2) was utilized to investigate the dissolution and release behaviour of SSD. Thereby SSD containing PCL/PEO and PLA/PEO composite nanofiber carriers were electrospun to achieve the enhancement in solubility, effective drug release and efficient drug loading of SSD. For this purpose, initially, the water-insoluble SSD was incorporated into highly aqueous soluble PEO to increase the solubility. Afterwards, the PEO+SSD solution was blended with PCL and PLA solution to produce composite PCL/(PEO+SSD) and PLA/(PEO+SSD) nanofibers and PCL/(PEO+SSD) casting films for topical drug delivery. The SSD loaded nanofibers were verified by FTIR, XRD, and EDS. The morphological characterization of nanofibers was carried out by SEM and AFM. The SSD loaded casting films were verified by FTIR, XRD, and EDS. The morphological characterization of the casting films was carried out by SEM and Optical Profilometer. The solubility of silver sulfadiazine in Water/Propylene Glycol / Phosphoric Acid (82:16:2) solution was evaluated. The amount of SSD release at various times up to 24 hours was quantified through UV-Visible spectrophotometer and the *in vitro* release profile was plotted.

2. THEORETICAL BACKGROUND

2.1 Nanofibers

Nanomaterials consist of a wide range of attractive materials with prominent physical and chemical properties such as zero-dimensional nanoparticles or quantum dots, one-dimensional nanowires, nanorods, nanofibers and nanotubes and two-dimensional nanosheets (Lim, 2017). Nanofibers are ultrafine, continuous, solid state textile fibers that have diameters less than 1 micrometre. Nanofibers are very fine fibers in comparison to conventional textile fibers to help the imagination, nanofibers approximately 1000 times thinner than a human hair as shown in Figure 2.1 (Peijs, 2018).

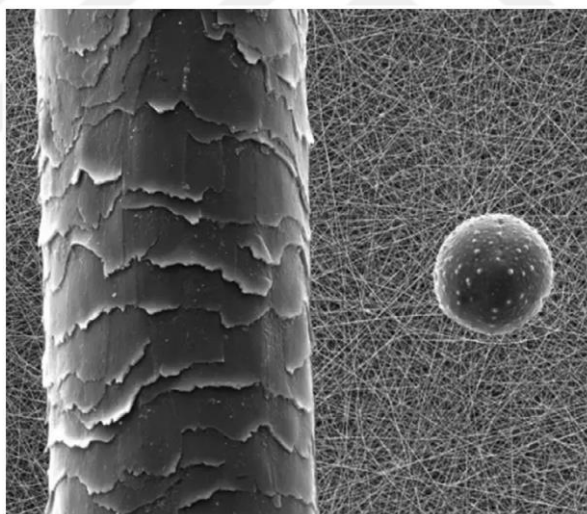


Figure 2.1 : Nanofiber scale (human hair, pollen grain, nanofiber mat) (Peijs, 2018).

Nanofibers possess small fiber diameters which give them unique properties. Reduced fiber diameter offers high surface area in relation to their mass because when the diameter decreases, the occupied place in terms of volume increases creating a high surface area to weight ratio. Smaller fiber diameter and high surface area represents high porosity and high pore interconnectivity with small pore size. These properties are essential for any filtration, separation processes, wound dressing and drug delivery applications. Figure 2.2 explains the relation between fiber diameter and surface area (Gibson et al., 2001). Moreover, nanofibers have enhanced mechanical properties,

notably toughness and high tenacity due to an increase in surface area. Indeed, the tensile strength of an individual nanofiber is very low but when their ultrafine diameters is considered, the values of the tensile strength is very high due to the high molecular orientation in the fiber structure. Thanks to this feature, nanofibers can be used in composites with high mechanical performance (Greiner & Wendorff, 2007).

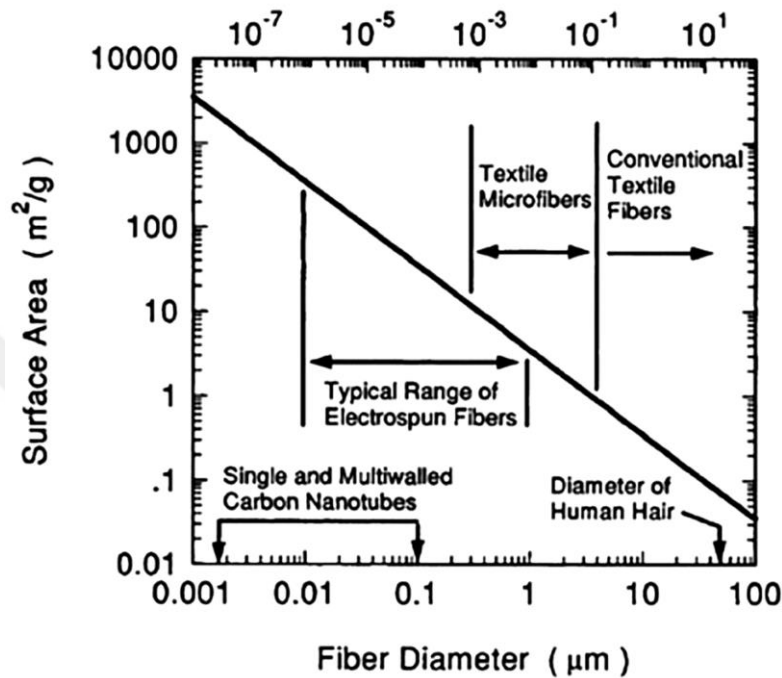


Figure 2.2 : Relationship between specific surface area and diameter of different fibers (Gibson et al., 2001).

As a result, due to the excellent properties, nanofibers may be used for many different applications (Lim, 2017). These are;

1. Environmental Applications

- Air /liquid/particle filtration
- Membrane technology
- Water treatment

2. Energy Applications

- Separators for batteries and fuel cells
- Energy storage cells
- Solar cells
- Supercapacitors

3. Biomedical Applications

- Tissue scaffolds,
- Wound dressings
- Drug delivery systems
- Artificial blood vessels
- Enzyme immobilizations
- Antimicrobial applications

4. Cosmetics

5. Protective clothing and materials

6. Sensor Devices

7. Composite Materials

8. Conductive Materials

9. Catalysis

There have been many methods for nanofiber fabrication for instance drawing, template synthesis, temperature-induced phase separation, molecular self-assembly, vapour grown, island in the sea and electrospinning methods. Electrospinning method has advantages over other nanofiber production methods (Kumbar et al., 2008). The major advantages of electrospinning process are:

- Simple equipment
- Continuous process
- Cost effective process
- Fibers can be obtained from few nanometres to several micrometres (Kumbar et al., 2008)

2.2 Electrospinning Process

Electrospinning is the cheapest, simplest and most convenient among all methods to fabricate fine fibers with diameters ranging from micrometers to nanometres (Dogan, 2013).

Basic electrospinning equipment contains a high voltage source, a solution feeding unit, a syringe with a tip and a collector. At first, high voltage is applied to the polymer solution to produce an electrical field between the tip and the collector to shape the droplet on the tip as Taylor Cone. When the electrostatic force is higher than the

surface tension of the polymer solution, polymer jet is pushed from the needle tip to the collector. Then, polymer jet reaches to collector following a spiral way by getting longer and thinner. Finally, nanoscaled fibers are obtained on the collector (Taylor, 1964; Sarac, 2017). The fiber diameter and properties can be controlled by changing the process (flow rate, voltage, distance), material (concentration, molecular weight, viscosity) or ambient parameters (humidity, temperature). Furthermore, aligned and regular fibers can be produced with using rotating collector at high speeds. Basic electrospinning equipment is shown in Figure 2.3.

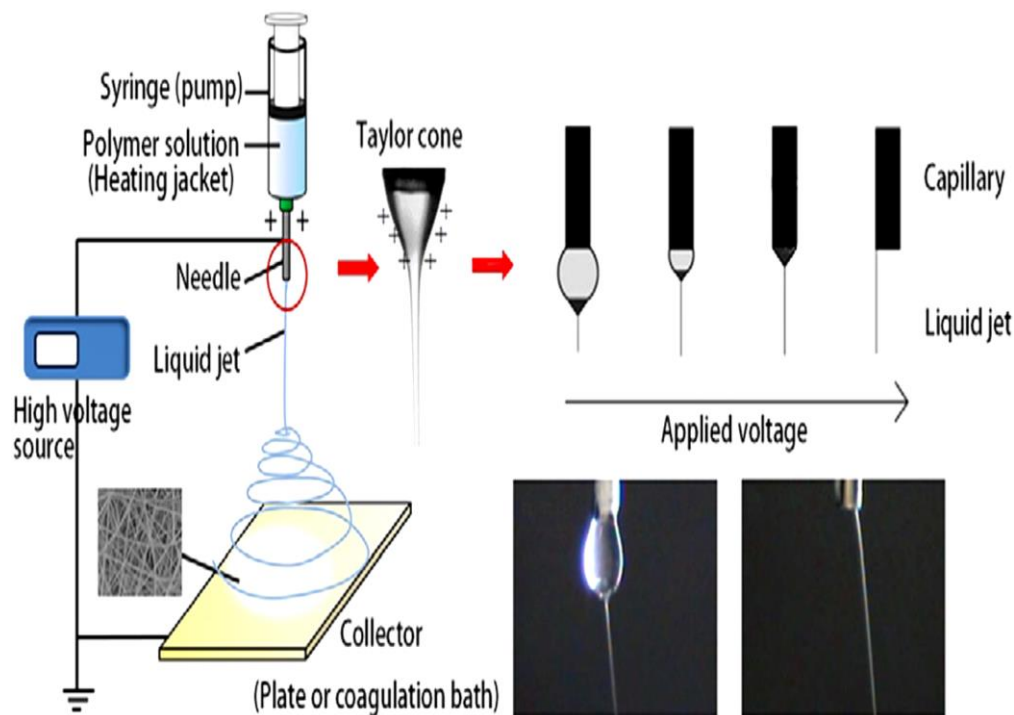


Figure 2.3 : Basic electrospinning equipment (Liu et al., 2017).

2.2.1 Parameters of electrospinning

The diameter, shape and surface morphology of the nanofibers are affected by a number of parameters during electrospinning. These parameters are first; the properties of the polymer solution, such as molecular weight and molecular weight distribution of the polymer, the conformation of polymer chains, viscosity, surface tension, electrical conductivity, solvent vapour pressure, and pH value, second; the process parameters, such as the applied voltage, occurring electrical field, electrode geometry, distance between the tip and collector, speed of the collector (for rotating collector), type and geometry of the collector (plate, rotating collector, rotating wire drum, rotating disk, water or ethanol coagulation bath with rollers), solution flow rate,

and third; the ambient factors, for instance the humidity, temperature and the air pressure of the environment (Sun et al., 2019).

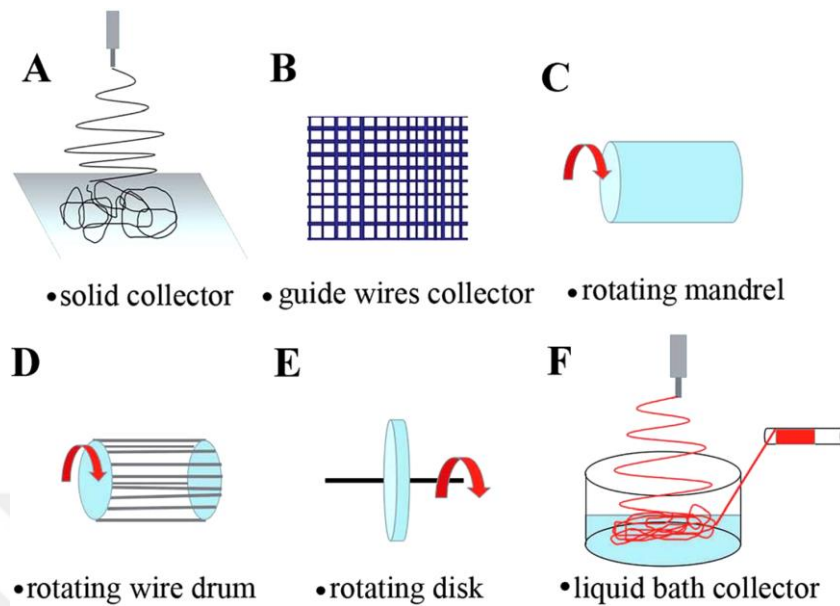


Figure 2.4 : Collector types using in electrospinning set up: (A) solid collector, (B) guidewire collector, (C) rotating mandrel, (D) rotating wire drum, (E) rotating disk, (F) liquid bath collector (Sun et al., 2019).

2.3 Biopolymers in Electrospinning

Electrospun nanofibers can be made from synthetic polymer and natural-derived polymers or their blends. A variety of synthetic degradable biopolymers, including Poly (ϵ -caprolactone) (PCL), Poly (lactic acid) (PLA), Poly (glycolic acid) (PGA), and Poly (lactic-*co*-glycolic acid) (PLGA) and Poly(ethylene) oxide (PEO), PVA and PU have been utilized for biomedical applications of electrospun nanofibers (Gunn & Zhang, 2010).

In recent years, remarkable attention has been given to natural biopolymers to form biomimetic nanofibers. A variety of natural biopolymers including collagen, gelatine, cellulose and cellulose derivatives, fibrinogen, chitosan and alginate have all been used for nanofiber preparation (Vert, 2001).

2.3.1 Polysaccharides

The most common polysaccharides in the biomedical applications are: cellulose, alginates, dextran and chitosan.

2.3.1.1 Cellulose and derivatives

Cellulose, the “sugar of plant cell wall,” is a polysaccharide based on glucose and it is the most plentiful biopolymer in the nature. The monomer unit of cellulose is β -D-anhydroglucopyranose that is shown in Figure 2.5.

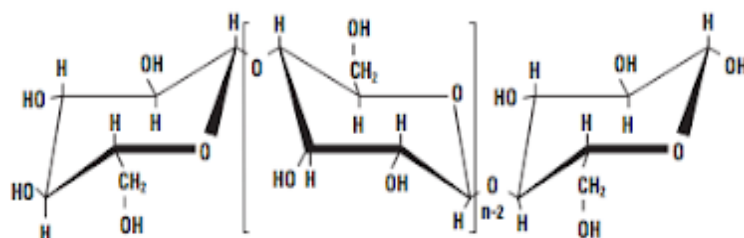


Figure 2.5 : Chemical structure of Cellulose (Url-7).

The macromolecular structure and the including intensive hydrogen-bonding in chemical structure of the cellulose lack the solubility properties in water and organic solvents. For this reason, cellulose has very low solubility in common solvents, low dimensional stability, limited thermos plasticity and antibacterial properties. To overcome these challenges, specific solvents such as *N,N*-dimethylacetamide/lithium chloride (DMA/LiCl) and dimethyl sulfoxide/tetrabutylammonium fluoride (DMSO/TBAF) are used commonly. These solvents break the hydrogen bonds in chemical structure of the cellulose. Although cellulose alone has been utilized with such strategies, as a polymer, derivatives of cellulose are easier to work and process as they overcome limitations that cellulose possesses. Derivatives of cellulose are; Acetyl esterase, Carbohydrate esterase (CE), Cellulose acetate (CA), Regenerated cellulose, Carboxymethyl cellulose (CMC), Hydroxypropyl cellulose (HPC), Hydroxyalkyl celluloses, Ethyl cellulose (EC) and Methyl cellulose (MC) (Aravamudhan et al., 2014).

Cellulose and derivatives are commonly utilized in wound dressings. Hydroxyalkyl celluloses and Carboxymethyl celluloses are in drug delivery and tissue engineering applications. Regenerated cellulose is widely preferred in haemodialysis membranes and hollow fibers applications (Vert, 2001). Cellulose acetate is used to fabricate blood filtration devices.

2.3.1.2 Alginates

Alginates include polysaccharide type polymer chains that consists of glucuronic and mannuronic acid (Timofeeva & Kleshcheva, 2011). Alginates are widely used in absorbable wound dressings. Because they are easily made into hydrogels form by occurring complex with calcium ions. Moreover, alginates are suitable biopolymers for drug delivery applications. However, they are not biodegradable in the body (Vert, 2001).

2.3.1.3 Chitin and chitosan

Chitin is a kind of polysaccharide which is widely found in the cell walls of the insect cuticles, of many fungal and of shellfish or mollusc exoskeletons. The basic monomer unit of the chitin is (1-4) 2 acetamide-2-desoxy-D-glucose (or N-acetyl glucosamine) that is represented in Figure 2.6 (Smith, 2005).

Chitosan is generated by the elimination of acetyl groups ($\text{CH}_3\text{-CO} \pm$ deacetylation) which are converted to amine group. The conversion is never really complete and occurs partially. This is defined by the deacetylation degree (DD) of the chitosan. DD value of the chitosan can be varying between 30 % to 95 %. By the means of the transition of chitin to chitosan, the polymer becomes more soluble and easier processable for different applications (Aravamudhan et al., 2014).

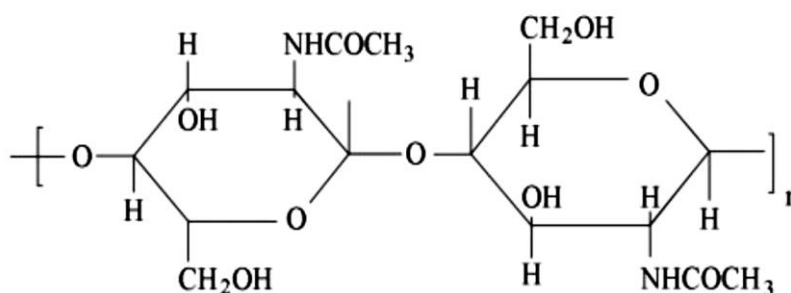


Figure 2.6 : Chemical structure of Chitin (Smith, 2005).

Molecular weight and deacetylation degree effect the properties of chitosan. Chitosan is dissolved in dilute acids. Chitin and chitosan are biocompatible and present anti thrombogenic and homeostatic properties. Therefore, they can be used in biomedical devices, drug delivery systems and tissue engineering (Smith, 2005).

Chitosan exhibits antibacterial activity that occurs with the interaction of negatively charged groups on the cell wall and the positively charged chitosan polymer. This

causes to destroy on cell wall of the bacteria so that it shows bactericidal effect. Moreover, antibacterial activity of chitosan is explained with attachment of chitosan to bacterial DNA. In this case, chitosan lacks the transcription of bacterial DNA (Aravamudhan et al., 2014).

2.3.1.4 Hyaluronic acid

Hyaluronic acid is a linear polysaccharide and is consist of *N*-acetyl-d-glucosamine and d-glucuronic acid. At solutions of hyaluronic acid, a gel structure is formed and these solutions show viscoelastic properties. Hence HA polymers are fantabulous biological absorbers and they are preferred for fabrication of hydrogels.

Hyaluronic acid is a highly water soluble polymer that results in rapid biodegradation in the body. For this reason, it is cross-linked to improve its stability and mechanical properties in applications. HA has a common use in tissue scaffolds, drug delivery systems and lubricants (Aravamudhan et al., 2014).

2.3.2 Proteins

Proteins consist of amino acids which are linked to each other by peptide-type amide bonds. Several protein based polymers are used in the biomedical applications.

2.3.2.1 Collagen

Collagen is a common protein in the human body that is the building block of the extracellular matrix (ECM) and it supports mechanical durability to the tissues. There are 29 different types of collagen that was identified. Chemical structure of collagen consists of hydroxyl proline, glycine and proline. Collagen can be cross-linked with the glutaraldehyde and other cross-linkers. Collagen is widely used in regenerative medicine and tissue scaffolds (Katoira et al., 2019).

2.3.2.2 Gelatine

Gelatine is a promising protein based biopolymer that is derived from collagens. There are two types of gelatine: Type A and Type B. Type A is obtained with acidic pre-treatment from collagens, but Type B is extracted with alkaline pre-treatment from collagens. Type B has more carboxylic acid than Type A because the alkaline pre-treatment converts glutamine and asparagine residues into glutamic and aspartic acid.

Due to the desirable properties of gelatine, such as its biocompatibility, biodegradability and commercial availability, gelatine is good candidate for biomedical applications. For instance, gelatine has been used in vascular prostheses, drug delivery carriers, wound dressings and tissues scaffolds (Zhang et al., 2004).

2.3.2.3 Fibrin

Fibrin is a natural biopolymer that is known with cell adhesive and homeostatic properties. They are primarily utilized in tissue scaffolds and drug delivery systems. Fibrin glue is produced from thrombin and fibrinogen which are derived from plasma. Perfect polymerization and crosslinking are essential to support optimum mechanical strength (Katoira et al., 2019).

2.3.3 Poly (ϵ -caprolactone) (PCL)

PCL is a type of aliphatic polyester obtained by ring-opening polymerization of ϵ -caprolactone monomers. Different catalysts such as stannous octoate or aluminium alkoxides can be used for the polymerization of caprolactones. Polymerization processes were carried out under different parameters which are, temperature and time of polymerization, concentrations and types of catalysts and the monomer ratio to solvent. PCL polymer can be obtained with different molecular weights (M_n) and poly-dispersity indices (PDI) with switching one or more of these parameters. Therefore, PCLs are formed varying with polymer degradation behaviour and mechanical properties. Chemical structure of PCL is shown in Figure 2.7.

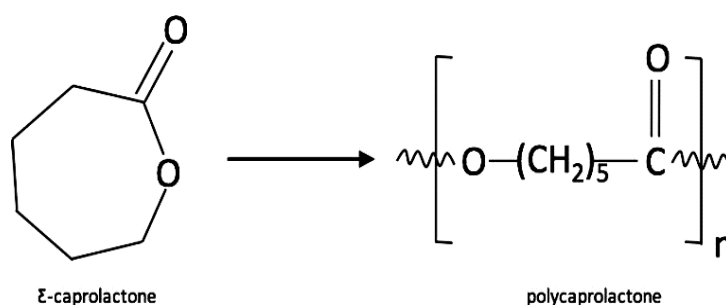


Figure 2.7 : Chemical structure of Poly (ϵ -caprolactone) (Osathanon et al., 2017).

PCL is easily soluble in chloroform, benzene, dichloromethane, cyclohexanone, toluene, and 2-nitropropane. However, it has limited solubility in acetone, acetonitrile, 2-butanone, dimethylformamide, ethyl acetate. PCL is a hydrophobic polymer hence it is unsolved in water and ethyl alcohol. PCL is a semi crystalline polymer at room temperatures. T_g of PCL is about -60°C and T_m is about 60°C . PCL shows rubbery

behaviours at room conditions. PCL is biodegradable but it has long degradation term due to having less frequent ester bonds per monomer to enzymatically hydrolyse in the body. PCL polymer degrades completely in 2-3 years. Enzymatic degradation is performed by the lipase enzyme. The ambient pH is an important factor on the degradation time. For example, PCL degrades in alkaline conditions faster than in acidic conditions (Malikmammadov et al., 2018).

Because of the long degradation term, PCL is especially preferred in long term implants, tissue scaffolds and sustained drug delivery applications. PCL can be blended with more degradable and hydrophilic polymers to optimize degradation rate of the applied material and to improve wettability of hydrophobic PCL. Many of drugs can be encapsulated into PCL for controlled drug release. The compatibility of PCL with different types of drugs enables uniform drug distribution and drug permeability in the polymer matrix and the slow degradation rate of PCL makes it favourable for prolonged drug delivery systems (Dubey & Gopinath, 2016; Kim & Park, 2009).

PCL has good mechanical properties such as high Young's modulus, elasticity and tensile strength. The tensile strength of PCL is around 10.5 - 16.1 MPa, tensile modulus is around 343.9 - 364.3 MPa, and the tensile yield strength is around 8.2 - 10.1 MPa (Hajiali et al., 2018; Eshraghi & Das, 2010).

For all these desirable properties of PCL, it is an ideal and promising biomaterial in drug delivery, wound dressings, tissue scaffolds and other medical applications.

2.3.4 Poly (lactic acid) (PLA)

PLA is a hydrophobic, aliphatic polyester that has renewable sources, such as corn starch, tapioca roots, chips or starch, or sugarcane. It is a biodegradable polymer that degrades by composting in 4 weeks and in the body from 6 months to 2 years. PLA can be dissolved in acetone (AC), chloroform (CHL), dichloromethane (DCM), dimethylacetamide (DMAc), dimethylformamide (DMF), dioxane (DX), tetrahydrofuran (THF) and benzene. (Toprakci et al., 2018; Laurencin & Deng, 2014).

Poly (lactic acid) can be obtained with condensation polymerisation of the free acid and with ring opening polymerisation of the lactide. There are three optically isomeric lactides: L-lactide (a dimer of L-lactic acid), D-lactide (a dimer of D-lactic acid) and *meso*-lactide (a dimer of D- and L- lactic acid) (McLauchlin & Thomas, 2012) which are shown in Figure 2.8.

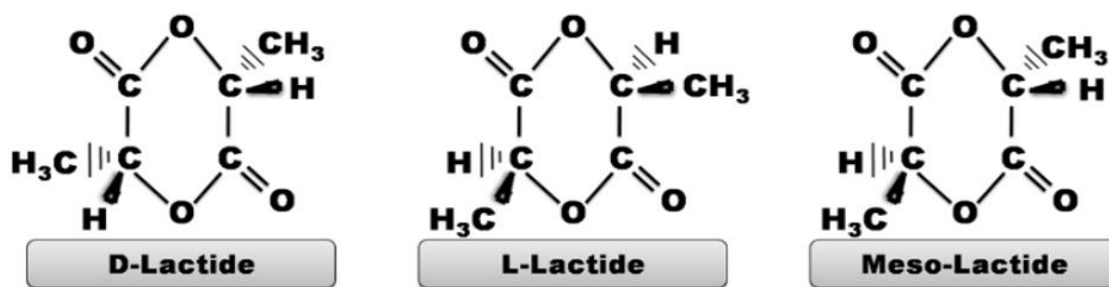


Figure 2.8 : Isomeric of lactides; L-lactide (a dimer of L-lactic acid), D-lactide (a dimer of D-lactic acid) and *meso*-lactide (a dimer of D- and L- lactic acid) (Toprakci et al.,2018).

Therefore, selection of the monomer and the polymerisation technic are important factors for the production of PLA polymer. Poly (D-lactic acid) or poly (L-lactic acid) are fabricated with condensation polymerization of pure L- or D-lactic acid respectively. Poly-L-lactide (PLLA) is a semi-crystalline and hard transparent polymer with a tensile strength of 45-70 MPa. However, Poly (DL-lactide) (PDLLA) is in amorphous state and has no melting point with lower tensile strength (Tyler et al., 2016).

High molecular weighted PLA is produced with excellent mechanical and physical properties by the ring-opening polymerisation. It is preferred in industrial production. However, low molecular weighted PLA obtained by condensation polymerization which has poor mechanical and physical properties. This is the important difference between the ring-opening polymerisation and condensation polymerisation methods (Toprakci et al., 2018). Polymerization of Lactic Acid to produce PLA is represented in Figure 2.9.

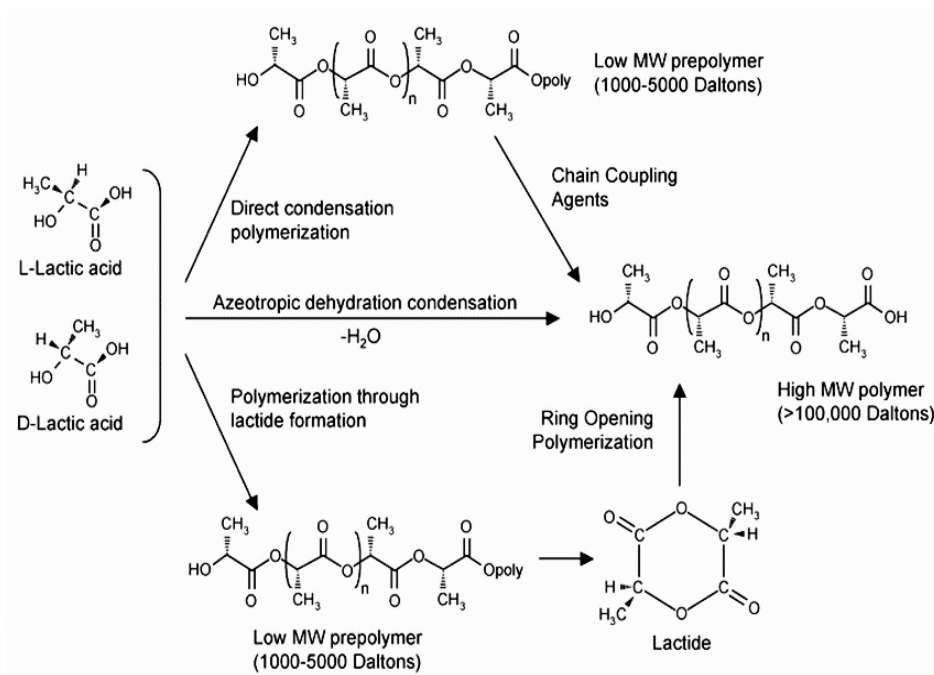


Figure 2.9 : Polymerization of Lactic Acid (Laurencin & Deng, 2014).

PLA is in semi crystalline state with a crystallinity between 10-50 %. It has a glass transition temperature about at 60°C, and a melting temperature about at 153°C. Furthermore, it has good mechanical properties with a tensile modulus about 4 GPa, a tensile strength around 53 MPa and an elongation at break of 4 % (McLauchlin & Thomas, 2012).

PLA is a green, biocompatible and biodegradable polymer for this reason it is extensively preferred in biomedical fields for instance, controlled drug delivery systems, tissue scaffolds, cardiac applications, orthopedically applications, plastic surgery, wound dressing, dental applications, biosensors, and preservations of biological agents (Tyler et al., 2016).

2.3.5 Poly (ethylene oxide) (PEO)

Poly (ethylene oxide) (PEO) is a nontoxic, non-ionic, highly aqueous soluble, biodegradable and easily processable polymer. The glass transition temperature of PEO is at around -50°C and melting temperature (T_m) at around 65°C hence it shows high crystallinity above the melting point. PEO has high solubility in water and it can be dissolved in various organic solvents, such as methanol or ethanol (Safdari et al., 2017; Polaskova et al., 2019).

PEO is synthesized commercially by suspension polymerization of ethylene oxide using different catalysts. The growing polymer chain should be held in solution during

the poly-condensation process. The polymerization reaction can be catalysed by magnesium-, aluminium-, or calcium-organo element compounds. Chemical structure of poly(ethylene) oxide (PEO) was shown in Figure 2.10. The average molecular weight of PEOs ranges from 200 to 5×10^6 / 7×10^6 , represented by the formula: $(\text{OCH}_2\text{CH}_2)_n$, where n denotes the average number of oxyethylene groups. When the molecular weight of PEO is below 25,000, that is classified as PEG (Zia et al., 2017).

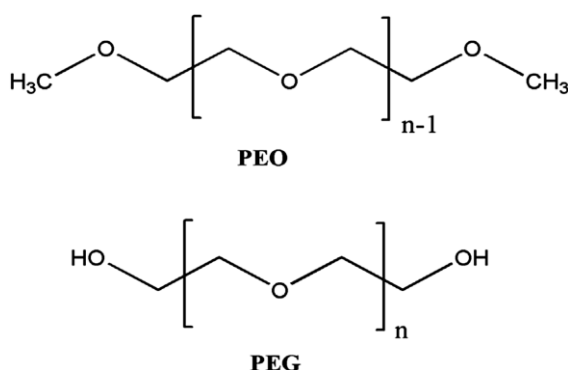


Figure 2.10 : Chemical structure of PEG and PEO (Zia et al., 2017).

PEO is widely used in the polymer matrix to increase bioavailability and solubility of drugs because of its high aqueous solubility and unique properties in drug delivery applications. It has also preferred applications of tissue scaffold, wound dressing, antibacterial membranes, super absorbents, tissue engineering (Kohsari et al., 2016; Wang et al., 2016; Cheng et al., 2015; Dubey et al., 2016; Gunn & Zhang, 2010).

PEO is a thickening, flocculent, dispersing, lubricating, binding, and water absorbable polymer. For this reason, PEO is utilized in hydrogel, dispersant, surfactant, flocculating agent and rheology modifier. However, pure PEO shows poor mechanical and thermal properties. Thermal and mechanical properties of PEO might be better by blending with different polymers such as Chitosan, PCL, PLGA (Zia et al., 2017; McLauchlin & Thomas, 2012).

2.4 Nanofibers in Medical Applications

Nanofibers possess remarkable properties such as high interconnected porosity, specific surface area, ability to imitate the Extra Cellular Matrix (ECM) and potential carrier for drug delivery. Due to these fascinating properties, nanofibers are attractive candidates for medical applications for instance wound dressings, tissue scaffolds and

artificial blood vessels (Wen et al., 2005; Huang et al., 2003). Applications of nanofibers in biomedical field were represented in Figure 2.12.

Figure 2.11. shows the increasing researches of nanofibers in the biomedical field with statistical information.

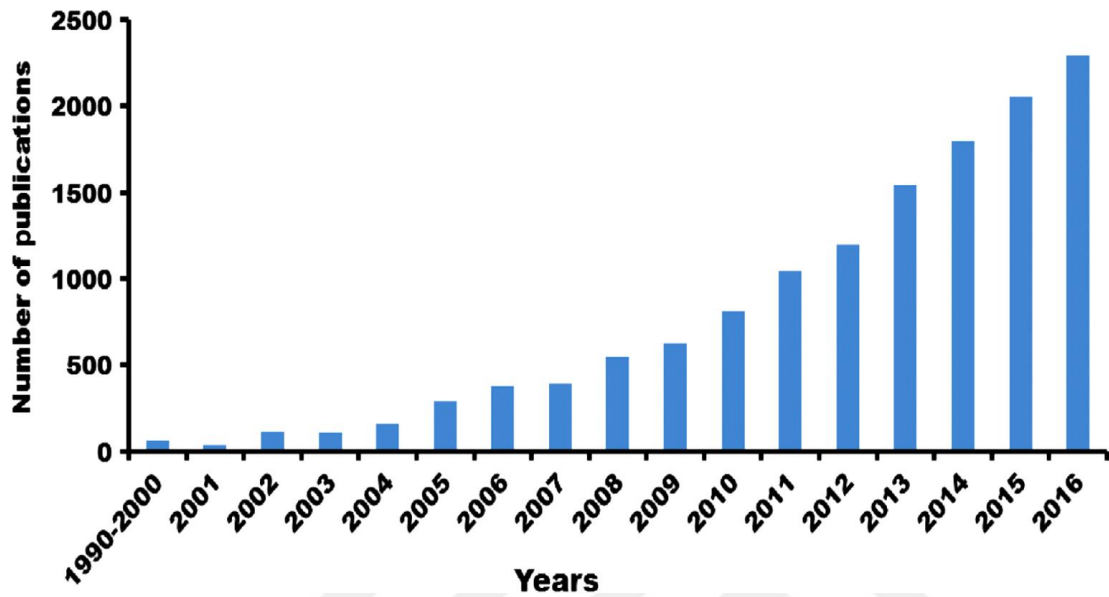


Figure 2.11 : Publication numbers of nanofiber researches in the biomedical field (Ramalingam & Ramakrishna, 2017).

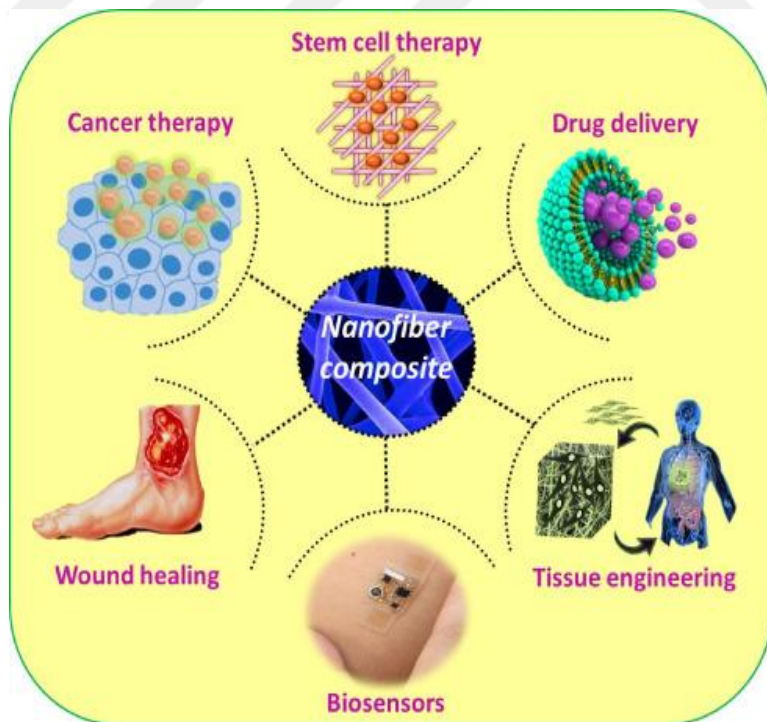


Figure 2.12 : Illustration of nanofibers in biomedical field (Ramalingam & Ramakrishna, 2017).

2.4.1 Wound dressings

Wound dressings are medical technical textiles which protect the wound from bacteria, infections and other external factors with helping the treatment of the wound. Electrospun nanofibers have attractive properties for the wound healing such as the homeostatic effect, permeation of enough oxygen and water vapour and protection of wound from infection and external factors. Due to the high porosity and pore interconnectivity nanofibrous materials exhibit good barrier properties and promoted fluid drainage ability for wound dressing. Moreover, different drugs with antiseptic and antibiotic effects can be integrated into nanofibers to promote wound healing process.

Rath et al. produced silver nanoparticles included collagen nanofibers based composite system through a sustained release of silver ions (Rath et al., 2015). Antimicrobial activity of the nanofiber composites was determined with in vivo studies by providing an aseptic environment at the wound site. Moreover, the in vivo studies nanofiber composites exhibited better wound healing efficiency with re-epithelization, collagen production and better wound closure compared to the control group (Ramalingam & Ramakrishna, 2017).

Ebrahimi-Hosseinzadeh et al., fabricated gelatine/hyaluronic acid composite nanofibers and compared its wound healing efficiency with the commercial product ChitoHeal Gel (Ebrahimi-Hosseinzadeh et al., 2016). The wound closure percentages were calculated with in vivo studies and 82 % was found for the nanofiber composites, 77.8 % ChitoHeal gels and 65 % for the control group. It is indicated with the histological studies that more epidermis and less inflammatory cells were seen at both nanofibers and the ChitoHeal gel applied groups in comparison with the control group (Ramalingam & Ramakrishna, 2017).

In another study, streptomycin incorporated polyurethane/cellulose acetate/zein composite nanofibers were fabricated. They exhibited antibacterial activity against gram positive and gram negative bacteria with optimum air permeation and moisturized environment thus wound healing was accelerated (Ramalingam & Ramakrishna, 2017).

2.4.2 Artificial blood vessels

Electrospun nanofibers are promising materials for artificial blood vessels that can mimic extracellular matrix (ECM) structure of the natural blood vessel and support adhesion, proliferation and improvement of the vascular cells.

Nottelet et al., fabricated Poly (ϵ -caprolactone) nanofibrous artificial blood vessels with a diameter of 2 mm and 4 mm. The artificial blood vessels exhibited favourable mechanical properties. Both tensile and extension force of the blood vessels were measured as 2-7.4 MPa and 200-1200 %. They have better mechanical properties compared to natural blood vessels (1.4 MPa and 100 %). That is an advantage in clinical conditions as the mechanical properties can decrease when the degradation of scaffold starts and the formation of new native tissues start (Nottelet et al., 2009).

In other work, gelatine nanofibrous blood vessels were electrospun with a diameter of 5 mm. Crosslinking of the fabricated vascular grafts was done by glutaraldehyde. The cross-linked grafts showed promising mechanical properties that the young's modulus of the cross-linked scaffolds was found around 33.8 MPa in the axial direction while native collagen was found around 5-10 MPa. Furthermore, the cross-linked vessels exhibited a good tenacity of 2.9 MPa in the axial direction in comparison with human coronary artery that has a tenacity of 60 KPa (Awad et al., 2018).

2.4.3 Tissue scaffolds

Tissue engineering is culturing of the cells taken from a patient or donor into a scaffold system that can promote proliferation of the cells in a tissue which is grafted back to impaired part of the patient (Rana et al., 2014). The nanofibers are often used in scaffold system as the nanofibers can mimic the native cellular microenvironment with its nano fibrillary porous structure.

Stout et al., fabricates PLGA/carbon composite nanofibers (25:75 wt %). The nanofibers were cultured with cardiomyocytes and neurons respectively. After 5 days an increase was observed in cell density of *in vitro* culture (Stout et al., 2011). Moreover, an increase was observed in conductivity for PLGA/carbon composite nanofibers compared to pure PLGA and pure carbon nanofibers. Conductivity is an important issue for myocardial tissue. Furthermore, these nanofibers could be used in neural tissue engineering.

In another work, sodium alginate (SA) coated PCL nanofibers were produced for neural tissue reconstruction by Shelke et al. Nanofibers provide mechanical strength to the nerve graft, while SA controls hydrophilicity of polymer matrix and release behaviour of the drug agent. The results indicated increased tensile strength in composite nanofibers in comparison with the pure PCL nanofibers. The high mechanical strength might be interrelated to the addition of SA reinforcement into the nanofiber structure (Shelke et al., 2016; Ramalingam & Ramakrishna, 2017).

2.5 Drug Delivery Systems

Drug delivery systems comprise of a formulation which facilitates the introduction of a drug in the body and enhances the treatment efficiency, maintains sufficient drug content in the blood for a period of time, carries drug to target point in a safe way and reduces side effects of release within the body (Zamani et al., 2013). The major aims of the DDSs are given below:

- 1) Enhancement in drug efficiency and safety
- 2) Reduction of side effects
- 3) Chrono-pharmacological benefits
- 4) Decrease of drug development cost
- 5) Extension of the drug life
- 6) Decrease of failing risks in new drug researches (Jain, 2008).

2.5.1 Structure of the skin

The skin is the largest organ of the human body. It saves the body from the foreign environment, acting as an early defence mechanism against the introduction of undesirable substances and microorganisms and also supports adjustment of the body temperature (Goyal et al., 2016).

Human skin is composed of three main layers which are epidermis, dermis and hypodermis. The epidermis includes stratum corneum and the viable epidermis. The stratum corneum (SC) is the outer layer of the skin. It performs barrier functions of the skin and the poor absorption of drugs. The matrix thickness of the SC is about 10-20 μm . SC consists of dehydrated and dead corneocytes (keratinocytes) which are installed in lipid layers. The viable epidermis is placed below the SC with a 0.06-0.8

mm thickness. It has the first layer of living cells and contains about 4-5 layers of dermal fibroblasts and keratinocytes. Dermis is the second layer of the skin and is placed under the epidermis with 0.3-5 mm thickness. This layer is composed of connective tissue, sweat glands, hair follicles and a network of capillaries, lymphatic vessels and nerve endings. Hypodermis is the third layer of the skin which includes loose, white, fibrous connective tissues (Goyal et al., 2016).

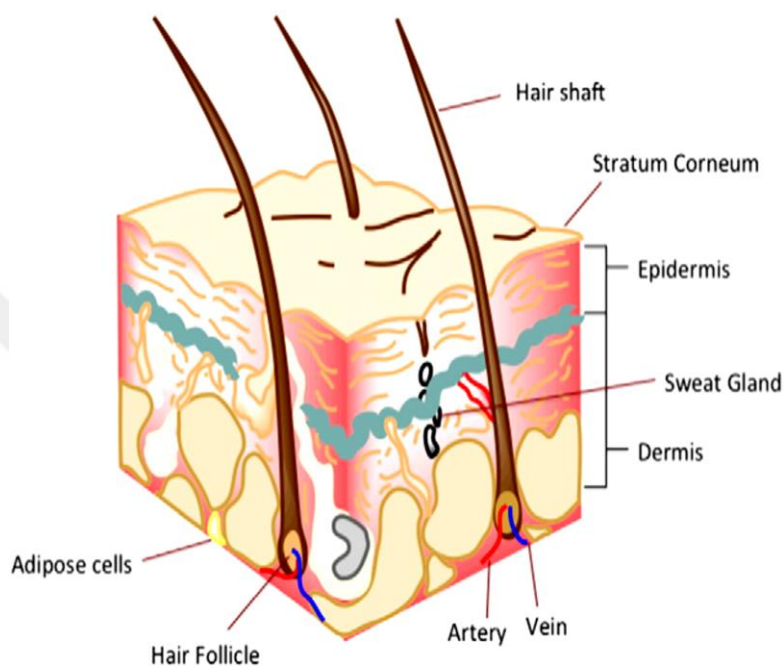


Figure 2.13 : Structure of the human skin (Goyal et al., 2016).

2.5.2 The skin and drug delivery

The human skin has high surface area (nearly 2 square metres) and it is a suitable path for drug delivery. In both topical and transdermal drug delivery, drug penetration through the SC is formulated by the Fick's second law:

$$J = DCP/L$$

Here J is the total released drug amount, D is the diffusion coefficient of the drug, C is the concentration of the drug in the formulation, P is the drug release coefficient, and L is the thickness of the SC. The applied drug passes the layers of the epidermis and travels to dermis facing both lipophilic and hydrophilic parts. Depending on the type of the drug and delivery method, the drug can remain locally (for topical) or penetrates towards the dermis (for transdermal). Hydrophilic drugs can be immediately included into the blood circulation with capillaries. The capillary bed expands into the

upper layers of the dermis right under the dermal to epidermal intersection (Goyal et al., 2016).

2.5.3 Topical drug delivery systems

Topical drug delivery systems are composed of a formulation that applied to the skin directly to heal disorders or disease of the skin which guide/target pharmacological effect of the drug to the skin surface. Some examples of topical agents are anti-fungal drugs, local anaesthetics, keratolytic agents, anti-inflammatory agents and antiseptics. Different pharmaceutical dosage forms can be used in topical drug delivery such as gels, creams, ointment, liquid preparation, sprays and solid powders (Verma et al., 2013).

Topical drug delivery has a local effect and it eliminates the necessity of systemically targeted drug delivery. However, transdermal drug delivery aims at a systemic drug effect and here the skin just acts as an entry portal of the drug into the body. Transdermal formulations pass through epidermis and dermis layers and get into the blood circulation, whereas topical formulations do not reach the layers under the epidermis (Url-4; Url-5). The difference of drug penetration levels between transdermal drug delivery and topical drug delivery is shown in Figure 2.14.

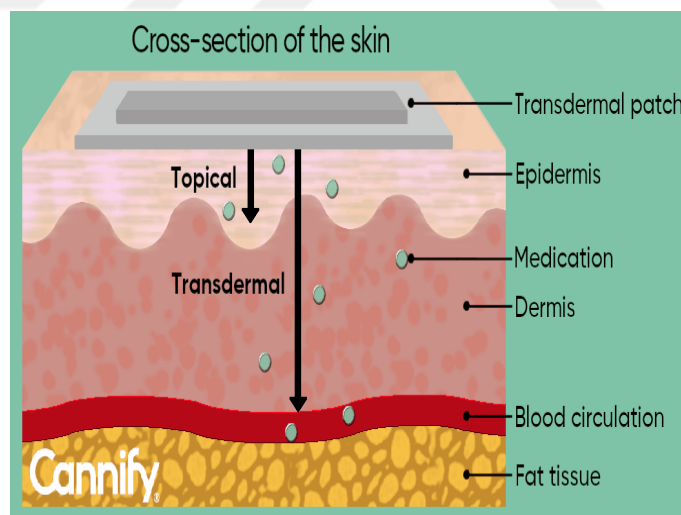


Figure 2.14 : Representation of the skin cross-section showing the difference of drug penetration levels between transdermal drug delivery and topical drug delivery (Url-4).

Topical DDSs have three major tasks:

- To help hydrate skin because of their moisturizing properties.
- To protect from external factors targeted area of the skin.

- To deliver drug to targeted site (skin) (Verma et al., 2013).

Advantages of topical DDSs are given below:

- Elimination of gastrointestinal (GI) drug absorption problems caused by GI pH, enzymatic activity and drug interactions of oral drugs.
- Patient acceptability is better since topical drug delivery system avoids the trouble of parenteral therapy.
- Reduction of required drug doses compared to oral drug delivery.
- Ability to dissolve different drugs or biological agents and making them combined within one formulation
- Providing extended drug release with a single application is possible.
- Drug release can be stopped rapidly by removing the formulation from the skin easily (Verma et al., 2013).

2.6 Nanofiber Based Drug Delivery Systems

Electrospun nanofibers are excellent materials for drug delivery systems due to high interconnected porosity, high surface area, ability to imitate the Extra Cellular Matrix (ECM), potential carrier for drug delivery. Utilization of nanofibers in drug delivery systems is based on the principle that the high surface area of the nanofibrous formulation increases the dissolution rate of the drug. Compared with other dosage forms such as; liposomes, micelles and hydrogels, major advantages of nanofibers are increment in drug loading efficiency and loading capacity, low systemic toxicity and excellent stability (Hu et al., 2014). Furthermore, several drugs can be carried within nanofibers with high local drug concentration due to their excellent targeting and drug transportation ability in a safe way (Morie et al., 2016).

Electrospinning is one of the simplest among all methods to fabricate nanoscaled fibers and it offers the opportunity for direct loading of drug or biological agents for instance antibacterial molecules, antibiotics, enzymes, growth factors, proteins, peptides, vitamins, DNA into the electrospun nanofibers (Taylor, 1964; Sarac, 2017). Many drugs and biomolecules are loaded into nanofibers for example; rifampin, paclitaxel, tetracycline hydrochloride, doxorubicin hydrochloride to improve bioavailability, bioactivity and control delivery (Zamani et al., 2013). Different polymers have been

electrospun into nanofibers such as gelatine, chitosan, silk fibroin, hyaluronic acid (HA), hydroxypropyl cellulose (HPC), polyurethane (PU), polyvinyl alcohol (PVA), poly (lactic acid) (PLA), poly (ϵ -caprolactone) (PCL), poly (ethylene oxide) (PEO) and poly (lactic-co-glycolic acid) (PLGA), to fabricate patches for drug-delivery applications (Hu et al., 2014; Gunn & Zhang, 2010; Esenturk et al., 2016; Sarac, 2017). Different biological molecules loaded electrospun nanofiber based drug delivery systems were represented in Table 2.1.



Table 2.1 : Biological molecules loaded nanofiber based polymer matrices.

| Biological Molecules | Polymer Matrix | Reference |
|---|--|-------------------------------|
| Drugs | | |
| Rifampicin | PLLA | (Zeng et al., 2003) |
| Doxorubicin Hydrochloric | PLLA | (Zeng et al., 2003) |
| Paclitaxel | PLLA | (Zeng et al., 2003) |
| Donepezil hydrochloride | PU/HPC | (Gencturk et al., 2017) |
| Sulfisoxazole | HPC | (Aytac et al., 2015) |
| DNA | | |
| pCMVb encoding a β -Galactosidase | PLGA and PLA-PEG | (Kim et al., 2004) |
| Growth Factors | | |
| Human β - nerve growth factor (NGF) | CLEEP | (Luu et al., 2003) |
| Human glial cell-derived neurotrophic factor (GDNF) | PCLEEP | (Chew et al., 2005) |
| Fibroblast growth factor-2 (FGF-2) | PCL/PLLA-PCL/Gelatin | (Gungor-Ozkerim et al., 2014) |
| Bone morfogenetic Protein -2 (BMP-2) | PLGA-Hap | (Chew et al., 2007) |
| Peptides | | |
| Lysozyme | PCL/PEO | (Duan et al., 2007) |
| Lysozyme | PCL/PEG | (Kowalczyk et al., 2008) |
| RGD peptide | Poly (ϵ -caprolactone)/Poly (m-anthranilic acid) (PCL/P3ANA) | (Guler et al., 2017) |
| Silver and silver compounds | | |
| Ag ⁺ | PCL/PEO | (Dubey et al., 2016) |
| Ag nano particles | PEO | (Khan et al., 2009) |
| Ag nanoparticles and Niclosamide | PCL/PEO | (Dubey et al., 2016) |
| Vitamin | | |
| B ₁₂ | PCL | (Madhaiyan et al., 2013) |

In recent years, there are a lot of studies on nanofiber based drug delivery systems in the literature. Gencturk et al. prepared Donepezil hydrochloride loaded polyurethane/hydroxypropyl cellulose (PU/HPC) composite nanofibers for transdermal drug delivery (Gencturk et al., 2017). PU/HPC/DNP (10:2:1, w/w/w) nanofiber patch exhibited a controlled release profile with releasing 80 % of DNP in 6 hours. Moreover, drug release mechanism of DNP is best fitted with Korsmeyer-Peppas mathematical model. The results showed that HPC/PU nanofibers can be used in transdermal drug delivery.

Guler et al immobilized RGD peptide on poly (ϵ -caprolactone)/poly (m-anthranilic acid) (PCL/P3ANA) and they produced electrospun nanofibers for bone tissue engineering (Guler et al., 2017). Schematic illustration of RGD functionalized nanofibers was shown in Figure 2.15. High amount of P3ANA included nanofibers with more carboxyl groups showed high surface area and excellent mechanical properties. The covalent RGD immobilization is demonstrated with FTIR-ATR and UV-visible measurements. The effects of RGD functionalized nanofibers (PCL/P3ANA-RGD) on Saos-2 cells were investigated with cell culture studies. This study showed that the RGD peptide promoted cell attachment and the interaction between Saos-2 cells and the PCL/P3ANA nanofibers. It is indicated that PCL/P3ANA-RGD nanofibers are promising materials for bone tissue engineering.

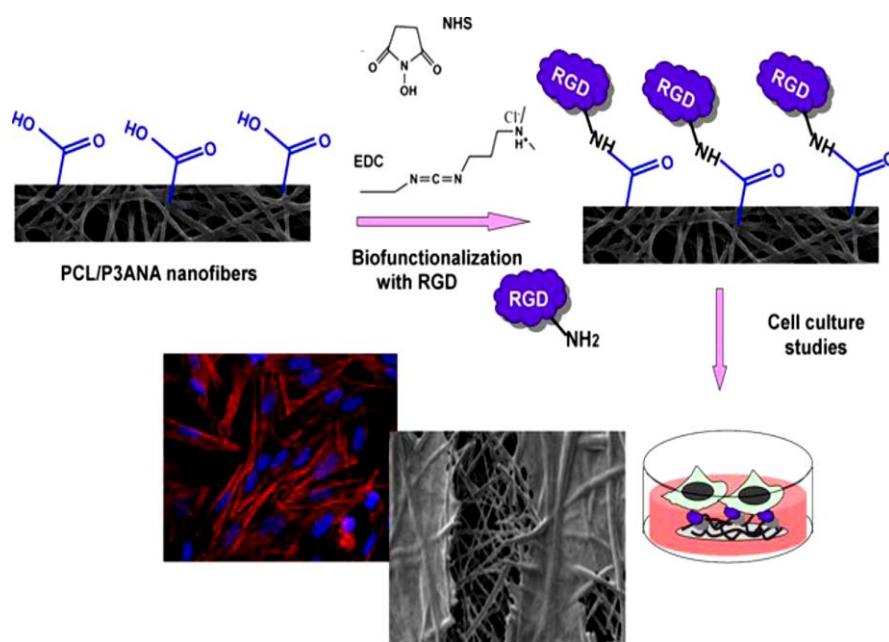


Figure 2.15 : Schematic illustration of RGD functionalized nanofibers (PCL/P3ANA-RGD) on Saos-2 cells (Guler et al., 2017).

Gungör- Özkerim et al. fabricated double-layer nanofibrous structure with the bottom layer from PCL (poly- ϵ -caprolactone)/PLLA (poly-L-lactic acid) composite nanofibers and the upper layer from PCL/Gelatine composite nanofibers and SEM Images of sandwiched nanofiber structure were shown in Figure 2.16. Fibroblast growth factor-2 (FGF-2) loaded microspheres were integrated into the middle of the two layers (Gungör- Özkerim et al., 2014). The cell culture results demonstrated that the FGF-2 can be loaded into the microspheres with promoting the cell attachment and proliferation.

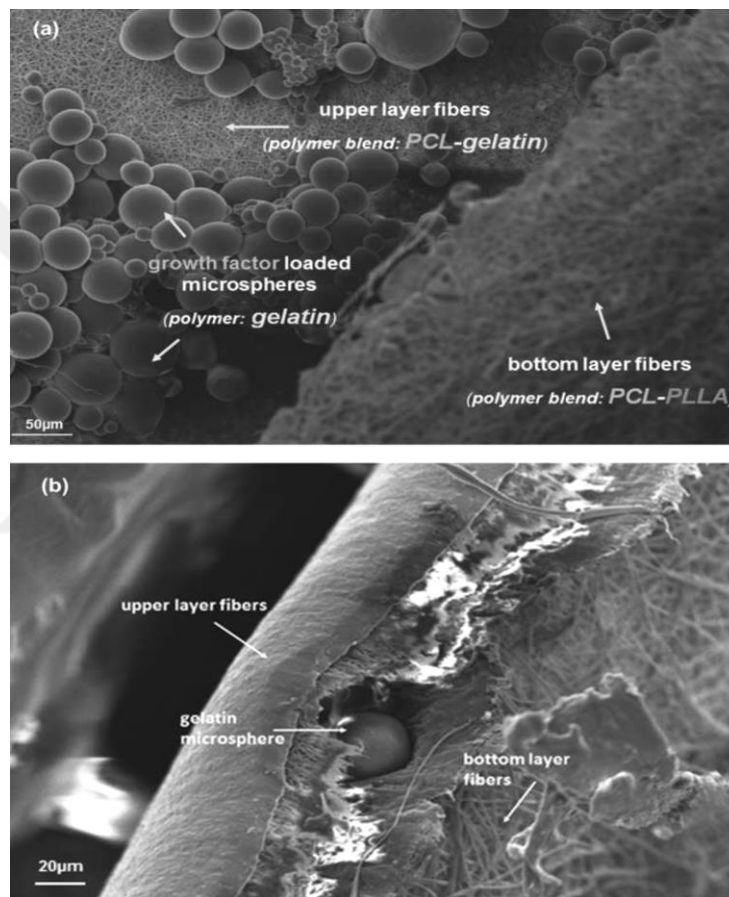


Figure 2.16 : SEM Images of sandwiched structure of PCL (poly- ϵ -caprolactone)/PLLA (poly-L-lactic acid) composite nanofibers (bottom layer) and PCL/Gelatine composite nanofibers (upper layer) (Gungor- Ozkerim et al., 2014).

Dubey et al studied to fabrication of 4 % PEO-1 % PCL blended and AgNPs incorporated nanofiber composites as wound dressing materials. In situ synthesis of AgNPs was done in PEO solution by reduction of Ag^+ (Dubey et al., 2015). In this blend PCL prevents the use of crosslinking agent and heat treatment. Synthesis of AgNPs and fabrication of PEO/PCL composite nanofibers were done successfully with an average size of 15-20 nm. Due to the addition of charged Ag particles fiber

diameter decreased from 224 nm to 116 nm. Surface roughness and wettability tests were carried out with AFM and contact angle measurements. Antibacterial effectivity studies were confirmed the bacterial activity of nanofibers against antibiotic-resistant *E. coli*. The results indicated that prepared composite nanofibers were suitable for wound dressings.

Khan et al studied a successful one-step fabrication of AgNPs-PEO composite nanofiber. PEO acts as both the reduction agent for Ag⁺ and the protection agent for the resulting AgNPs in solution (Khan et al., 2009). Schematic illustration of Ag⁺ reduction mechanism was shown in Figure 2.17. This procedure prevents the separately synthesis of AgNPs and it eliminates the use of chemical, thermal or radiolytic reduction processes and need of protection agent. The formation of AgNPs in the PEO solution is reduced the fiber diameter and bead fiber formations. Fiber diameter decreases from 313 nm to 214 -197 nm with the addition of 0.17 and 0.26 wt % AgNO₃ respectively. This result is related to the increased in electrical conductivity with the formation of AgNPs.

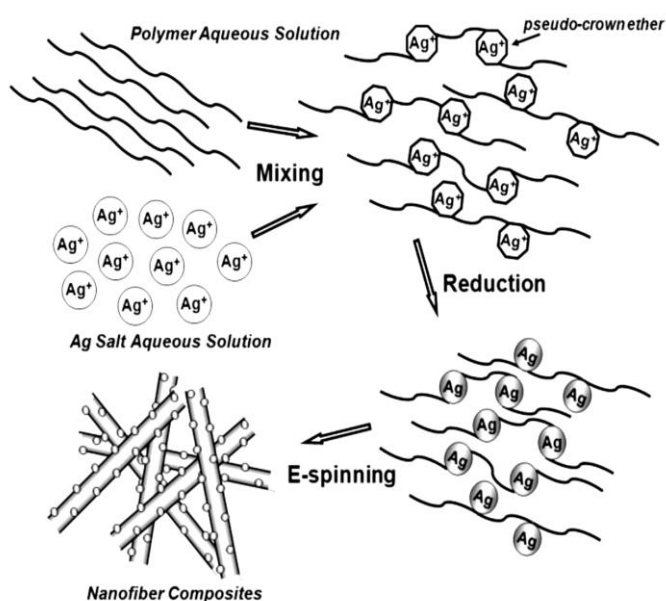


Figure 2.17 : Schematic illustration of Ag⁺ reduction mechanism (Khan et al., 2009).

To enhance water solubility and bioavailability of niclosamide, Dubey and Gopinath studied niclosamide loaded PEO nanofibers using electrospinning method (Dubey & Gopinath, 2016). Moreover, the co-delivery of drugs in nanofibers, is a good way to overcome drug resistance and to increase therapeutic effectiveness. For his goal,

niclosamide and AgNPs were added separately and together into the nanofiber. Poly (ethylene oxide) (PEO) acts as a template for the in-situ synthesis of AgNPs by reduction of Ag^+ . 3.5 % PEO drug loaded and 3 wt % PCL solutions were mixed and electrospun. Contact angle studies showed that drug loaded NFs have better hydrophilicity than the drug alone. Because of the hydrophilic structure of PEO, crystalline drug is converted to amorphous state in the polymer matrix. DTA analysis showed enhancement in water solubility of the drug with an increase in amorphous structure. Cumulative drug release profiles are represented in Figure 2.18.

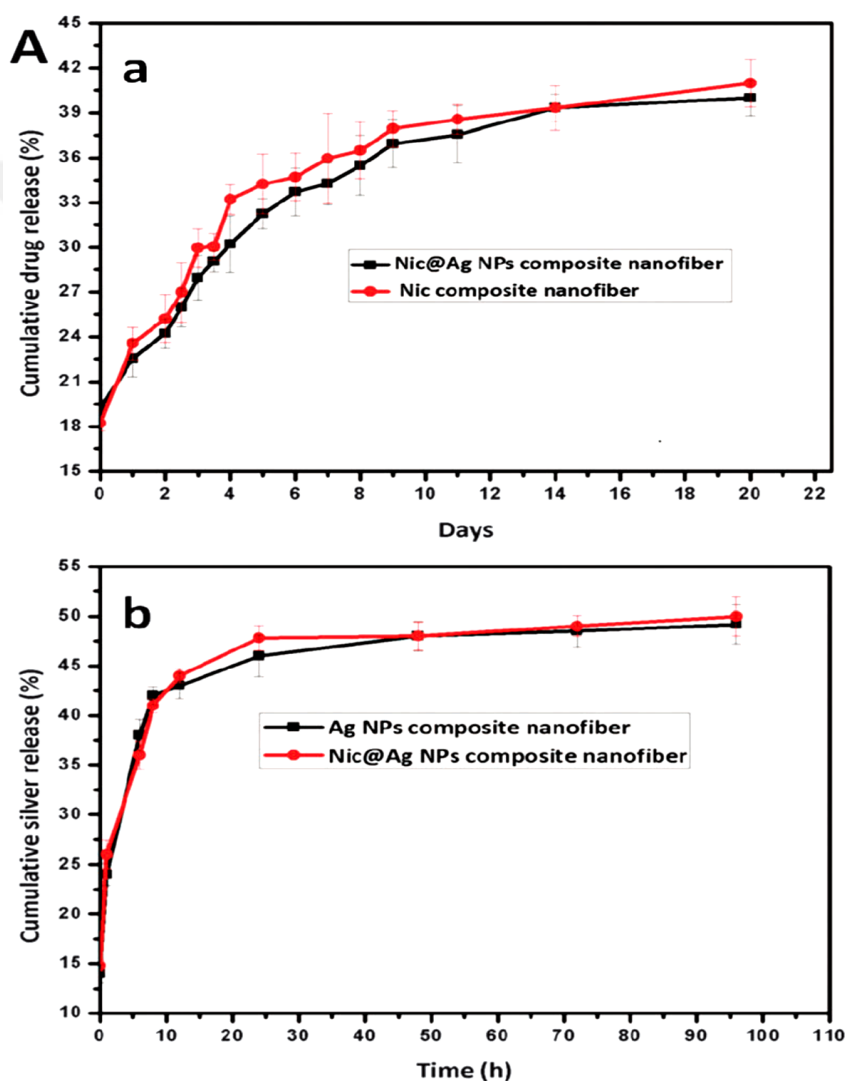


Figure 2.18 : a) Drug release profile of the only niclosamide loaded and the nic@Ag NP loaded composite nanofibers. (b) Ag NP release profile of only Ag NPs loaded and nic@Ag NP loaded composite nanofibers (Dubey & Gopinath, 2016).

Madhaiyan et al. incorporated water soluble vitamin B₁₂ into hydrophobic PCL nanofiber structure to success sustained drug release for transdermal patch applications

(Madhaiyan et al., 2013). For enhancement of the vitamin B₁₂ release from the polymer matrix and obtaining more hydrophilic surfaces, plasma treatment was applied on nanofibers at different length of time. Due to the increased surface area and effective drug loading, a sustained drug release was obtained. Cumulative drug release measurements of vitamin B₁₂ with plasma treatment are shown in Figure 2.19.

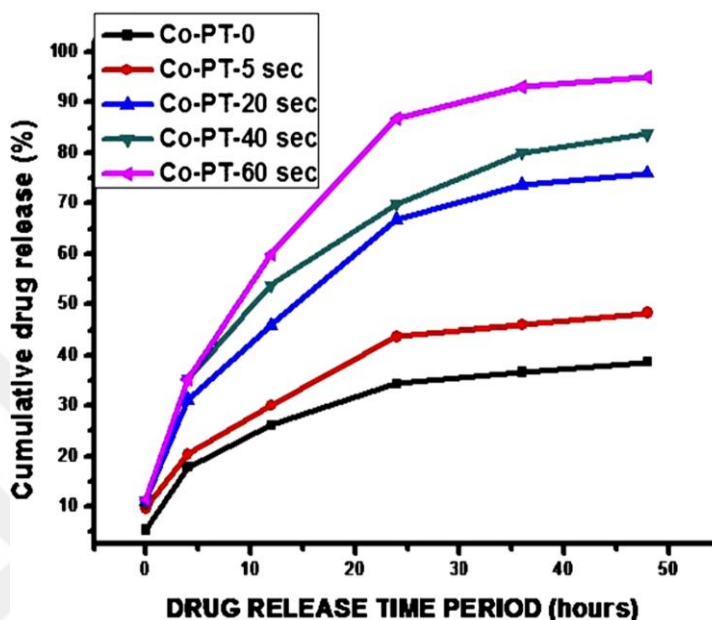


Figure 2.19 : Cumulative drug release profile of vitamin B₁₂ with plasma treatment (Madhaiyan et al., 2013).

2.7 Silver Sulfadiazine

Silver sulfadiazine (SSD) is a non-ionized, water-insoluble, topical agent with a melting point of 285°C and a molecular weight of 357.14 g/mol. It has a wide range of antimicrobial activity that is affected both on bacteria and fungi. SSD is a sulfonamide based drug that is formed by the reaction of sulfadiazine with silver nitrate to form complex silver salt. SSD is used extensively in the topical treatment of infected burns (White and Cooper, 2005; Url-3). Chemical structure of SSD is shown in Figure 2.20, where six Ag⁺ ions bind to six sulfadiazine via the nitrogen atoms of the sulfadiazine pyrimidine rings (Url-2).

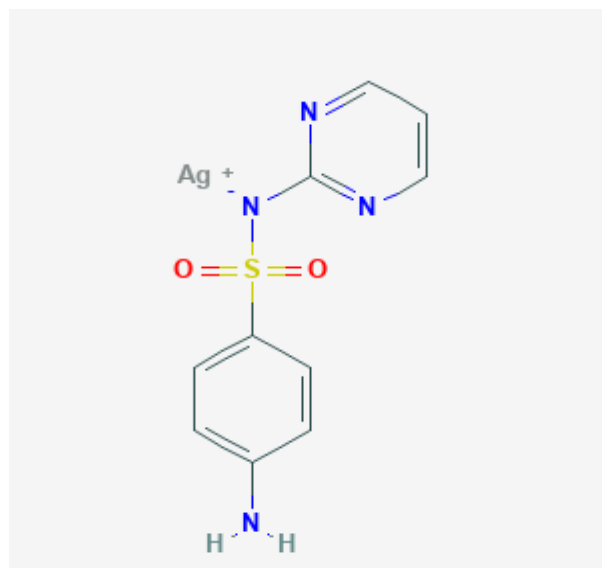


Figure 2.20 : Chemical structure of SSD (Url-2).

SSD is commercially produced in cream form with a brand name of Dermazin[®], Flamazine[®], Silvadene[®], Silverdine[®], Thermazene[®] and SSD cream[®] for burn healing. These products are soft, white, water-miscible creams that contain 1 % SSD active agent (Url-2; Url-3). In other words, each gram of SSD cream includes 10 mg of silver sulfadiazine agent. These commercial products are applied on the targeted areas of skin topically for two to four times in a day.

Silver sulfadiazine provides a long-term release of silver ions, whereas in the case of other silver salts, such as silver nitrate, large amounts of silver ions are released all at once. Thus, the use of SSD decreases the need for frequent application. This makes SSD a desirable and favourable agent since the frequent application is not always practical or possible for patients. In a research, the drug release rates of different silver salts were studied by Fox and Modak (Url-1). The release rate of ionized silver into human serum were measured and unreacted percentage (%) of silver salts versus time graph was plotted. As shown in Figure 2.21 silver sulfadiazine releases gradually into the human serum media. However, some of the silver salts such as silver sulfamerazine releases a very small amount of its silver ions into the media whereas silver nitrate shows an immediate release (Fox & Modak, 1974). Because of these reasons, silver sulfadiazine is more effective than the other silver salts such as silver nitrate, silver sulphanilamide or silver sulfamerazine which are mentioned in Figure 2.21.

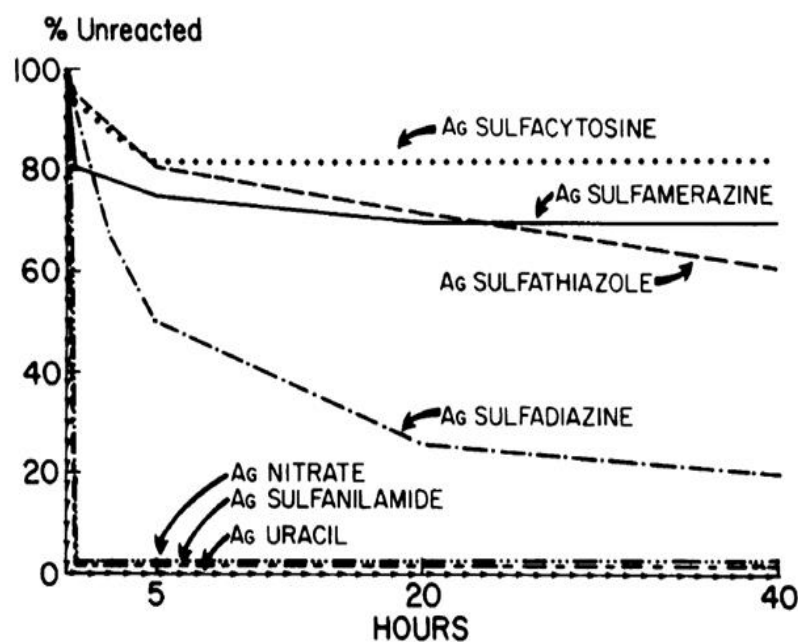


Figure 2.21 : Percentage of unreacted silver compounds in human serum (Fox & Modak, 1974).

2.7.1 Antibacterial activity mechanism

Silver Sulfadiazine is a sulfonamide group topical drug with wide range of antibacterial activity. Silver sulfadiazine performs on the cell membrane and cell wall to exhibit antibacterial effect. The antibacterial action of SSD is not clarified, and whether the broad-spectrum antimicrobial activity is attributable to either the silver or the sulfadiazine parts, or a synergistic interaction of both, has been considered and discussed. However, the synergistic interaction of silver and sulfadiazine or the action of each part is more probable and well accepted (Url-2). When SSD interacts wound fluid, which contains electrolytes of Na⁺, K⁺, Cl⁻, silver ions release sustainably into wounded areas of skin (White & Cooper, 2005). Ionized silvers catalyse the formation of disulfide bonds causing protein structural changes and inhibition of thiol-containing enzymes. Furthermore, silver ions can intercalate DNA interrupting the replication and transcription of bacterial DNA. Para-amino benzoic acid (PABA) is a substrate of the dihydropteroate synthetize enzyme. SSD inactivates bacterial dihydropteroate synthase with resulting in damage of folic acid metabolism and interruption of DNA synthesis (Url-2; Url-3).

2.7.2 SSD based drug delivery systems

SSD is a poorly aqueous soluble drug (3.4 mg/l at pH = 6.8). The low solubility restricts the drug efficiency, bioavailability and potential antimicrobial activity of SSD

thus its applications are limited. Drug solubility is an important issue since efficient drug release and antimicrobial efficiency is contributed just by decomposition of SSD to sulfadiazine and silver ions. Also, the solubility problem of SSD makes it difficult to be stabilized and incorporated into the polymer matrix. Water insolubility of SSD is a challenge, therefore researchers have focused on the improvement of its solubility, bioavailability and antibacterial activity. To this end, SSD was formed as nanoparticles, nanorods, nano suspensions or loaded into different types of polymeric carriers by formulating as film, hydrogel, composite and fiber-based drug delivery systems (Szegedi et al., 2014; Li et al., 2015; Liu et al., 2019; Shao et al., 2016). Herein, the literature survey related to different dosage forms of SSD was summarized and represented in Table 2.2.

Table 2.2 : SSD loaded polymer matrices.

| Biologic Molecules | Polymer Matrix | Reference |
|---------------------------|--|------------------------|
| SSD and Bupivacaine | PEG-Gelatine composed semi-interpenetrating networks | (Kao et al.,2009) |
| SSD | Nano porous silica carriers | (Szegedi et al., 2014) |
| Silver nanoparticle | Sulfadiazine/ polyvinyl alcohol nanorods | (Li et al., 2015) |
| SSD | PLLA nano sheets | (Ito et al., 2015) |
| SSD | Bacterial Cellulose composites | (Shao et al., 2016) |
| SSD | Ploxomer thermosensitive hydrogel | (Liu et al., 2019) |

Kao et al, produced PEG-Gelatine composed semi-interpenetrating networks for dermal wound treatment. SSD and Bupivacaine are loaded together and separately into the network and antibacterial activities were investigated (Kao et al., 2009). Antibacterial efficiency of SSD and bupivacaine against *E. Coli*, *S. Aerey* and *Pseudomonas Aeruginosa* is performed. Literature on SSD inhibition of *P. Aeruginosa* and other gram-negative bacteria is conflicting. In this study, it is shown that SSD loaded networks killed gram-positive and gram-negative bacteria. Also, it can be said that antibacterial activity of SSD against to gram negative bacteria is enhanced in this

work. The results showed that PEG-Gelatine composed semi-interpenetrating networks are potential matrix for dermal wounds.

Szegedi et al. produced silver and sulfadiazine loaded nanostructured silica materials (MCM-41 or SBA-15) to improve aqueous solubility of SSD (Szegedi et al., 2014). The nanoporous silica has empty channels and it was shown that these channels provided suitable conditions for carriage of sulfadiazine and silver ions.

Li et al. fabricated silver nanoparticle loaded sulfadiazine/ polyvinyl alcohol nanorods (Li et al., 2015). Formation of Ag-SD/PVA nanorods was represented in Figure 22. Moreover, XRD, FT-IR, SEM and TEM characterization methods were done. In this study, the role of the PVA was both controlling the size of the silver sulfadiazine (SSD) and reduction of SSD to produce Ag-SD/PVA NRs.

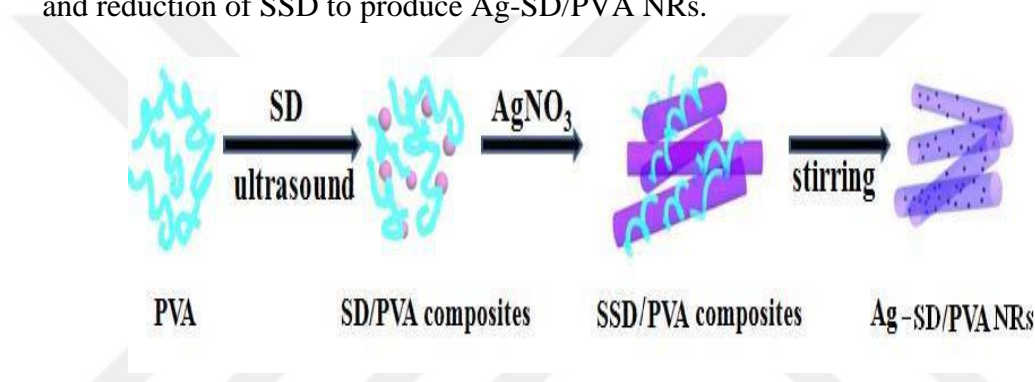


Figure 2.22 : Formation of Ag-SD/PVA nanorods (Li et al., 2015).

The Ag-SD/PVA nanorods showed higher antibacterial activity against the *S. aureus*, *P. aeruginosa* and *E. coli* when compared to the Ag NPs and SSD microrods (MRs) alone. It can be related to synergistic effects of the Ag NPs and SD NRs.

Ito et. al. produced SSD loaded PLA nanosheets by spin coating method. Here in, SSD drug sandwiched between two PLA layers (Ito et al., 2015). The SSD loaded nanosheet exhibited sustained release properties for more than 3 days. Antibacterial activity was evaluated with *in vitro* Kirby-Bauer test and the antibacterial efficiency of the nanosheet against methicillin-resistant *Staphylococcus aureus* (MRSA) is confirmed. *In vivo* studies were carried out with a burned mouse model. The *in vivo* evaluation indicated that the nanosheet reduced the number of MRSA bacteria on the lesion and hindered the inflammatory reaction of MRSA in the wound area. Therefore, potential application of SSD loaded nanosheets for wound dressings were represented.

Shao et. al. prepared SSD containing Bacterial Cellulose (BC) composites by simple blending (Shao et al., 2016). The impregnation of SSD into the BC polymer matrix is

verified with XRD, FT-IR and SEM characterizations. Drug release studies was performed at different pH values. pH-sensitive controlled drug release of both silver and sulfadiazine ions was achieved. The antibacterial efficiency of BC-SSD composites were evaluated with disc diffusion method and the bacterial inhibition of *Candida albicans* and *Staphylococcus aureus* were determined. Furthermore, the cytotoxicity test of the composites was carried out on HEK293 cells. Therefore, BC-SSD composites can be good candidates for drug delivery and wound dressing field with excellent antibacterial activity and biocompatibility. Antibacterial activity images of the study are represented in Figure 2.23.

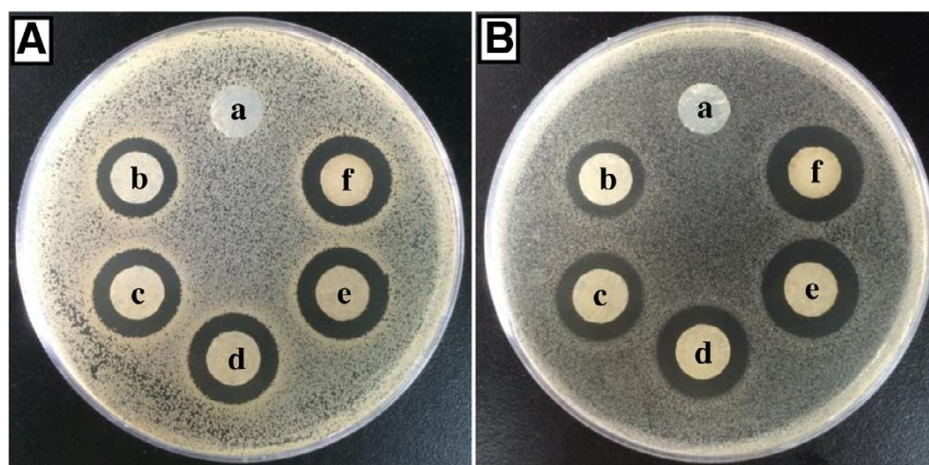


Figure 2.23 : Antibacterial activity studies of BC and BC-AgSD composites: *S. aureus* (A) and *C. albicans* (B). (In all plates, a is BC as the control, b-f are BC 1, BC 2, BC 3, BC 4 and BC 5). (Shao et al., 2016).

In the other study, Liu et al. fabricated SSD incorporated thermo sensitive hydrogel with distinctive advantages over the commercial SSD cream (Liu et al., 2019). The SEM images of SSD/NS gel showed the hydrogel matrix with SSD packaged in it. The reversed physicochemical properties of AgSD in hydrogel were confirmed with XRD and FT-IR studies. Accumulated drug release (%) of AgSD from AgSD/NSgel, commercial AgSD cream, AgSD bulk, and AgSD NS solution was represented in Figure 2.24. SSD loaded hydrogels showed more sustained drug release profile compared with commercial SSD cream.

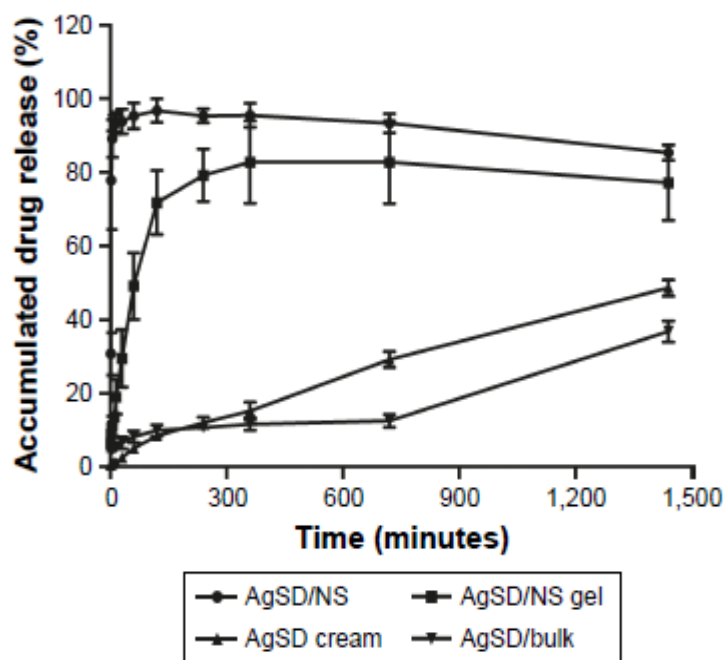


Figure 2.24 : Accumulated drug release (%) of AgSD from AgSD/NS gel, commercial AgSD cream, AgSD bulk, and AgSD NS solution. **Abbreviations:** AgSD, silver sulfadiazine; NS, nanosuspension. (Liu et al., 2019).

Moreover, the hydrogel was found efficient on *Pseudomonas aeruginosa*, *Staphylococcus aureus* and *Escherichia coli* bacteria. The cytotoxicity of SSD was carried out with MTT assay and the result indicated that the poloxamer hydrogel decreases the possible toxicity of SSD drug. As a conclusion, this thermo responsive hydrogel delivery system can be a suitable carrier for SSD.

2.7.3 Silver Sulfadiazine in nanofiber drug delivery applications

SSD was incorporated into different carrier matrices such as nanorods, semi-interpenetrating networks, nanoporous silica carriers, lipid-based films and nanocomposites (Li et al., 2015; Aguzzi et al., 2014; Szegedi et al., 2014; Piyush et al., 2013; Kao et al., 2009; Azevedo et al., 2006). However, in the literature, there are limited number of studies related to loading SSD in electrospun nanofibers. Herein, the literature survey on SSD loaded nanofibers was summarized and represented in Table 2.3.

Table 2.3 : SSD loaded nanofibers.

| Biological Molecules | Polymer Matrix | Reference |
|----------------------|---|-------------------------------|
| SSD | Zein nanofibers | (Ullah et al, 2019a) |
| SSD | Silk Fibroin nanofibers | (Jeong et al., 2014) |
| SSD | Cyclo Dextrin containing PVA nanofibers | (Nalbandi and Amiri, 2019) |
| SSD | PAN | (Kharaghani et al., 2019) |
| SSD | PCL nanofibers incorporating β - cyclodextrin | (Souza et al., 2019) |
| SSD | PCL/PVA nanofibers | (Mohseni et al., 2016) |
| SSD | PU/ gelatine nanofiber | (Heo et al., 2013) |

Recently, Ullah et al. produced SSD loaded electrospun zein nanofibers (Ullah et al, 2019a). They investigated the drug release properties and antibacterial efficiency. Antibacterial activity test results demonstrate that nanofiber mats are effective on for both Gram positive as well as Gram negative bacteria. Release studies exhibited remarkable release properties of the zein nanofiber mats with 0.6 % wt SSD compared with other samples with low concentration of SSD. Moreover, incorporation of SSD into the zein matrix was characterized by FTIR, XRD and XPS. FTIR results showed there is no chemical interaction between SSD and zein. The crystalline structure of the SSD in nanofiber matrix was verified with XRD and Ag and S contents of the nanofibers were confirmed with XPS analysis.

Jeong et.al. fabricated SSD containing silk fibroin (SF) nanofibers by electrospinning to determine the wound healing effect (Jeong et al., 2014). SSD loaded SF nanofibers were compared with the commercial wound dressing Acticoat™ in a rat wound model. Re-epithelialization and wound closure are two main parts of the healing process. They are controlled with fibroblasts and keratinocytes. Hence, the cell adhesion and proliferation of normal human epidermal keratinocytes (NHEK) and normal human epidermal fibroblasts (NHEF) on SSD included SF nanofibers were determined. The SSD containing SF nanofibers has faster wound healing than the marketed product Acticoat™. Wound photos treated with Ag-based wound dressings at 3, 7 and 14 days after wounding were shown in Figure 2.25.

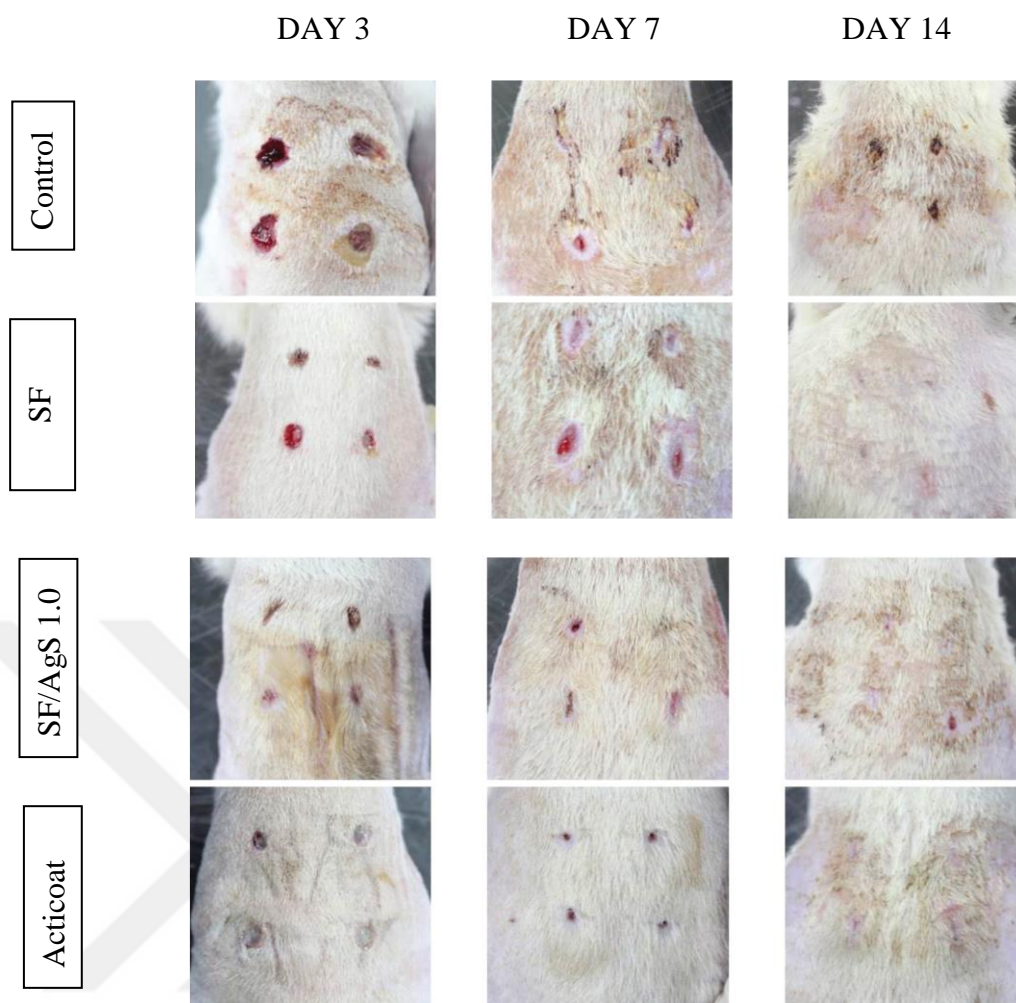


Figure 2.25 : Photos of wounds that treated with Ag-based wound dressings at 3, 7 and 14 days after wounding **Abbreviations:** AgS silver sulfadiazine; SF, silk fibroin; AgS 1.0, 1.0 wt % SSD (Jeong et al., 2014).

In another research, Nalbandi and Amiri studied electrospun polyvinyl alcohol (PVA) nanofibers containing Cyclo Dextrin (CDs) complexes to clarify the solubility problem of SSD (Nalbandi & Amiri, 2019). Cyclodextrin nanocontainers (b-CD or HPb-CD)/SSD were obtained by forming inclusion complex (IC) between SSD and cyclodextrins. After preparation of SSD included nanocapsules, these inclusion complexes incorporated to PVA nanofibers. FTIR, SEM and EDX analysis of the nanofibers were performed. Results showed that solubility and bioavailability of SSD were enhanced by loading into CDs and controlled release was obtained due to the encapsulation cavity of CDs. Electrospun PVA nanofibers loading with SSD/CDs inclusion complex exhibited significant antibacterial activity against *Staphylococcus aureus* and *Escherichia coli* bacteria. Schematic formation of Cyclodextrin SSD inclusion complex loaded PVA nanofibers was shown in Figure 2.26.

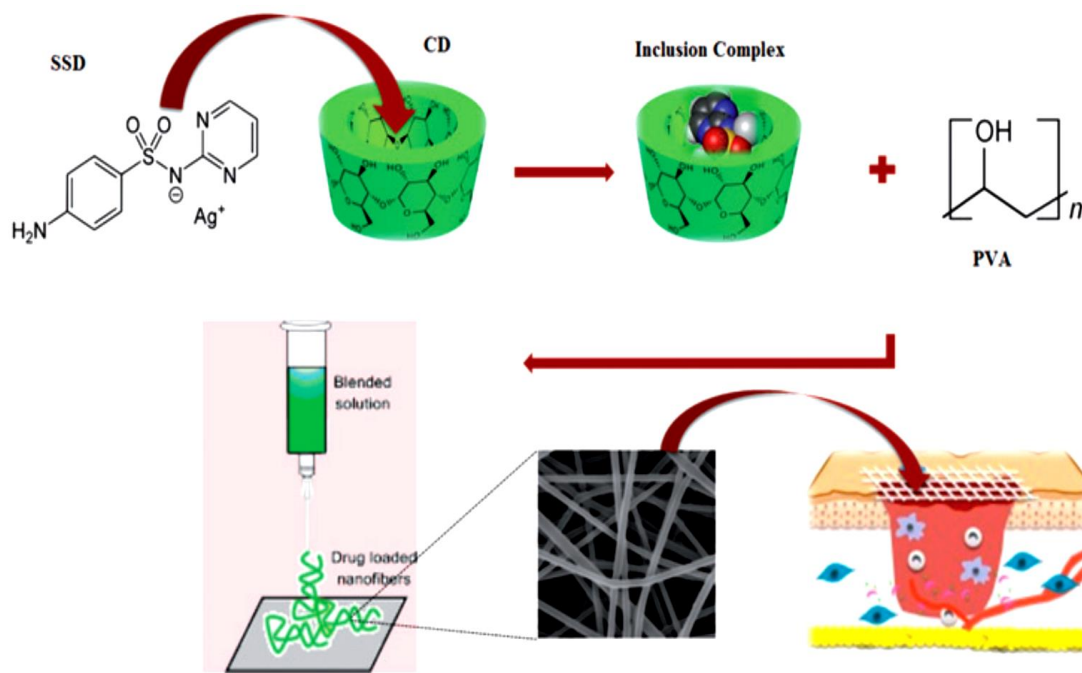


Figure 2.26 : Cyclodextrin SSD inclusion complex loaded PVA nanofibers (Nalbandi & Amiri, 2019).

Kharaghani et al. prepared PAN/SSD nanofiber patches for wound dressing and the antibacterial activity of the nanofibers were investigated by the disc diffusion test method (Kharaghani et al., 2019). Fiber morphology was investigated with SEM instrument. The SEM images demonstrated that the bead free and uniform fibers were obtained. The nanofiber mats showed the efficient antibacterial activity on *E. coli* and *Bacillus* bacteria. Moreover, stability of SSD in the polymer matrix was verified with FTIR and crystalline structure was confirmed with XRD. It is concluded that SSD containing nanofibers have good potential for antibacterial applications.

Souza et. al., carried out the fabrication of the electrospun PCL nanofibers incorporating β -cyclodextrin/silver sulfadiazine inclusion complexes for use as wound dressings (Souza et al., 2019). They aimed to reduce the direct contact between silver and skin and to optimize the drug release. Hence, antibacterial activity and drug release properties of PCL nanofibers including silver sulfadiazine β -cyclodextrin complexes were evaluated. The nanofiber patches represented desirable antibacterial effect against *S. aureus*, *S. epidermidis*, *E. coli* and *K. pneumonia* bacteria. SSD drug release was predominantly released by diffusion within 24 hours. Furthermore, drug stability in the polymer matrix was confirmed with FT-IR and fiber morphology was investigated with SEM instruments. Release profile of SSD Cyclodextrin complex

loaded PCL nanofibers is represented in Figure 2.27 and antibacterial efficiency evaluation is shown in Figure 2.28.

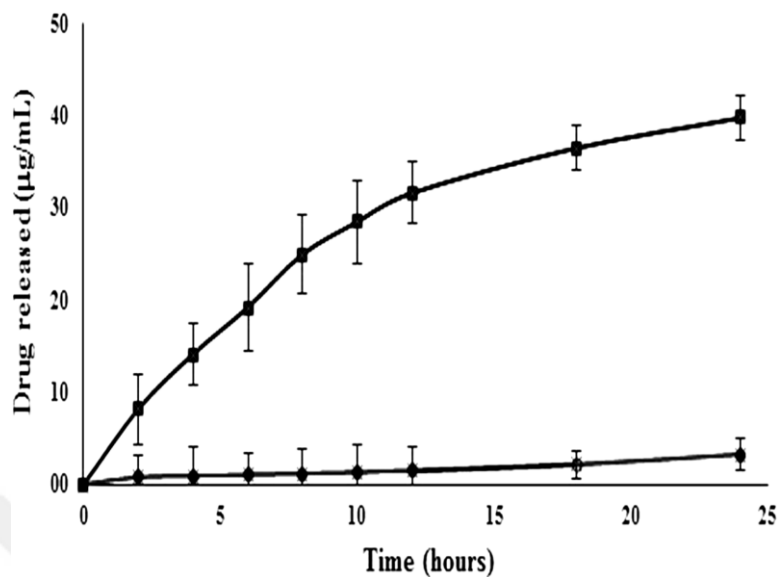


Figure 2.27 : SSD release amount (Souza et al., 2019).

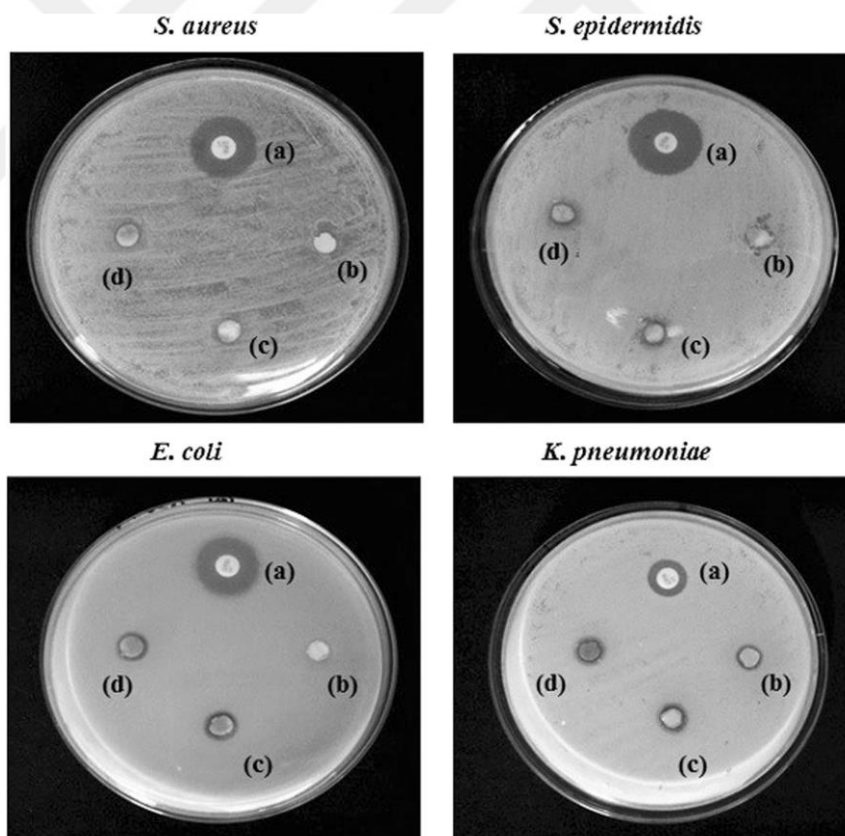


Figure 2.28 : Antibacterial activity evaluation of SSD Cyclodextrin complex loaded PCL nanofibers (Souza et al., 2019).

Mohseni et al. fabricated SSD loaded PCL/PVA electrospun mats to be utilized in wound treatment (Mohseni et al., 2016). To evaluate wound dressing biocompatibility,

cell attachment and proliferation studies were also examined by MTT assay and SEM analysis of cell seeded scaffolds. Since the sample with highest SSD concentration showed the lowest cell proliferation it is demonstrated that the cell proliferation was significantly affected by concentration of SSD. Approximately, 70 % of silver ions were released at the end of the first week.

Heo et al., designed SSD loaded polyurethane (PU) and gelatine nanofiber scaffolds for burn healing with controlled SSD delivery. They compared burn-wound healing performance of the SSD loaded nanofiber scaffolds (NFSSD-1 and NFSSD-2), nanofiber scaffold without SSD (NF) and gauze (Heo et al., 2013).

It was seen that the size of the burn area which was treated with NFSSD-2 decreased more during 21-day period when compared to gauze, NF and NFSSD-1. Therefore, the NFSSD-2 showed the best burn-wound closure rate as represented in Figure 2.29. These results can be explaining the effective antibacterial efficiency of SSD. Because release of SSD inhibits bacterial growth and accelerate the burn healing process by preventing bacterial infection. In this study, it is estimated that SSD incorporated PU/gelatine nanofibers are good candidates for burns.

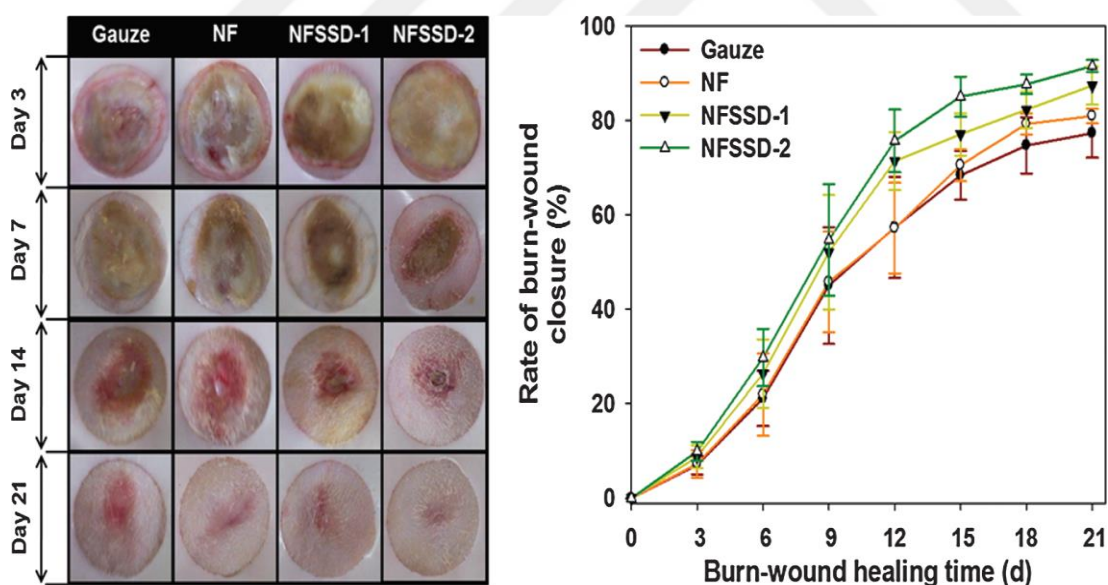


Figure 2.29 : A) Photos of burn healing process B) Comparison of wound closure rates of Gauze, PU/ Gelatine nanofiber without SSD (NF), different amount SSD loaded PU/ Gelatine nanofibers (NFSSD-1 and NFSSD-2) during the healing period (Heo et al., 2013).

3. EXPERIMENTAL STUDIES

3.1 Materials

Poly (ϵ -caprolactone) (PCL) (average molecular weight=70,000-90,000), Poly (ethylene oxide) (PEO) (average molecular weight =900,000), Ethanol (≥ 99.8 % (GC)), Chloroform (99–99.4 % (GC)), Acetic acid (≥ 99 %), Acetonitrile (≥ 98.0 %), Phosphoric acid (ACS reagent, ≥ 85 wt. % in H₂O), Polyethylene glycol 400 (PEG 400), 1,2-Propanediol, Propylene glycol, Phosphate buffer saline 7.4 (PBS 7.4), Phosphate buffer saline 5.5 (PBS 5.5), 0.05 % NH₃ solution were purchased from Sigma Aldrich (USA). Poly (lactic acid) (PLA) (Product number: 2003D) was purchased from Nature Works LLC Co. (USA). Silver sulfadiazine (SSD) was gifted from Deva Pharma (Turkey). Distilled water was supplied from the Millipore Milli-Q Ultrapure Water System. All chemical solvents were of analytical grade and used without any purifications.

For drug release studies, dialysis tubing cellulose membrane (avg. flat width 25 mm), consisting of regenerated cellulose made from virgin wood pulp, was purchased from Sigma Aldrich (USA). Polytetrafluoroethylene (PTFE) Syringe Filters (13mm Diameter, 0.45um Pore Size) were supplied from Biomed Scientific Limited.

For antibacterial activity studies, Nutrient agar (NA) and Nutrient broth (NB) were purchase from Merck (Darmstadt, Germany). *E. coli* (Gram-negative; ATCC 25922), *Pseudomonas aeruginosa* (Gram- negative; ATCC 27853), *S. aureus* (Gram-positive; ATCC 25023), bacteria were obtained from the Food Engineering Department of Yıldız Technical University.

3.2 Electrospinning Process

Electrospinning method was used to produce drug-free and drug loaded nanofiber patches. Electrospinning is one of the simplest among all methods to fabricate fine fibers with diameters ranging from micrometres to nanometres. The electrospinning equipment contains a high voltage source (0-50 kV, ES 30 Model, Gamma High

Voltage Inc., USA), a solution feeding unit (0.1-400 ml/hour, NE-500 Model, New Era Pump Systems, Inc. USA), a 2 ml syringe with a needle tip (18 G) and a grounded collector. The grounded collector is a rectangular plate which is made of stainless steel and covered with an aluminium foil.

At first, high voltage is applied to the polymer solution to produce an electrical field between the tip and the collector to shape the droplet on the tip as Taylor Cone. When the electrostatic force is higher than the surface tension of the polymer solution, polymer jet is pushed from the needle tip to the collector. Then, polymer jet reaches to collector following a spiral way by getting longer and thinner. Finally, nanoscale fibers are obtained on the collector (Taylor, 1964; Sarac, 2017).



Figure 3.1 : Photograph of the electrospinning set up.

3.3 Tape Casting Method (Doctor Blade)

Doctor blade or tape casting is one of the common methods for fabrication of thin films. This method was first developed during the 1940's to form thin sheets of piezoelectric materials and capacitors and now it is an accepted coating method (Aegerter & Mennig, 2013).

In the doctor blade technic, a well-mixed solution is placed on a substrate. When a constant movement is constituted between the blade and the substrate, the solution is spread, smoothed and thinned on the substrate surface with the doctor blade to form a thin film (Aegerter & Mennig, 2013). During the process, the film thickness is controlled by the gap between the blade and the substrate and is possible to obtain films with thicknesses from 20 to several hundred microns (Pasquarelli et al., 2011).

The dual doctor blades can be utilized to provide very precise thickness control of the final layers. Furthermore, this method enables the coating of large surface areas and it is possible to control the process speed up to several meters per minute.

3.4 Preparation of the Polymer Solutions

3.4.1 Preparation of the PEO, PCL, PCL/PEO and PCL/(PEO+SSD)

3.5 % (w/w) PEO solution was prepared in Acetonitrile/acetic acid (3:1/v:v) solvent and SSD was added into the PEO solution at the amount of 12 wt % with respect to the PEO polymer. The SSD was completely dissolved in the PEO solution. Besides 4 % (w/w) PCL solution was prepared in Chloroform/Ethanol (3:2/v:v) individually. PCL and SSD loaded PEO solutions were mixed at a ratio of 7:3 (w/w) and stirred for an hour to get a homogeneous blend solution. PEO and PCL solutions were miscible and phase separation was not seen in the PCL/PEO blend solution. Consequently; PEO, PEO+SSD, PCL, PCL/PEO (7:3), PCL/(PEO+SSD) (7:3) solutions were prepared respectively for electrospinning. In the final solution, PCL/(PEO+SSD) (7:3), the amount of SSD was 3.2 wt % with respect to the total polymer matrix.

Different concentrations of PEO between (2-4 wt %) and PCL between (3-6 wt %) were used for the optimization of the continuous and uniform composite nanofibers. Bead defects occurred at concentrations of 2 wt % PEO and 3 wt % PCL. At concentrations of 4 wt % PEO and 6 wt % PCL the solution could not be electrospun as the solution got so viscous that it could not be ejected from the tip. Thus, 3.5 wt % for PEO and 4 wt % for PCL were selected as the optimum concentrations for fiber formation. Hydrophobic PCL should dominate the polymer matrix to provide sustained and prolonged release thus, PCL/PEO were blended at a ratio of 7/3 (w/w).

Three different concentrations (1.6, 3.2, 6.4 wt %) of SSD were used for the optimization of drug dosage in the polymer matrix. Drug dosage was optimized according to drug solubility of SSD in the PCL /PEO blend solution and that was controlled visually. At high concentration, 6.4 wt % SSD was not dissolved completely. Low concentrations of 1.6 and 3.2 wt % SSD were dissolved perfectly but 1.6 wt % was elected due to more SSD dosage into the polymer matrix. Thus, 3.2 wt % was selected the optimum soluble concentration of SSD in the PCL/PEO blend solution and it is used for the fabrication of SSD loaded nanofibers.

3.4.2 Preparation of the PEO, PLA, PLA/PEO and PLA/(PEO+SSD)

3.5 % (w/w) PEO solution was prepared in Acetonitrile/acetic acid (3:1/v:v) solvent and SSD was added into the PEO solution at the amount of 20 wt % with respect to the PEO polymer. The SSD was completely dissolved in the PEO solution. Besides 6 % (w/w) PLA solution was prepared in Acetonitrile/Chloroform (3:2/v:v) individually. PLA and SSD loaded PEO solutions were mixed at a ratio of 7:3 (w/w) and stirred for an hour to get a homogeneous blend solution. PEO and PLA solutions were miscible and phase separation was not seen in the PLA/PEO blend solution. Consequently; PEO, PEO+SSD, PLA, PLA/PEO (7:3) solutions were prepared respectively for electrospinning. In the final solution, PLA/(PEO+SSD) (7:3), the amount of SSD was 4 wt % with respect to the total polymer matrix.

Different concentrations of PLA between (4-8 wt %) were used for the optimization of the continuous and uniform composite nanofibers. Bead defects occurred at concentrations of 4 wt % and 5 wt % PLA. At concentrations of 7-8 wt % PLA and 3.5 wt % PEO, the blend solution could not be electrospun as the solution got so viscous that it could not be ejected from the tip. Thus, 3.5 wt % for PEO and 6 wt % for PLA were selected as the optimum concentrations for fiber formation. Hydrophobic PLA should dominate the polymer matrix to provide sustained and prolonged release. Therefore, PLA/PEO were blended at a ratio of 7/3 (w/w).

Three different concentrations (3, 4 and 6 wt %) of SSD were used for the optimization of drug dosage in the polymer matrix. Drug dosage was optimized according to drug solubility of SSD in the PLA /PEO blend solution and that was controlled visually. At high concentration, 6 wt % SSD was not dissolved completely. Low concentrations of 3 and 4 wt % SSD were dissolved perfectly but 3 wt % was elected due to dosage of more SSD into the polymer matrix. Thus, 4 wt % was selected the optimum soluble concentration of SSD in the PLA/PEO blend solution and it is used for the fabrication of SSD loaded nanofibers.

3.5 Fabrication of Electrospun Nanofibers

The electrospinning method was utilized for fabrication of composite nanofibers. The homogeneous polymer solutions were loaded into 2 ml syringe with a mounted 18 G needle. The syringe was placed horizontally on the pump and the solution was forced to the metallic needle tip with a 1 ml/h feeding rate to provide a constant flow. The

nanofiber production was carried out with an applied high-voltage of 15-17 kV, a working distance of 12-15 cm from tip to collector and a grounded rectangular electrode plate covered with aluminium foil was utilized as a collector. When the high voltage was applied to the needle tip, the nanofibers were deposited on the grounded collector plate. The experiments were done at room temperature and 40-60 % of relative humidity in enclosed Plexi glass box. Several parameters such as voltage, viscosity, flow rate and working distance were optimized to produce smooth and continuous fibers. The optimized parameters for fabrication of nanofibers were as following; the 15 kV applied voltage and 15 cm tip to collector distance for the pure PEO and PEO+SSD nanofibers, 17 kV and 12 cm for the pure PCL, PCL/PEO and SSD loaded PCL/PEO, 17 kV and 13 cm for the pure PLA, PLA/PEO and SSD loaded PLA/PEO composite nanofibers.

The dried nanofibers were fabricated via electrospinning since the solvents evaporated easily while the way of polymer jet was directed towards the collector. Additional drying of the nanofibers was done in a vacuum oven at 30°C for 12 hours to remove the residual solvents completely. The samples were kept in desiccators in the presence of silica for further testing. Schematic illustration of PCL/(PEO+SSD) and PLA/(PEO+SSD) composite nanofiber fabrication and was shown in Figure 3.2.

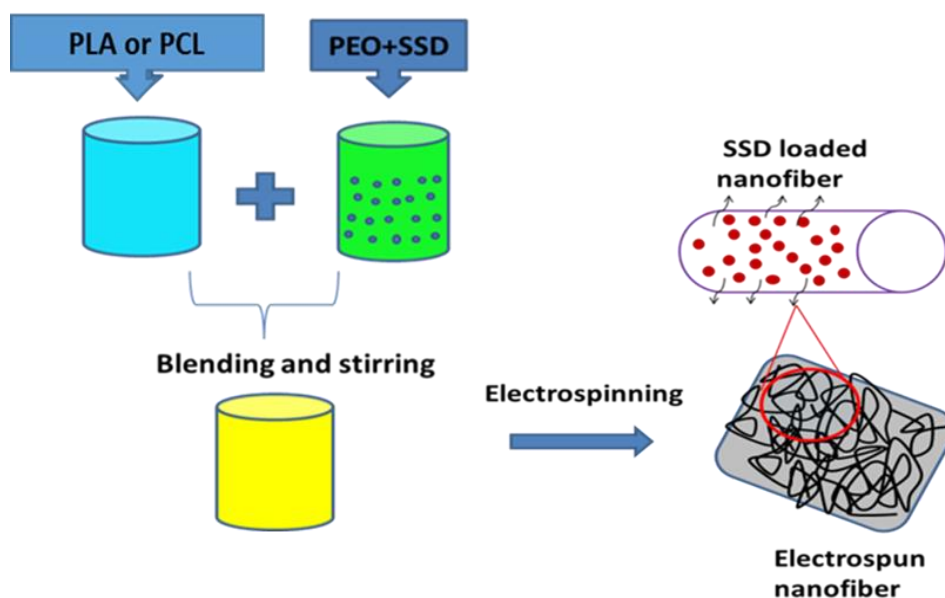


Figure 3.2 : Schematic illustration of PCL/(PEO+SSD) and PLA/(PEO+SSD) composite nanofiber fabrication.

3.6 Fabrication of Casting Films

Film casting technique was used for the fabrication of the composite films. This method was used to compare nanofiber and casting films which were fabricated by using the same solutions. For this purpose, from the drug loaded and drug-free PCL/PEO solutions, both electrospun nanofibers and casting films were prepared. The prepared PCL, PEO, PCL/PEO and PCL/(PEO+SSD) solution was dropped on aluminium foil, then solution was sheared in a rapid by doctor blade micrometre. The solution formed as a film and the film samples were dried in the oven at 40°C for 30 minutes. The principle is represented in Figure 3.3.

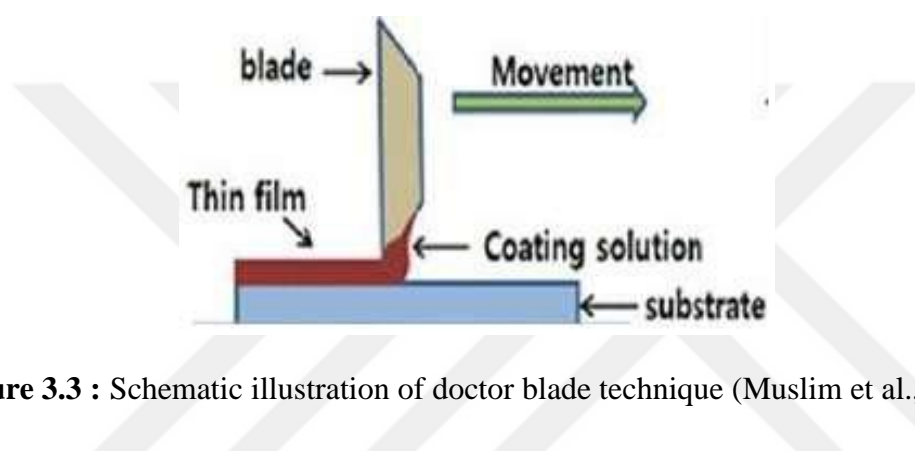


Figure 3.3 : Schematic illustration of doctor blade technique (Muslim et al., 2018).

3.7 *In vitro* Release Studies of SSD with UV Method

UV-Visible spectrophotometer (Hach -Lange-DR 5000) was used for *in vitro* drug release studies. UV-Visible spectrophotometry is a simple and commonly used method in pharmaceutical analysis. It determines the amount of UV radiation that is absorbed by a substance in solution. Thus, the substance is recognized and detected with the spectrophotometer. Ultraviolet-Visible spectrophotometers are instruments which measure the intensity ratio of two beams of light in the UV-Visible zone. The working principle of the UV spectrophotometer is based on the Beer -Lambert law. The Beer-Lambert equation is as given below (Behera et al., :2012):

$$A = a b c$$

Here, A=absorbance, a= coefficient of absorptivity, b=path length of UV radiation (cm), c=concentration of substance in solution.

3.7.1 Solubility studies of SSD

SSD is a low aqueous soluble drug. In literature, there are few studies on solubility and release of SSD. At known concentration of SSD (0.1, 0.5 and 0.7 mg/ml) was dissolved in different buffers to examine the solubility behaviour of SSD. The solubility test was performed in distilled water, ethanol, Phosphate Buffer Saline 7.4 (PBS 7.4), Phosphate Buffer Saline 5.5 (PBS 5.5), 0.05 % NH₃, EtOH +distilled water, and EtOH+PBS 5.5 solutions. However, SSD was not dissolved in these solvents. Therefore, organic solvents and phosphoric acid were blended with distilled water. Water/ Polyethylene glycol400/ Phosphoric Acid (82:16:2), Water/Propylene Glycol/Phosphoric Acid (82:16:2), Water/EtOH/Phosphoric Acid (82:16:2) cosolvent medias were prepared to perform SSD dissolution. Among them, Water/Propylene Glycol / Phosphoric Acid (82:16:2) was used as buffer media owing to the better solubility and enabling sink condition for drug release study. Solubility test results in the definite buffers were represented in Table 3.1 and the sign of (+) refers to solubility and sign of (-) refers to insolubility of SSD in the used buffer (Szegedi et al., 2014; Piyush et al., 2013; Venkataraman & Nagarsenker, 2013; Jangra et al., 2016).

Table 3.1 : Solubility study of SSD in different buffers (+ soluble, - insoluble).

| Buffer | Silver sulfadiazine concentration | | Solubility | |
|---|-----------------------------------|----------|------------|---|
| | | | | |
| PBS 7.4 | 0.1 mg/ml | | - | |
| 30 % EtOH +70% Water | 0.1 mg/ml | | - | |
| EtOH | 0.1 mg/ml | | - | |
| Water | 0.1 mg/ml | | - | |
| PBS 5.5 | 0.1 mg/ml | | - | |
| 30 % EtOH+70% PBS 5.5 | 0.1 mg/ml | | - | |
| 0.05 % NH ₃ Solution | 0.1 mg/ml | | - | |
| Water/Polyethylene glycol 400/Phosphoric Acid (82:16:2) | 0.5 mg/ml | 0.7mg/ml | + | - |
| Water/Propylene Glycol/Phosphoric Acid (82:16:2) | 0.5 mg/ml | 0.7mg/ml | + | + |
| Water/EtOH/Phosphoric Acid (82:16:2) | 0.5 mg/ml | 0.7mg/ml | + | - |

After the choice of Water/Propylene Glycol / Phosphoric Acid (82:16:2) buffer media, the maximum soluble SSD amount in the buffer was determined. For this purpose, the excess amount of drug (30 mg) was transferred into 10 ml volumetric flask and the buffer was added up to the mark on the volumetric flask. The mixture was stirred on a magnetic stirrer for 24 hours and then transferred to a centrifuge tube. After 24 hours the solution was centrifuged at 12,000 rpm for 10 minutes. The aliquot of 5 ml was withdrawn of the supernatant from the centrifuge tube for determining drug concentration by UV-Visible Spectrophotometer at 285 nm. The maximum solubility of SSD in Water/ Propylene Glycol/ Phosphoric Acid (82:16:2) was recorded as 836 µg/ml.

3.7.2 Preparation of calibration curve

0.5 mg/ml standard stock solution of SSD was prepared by dissolving 5 mg of SSD powder in 10 ml of the buffer solution. By diluting the stock solution of SSD (500 µg/ml), standard solutions were obtained in the concentration range between 5 µg/ml and 90 µg/ml (10 points) by transferring an appropriate volume of stock solution to 10

ml volumetric flask and making up the volume of flasks with buffer solution. All standard solutions were scanned in UV-Visible Spectrophotometer, between the wavelength range of 200-400 nm. The wavelength of the maximum absorbance peak was found to be 285 nm. The absorbance values were plotted against the corresponding concentration of standard solutions to get the calibration curve of SSD which was shown in Figure 3.4. Each experiment was done triplicate.

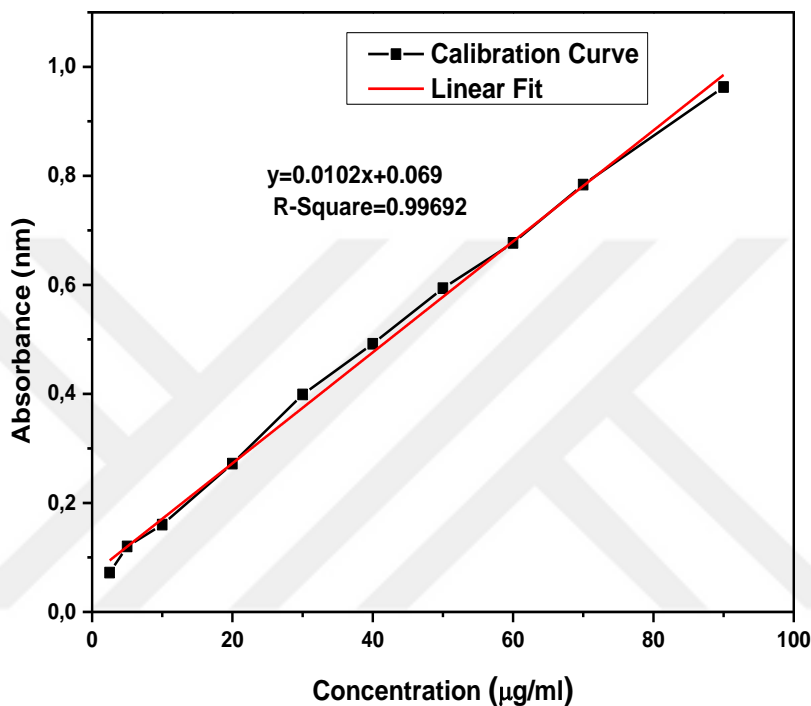


Figure 3.4 : Calibration curve of SSD.

3.7.3 UV method validation

Method validation is an important part of analytical studies that ensures if the measurement process generates valid measurements or not. The method validation results provide evaluation of the analytical results for quality, reliability and consistency. A simple, rapid, reliable and economical UV-spectrophotometric method was developed to estimate the release amount of SSD from composite nanofiber formulations with using Water/Acetonitrile/ Phosphoric Acid buffer system.

UV method validation was done according to the ICH Guidelines (ICH Q2R1) which presents the analytical procedure that should be followed during the validation. Standard validation parameters that were estimated are; accuracy, precision, linearity, specificity, detection limit, quantification limit and solution stability (Rao et al, 2011).

3.7.3.1 Specificity

Specificity is the ability to evaluate unambiguously the drug substance in the presence of other components which are desired to found in the formulation. Assuring specificity is the first step of the UV method validation. If specificity is not determined, other parameters such as accuracy, precision and linearity are all insignificant. Solution of each of the component of formulation was prepared and the solutions were scanned in UV spectroscopy to check if there is an absorbance peak at the area of specific peak of SSD (at the 285 nm) or not (Rao et al, 2011).

3.7.3.2 Linearity

The linearity of the method is to obtain direct proportional correlation between absorbance and concentration of the aliquots. Linearity is determined with calculating correlation coefficient of absorbance vs. concentration plot and the correlation coefficient value should be above 0.9 for the validated methods.

500µg/mL stock solution was prepared and diluted with the used buffer to obtain 5µg/mL, 10µg/mL, 20µg/mL, 30µg/mL, 40µg/mL, 60µg/mL, 70µg/mL, 80µg/mL standard solutions. The absorbances of all standard solutions were measured at 285 nm. The calibration curve was plotted as absorbance versus concentration and the linearity of the curve was evaluated with correlation coefficient which is calculated by regression equation (Rao et al, 2011).

3.7.3.3 Precision

Precision is the repeatability of the method under the same conditions after a period of time. This can be determined with intraday (on same day) and/or interday (on different days) studies. Working solutions were prepared and performed to estimate interday precision of the UV method. Experiments were done for consecutive 3 days and all samples were triplicate per day (n=3). The percentage of standard deviation (SD %) and relative standard deviation (RSD %) were estimated to evaluate the precision (Bushra et al, 2013).

3.7.3.4 Accuracy

Accuracy is the similarity or nearness between the measured absorbance values and reference absorbance values. It is represented and determined by recovery studies.

Accuracy of the UV Method was done by standard addition method. The accuracy was evaluated with recovery studies. From diluting the stock solution, sample solutions were prepared at different concentrations (Bushra et al, 2013).

All components of the formulation were added into the sample solutions and were mixed well. Preparation samples were filtered with 0.45 µm syringe filter and each filtered aliquot was triplicate. the absorbance values were measured at 285 nm and amount of SSD was estimated with the equation of the calibration curve. Then the recovery % value was calculated by using the following formula to evaluate the accuracy (Rao et al, 2011).

$$\text{Recovery \%} = (N \sum xy - \sum x \sum y) / (N \sum x^2 - (\sum x)^2) * 100$$

3.7.4 *In Vitro* drug release studies (Dialysis bag method)

The drug release studies of SSD loaded composite nanofibers was investigated in Water/Propylene Glycol /Phosphoric Acid (82:16:2) mixture under sink conditions. Sink condition is defined as the drug concentration in the course of the *in vitro* release as it should not be over 10 % of the drug saturation concentration (Larsen & Larsen, 2009). Three drug-loaded fiber samples of about 23-25 mg were cut in a circular shape with a diameter of 30 mm. Dialysis bag method were used for *in vitro* release studies. This bag consists of regenerated cellulose made from virgin wood pulp. The dialysis bag was suspended in distilled water for activation of the membrane and each nanofiber patch was put in a dialysis bag of 2.5 cm in length. Both ends were tied. The dialysis bag was suspended in 20 mL release media under stirring at 100 rpm and 37°C. Drug release studies were performed in 25 ml conical flasks and the conical flasks were closed with cylindrical cork stopper, then tightly sealed with parafilm to ensure constant volume of release media (to avoid evaporation or any volume loss from the release media). The conical flasks were covered with aluminium foil to prevent entering of the light. At predetermined time intervals of 0.5, 1, 1.5, 2, 3, 4, 5, 6, 7, 8 and 24 hour 1.5 mL aliquots were sampled and replaced with 1.5 mL fresh buffer. The aliquots were filtered with 0.45 µm PTFE syringe filter. The filtered aliquots were scanned on UV Spectrophotometer at excitation of 285 nm and drug concentrations were quantified. Using the calibration curve, amount of SSD release was calculated. Finally, release amount of SSD versus time and percentage of SSD release versus time graphs were plotted. All experiments were performed triplicate.



Figure 3.5 : Photographs of *in vitro* drug release studies.

3.7.5 Controlling the drug release with conductivity

Drug release studies were also verified with conductivity measurement due to the conductive nature of SSD. At predetermined time intervals of 0.5, 1, 1.5, 2, 3, 4, 5, 6, 7, 8 and 24-hour 1.5 mL aliquots were sampled. The conductivity of aliquots was measured using Multiparameter InoLabMulti 720 (WTW) at room temperature. All experiments were performed triplicate and conductivity of aliquots versus time graph was plotted.

3.7.6 Drug release kinetics

The regression coefficients (R^2) of the release profile were evaluated according to different mathematical models to describe the release mechanism of SSD loaded nanofiber patches. These models are, Zero Order, First Order, Hixson-Crowell, Higuchi Square Root and Korsmeyer-Peppas (Gouda et al., 2017).

3.7.6.1 Zero Order kinetic model

Zero order kinetics model describes the constant drug release from a formulation and drug level in the blood remains constant during the drug release action. This mathematical model describes the drug release with the following formula as (Gouda et al., 2017):

$$C_0 - C_t = K_0 t$$

$$C_t = C_0 - K_0 t$$

C_t is the amount of released drug at time t ,

C_0 is the initial drug concentration at time $t=0$,

K_0 is the zero-order rate constant.

The cumulative drug release versus time graph was plotted and the (R^2) value of the curve was calculated to see whether the release is fitted with zero order kinetics model or not.

3.7.6.2 First Order kinetic model

In First Order Kinetic Model, rate of the release process is directly proportional to the concentration. Hence, it has linear kinetics. This mathematical model describes the drug release with the following formula as (Gouda et al., 2017):

$$\log C = \log C_0 - K_1 t / 2.303$$

K_1 is the first order rate constant in time^{-1} ,

C_0 is the initial drug concentration,

C is the percentage of remaining drug at time t .

The cumulative log % of the drug remaining versus time graph was plotted and the correlation coefficient (R^2) of the curve was found to show whether the drug release is fitted with first order kinetics model or not.

3.7.6.3 Higuchi square root kinetic model

Higuchi kinetics model defines the drug release mechanism as diffusion controlled process that is square root of time dependent. This kinetics model defines the drug release with the following formula as (Gouda et al., 2017):

$$Q = K_H \times t^{1/2}$$

Here, K_H is the dissolution constant of Higuchi. Q is the cumulative amount of drug release in time t .

The cumulative percentage drug release (Q) versus square root of time graph were plotted. There is a linear correlation between Q and $t^{1/2}$ for the basic Higuchi model. Moreover, if the slope of the plot equals to K_H , it shows that the drug release follows $t^{1/2}$ Higuchi kinetics model.

3.7.6.4 Hixson-Crowell kinetic model

The Hixson-Crowell kinetics model defines the drug release process when there is a change in surface area of the formulations. Therefore, particles of regular area are proportional to the cube root of its volume. This mathematical model defines

dissolution based drug release mechanism with the following formula as (Gouda et al., 2017):

$$W_0^{1/3} - W_t^{1/3} = k_{HC}$$

Here, W_0 is the initial drug amount of the formulation (amount of drug remaining at time 0) W_t is the remaining drug amount of the formulation at time t ; K_{HC} is the Hixson-Crowell constant that describes the correlation between surface and volume. The cube root of percentage of remaining drug in formulation versus time graph was plotted and correlation coefficient was calculated whether the release process is fitted with The Hixson-Crowell kinetics model or not.

3.7.6.5 Korsmeyer-Peppas kinetics model

This mathematical model describes the drug release with the following formula as (Gouda et al., 2017):

$$M_t / M_\infty = kt^n \quad (3)$$

M_t/M_∞ is the amount of released drug at time (t), M_∞ is the total amount of released drug after time ∞ (total amount of drug in the formulation), n is the drug release exponent which defines the release mechanism, k is the constant of the release rate. For the cylindrical-shaped matrices; $0.45 \leq n$ represents Fickian diffusion mechanism and non-Fickian or anomalous transport exhibits when $0.45 < n < 0.89$, $n = 0.89$ corresponding to Case II (relaxational) transport and $n > 0.89$ indicates super case II transport. To determine the exponent of n the portion of the drug release curve, where $M_t / M_\infty < 0.6$ should be used only. The log cumulative percentage of drug release versus log time curve was plotted to estimate the release kinetics.

3.7.7 Drug loading efficiency

The drug loading efficiency of nanofibers indicates the comparison of the actual drug loading into the nanofibers and the initially used drug that can be calculated by UV-Visible spectrophotometry (Hach -Lange-DR 5000) with the absorbance peak at 285 nm wavelength for SSD. A sample piece of SSD loaded nanofiber was cut and weighted as 5 mg. The 5 mg weighted sample was suspended in 5 mL chloroform/acetonitrile cosolvent and then the suspension was shaken for 24 hours to re-dissolve the sample. The next day it was filtered and the absorbance of SSD was

measured and the experiment was triplicate. The drug loading efficiency was calculated by the following equation:

$$\text{Drug Loading Efficiency (\%)} = (A_{\text{act}}/A_{\text{int}})*100 \text{ (1)}$$

In the *Equation 1*; A_{act} is the amount of actual drug loading and A_{int} is the amount of initial (theoretical) drug loading into the nanofibers. Three nanofiber patches were examined to calculate drug loading efficiency and the average values was recorded.

3.8 Characterizations and Measurements

3.8.1 SEM analysis

The surface morphology of the nanofibers was examined by using the SEM instrument (Zeiss EVO® LS 10) with a 10 kV voltage and a 9 mm working distance. A small piece of the nanofibers was prepared and then coated with gold (Au) for a minute with a sputter-coating unit. The fiber diameters were measured by using the Image J Program from 50 different fiber sections of a scanning electron microscopy (SEM) image. Average fiber diameters and fiber diameter distributions were performed with Origin Pro 9 software.

3.8.2 SEM-EDS and EDS-Mapping analysis

Energy dispersive spectra (EDS) analysis was performed to confirm that PCL/(PEO+SSD) nanofibers contain SSD. For this purpose, Silver (Ag), Nitrogen (N), Sulphur (S) atoms were detected representing the SSD in content of the nanofibers. EDS graph give information about drug content of composite nanofibers. Moreover, these Ag, N and S atoms were scanned and mapped as an image with EDS-Mapping study. EDS-Mapping Images were carried out to show the distributions of these elements in composite nanofibers.

3.8.3 Water uptake measurement

The water uptake was evaluated by immersing electrospun patches in 20 mL buffer solution at the room temperature for 24 hours. The weight of the wet sample was measured after being dried in the incubator to remove the surface water. The water uptake percentage was calculated by the following formula:

$$\text{Water Uptake \%} = (W_w - W_d) / W_d * 100 \text{ (2)}$$

In the *Equation 2*; W_d is dried weight of the patch and W_w is the wet weight of the patch. Three nanofiber patches were examined to calculate the water uptake percentage and the average value was recorded.

3.8.4 Optical Profilometer

The surface morphology and surface roughness of the casting films were determined with the ZEISS Axio CSM 700 Optical Profilometer.

3.8.5 Viscosity measurement

The viscosities of the electrospinning solutions were determined with the Anton Paar Physica MCR 302 rheometer which was fitted out with a cone-plate at a 100 1/s constant shear rate.

3.8.6 Attenuated Total Reflectance Infrared (FTIR-ATR) spectroscopy analysis

Nanofiber patches were characterized by Attenuated Total Reflectance infrared spectroscopy (FTIR-ATR) (Perkin Elmer Spectrum 100) to check the presence of chemical bonding between SSD and polymer matrix and surface molecular interactions of the samples. The absorbances of all specimens were analysed between the frequency range of 500 - 4000 cm^{-1}

3.8.7 X-Ray diffraction (XRD) analysis

X-ray diffraction (XRD) was done by using the PANalytical X-Pert PRO diffractometer. XRD analysis was carried out to observe crystallinity of both drug-free and SSD loaded nanofibers. XRD patterns were plotted by the X-ray diffractometer between the range of 4-50° at a 0.05°/min scan speed.

3.8.8 Contact angle measurements

Hydrophilicity of the SSD loaded nanofibers was evaluated by using the contact angle instrument (VCA-optima, AST, Inc.). Deionized water (0.25 L) was dropped onto the nanofiber mats and the contact angles of the samples were measured. All measurements were done from 5 different points of a sample.

3.8.9 Atomic Force Microscope (AFM) studies

The surface roughness values of composite nanofibers were calculated with using AFM instrument. Very few nanofibers were deposited on the cover glass for 20 second with electrospinning and the samples were examined by AFM (NANO MAGNETICS INSTRUMENTS) in semi contact mode. The images were analysed with NMI Image Analyser software.

3.8.10 Antibacterial activity test

Antibacterial activity performance of PCL/(PEO+SSD) and PLA/(PEO+SSD) composite nanofibers were evaluated with two different methods which are;

- Disc Diffusion Method
- Minimum Inhibition Concentration (MIC) and Minimum Bactericidal Concentration (MBC) Methods

3.8.10.1 Disc diffusion method

Antimicrobial activities of the composite and pure nanofibers against gram negative *Pseudomonas aeruginosa* (*P. aeruginosa*), *Escherichia coli* (*E. coli*) and gram positive *Staphylococcus aureus* (*S. aureus*) bacteria were performed. The evaluation was performed according to the disc diffusion method of the US Clinical and Laboratory Standards Institute (CLSI) (AATCC 147-1998 test parameters).

The inoculum is prepared in agar plates (Nutrient agar) by using a 24-hour inoculum suspension from single fallen colonies directly in the Nutrient broth. The turbidity of the suspension is set to a turbidity equivalent to the Mc Farland 0.5 standard (1.5×10^8 CFU/mL). The UV-Vis device was used to adjust the intensity of the suspension. The *E. coli*, *S. aureus* and *P. aeruginosa* bacteria were inoculated into the agar before the drug impregnated discs and mats were applied (0.1 ml) and the plaque was allowed to stand for five minutes to be absorbed and to remove any excess moisture from the surface.

For antibacterial tests, the PCL(PEO+SSD), PCL+PEO, PLA(PEO+SSD), PLA+PEO nanofiber mats were cut into 1.2 cm circular shaped pieces and the same weighted of the nanofiber samples were chosen to have same amount of SSD. SSD powder was weighed and SSD solution were prepared in the buffer for positive control. Drug-free composite nanofibers were utilized as the negative control for antibacterial activity. The antibacterial activity of commercial SSD cream was also evaluated to compare with composite nanofibers. Hence, SSD cream was weighted in order to adjust SSD amount within the nanofiber formulations. Then the SSD cream was impregnated on to discs ($d=6$ mm).

The nanofiber mats were sterilized by UV light for 30 min and placed at the centre of petri plates containing sterilized nutrient agar (NA). Each sample and the control

groups were placed on NA in a Petri dish, and then incubated at 37°C for 24 h. The mortality of the bacteria was observed with formation of the clean zone around the samples. The diameters of the clean zones were measured and photographed. The inhibition zones of the nanofiber formulations were compared with commercial SSD Cream. All specimens were three replicates. The antibacterial effectivity test was performed for the period of 24, 48 and 72 hours.

3.8.10.2 Minimum Inhibition Concentration (MIC) and Minimum Bactericidal Concentration (MBC) methods

Antibacterial activity of the SSD loaded PCL/PEO and PLA/PEO nanofibers were examined against *Pseudomonas aeruginosa* (ATCC 27853), *Staphylococcus aureus* (ATCC 25023), and *Escherichia coli* (ATCC 25922) with determining MIC and MBC values. These values were measured using broth dilution (micro dilution) method.

The Minimum Inhibitory Concentration (MIC) is the lowest concentration of the drug substance that has bacteriostatic effect. It means, preventing the growth and proliferation of bacteria without killing. MIC is used to determine the antibacterial activity of drugs or biological agents by estimating the effect of decreasing concentrations of them. This method is used for determination of appropriate concentrations that is required in the drug formulation (Url-6).

Series of sample solutions at concentrations of 2560, 1280, 640, 480, 320, 160, 80, 40 µg/mL were prepared and dispersed in 2 mL of broth media. Then, 20 µL of bacterial suspensions (10⁸ CFU/mL) were added into the series of tubes. Therefore, the bacterial cultures were appropriately diluted to get 10⁸ CFU/mL and used as primary inoculum. Sample concentrations of the formulations were incubated at 37°C for 24 h. Growth or no growth was determined by visually.

The Minimum Bactericidal Concentration (MBC) is the lowest concentration of the drug substance that shows bactericidal effect reducing the bacterial viability over a period of time. It can be determined from the broth dilution of MIC tests by subculturing to agar plates that do not contain the test agent. The difference between MBC and MIC is; while the MIC test exhibits the lowest level of antimicrobial agent that inhibits bacterial growth, the MBC exhibits the lowest level of antimicrobial agent that results in microbial death (Url-6).

For the estimation of MBC (Minimum Bactericidal Concentration), the invisible bacterial suspension samples at different concentrations (2560, 1280, 640, 480, 320, 160, 80, 40 $\mu\text{g}/\text{mL}$) were prepared. They were cultured to the agar plates and incubated at 37°C for 24 h. The number of surviving colonies was calculated to find out the MBC values of the nanofiber specimens.

3.8.11 Stability studies of formulations

Stability testing is an important part of formulation development. It gives information about drug quality or how a drug substance is affected by environmental factors over a period of time. Thus, it appoints shelf-life and storage conditions of the drug products. For this purpose, stability studies of the composite nanofibers were carried out for 3- and 6-months periods. Nanofiber samples were kept both at refrigerator conditions (+4°C) and room temperature (25 \pm 2°C) to evaluate stability of nanofiber patches. Stability tests were performed with calculating drug loading amount, cumulative drug release by UV absorption measurements, analysing surface morphology by SEM analysis.

3.8.11.1 Stability testing with SEM analysis

Drug loaded and drug-free nanofiber formulations were waited for 3 and 6 months at 25 \pm 2°C and +4°C refrigerator conditions. Then surface morphologies of the formulations were examined.

3.8.11.2 Stability testing with calculating the drug loading efficiency

Drug loaded and drug-free nanofiber formulations were waited for 3 and 6 months at 25 \pm 2°C and +4°C refrigerator conditions. Then drug loading efficiency (loading drug amount) of the formulations were estimated.

3.8.11.3 Stability testing with cumulative drug release

Drug loaded and drug-free nanofiber formulations were waited for 3 and 6 months at 25 \pm 2°C and +4°C refrigerator conditions. Then the cumulative drug release of the formulations was examined.

3.8.12 Cytotoxicity

The cytotoxicity studies of the drug loaded and drug-free PCL/PEO and PLA/PEO nanofiber patches were done with using the cell viability assay (MTT assay). The cytotoxicity tests were performed according to the ISO10993-5 direct contact testing

method. Four samples were prepared for each composite nanofiber patch in a circular shape with 10 mm diameter. The samples were sterilized under UV light for 30 minutes to avoid contamination.

L929 mouse fibroblast cells were used for the experiment. The L929 cells were grown in 25 T-flasks, subcultured three times a week at 37°C, 5 % CO₂ in air for 24 hours. The culture medium was Dulbecco's Modified Eagle Medium (DMEM) nutrient mixture supplemented with 10 % (v/v) fetal bovine serum (FBS) and 1 % gentamycin. Adherent cells at a logarithmic phase were detached with a mixture of 0.05 % trypsin and 0.02 % EDTA incubated for 5-10 min at 37°C and used for cell inoculation. 100 µl DMEM medium was used as negative control and 1 % phenol solution was used as positive control.

L 929 cells are seeded into 96-well cell culture plates. The plates were incubated in DMEM culture media at 37°C, 5 % CO₂ in air for 24 hours to form a self-confluent monolayer. After the incubation, the culture medium was removed from the wells and then fresh culture medium was added into the each well. Nanofiber samples were placed wells and treated with cells. After 24 hours treatment, the cells were inoculated in 100 µl growth DMEM medium and 100 µl MTT medium (tetrazolium salt 3- [4,5-dimethylthiazol-2-yl]-2,5-diphenyltetrazolium bromide). The well culture plate was kept in a dark environment for 4 h at 37°C. Then, MTT was removed, the cells were rinsed with glycine buffer and 100 µl DMSO was added to each well respectively. Finally, the absorbance at 570 nm was measured using a UV-visible spectrophotometer (Ozdemir et al., 2009).

The cell viability (%) was calculated with the following formula (Tonglairoum et al., 2014):

The cell viability (%) = $(OD_{570; \text{sample}} - OD_{570; \text{blank}}) / (OD_{570; \text{control}} - OD_{570; \text{blank}}) * 100$

4. RESULTS AND DISCUSSION

4.1 Preparation of the Polymer Solutions

Optimum parameters of the polymer solutions were stated after several tries which were described in materials and method section. Herein, preparation of the optimized solutions is explained.

3.5 % (w/w) PEO solution was prepared in acetonitrile/acetic acid (3:1/v:v) solvent and SSD was added into the PEO solution at the amount of 12 wt % with respect to the PEO polymer. The SSD was completely dissolved in the PEO solution. Besides 4 % (w/w) PCL solution was prepared in chloroform/ethanol (3:2/v:v) individually. PCL and SSD loaded PEO solutions were mixed at a ratio of 7:3 (w/w) and stirred for an hour to get a homogeneous blend solution. PEO and PCL solutions were miscible and phase separation was not seen in the PCL/PEO blend solution. Consequently; PEO, PEO+SSD, PCL, PCL/PEO (7:3), PCL/(PEO+SSD) (7:3) solutions were prepared respectively for electrospinning. In the final PCL/(PEO+SSD) (7:3) solution, the amount of SSD was 3.2 wt % with respect to the total polymer matrix. The photograph of PEO, PEO+SSD, PCL, PCL/PEO and PCL/(PEO+SSD) solutions was represented in Figure 4.1.



Figure 4.1 : Photograph of PEO, PEO+SSD, PCL, PCL/PEO and PCL/(PEO+SSD) solutions.

3.5 % (w/w) PEO solution was prepared in acetonitrile/acetic acid (3:1/v:v) solvent and SSD was added into the PEO solution at the amount of 20 wt % with respect to the PEO polymer. The SSD was completely dissolved in the PEO solution. Besides 6

% (w/w) PLA solution was prepared in acetonitrile/chloroform (3:2/v:v) individually. PLA and SSD loaded PEO solutions were mixed at a ratio of 7:3 (w/w) and stirred for an hour to get a homogeneous blend solution. PEO and PLA solutions were miscible and phase separation was not seen in the PLA/PEO blend solution. Consequently; PEO, PEO+SSD, PLA, PLA/PEO (7:3), PLA/(PEO+SSD) (7:3) solutions were prepared respectively for electrospinning. In the final solution, PLA/(PEO+SSD) (7:3), the amount of SSD was 4 wt % with respect to the total polymer matrix. The photograph of PEO, PEO+SSD, PLA, PLA/PEO and PLA/(PEO+SSD) solutions was represented in Figure 4.2.



Figure 4.2 : Photograph of PEO, PEO+SSD, PLA, PLA+PEO and PLA/(PEO+SSD) electrospinning solutions.

4.1.1 Viscosity measurements of the solutions

The viscosities of the prepared solutions were measured by using the Anton Paar Physica MCR 302 rheometer which was fitted out with a cone-plate at a 100 1/s constant shear rate. Viscosity values of the solutions were represented in Table 4.1. The viscosity was found between the range of 0.014 and 0.3 Pa.s. The viscosity of the solutions increased with addition of SDD that was an expected result. Because, polymer drug interactions occur with distribution of SSD into the PEO and PCL/PEO solution.

It is stated that the viscosity values of the PCL and PLA solutions increased by blending with PEO in PCL/PEO and PLA/PEO solutions. PEO gives higher viscosity to the solutions due to its gelling properties and high molecular weighted polymer chain with 900.000 Mw (Kashmola & Kamil, 2014).

Table 4.1 : Viscosity values of the solutions.

| Viscosity (Pa.s) | Solutions |
|------------------|---------------|
| 0.190 | PEO |
| 0.300 | PEO+SSD (1) |
| 0.320 | PEO+SSD (2) |
| 0.014 | PCL |
| 0.021 | PLA |
| 0.059 | PCL/PEO |
| 0.061 | PLA/PEO |
| 0.062 | PCL/(PEO+SSD) |
| 0.063 | PLA/(PEO+SSD) |

4.2 Electrospinning Process

Drug loaded and drug-free electrospun fibers were prepared by electrospinning technique. Different electrospinning parameters were tried for the optimization of process parameters to obtain smooth, bead free and uniform fiber morphology. Optimum parameters for PEO, PEO+SSD, PCL, PLA, PEO/ PCL, PLA/PEO, PCL/(PEO+SSD) and PLA/(PEO+SSD) nanofibers were given in Table 4.2 and Table 4.3. A photograph of electrospinning process was seen in Figure 4.3.



Figure 4.3 : Photograph of the electrospinning process.

Table 4.2 : Optimized electrospinning parameters for PCL/(PEO+SSD) formulations.

| Parameters | PEO | PEO+SSD | PCL | PCL/PEO | PCL/ (PEO+SSD) |
|---------------------|-----|---------|-----|---------|-------------------|
| Voltage (kV) | 15 | 15 | 17 | 17 | 17 |
| Distance (cm) | 15 | 15 | 12 | 12 | 12 |
| Flow rate (ml/hour) | 1 | 1 | 1 | 1 | 1 |

Table 4.3 : Optimized electrospinning parameters for PLA/(PEO+SSD) formulations.

| Parameters | PEO | PEO+SSD | PLA | PLA/PEO | PLA/(PEO +SSD) |
|---------------------|-----|---------|-----|---------|-------------------|
| Voltage (kV) | 15 | 15 | 17 | 17 | 17 |
| Distance (cm) | 15 | 15 | 13 | 13 | 13 |
| Flow rate (ml/hour) | 1 | 1 | 1 | 1 | 1 |

4.3 Doctor Blading Process

Doctor blade technique was used for the production of the composite films. This method was used to compare nanofiber and casting films which were fabricated by using the same solutions. For this purpose, from the drug loaded and drug-free PCL/PEO solutions, both electrospun nanofibers and casting films were prepared. The prepared PCL, PEO, PCL/PEO and PCL/(PEO+SSD) solution was dropped on

aluminium foil, then solution was sheared in a rapid by doctor blade micrometre. The solution formed as a film and the film samples were dried in oven at 40°C for 30 min. Release properties and performance of PCL/(PEO+SSD) casting film and PCL/(PEO+SSD) composite nanofiber formulations were compared. A photograph of the doctor blade process was seen in Figure 4.4.

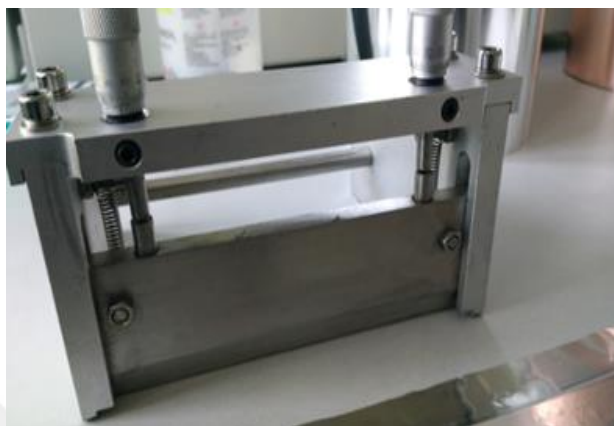


Figure 4.4 : Fabrication of casting films with Doctor Blade.

4.4 UV Method Validation

4.4.1 Specificity

Solution of each of the component of formulation was prepared and the solutions were scanned in UV spectroscopy to check if there is an absorbance peak at the area of specific peak of SSD (at the 285 nm) or not. According to specificity study there was no peak appear from the other components of the formulation at the 285 nm.

4.4.2 Linearity

500 µg/mL stock solution was prepared and diluted with the used buffer to obtain 5 µg/mL, 10 µg/mL, 20 µg/mL, 30 µg/mL, 40 µg/mL, 60 µg/mL, 70 µg/mL, 80 µg/mL standard solutions. The absorbances of the all standard solutions were measured at 285 nm. The calibration curve was plotted absorbance versus concentration (Figure 3.4) and the linearity of the curve was evaluated with correlation coefficient value (R^2) which is calculated by regression equation. The calibration curve of SSD was found to be linear and the regression equation was $y = 0.0087x + 0.697$ with correlation coefficient (R^2) 0.9928.

4.4.3 Precision

Working solutions were prepared and performed to estimate interday precision the UV method. Experiments were done for consecutive 3 days and all samples were triplicate

per day (n=3). The percentage of standard deviation (SD %) and relative standard deviation (RSD %) were calculated to evaluate the precision. The results of precision study were shown in Table 4.4. The developed UV method was precise since the RSD % values were less than 2.99.

Table 4.4 : Evaluation data of precision study.

| Concentration (µg/ml) | 1.Day | 2.Day | 3.Day | Mean | SD % | RSD % |
|-----------------------|-------|-------|--------|-------|--------|-------|
| 5 | 0.086 | 0.088 | 0.09 | 0.088 | 0.002 | 2.27 |
| 10 | 0.145 | 0.147 | 0.1475 | 0.146 | 0.001 | 0.9 |
| 20 | 0.26 | 0.267 | 0.273 | 0.266 | 0.0015 | 2.44 |
| 30 | 0.345 | 0.348 | 0.3495 | 0.347 | 0.002 | 0.66 |
| 40 | 0.444 | 0.45 | 0.47 | 0.454 | 0.013 | 2.99 |
| 60 | 0.585 | 0.595 | 0.61 | 0.596 | 0.0125 | 2.11 |
| 70 | 0.69 | 0.705 | 0.71 | 0.701 | 0.01 | 1.48 |
| 80 | 0.737 | 0.74 | 0.76 | 0.745 | 0.0125 | 1.68 |

4.4.4 Accuracy

Accuracy of the UV Method was done by standard addition method. The accuracy was evaluated with recovery studies. From diluting the stock solution, sample solutions were prepared at different concentrations. All components of the formulation were added into the sample solutions and were mixed well. Preparation samples were filtered with 0.45 µm syringe filter and each filtered aliquot was triplicate. The absorbance values were measured at 285 nm and amount of SSD was estimated with the equation of the calibration curve. Then the recovery % value was calculated by using the following formula to evaluate the accuracy (Rao et al, 2011).

$$\text{Recovery \%} = (N \sum xy - \sum x \sum y) / (N \sum x^2 - (\sum x)^2) * 100$$

Evaluation data of accuracy study was given at Table 4.5.

Table 4.5 : Evaluation data of accuracy study.

| Concentration (µg/ml) | Recovery % | SD | RSD % |
|----------------------------------|-------------------|-----------|--------------|
| 80 | 97.5 | 0.5 | 0.51 |
| 70 | 96 | 1 | 1.04 |
| 60 | 98 | 0.92 | 1.05 |
| 40 | 97 | 1 | 1.03 |
| 30 | 96.8 | 1.587 | 1.64 |
| 20 | 94.8 | 1.276 | 1.35 |
| 10 | 92.3 | 1.059 | 1.15 |
| 5 | 94.73 | 0.55 | 0.58 |

4.5 Measurement and Characterization Studies of Silver Sulfadiazine (SSD)

In this section FT-IR and XRD characterization of pure SSD in a powder form were performed.

4.5.1 FT-IR ATR spectrum of Silver Sulfadiazine

FT-IR Spectrum of pure SSD were represented in Figure 4.5.

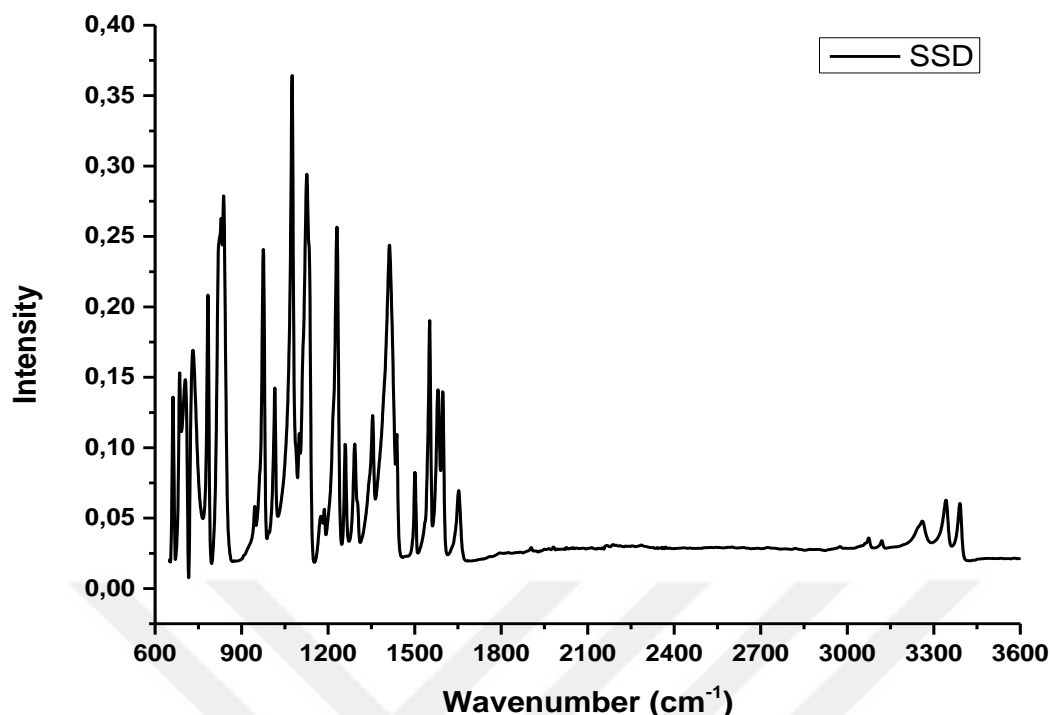


Figure 4.5 : FT-IR ATR Spectrum of SSD.

SSD presented peaks at 3343 and 3393 cm^{-1} were due to the amine (NH_2) stretching mode. Exhibited peaks at 1651 cm^{-1} associated with NH_2 bending, at 1595, 1581, 1552 and 1500 cm^{-1} were attributed to the aromatic $\text{C}=\text{C}$ stretching, at 783, 1016, 1356 cm^{-1} were due to the asymmetric and at 1124 cm^{-1} conjugated the symmetric stretching of SO_2 (Ghodekar et al., 2012; Patel et al., 2019; Zepon et al., 2014). Finally, the peaks exhibited at around 1230 cm^{-1} conjugated to aromatic $\text{C}-\text{N}$ stretching and at 1075 cm^{-1} corresponding to aromatic vibrations.

4.5.2 XRD spectrum of Silver Sulfadiazine

XRD Spectrum of pure SSD were represented in Figure 4.6. SSD showed its characteristic peaks at around $2\theta = 8.8^\circ$ and 10.2° corresponding to the (0 0 2), (0 1 1) planes as explained in literature (Aguzzi et al., 2014; Ghodekar et al., 2012; Luan et al., 2012).

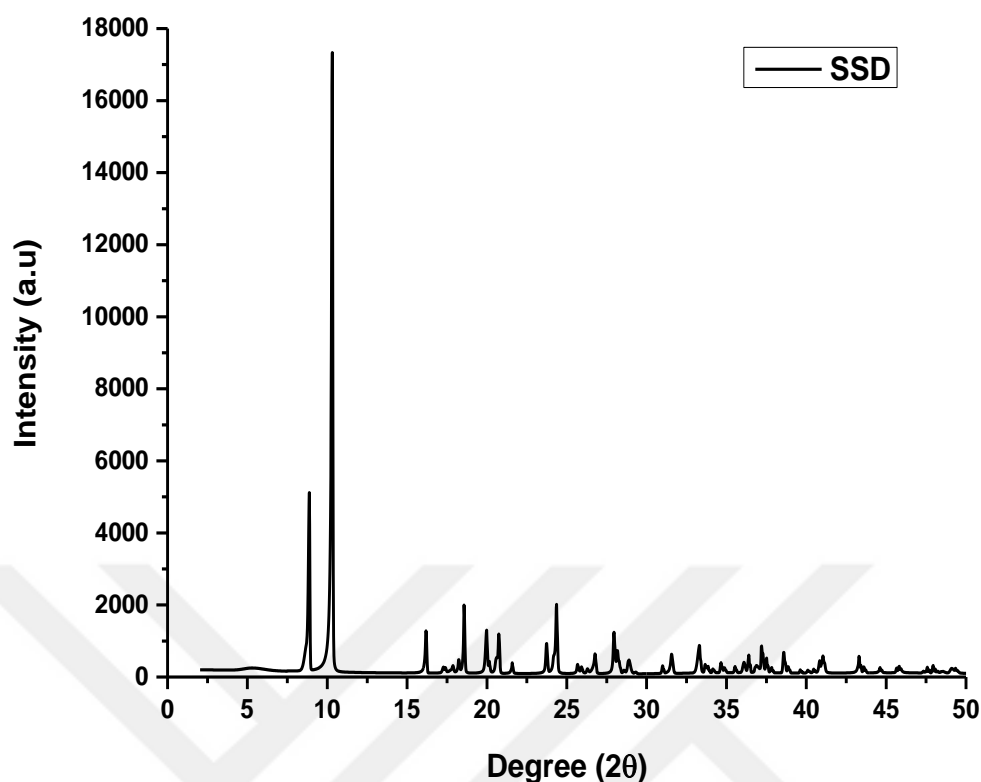


Figure 4.6 : XRD Spectrum of SSD.

4.6 Measurements and Characterization Studies of PCL/(PEO+SSD) Nanofiber Formulations

SEM, SEM-EDS, SEM-EDS Mapping, AFM, FTIR-ATR Spectroscopy, XRD, analysis, water uptake and contact angle measurements were performed to characterize PEO, PEO+SSD, PCL, PCL/PEO and PCL/(PEO+SSD) electrospun nanofibers.

4.6.1 SEM analysis

Morphology of fibers such as fiber diameter, structure and frequency of the pores, getting beadles and smooth surface is an important parameter for nanofiber based drug delivery systems. It is significant to provide the appropriate conditions for loading, carrying and releasing the drugs (Sill&Von Recum, 2008). Therefore, it was aimed to obtain fiber morphology with appropriate properties for drug delivery. In this part, SEM analysis was performed for the morphological characterization of the nanofibers to verify the fiber diameter, fiber morphology, bead defects, smoothness, uniformity and diameter distribution of nanofibers. The average fiber diameters were calculated

from 30 different fiber sections of an SEM image and histograms of fiber diameter distributions were plotted.

4.6.1.1 SEM analysis of PEO and PEO+SSD nanofiber

General surface images of PEO and PEO+SSD nanowebs were represented in Figure 4.7 at 2000 magnification. The SEM images at 10,000 magnification and diameter distribution of PEO and PEO+SSD nanofibers were shown in Figure 4.8. Uniform, solid, continuous, bead-free and porous fiber morphologies with nanoscaled diameters were observed in the SEM images.

The average diameter was 313 ± 67 nm for the pure PEO nanofibers and 297 ± 38 nm for the PEO+SSD. Compared to pure PEO fibers, the SSD loaded PEO nanofibers had lower diameter and a narrow diameter distribution with smooth fiber morphology. It demonstrated that SSD was dissolved perfectly in PEO polymer solution and distributed in PEO nanofiber mats homogeneously.

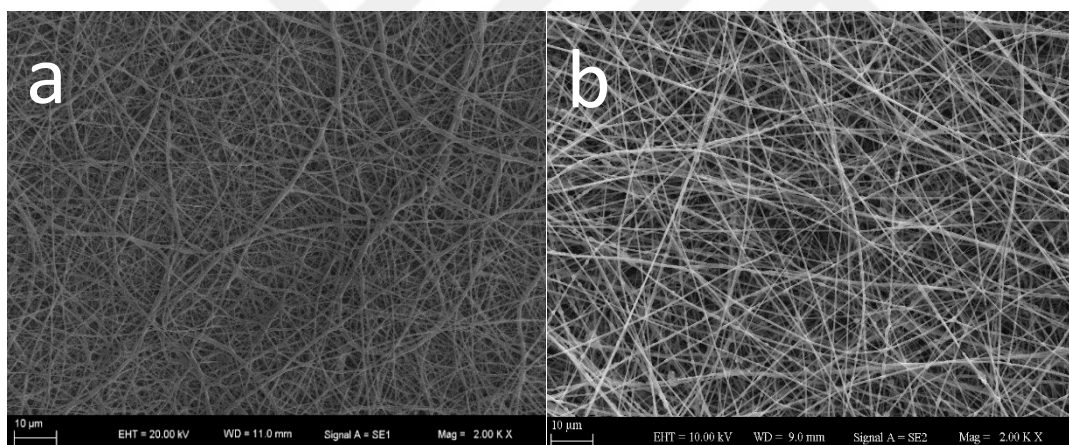


Figure 4.7 : General surface images of a) PEO and b) PEO+SSD (at X 2000 magnification).

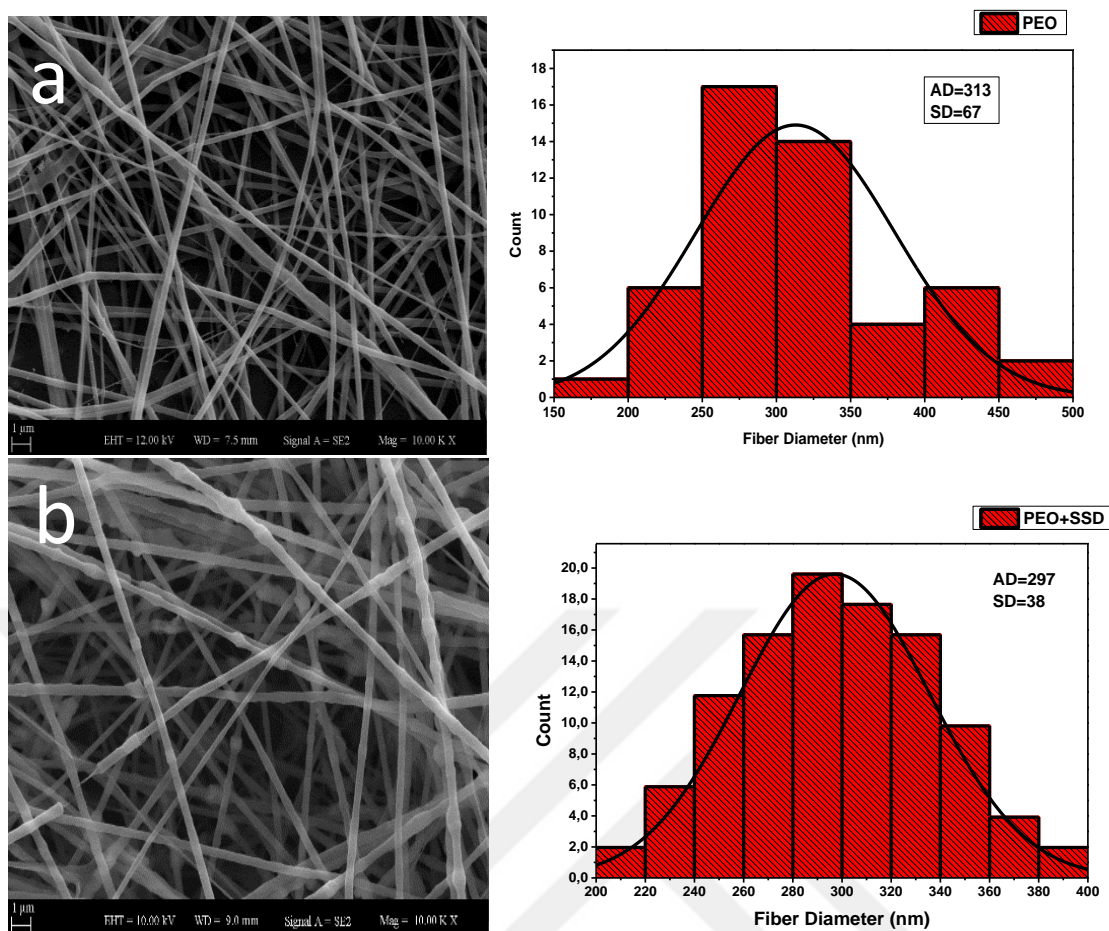


Figure 4.8 : SEM Images and corresponding diameter distribution histograms of a) Pure PEO and b) PEO+SSD nanofibers.

4.6.1.2 SEM analysis of PCL, PCL/PEO and PCL/(PEO+SSD) nanofibers

Nanoscaled, solid, continuous and porous PCL and PCL+PEO, PCL/(PEO+SSD) nanofibers were fabricated via electrospinning. General surface images of the PCL, PCL /PEO and PCL/(PEO+SSD) nanowebs were represented in Figure 4.9 at 2000 magnification. The SEM images at 10,000 magnification and diameter distribution of PCL, PCL/PEO and PCL/(PEO+SSD) nanofibers were shown in Figure 4.10.

Some fibers with bead defects were seen in the pure PCL nanofibers. However, The PCL/PEO and PCL/(PEO+SSD) composite nanofibers had smooth morphology without bead defects and greater fiber uniformity with less standard deviation (\pm SD) compared to pure PCL. This indicates that PCL and PEO blended homogeneously and phase separation did not occur during electrospinning. Additionally, blend of PCL, PEO and SSD molecules were bonded physically and had a good interaction in the composite fiber structure (Dubey & Gopinath, 2016). The photograph of the homogenous mixture of PEO and PCL was shown in Figure 4.1. The average diameter

was 220 ± 62 nm for pure PCL nanofibers, 372 ± 46 nm for PCL/PEO nanofibers and 354 ± 34 nm for SSD loaded PCL/PEO nanofibers.

Compared to drug-free PCL/PEO nanofibers (372 ± 46 nm), the SSD loaded composite nanofibers (354 ± 34 nm) had smaller fiber diameters with lower \pm SD. According to the literature, the reason is related to the presence of conductive SSD particles in the composite nanofibers (Lee et al., 2016). SSD is a silver salt and is conductive in nature. Electrospinning solution contains a high amount of charged silver and sulfadiazine ions by the addition of SSD into the PEO solution. It supplies more electric charges to the electrospinning jet in order to overcome the surface tension of the solution. The bead defects are formed on the fiber surface if the polymer jet is not fully stretched. Therefore, when SSD is added to the solution, the electrical conductivity of the solution increases, resulting in the stretching of the solution. Consequently, smooth fibers were formed and fiber diameter decreases with greater uniformity by cause of a high stretching force (Saquing et al., 2009). Thus, when compared to pure PEO (313 ± 67 nm) and the PEO-PCL (372 ± 46 nm) blended nanofibers, the SSD loaded PEO (297 ± 38 nm) and SSD loaded PCL/PEO (354 ± 34 nm) composite nanofibers diameters were smaller with less \pm SD. Moreover, the smaller diameter of SSD containing nanofibers can be related to following reasons: the uniform distribution of the SSD in the nanofiber matrix without aggregation and with strong physical bonding between polymer matrix and SSD as it was recently reported that the diameter of the nanofibers gradually decreased with an increase in the amount of silver sulfadiazine (Ullah et al., 2019b).

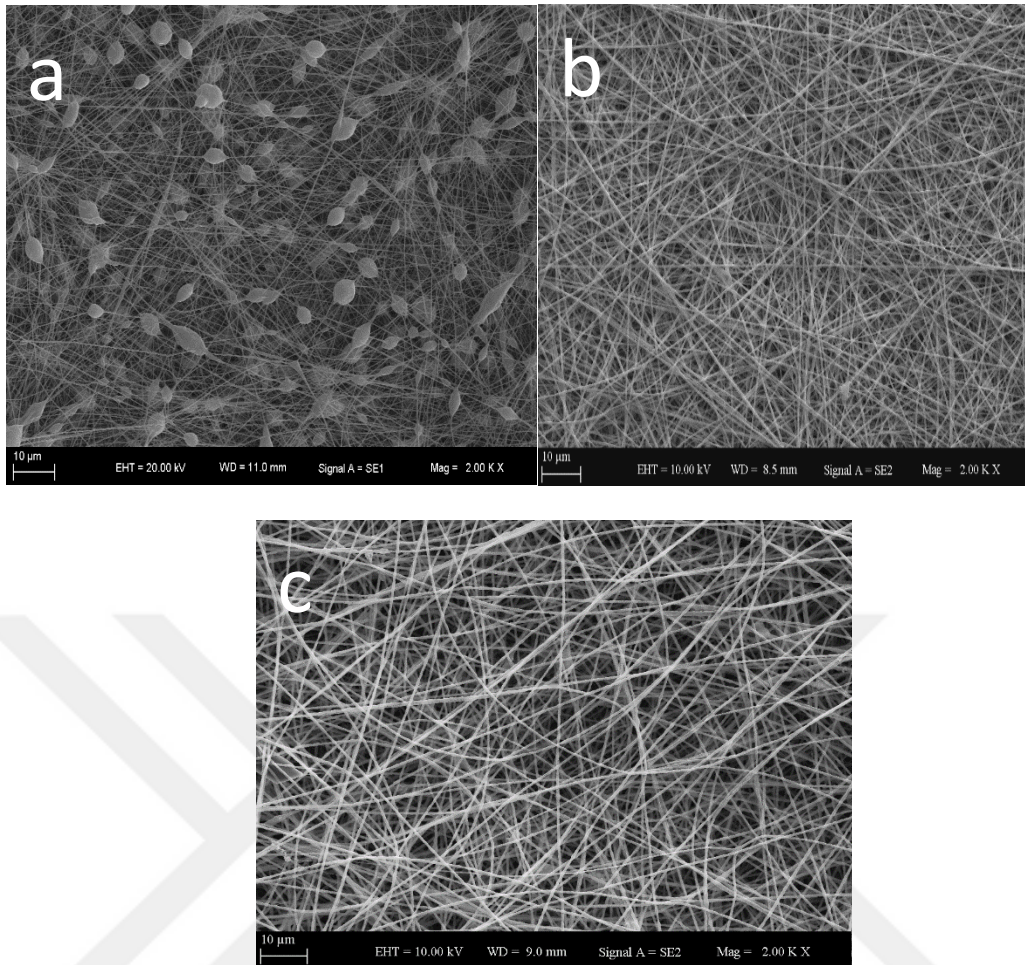


Figure 4.9 : General surface images of a) PCL and b) PCL/PEO c) PCL/(PEO+SSD) (at X 2000 magnification).

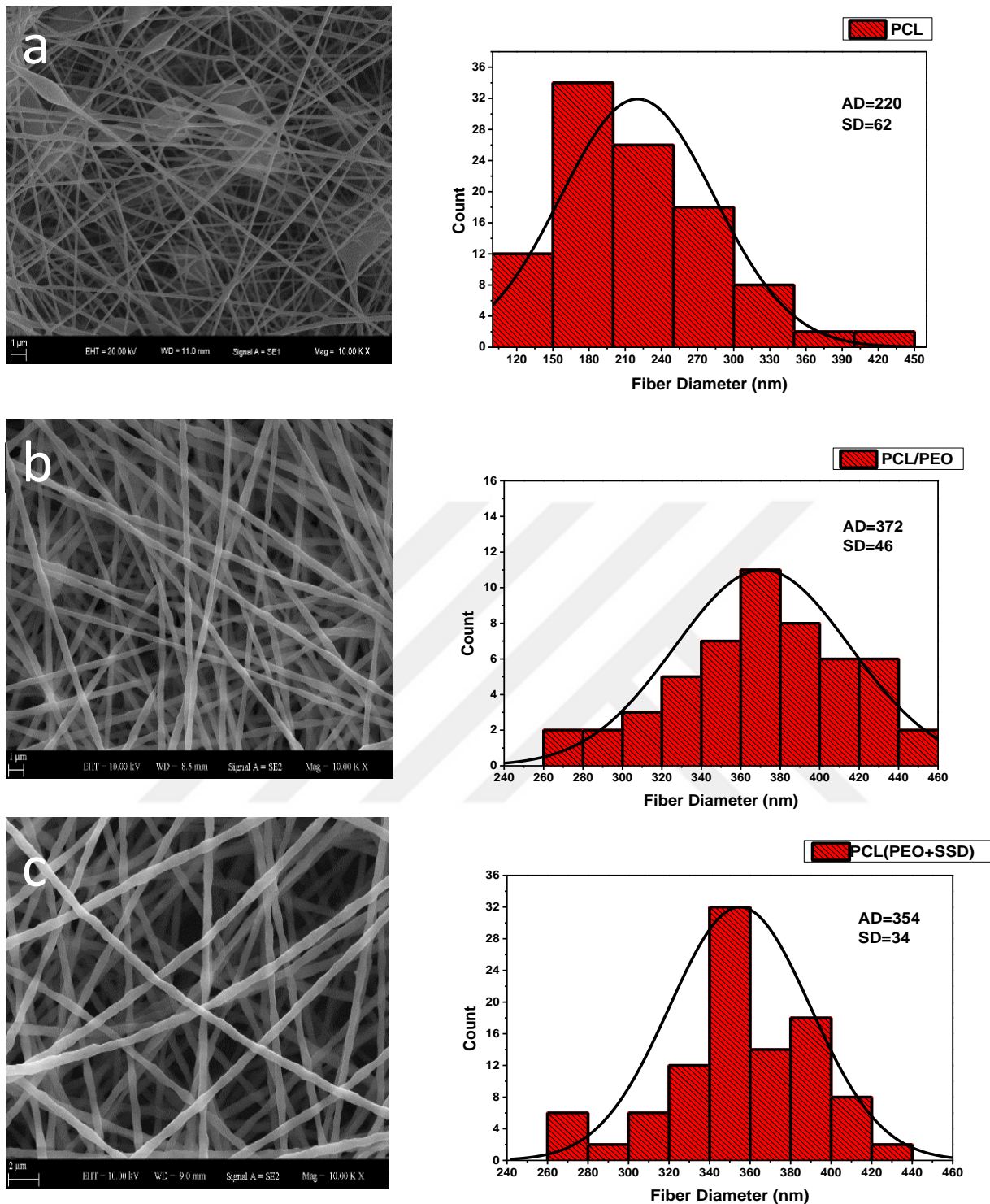


Figure 4.10 : SEM images and corresponding diameter distribution histograms of a) Pure PCL, b) PCL+PEO, c) PCL/(PEO+SSD) nanofibers.

4.6.1.3 Effect of viscosity on nanofiber morphology

Viscosity has reverse effects on the fiber diameter (Zeng et al., 2003). PCL solution has a lower viscosity than the PEO solution. PCL/ PEO blend solution exhibited higher viscosity compared to pure PCL solution. In agreement with the literature, the increase

of solution viscosity led to an increase in average fiber diameter from 220 nm (PCL) to 354 nm (PCL/PEO+SSD) and 372 nm (PCL/PEO). Furthermore, high viscosity solution promoted smooth fiber formation, for this reason, pure PCL nanofibers had bead defects whereas PCL/PEO had no beads (Souza et. al., 2018; Dubey & Gopinath, 2016). However, while the viscosity of the PEO+SSD was higher than the PEO solution, the diameter of PEO+SSD (297 ±38 nm) was smaller than pure PEO (313 ±67 nm) nanofibers. It shows that increased conductivity with the SSD addition was more effective than viscosity on the fiber diameter. In other words, the conductivity factor was more effective than the viscosity factor on the fiber diameters. The addition of SSD causes increased conductivity and contributes to the generation of nanofibers with smaller diameters. Viscosity values of the prepared solutions were shown in Table 4.6.

Table 4.6 : Viscosity values of electrospinning solutions.

| | PEO | PEO+SSD (1) | PCL | PCL/PEO (7:3) | PCL(PEO+SSD) (7:3) |
|-------------------------|------------------|----------------|----------------|---------------|--------------------|
| Viscosity (Pa.s) | 0.190 | 0.300 | 0.014 | 0.059 | 0.062 |
| Fiber Diameters (nm) | 313 ±67 nm | 297 ±38 nm | 220 ± 62 nm | 372 ±46 nm | 354 ±34 nm |

4.6.1.4 Water uptake

The water uptake was evaluated by immersing electrospun nanofiber patches in buffer solution at room temperature for 24 hours. The weight of the wet sample was measured after drying in incubator to remove the surface water. Swelling and surface destruction were investigated by SEM as shown in Figure 4.11. The water uptake percentage was calculated by *Equation 2* and was found 60 % ±8 as mean value.

In the equation; W_d is dried weight of the patch and W_w is the wet weight of the patch. Three nanofiber patches were examined to calculate water uptake percentage and the average value was recorded.

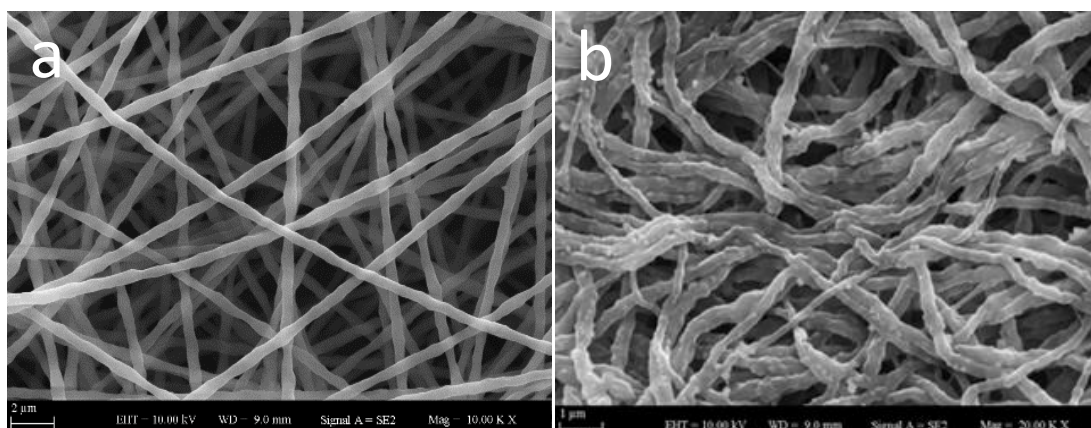


Figure 4.11 : SEM Images of PCL/(PEO+SSD) a) before and b) after immersing in buffer solution.

SEM images demonstrate that diameter of nanofibers increase due to swelling of PCL and smoothness of nanofibers is damaged because of destruction and polymer erosion of the PCL/PEO matrix. Moreover, the nanofiber structure shifted from straight to the entangled state.

SEM images demonstrate that diameter of nanofibers increase due to swelling of PCL and smoothness of nanofibers is damaged because of destruction and polymer erosion of the PCL/PEO matrix. Moreover, the nanofiber structure shifted from straight to the entangled state.

4.6.2 Elemental analyses of SSD loaded composite nanofibers

Energy dispersive spectra (EDS) analysis was performed to confirm that PCL/(PEO+SSD) nanofibers contain SSD, by detecting the Silver (Ag), Nitrogen (N), Sulphur (S) content of the nanofibers. Moreover, EDS-Mapping was carried out to show the distributions of these elements in composite nanofibers. SEM-EDS spectra and EDS-Mapping images of PCL/(PEO+SSD) composite nanofibers were seen in Figure 4.12. Elemental distributions of S, N and Ag atoms in the formulation with SEM-EDS Mapping Image were represented in Figure 4.13. The peaks of Ag, N, S within the EDS spectra indicate their presence in the fiber structure, indicating that the nanofiber mats are evenly loaded with SSD. The elemental distribution of the Ag, S, N is represented with their corresponding amount in Table 4.7. EDS-Mapping images demonstrated that SSD molecules were distributed homogeneously in the fiber structure without any aggregation.

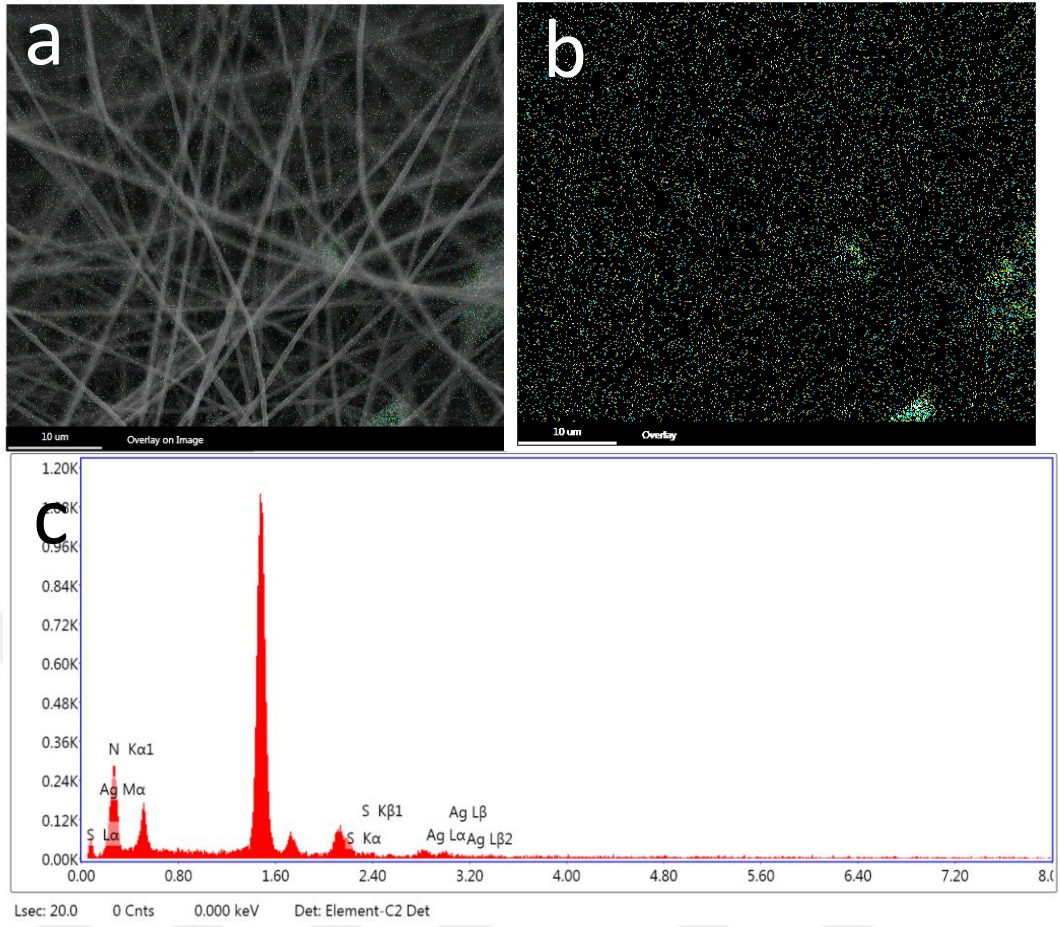


Figure 4.12 : EDS Mapping image (a,b) and spectra (c) of PCL/(PEO+SSD).

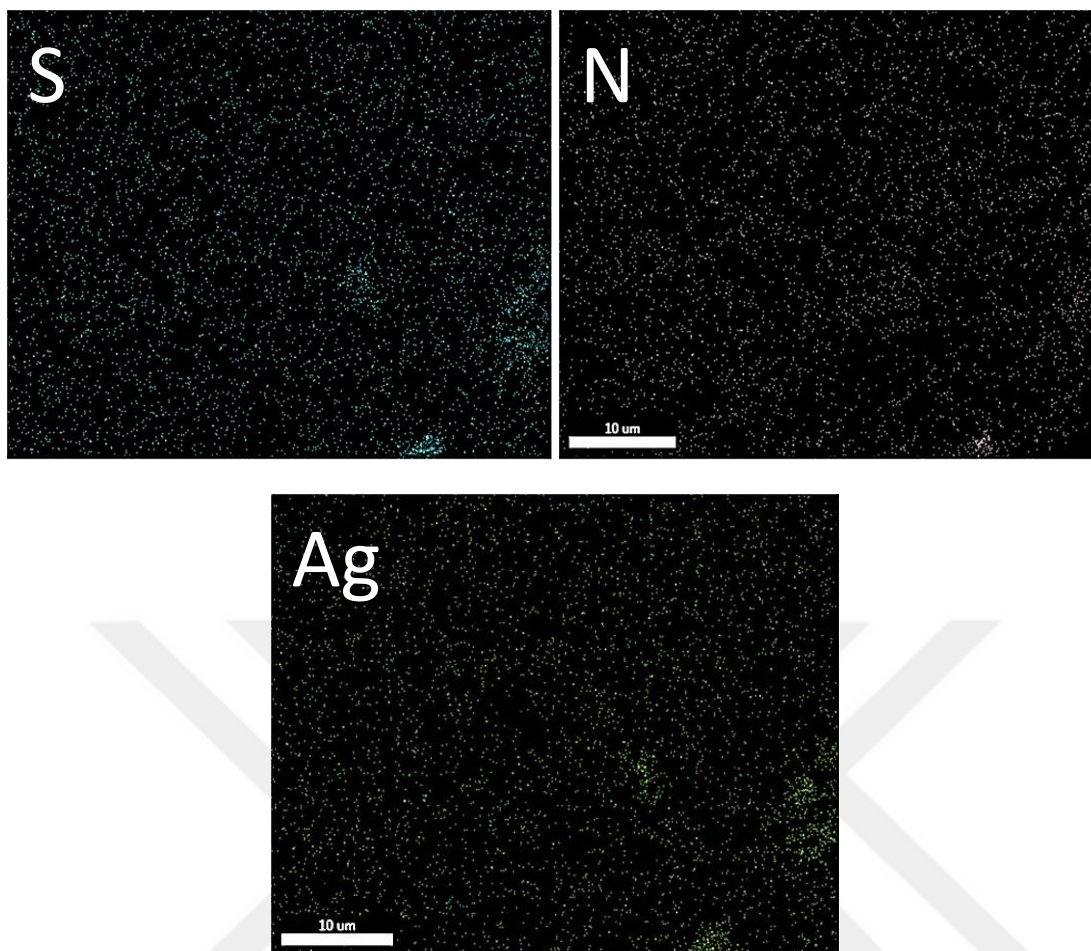


Figure 4.13 : Representation of elemental distribution of S, N and Ag atoms on formulation with SEM-EDS Mapping image.

Table 4.7 : Elemental distribution of Ag, S and N on EDS Mapping image.

| Elements | Ag | N | S |
|----------------|----|----|----|
| Distribution % | 30 | 31 | 39 |

4.6.3 Atomic Force Microscopy (AFM)

AFM was used to investigate the surface topography and to determine the surface roughness of the nanofibers. AFM Images of PCL/PEO was represented in Figure 4.15 and PCL/(PEO+SSD) was represented in Figure 4.16 with 3D images.

Very few nanofibers were electrospun on the cover glass for 20 second and the specimens were analysed. AFM Images shows the roughness structure of nanofibers. Moreover, it is determined that the surface roughness of the drug loaded nanofibers was higher than pure PCL/PEO nanofibers (from 150 to 200 nm). This can be attributed to the presence of SSD on the surface of the nanofibers as well as it presents inside the nanofibers.

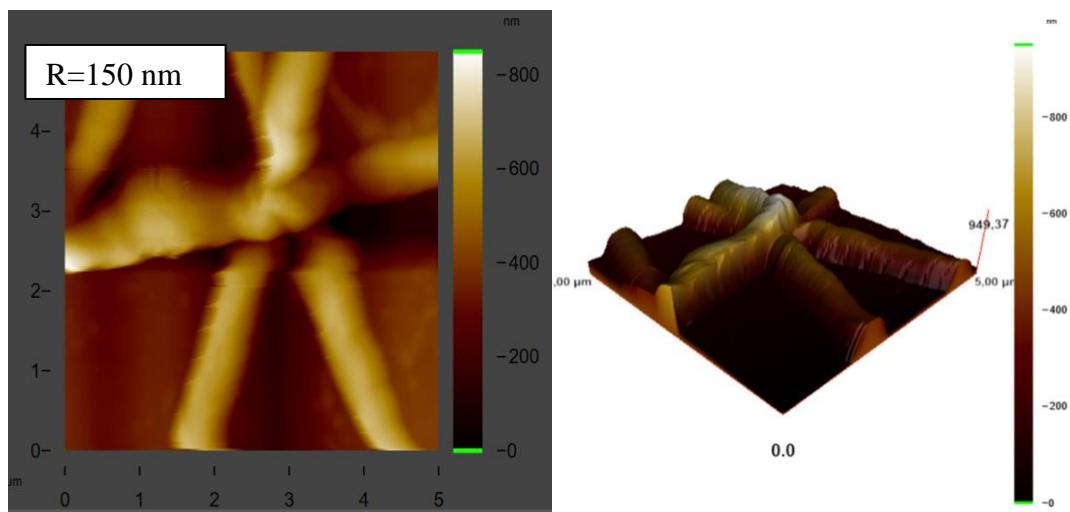


Figure 4.14 : AFM images of pure PCL/ PEO nanofibers.

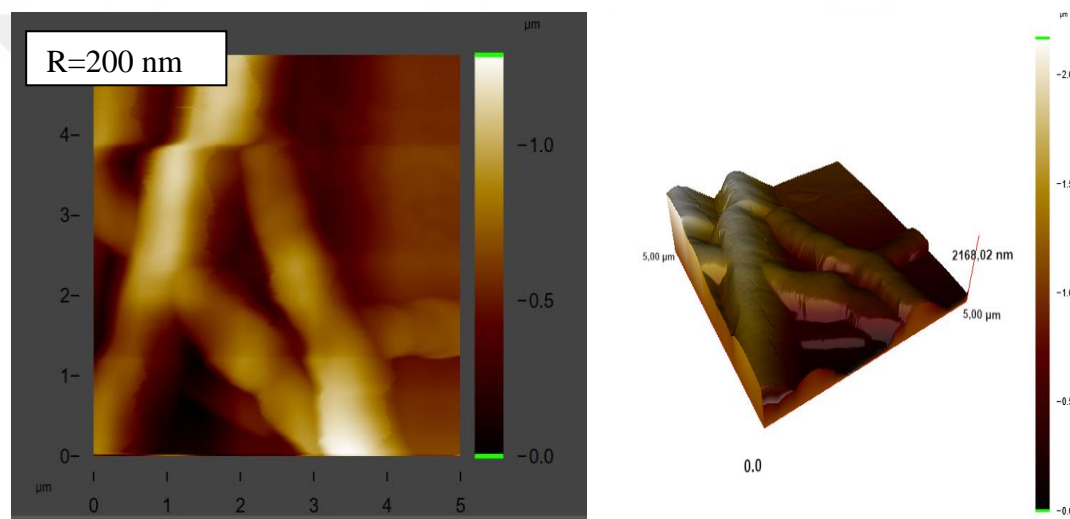


Figure 4.15 : AFM images of SSD loaded PCL/ PEO nanofibers.

4.6.4 Wettability-Contact angle measurements

Wettability is an important issue to perform for biomedical applications such as scaffolds, wound healing, tissue engineering and drug delivery systems as these biomaterials will contact with body fluid, blood, water, exudate etc. Water contact angle measurement is a widely used method for estimation the surface wettability of the materials (Madhaiyana et al., 2013). It gives a clear idea about hydrophilicity or hydrophobicity of material surface. In this study, because of the inherent hydrophilic nature of the PEO polymer, there was a necessity to combine it with a hydrophobic polymer. For this reason, a well-known hydrophobic polymer PCL was added to the PEO. Wettability of PCL, PEO, PCL/PEO, PCL/PEO+SSD were evaluated with contact angle measurements. Contact angle test photographs were shown in Figure 4.17 and contact angle values were given as graph in Figure 4.18.

When PEO nanofiber patch contacts with water, because of its super hydrophilic nature, PEO patch is spread on the surface immediately. For this reason, contact angle of the pure PEO nanofibers could not be measured. On the other hand, PCL is a very hydrophobic polymer and it has low wettability. Therefore, using PCL alone is a challenge in biomedical field because there is a necessity of contact with body fluids of the material. Stabilization of the polymer matrix was done by blending PEO with a hydrophobic PCL polymer. Otherwise, there is no important difference but the contact angle values of the drug-free composite nanofibers were lower than the SSD loaded composite nanofibers. This can be attributed to the hydrophobic characteristic of SSD that decreased the surface hydrophilicity of the formulation.



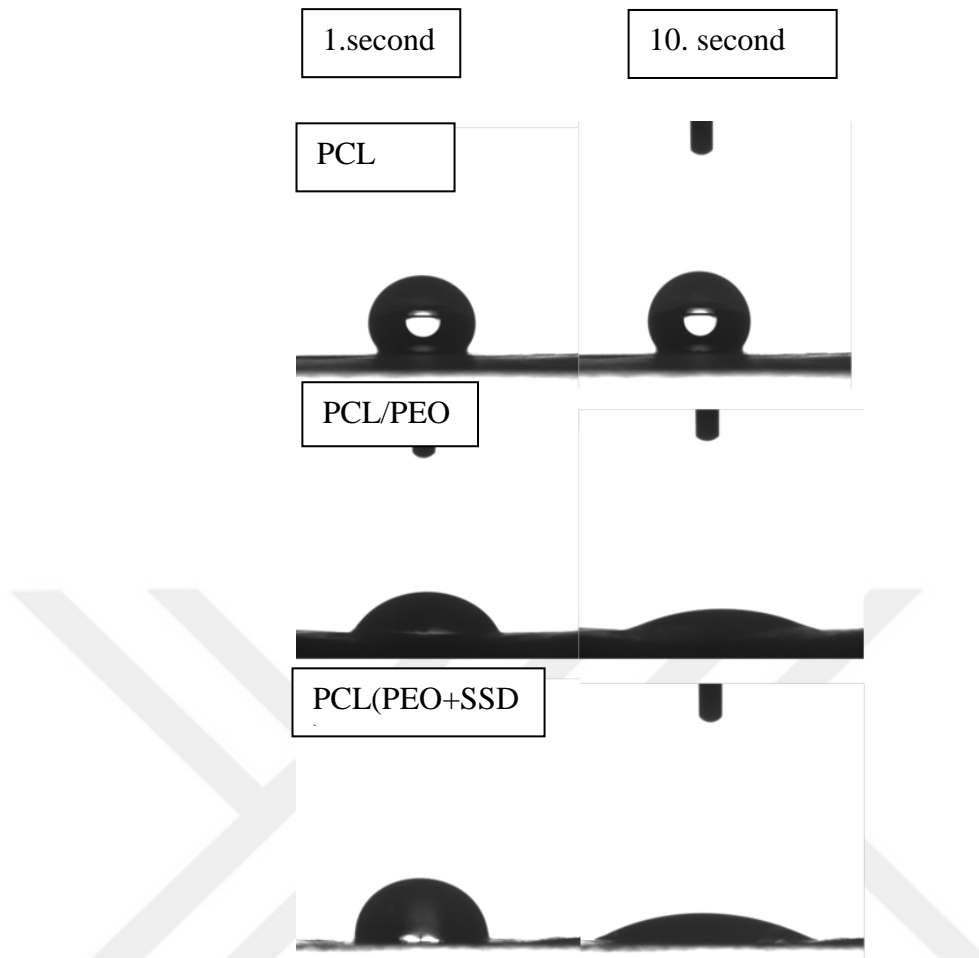


Figure 4.16 : Contact angle photographs of nanofibers.

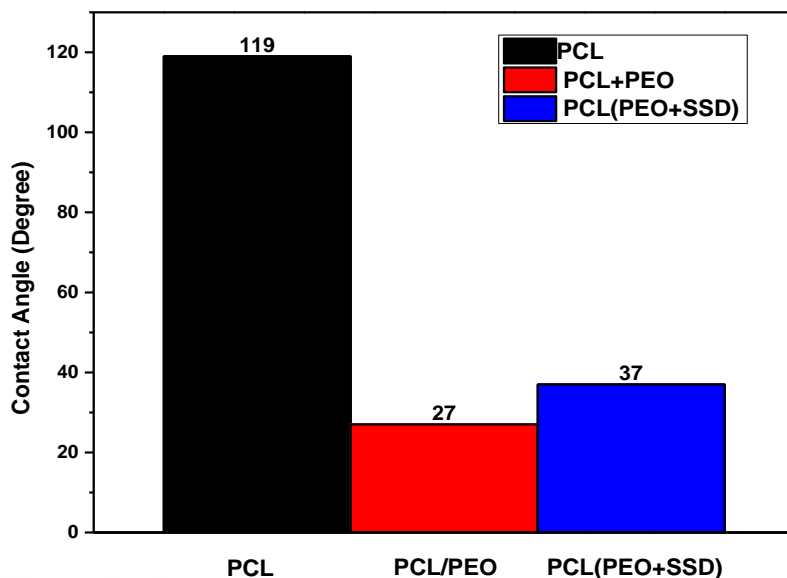


Figure 4.17 : Contact Angle values of nanofibers.

4.6.5 X-ray diffraction (XRD) study

X-ray diffraction (XRD) analysis was performed to examine the crystalline structure of the SSD loaded electrospun nanofibers. XRD pattern of silver sulfadiazine powder and PEO+SSD, PCL/PEO, PCL/(PEO+SSD) nanofiber patches were shown in Figure 4.19.

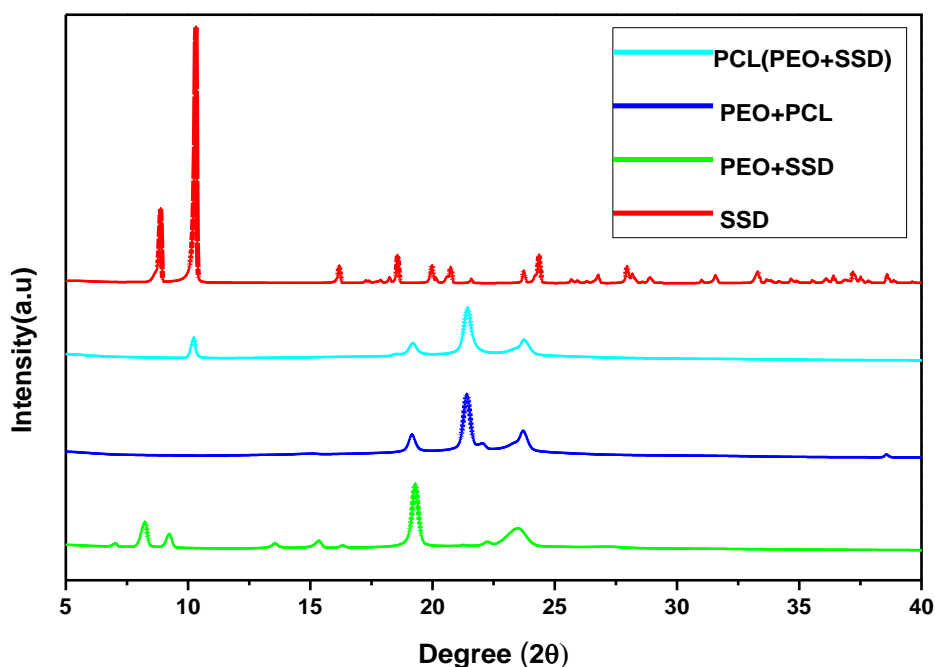


Figure 4.18 : XRD pattern of SSD, PEO+SSD, PEO+PCL and PCL (PEO+SSD) nanofibers.

SSD showed its characteristic peaks at around $2\theta = 8.8^\circ$ and 10.2° corresponding to the (0 0 2), (0 1 1) planes as explained in literature (Aguzzi et al., 2014; Ghodekar et al., 2012; Luan et al., 2012). X-ray diffraction (XRD) pattern of PEO+SSD nanofibers showed diffraction peaks of semicrystalline PEO at $2\theta = 19^\circ$ and 23° interrelated to the (1 2 0) and (0 3 2) helical structure of the PEO crystal. Also, in the pattern of PEO+SSD, SSD was confirmed with its distinctive peaks, which were shifted from 8.8° to 8.2° and 10.2° to 9.3° , respectively. The XRD pattern of PCL/PEO nanofibers represented the diffraction peaks of semicrystalline PCL at $2\theta = 21^\circ$ and $2\theta = 23^\circ$ associated with the (1 1 0) and (2 0 0) crystallographic planes of the PCL crystal (Oliveira et al., 2013; Yao et al., 2015; Li et al., 2014).

The XRD pattern of SSD loaded PCL/PEO nanofibers exhibited microcrystalline nature of SSD, by the distinctive one single peak at 10.2° . However, the other distinctive peak of SSD at 8.8° did not appear in the diffraction pattern of PCL/(PEO+SSD) whereas it appears in PEO+SSD with shifting to 8.2° . This is related to the addition of PCL that decreases the percentage of SSD in the formulation. Moreover, the weak peak at $2\theta = 8.8^\circ$ totally disappeared while the stronger peak at $2\theta = 10.2^\circ$ was still observed in the XRD pattern. PCL/(PEO+SSD) formulation showed the characteristic peak of SSD at 10.2° with a low intensity that points out the loss in crystallinity. Moreover, loaded SSD into the nanofiber matrix was crystalline with reduced crystallinity determining that structural stability of SSD was achieved during electrospinning.

4.6.6 Attenuated Total Reflectance Infrared (FTIR-ATR) spectroscopy analysis

The stability of SSD in the fiber structure and the molecular interactions in the drug-free and drug loaded nanofibers were examined by Attenuated Total Reflectance Infrared (FTIR-ATR) Spectroscopy. FTIR-ATR spectra of silver sulfadiazine powder and PCL, PEO nanofibers and interaction between PCL, PEO, and Silver sulfadiazine were shown in Figure 9a; PEO+SSD, PCL/PEO, PCL/(PEO+SSD) nanofiber patches were shown in Figure 9b.

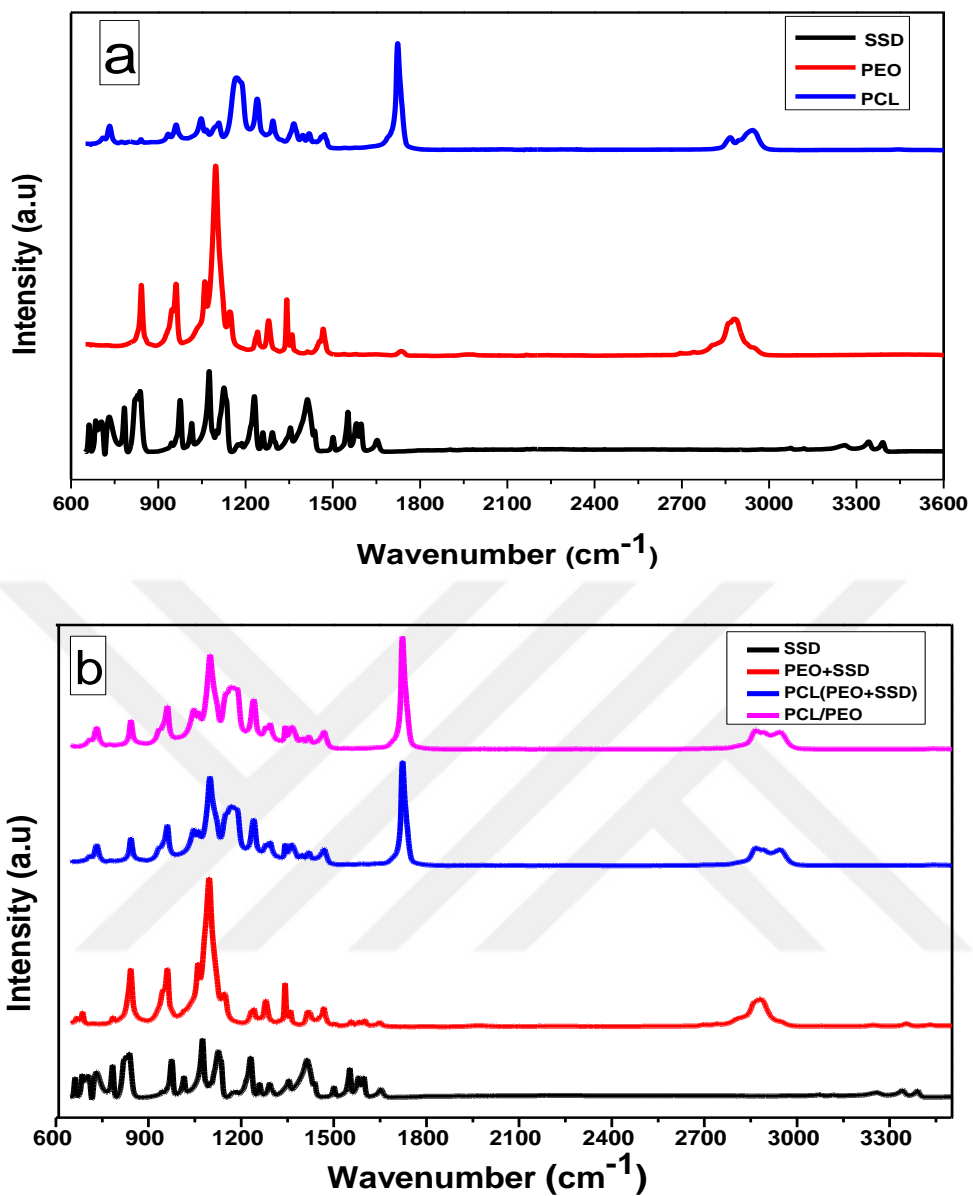


Figure 4.19 : FTIR -ATR Spectra of a) SSD, PCL, PEO and b) PEO+SSD, PCL/PEO, PCL/(PEO+SSD) nanofibers.

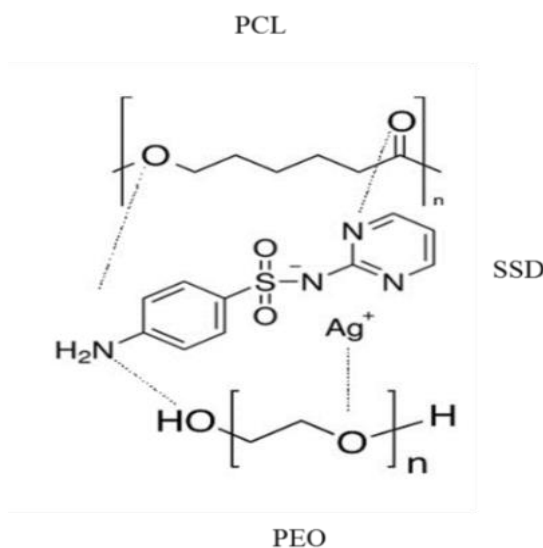


Figure 4.20 : Interaction between PCL, PEO and SSD.

SSD presented peaks at 3343 and 3393 cm^{-1} were due to the amine (NH_2) stretching mode. Exhibited peaks at 1651 cm^{-1} associated with NH_2 bending, at 1595, 1581, 1552 and 1500 cm^{-1} were attributed to the aromatic $\text{C}=\text{C}$ stretching, at 783, 1016, 1356 cm^{-1} were due to the asymmetric and at 1124 cm^{-1} conjugated to the symmetric stretching of SO_2 (Ghodekar et al., 2012; Patel et al., 2019; Zepon et al., 2014). Finally, the peaks exhibited at around 1230 cm^{-1} conjugated to aromatic $\text{C}-\text{N}$ stretching and at 1075 cm^{-1} corresponding to aromatic vibrations.

All characteristic peaks of PEO appeared at around 2880-2885 cm^{-1} due to $\text{C}-\text{H}$ stretching vibration, at 1465 cm^{-1} attributed to CH_2 scissoring vibration, at 1360 and 1340 cm^{-1} associated with wagging vibration of CH_2 , at 1280 cm^{-1} due to CH_2 twisting vibration, at 840 cm^{-1} and 960 cm^{-1} belonging to CH_2 rocking vibrations. Also, the semicrystalline structure of PEO was observed by the triplet peak of $\text{C}-\text{O}-\text{C}$ stretching vibrations at 1147, 1100, and 1060 cm^{-1} (Aguzzi et al., 2014).

Typical peaks for the PCL were seen at 2949, 2865 and 730 cm^{-1} corresponding to the asymmetric stretching, symmetrical stretching and long-chain rocking motion of vibrations of CH_2 . The peak at 1730 cm^{-1} conjugated to $\text{C}-\text{O}$ carbonyl stretching mode; at 1471 cm^{-1} , 1397 cm^{-1} , and 1365 cm^{-1} belonging to CH_2 bending modes. Also, $\text{C}-\text{O}$ and $\text{C}-\text{C}$ stretching vibrations at 1293 cm^{-1} , $\text{C}-\text{O}-\text{C}$ stretching vibrations at 1240 cm^{-1} , 1169 cm^{-1} , 1108 cm^{-1} , and 1048 cm^{-1} were shown (Hu et al., 2018; Narayanan et al., 2015). The peaks at 3431 cm^{-1} and 1640 cm^{-1} are associated with $-\text{OH}$ and the carboxyl ($\text{C}-\text{O}$) stretching. The peaks exhibited at 1026 and 1074 cm^{-1} correspond to the

asymmetric vibration of C-O-C. The peak at around 1730 cm^{-1} could be related to the ester bond in PCL (Oliveria et al., 2013; Yao et al., 2015; Zander et al., 2013).

SSD loaded PEO nanofibers represented the specific peaks of SSD at 784 cm^{-1} due to the asymmetric stretching of SO_2 , at 1583 and 1556 cm^{-1} attributed to aromatic C=C stretching, 1649 cm^{-1} conjugated to NH_2 stretching. Drug-free PCL/PEO nanofibers were not influenced significantly by the addition of SSD in PCL/PEO nanofibers. This means SSD bounded to polymer matrix physically and overall symmetry of the SSD molecule did not significantly change in the electrospun nanofiber matrix (Xue et al., 2014).

4.6.7 Loading efficiency, drug release profile and kinetics

The drug loading efficiency of nanofibers was calculated by *Equation 1* and was found to be $86\% \pm 5$ on average.

Percentage cumulative drug release was determined via the amount of SSD present in the composite nanofiber formulation and the plot was shown in Figure 4.22 for cumulative release % vs time. It was also observed that nanofiber formulations were stable in buffer media over 24 hours. PCL/PEO nanofibers were blended homogeneously so that smooth, continuous and uniform fiber morphology were obtained (Figure 4.10) and phase separation did not occur during electrospinning. In addition, the photograph of the homogeneous mixture of PEO and PCL was shown in Figure 4.1. Due to the good composition of PCL and PEO in the fiber matrix, composite nanofiber formulation exhibited one phase release kinetics hence biphasic release kinetics were not observed in the drug release profile.

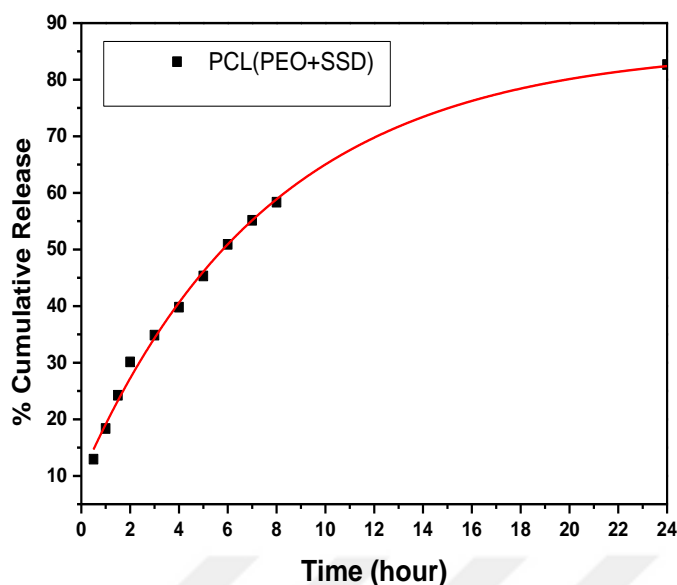


Figure 4.21 : Cumulative release % of SSD from PCL/(PEO+SSD) nanofibers.

The SSD showed an initial release of approximately 15 % which could be due to the adhered particles to the nanofiber surface and also the high dissolution rate of the PEO polymer (Dubey & Gopinath, 2016). The initial release was followed by sustained release of SSD which was around 58 % ± 2 in 8 hours. Afterwards, the controlled release of SSD was proceeded up to 24 h and it was around 82 % ± 4 , exhibiting a retarded rate of release.

Commercial products of SSD in the form of creams are applied on the targeted areas of skin topically two to four times a day. The control of drug release provides increment in the therapeutic efficiency of treatment and to improve the patient comfort with reducing the number of applications (El-Feky et al., 2017; Ghedini et al., 2017). The amount of drug released from the composite PCL/(PEO+SSD) nanofiber patch increased over time. After 24 hours, approximately 82 % of the drug was released from the nanofiber formulation. Generally, for burn healing applications, drug carriers should be able to fast and gradual degradation thus leading to action than with a slower and sustained progress (Heo et al., 2018; Mohseni et al., 2016; Heo et al., 2013). Hence, hydrophilic and hydrophobic polymer combinations were utilized in the drug carrier matrix (Heunis & Dicks, 2010; Hanumantharao & Rao, 2019).

Both diffusion and polymer degradation are key factors in controlling the drug release of SSD from the PCL/PEO nanofiber matrix. Highly soluble and degradable PEO rapidly induces the SSD release whereas hydrophobicity and slow degradation rate of

PCL provide a gradual release of SSD (Yoo et al., 2009). Moreover, the high surface area of nanofibers enhances the drug dissolution. Basically, the micro-porous structure of PCL/PEO nanofibers enables the drug diffusion from the matrix in two steps: one is the buffer diffusion into the pores to dissolve the SSD drug and the second one is the diffusion of dissolved drug to the outer of the pores. Therefore, the controlled drug release from nanofiber is associated with its micro-porous structure which balances the free access of the buffer into the matrix and diffusion of SSD out of the matrix (Garg et al., 2014).

To understand the SSD drug release mechanisms from SSD loaded composite nanofiber; Zero Order, First Order, Higuchi, Hixon Crowell and Korsmeyer-Peppas kinetics models were applied in the drug release profile. The regression coefficients (R^2) according to different kinetic models are given in Table 4.8.

Table 4.8 : Drug release kinetics models for PCL/(PEO+SSD) nanofibers with regression coefficient (R^2).

| Release Kinetics Models | R^2 |
|-------------------------|--------------------|
| Zero Order | 0.815931598 |
| First Order | 0.58881582 |
| Hixon Crowell | 0.669240218 |
| Higuchi | 0.965408626 |
| Korsmeyer-Peppas | 0.995978862 |

The result best fits with the Korsmeyer-Peppas model that indicates the regression coefficient $R^2 = 0.995$. This mathematical model describes the drug release with the following formula as:

$$M_t / M_\infty = k t^n \quad (3)$$

M_t/M_∞ is the released amount of drug at time (t), M_∞ is the total released amount of drug after time ∞ (total drug amount in the formulation), n is the drug release exponent which defines the release mechanism, k is the constant of the release rate. Hence, the exponent of n was found as 0.544. For the cylindrical-shaped matrices; $0.45 \leq n$ represents Fickian diffusion mechanism and non-Fickian or anomalous transport exhibits when $0.45 < n < 0.89$, $n = 0.89$ corresponding to Case II (relaxational) transport and $n > 0.89$ indicates super case II transport (Gouda et al., 2017). In this

work, the release profile value of n is higher than 0.45, pointing clearly to the non-Fickian mass transport mechanism, which means that diffusion and dissolution are the key factors of the drug release mechanism for SSD loaded composite nanofibers.

4.6.8 Controlling the drug release with conductivity

Drug release studies were also verified with conductivity measurement due to the conductive nature of SSD. At predetermined time intervals of 0.5, 1, 1.5, 2, 3, 4, 5, 6, 7, 8 and 24-hour 1.5 mL aliquots were sampled. The conductivity of aliquots was measured using Multiparameter meter InoLabMulti 720 (WTW) at room temperature.

Conductivity of aliquots versus time plot was represented in Figure 4.23. It is shown that the conductivity increased with time. The reason is related to the release of conductive SSD particles from nanofiber matrix to the buffer solution. SSD is a silver salt and is conductive in nature. Therefore, when SSD is released to the buffer solution, the electrical conductivity of the solution increases with time.

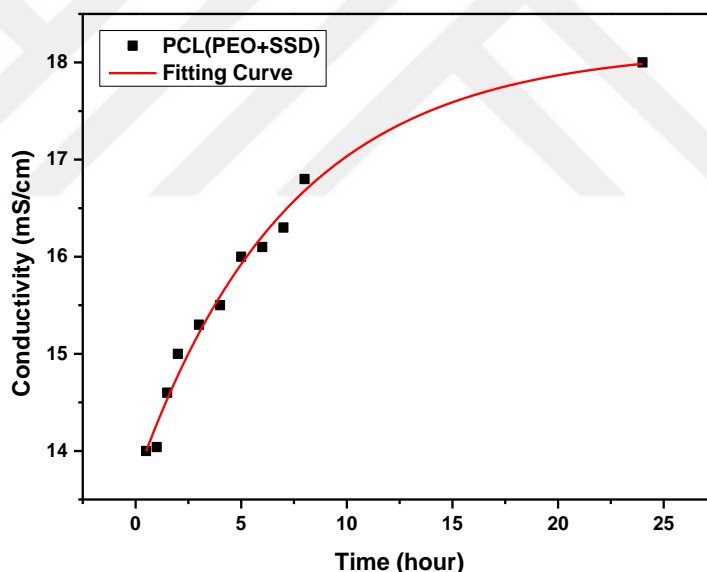


Figure 4.22 : Conductivity measurement of the released aliquots versus time.

4.7 Measurements and Characterization Studies of PCL/(PEO+SSD) Film Casting Formulations

SEM, SEM-EDS, SEM-EDS Mapping, optical profilometer and contact angle measurements were performed to characterize PEO, PEO+SSD, PCL, PCL/PEO and PCL/(PEO+SSD) casting films.

4.7.1 SEM Analysis of the PEO, PEO+SSD, PCL, PCL/ PEO, PCL/(PEO+SSD) casting films

Surface morphology is an important parameter for drug delivery systems. Therefore, SEM analysis was performed for the morphological characterization of the casting films. SEM images of casting films were represented in Figure 4.24 and 4.25. The SEM images showed that, film defects decrease addition of PCL polymer into the PEO solution. Also compared to pure film, SSD loaded films have less defects.

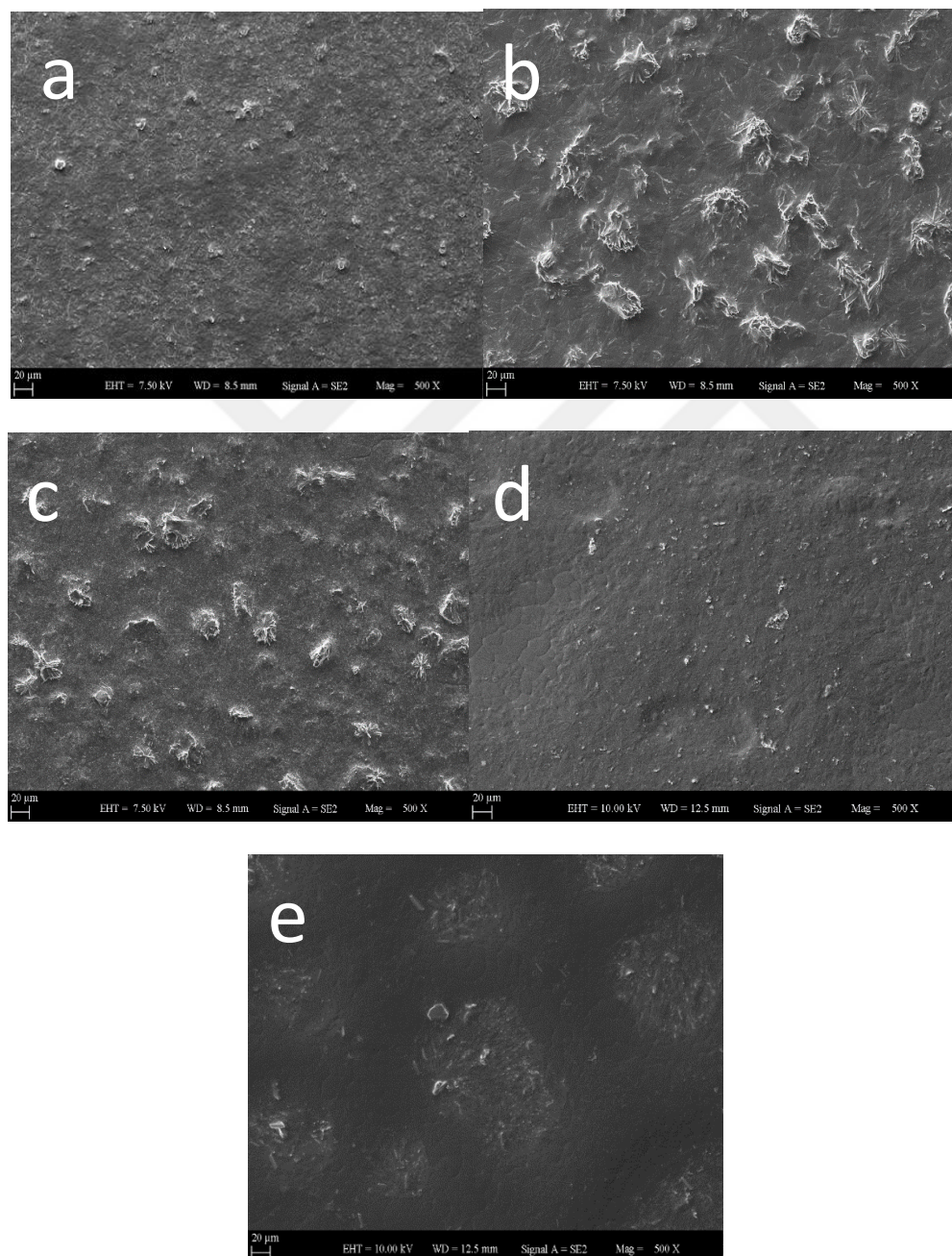


Figure 4.23 : SEM Images of a) PEO, b) PEO+SSD, c) PCL, d) PCL/PEO, e) PCL/(PEO+SSD) casting films (at X500 magnification).

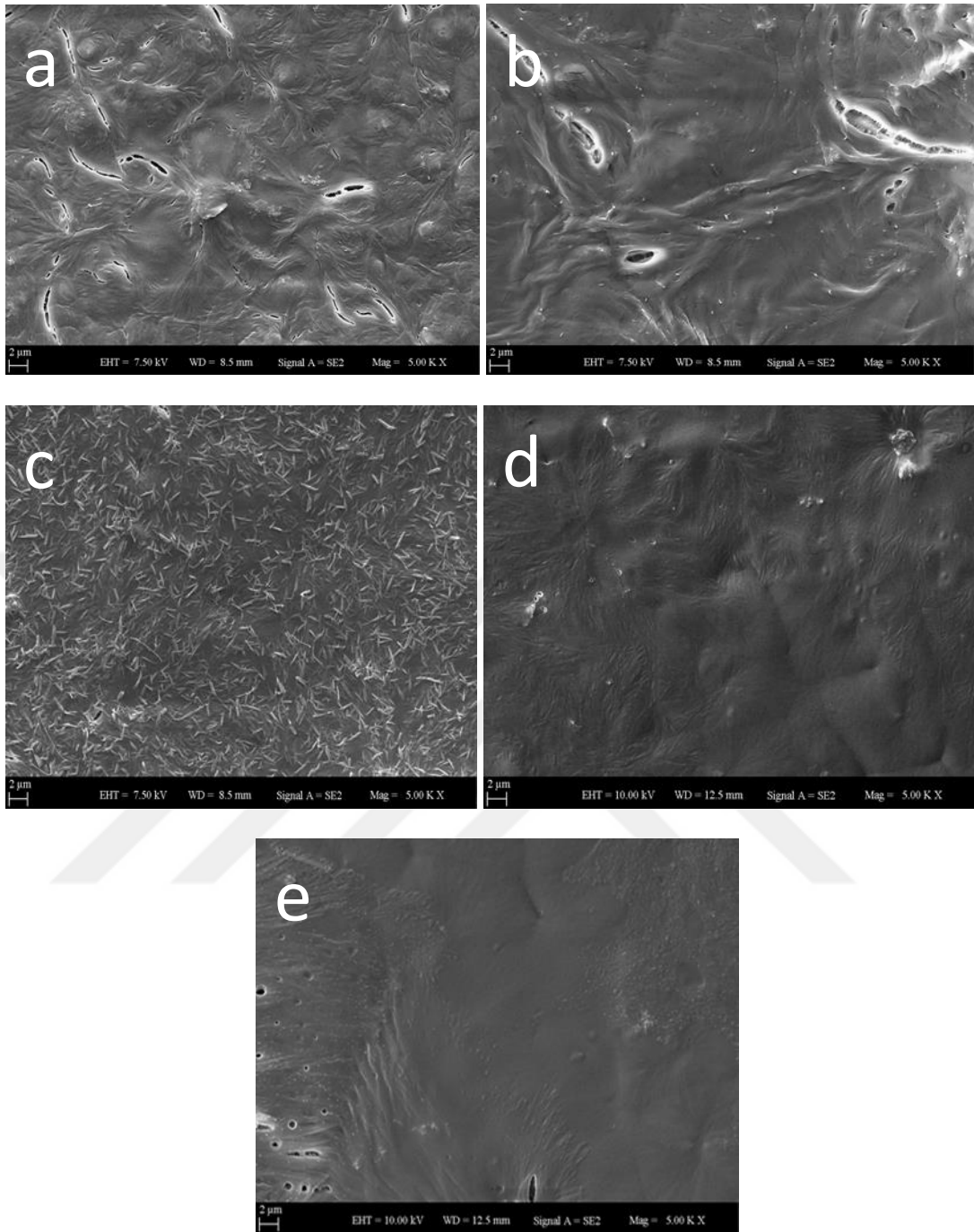


Figure 4.24 : SEM Images of a) PEO, b) PEO+SSD, c) PCL, d) PCL/PEO, e) PCL/(PEO+SSD) casting films (at X5000 magnification).

4.7.2 Elemental analysis of PCL/(PEO+SSD) casting film

Energy dispersive spectra (EDS) analysis was performed to confirm that PCL/(PEO+SSD) casting films contain SSD, by detecting the Silver (Ag), Nitrogen (N), Sulphur (S) content of the casting films. Moreover, EDS-Mapping was carried out to show the distributions of these elements. SEM-EDS spectra and EDS-Mapping images of PCL/(PEO+SSD) casting films can be seen in Figure 4.26. The peaks of Ag,

N, S within the EDS spectra indicate their presence in the film structure, indicating that the films are evenly loaded with SSD. Elemental distribution of S, N and Ag atoms on formulation with SEM-EDS Mapping Image was represented in Figure 4.27.

The elemental distribution of the Ag, S, N is represented with their corresponding amount in Table 4.9. EDS Mapping images showed that SSD molecules were distributed in the film structure with some agglomeration, not as homogeneously as in the fiber structure.

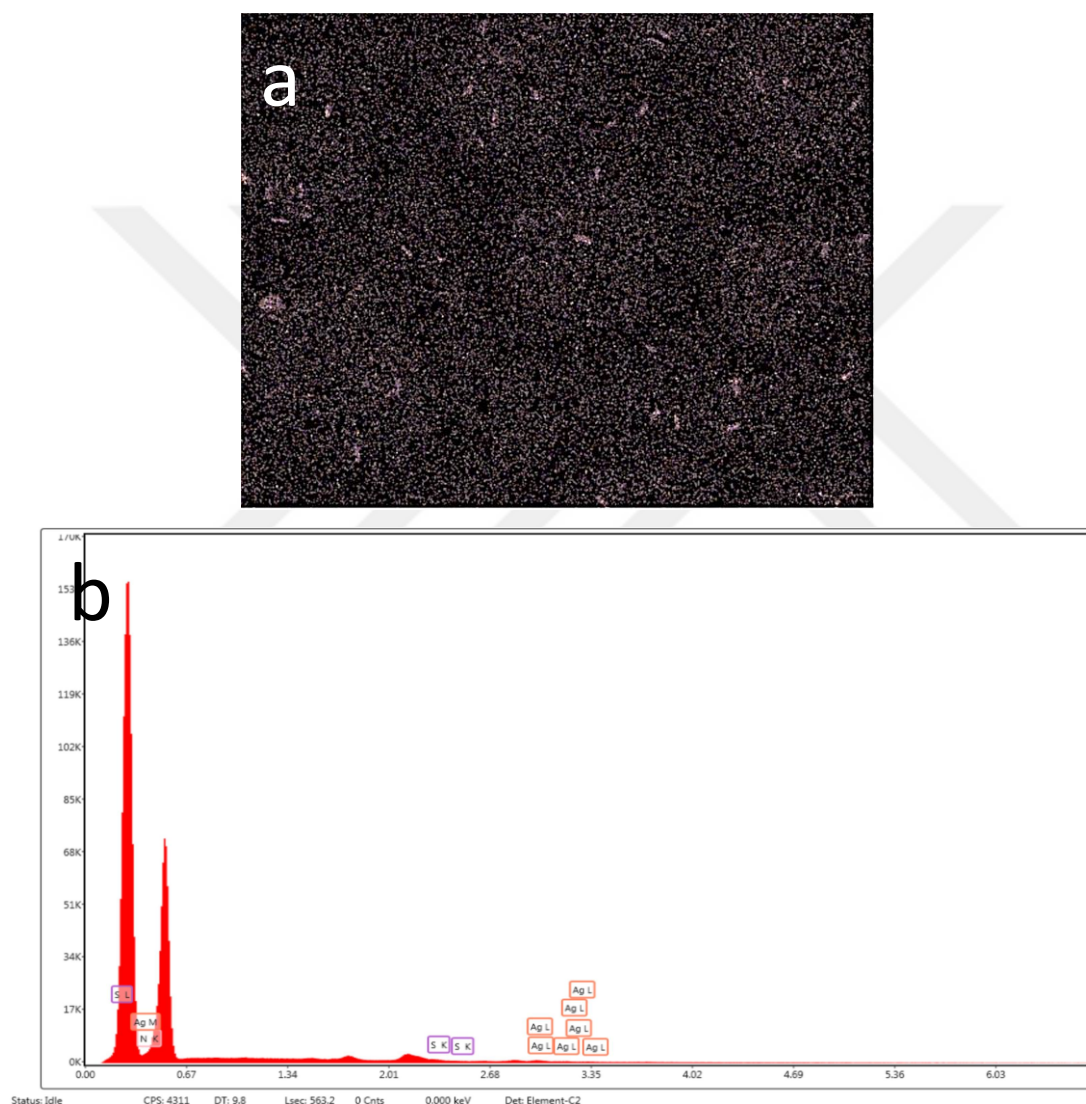


Figure 4.25 : EDS Mapping image (a) and Spectra (b) of PCL/(PEO+SSD) casting film.

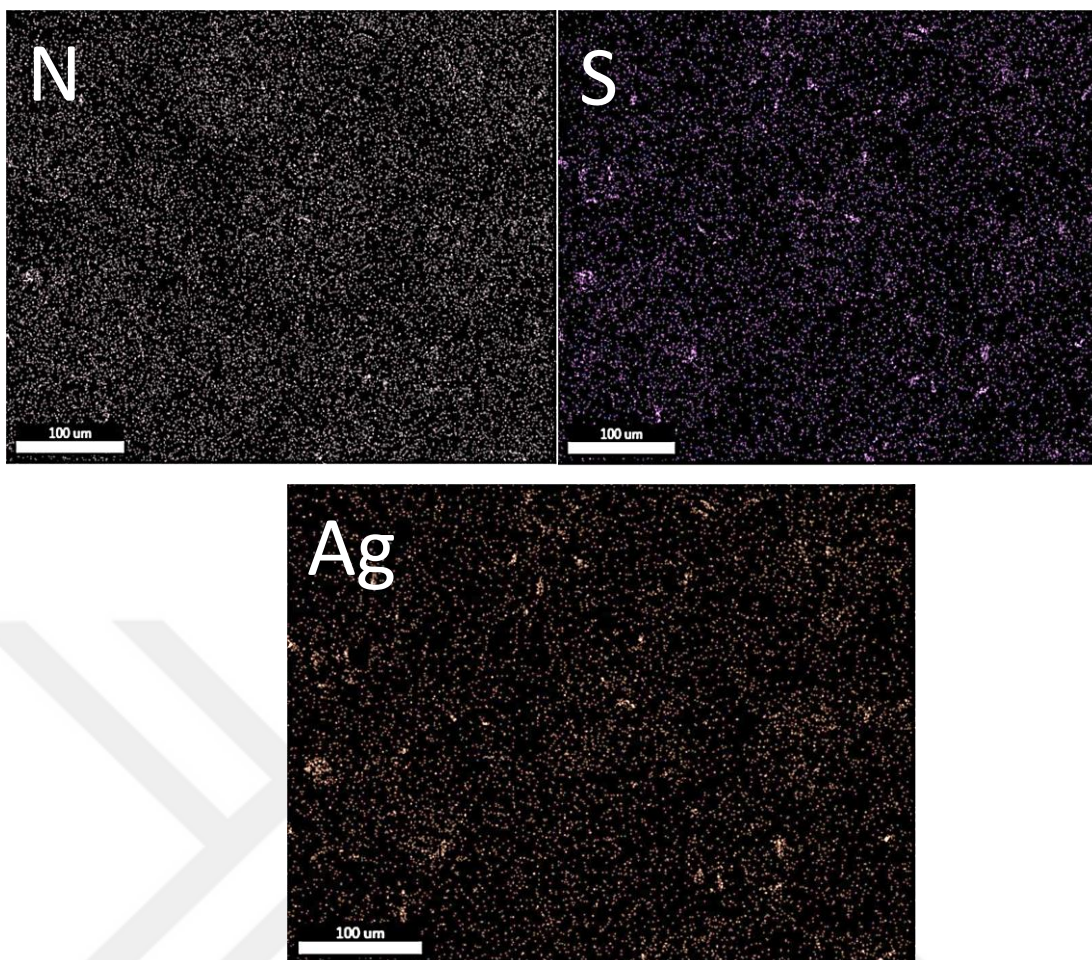


Figure 4.26 : Representation of elemental distribution of S, N and Ag atoms on formulation with SEM-EDS Mapping image.

Table 4.9 : Elemental distribution of Ag, S and N on EDS Mapping image.

| Elements | Ag | N | S |
|----------------|----|----|----|
| Distribution % | 21 | 50 | 29 |

4.7.3 Optical Profilometer analysis

The surface roughness was determined with Optical Profilometer. The dried samples were analysed using Optical Profilometer. It is seen that surface roughness values of the drug loaded films were greater than the drug-free films. In other words, the roughness value increased with the presence of SSD. This can be attributed to the presence of SSD on the surface of the film as well as it presents inside the film. Optical profilometer images are seen in Figure 4.28 and the roughness values are represented in Table 4.10.

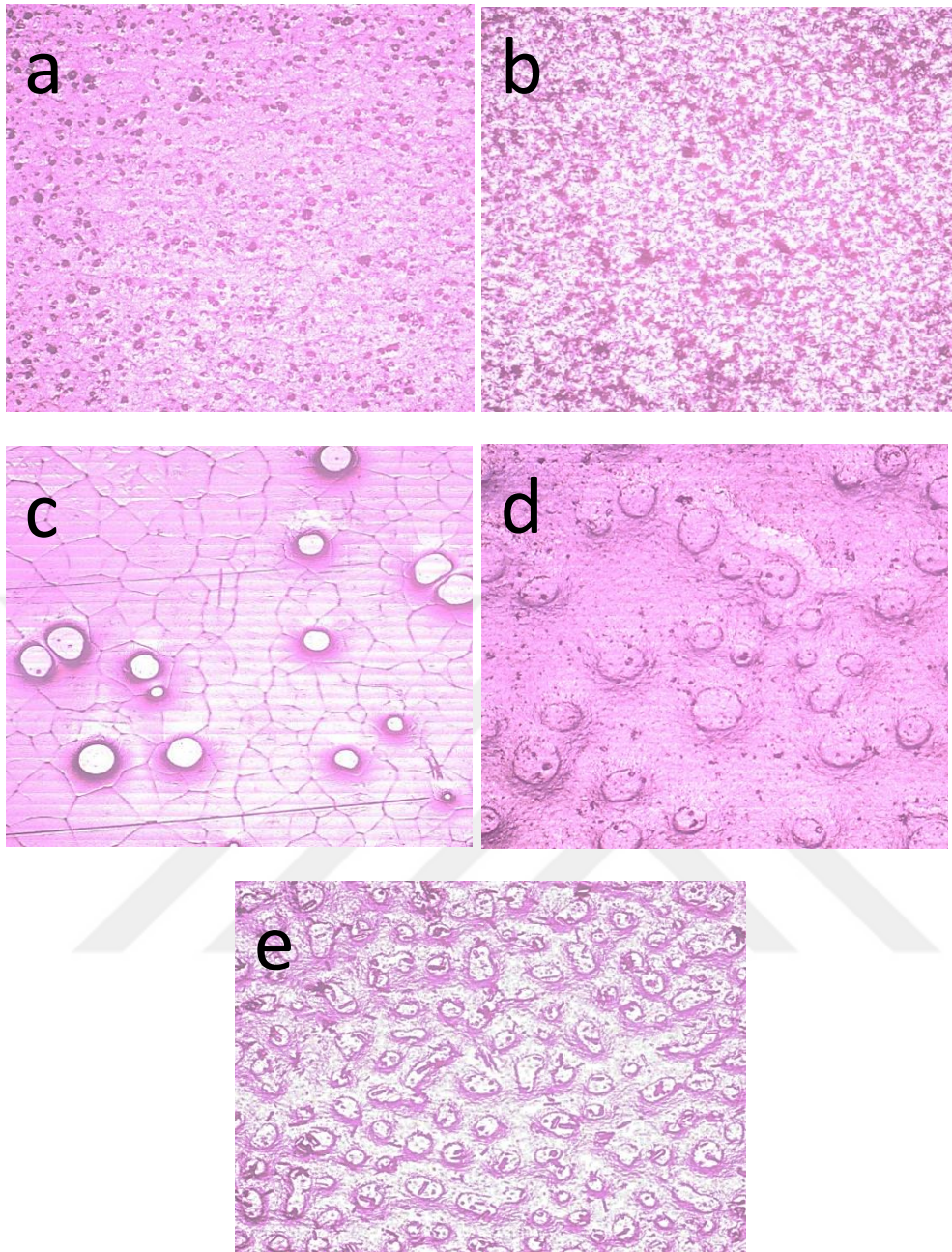


Figure 4.27 : Optical profilometer images of PEO, PEO+SSD, PCL, PCL/PEO and PCL/(PEO+SSD) casting films.

Table 4.10 : Roughness values of the casting films.

| Samples | PEO | PEO+SSD | PCL | PCL/PEO | PCL(PEO+SSD) |
|-----------------------------|-----|---------|-----|---------|--------------|
| Roughness (μm) | 3.7 | 5.3 | 5.5 | 3 | 4.1 |

4.7.4 Wettability-Contact angle measurements

Wettability studies were performed to measure contact angles of the samples. Contact angle test photographs were shown in Figure 4.29 and contact angle values were given as graph in Figure 4.30.

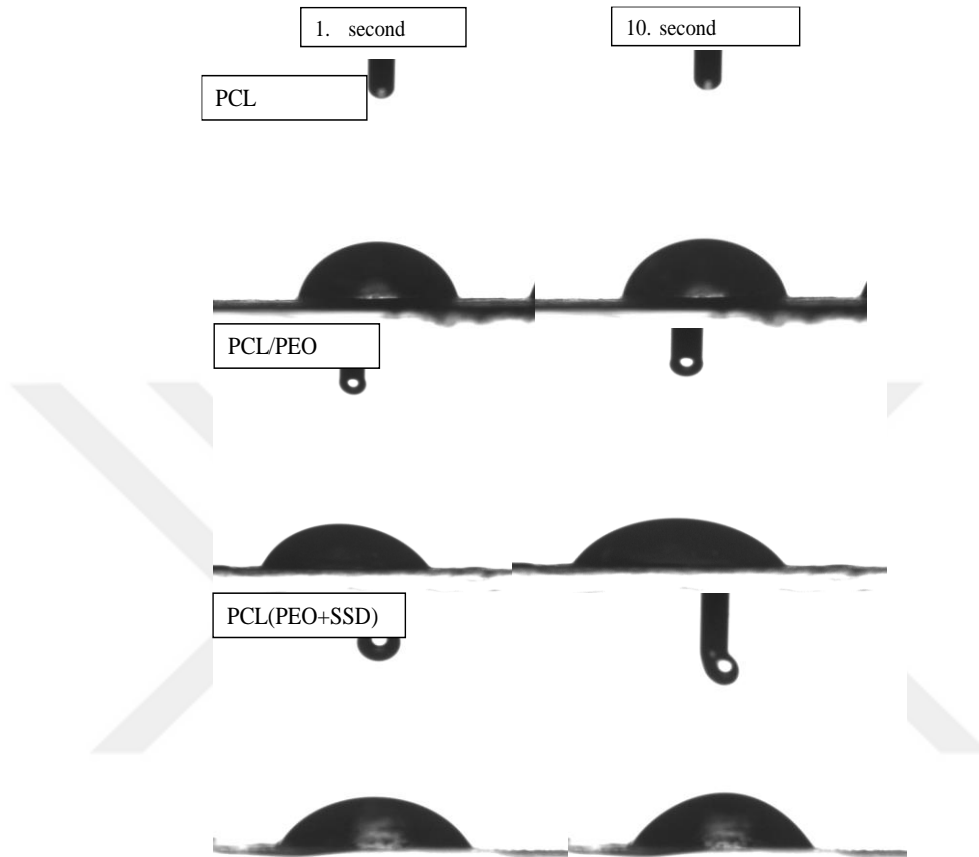


Figure 4.28 : Contact angle photographs of casting films.

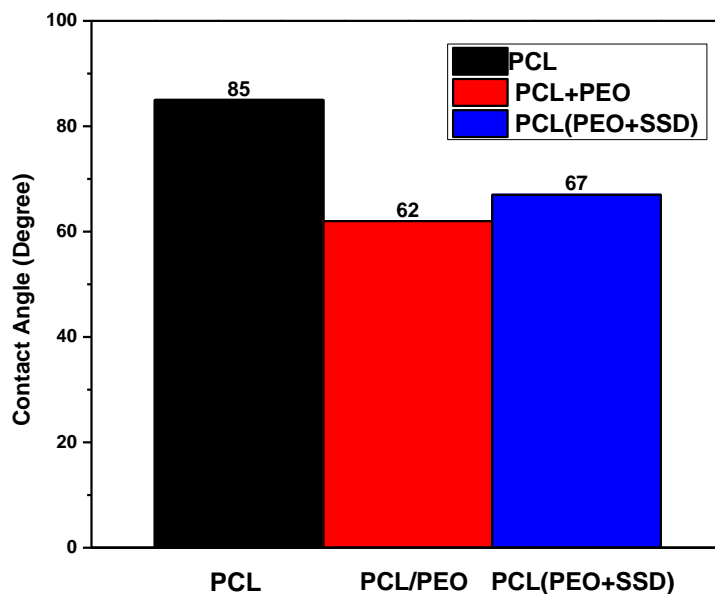


Figure 4.29 : Contact angle values of casting films.

When PEO film contacts with water, because of its super hydrophilic nature, PEO film is spread on the surface immediately. For this reason, contact angle of the PEO film could not be measured. On the other hand, PCL is a hydrophobic polymer and it has low wettability. Therefore, using PCL alone is a challenge in biomedical field because there is a necessity of contact with body fluids of the material.

In this study, stabilization of the polymer matrix was done by blending PEO with a hydrophobic PCL polymer. Otherwise, there is no significant difference but the contact angle values of the drug-free films were lower than the SSD loaded films. This can be attributed to the hydrophobic characteristic of SSD, that decreased the surface hydrophilicity of the formulation.

4.7.5 Loading efficiency, drug release profile and kinetics

The drug loading efficiency of the casting film was calculated by *Equation 1* and was found 65 % \pm 2 on average. In comparison with the PCL/(PEO+SSD) nanofiber formulation, the casting film formulation showed low loading efficiency. It is indicated that the nanofiber are better candidates than the casting films.

Percentage cumulative drug release was determined via the amount of SSD present in the casting film formulation and the plot was shown in Figure 4.31 for cumulative release % vs time. It was also observed that film formulations were stable in buffer media over 24 hours.

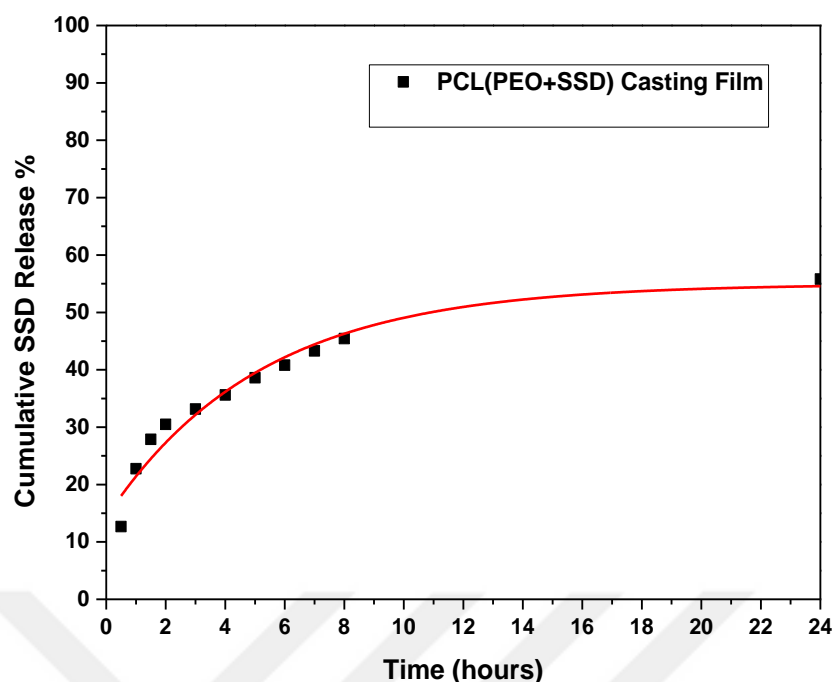


Figure 4.30 : Cumulative release % of SSD from PCL/(PEO+SSD) casting film.

The SSD showed an initial release of around 12 % which could be due to the adhered SSD particles to the film surface and high dissolution of the PEO polymer. The initial phase was followed by sustained release of SSD which was around 45 % ± 2 in 8 hours. Afterwards, controlled release of SSD was proceeded up to 24 h and it was around 55 % ± 3 exhibiting a retarded rate of release. SSD release % of PCL/(PEO+SSD) casting film was significantly lower than the PCL/(PEO+SSD) nanofiber formulation.

To explain the SSD drug release mechanisms from SSD loaded composite nanofiber; Zero Order, First Order, Higuchi, Hixon Crowell and Korsmeyer-Peppas kinetics models were applied in the drug release profile. The regression coefficients (R^2) according to different kinetic models were given in Table 4.11.

Table 4.11 : Drug release kinetics models for PCL/(PEO+SSD) nanofibers with regression coefficient (R^2).

| Release Kinetic Models | R^2 |
|------------------------|-------------|
| Zero Order | 0.683245827 |
| First Order | 0.711151507 |
| Hixon Crowell | 0.769159238 |
| Higuchi | 0.881730688 |
| Korsmeyer-Peppas | 0.930434932 |

The result best fits with the Korsmeyer-Peppas model that indicates the regression coefficient $R^2 = 0.9304$. This mathematical model describes the drug release with the following formula as:

$$M_t / M_\infty = k t^n \quad (3)$$

M_t/M_∞ is the released amount of drug at time (t), M_∞ is the total released amount of drug after time ∞ (total drug amount in the formulation), n is the drug release exponent which defines the release mechanism, k is the constant of the release rate. Hence, the exponent of n was found as 0.355. For the cylindrical-shaped matrices; $0.45 \leq n$ represents Fickian diffusion mechanism and non-Fickian or anomalous transport exhibits when $0.45 < n < 0.89$, $n = 0.89$ corresponding to Case II (relaxational) transport and $n > 0.89$ indicates super case II transport (Gouda et al., 2017). In this study, the release profile value of n is lower than 0.45, pointing clearly to the Fickian mass transport mechanism. This shows that diffusion is the main factor of the drug release mechanism for SSD loaded casting films.

4.8 Measurements and Characterization Studies of PLA/(PEO+SSD) Nanofiber Formulations

SEM, SEM-EDS, SEM-EDS Mapping, AFM, FTIR-ATR Spectroscopy, XRD analysis, water uptake and contact angle measurements were performed to characterize PEO, PEO+SSD, PCL, PCL/PEO and PCL/(PEO+SSD) electrospun nanofibers.

4.8.1 SEM analysis

Morphology of fibers such as fiber diameter, structure and frequency of the pores, getting beadless and smooth surface is an important parameter for nanofiber based drug delivery systems. It is significant to provide the appropriate conditions for loading, carrying and releasing the drugs (Sill&Von Recum, 2008). Therefore, it was aimed to obtain fiber morphology with appropriate properties for drug delivery. In this part, SEM analysis was performed for the morphological characterization of the nanofibers to verify the fiber diameter, fiber morphology, bead defects, smoothness, uniformity and diameter distribution of nanofibers. The average fiber diameters were calculated from 30 different fiber sections of an SEM image and histograms of fiber diameter distributions were plotted.

4.8.1.1 SEM analysis of PEO and PEO+SSD nanofibers

General surface images of PEO and PEO+SSD nanowebs were represented in Figure 4.32 at 2000 magnification. The SEM images at 10000 magnification and diameter distribution of PEO and PEO+SSD nanofibers were shown in Figure 4.33. Uniform, solid, continuous, bead-free and porous fiber morphologies with nanoscaled diameters were observed in the SEM images.

The average diameter was 313 ± 67 nm for the pure PEO nanofibers and 251 ± 90 nm for the PEO+SSD. Compared to pure PEO fibers, the SSD loaded PEO nanofibers had smaller fiber diameter. However, they had some irregularities, weak and immature fiber morphologies and wider fiber diameter distribution.

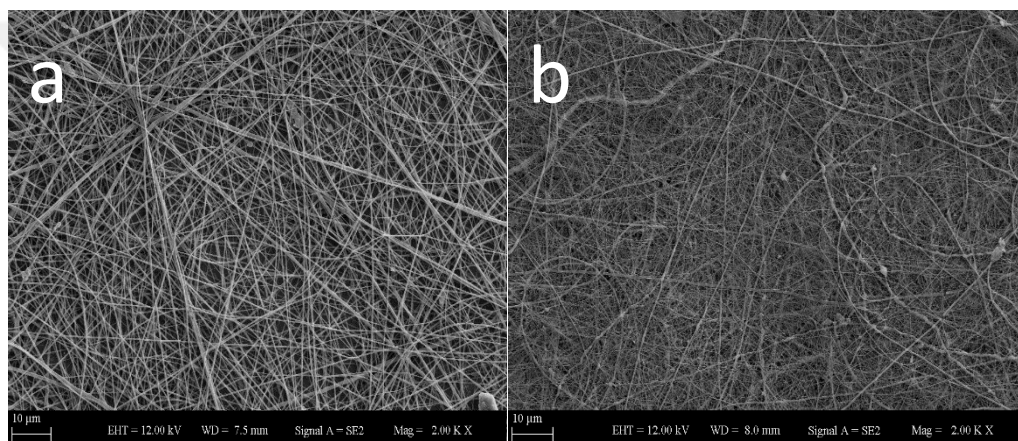


Figure 4.31 : General surface images of a) PEO and b) PEO+SSD nanofibers (X 2000 magnification).

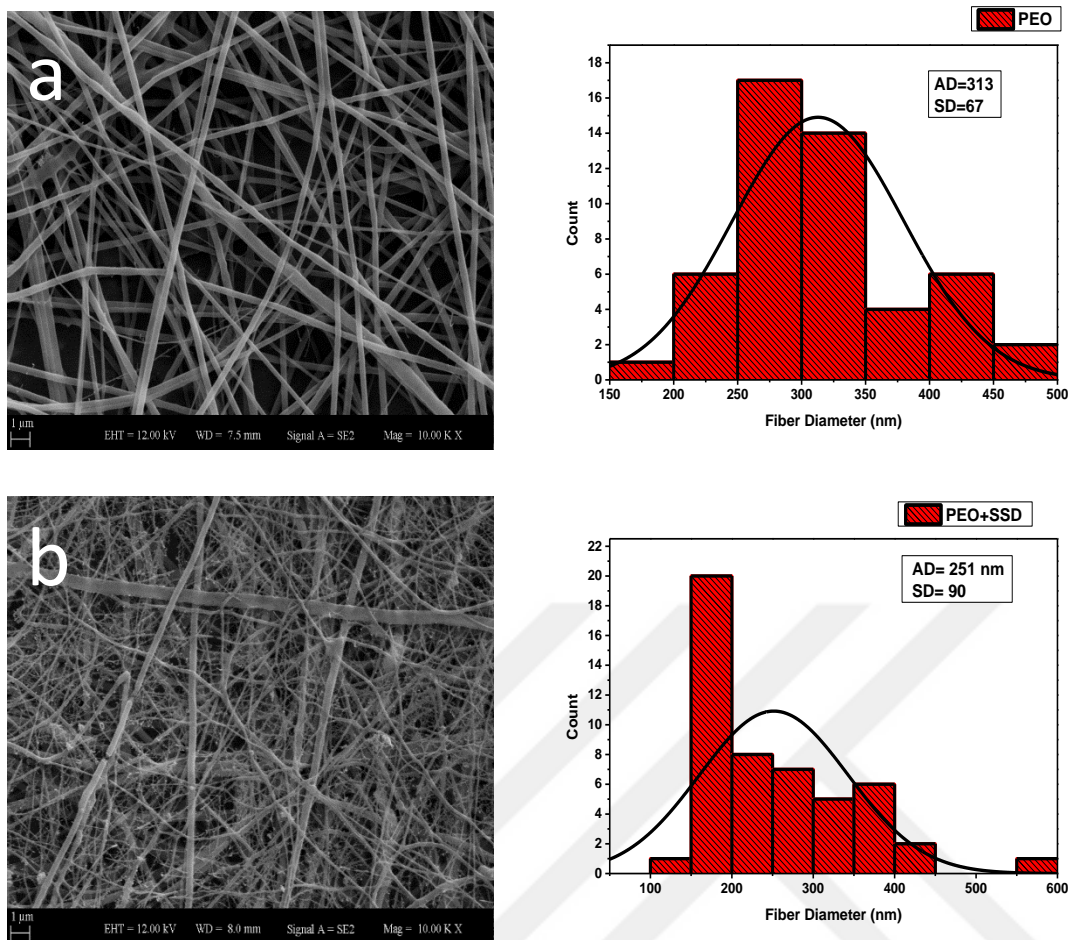


Figure 4.32 : SEM images and corresponding the diameter distribution histograms of a) Pure PEO b) PEO+SSD nanofibers.

4.8.1.2 SEM analysis of PLA, PLA+PEO and PLA/(PEO+SSD) nanofibers

Nanoscaled, solid, continuous and porous PLA and PLA+PEO, PLA/(PEO+SSD) nanofibers were fabricated via electrospinning. General surface images of PLA, PLA/PEO and PLA/(PEO+SSD) nanowebbs were represented in Figure 4.34 at 2000 magnification. The SEM images of PLA, PLA/PEO and PLA/(PEO+SSD) nanofibers at 10000 magnification and average diameter distribution of them were shown in Figure 4.35. Some fibers with beaded structures were observed in the pure PLA nanofibers. However, The PLA/PEO and PLA/(PEO+SSD) composite nanofibers had smooth and uniform morphology without bead defects compared to pure PLA. This indicates that PLA and PEO blended homogeneously and phase separation did not occur during electrospinning. Additionally, blend of PLA, PEO and SSD molecules were bonded physically and had a good interaction in the composite fiber structure (Dubey & Gopinath, 2016). The photograph of the homogenous mixture of PEO and PLA was shown in Figure 4.2. The average diameter was 227 ± 75 nm for pure PLA

nanofibers, 554 ± 90 nm for PLA/PEO nanofibers and 311 ± 63 nm for SSD loaded PLA/PEO nanofibers.

Compared to drug-free PLA/PEO nanofibers (554 ± 90 nm), the SSD loaded composite nanofibers (311 ± 63 nm) had smaller fiber diameters with lower \pm SD. According to the literature, the reason is related to the presence of conductive SSD particles in the composite nanofibers (Lee et al., 2016). SSD is a silver salt and is conductive in nature. Electrospinning solution contains a high amount of charged silver and sulfadiazine ions by the addition of SSD into the PEO solution. It supplies more electric charges to the electrospinning jet in order to overcome the surface tension of the solution. The bead defects are formed on the fiber surface if the polymer jet is not fully stretched. Therefore, when SSD is added to the solution, the electrical conductivity of the solution increases, resulting in the stretching of the solution. Consequently, smooth fibers were formed and fiber diameter decreases with greater uniformity by cause of a high stretching force (Saquing et al., 2009). Thus, when compared to pure PEO (315 ± 59 nm) and the PEO-PLA (554 ± 90 nm) blended nanofibers, the SSD loaded PEO (251 ± 90 nm) and SSD loaded PLA/PEO (311 ± 63 nm) composite nanofibers have less fiber diameters. Moreover, the smaller diameter of SSD containing nanofibers can be related to following reasons: the uniform distribution of the SSD in the nanofiber matrix without aggregation and with strong physical bonding between polymer matrix and SSD as it was recently reported that the nanofibers diameters gradually decreased with an increase in the amount of silver sulfadiazine (Ullah et al., 2019b).

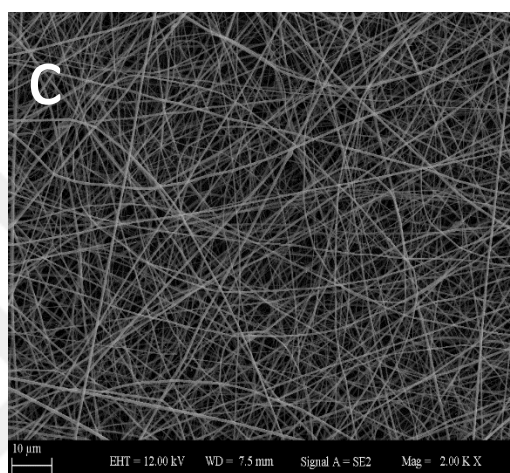
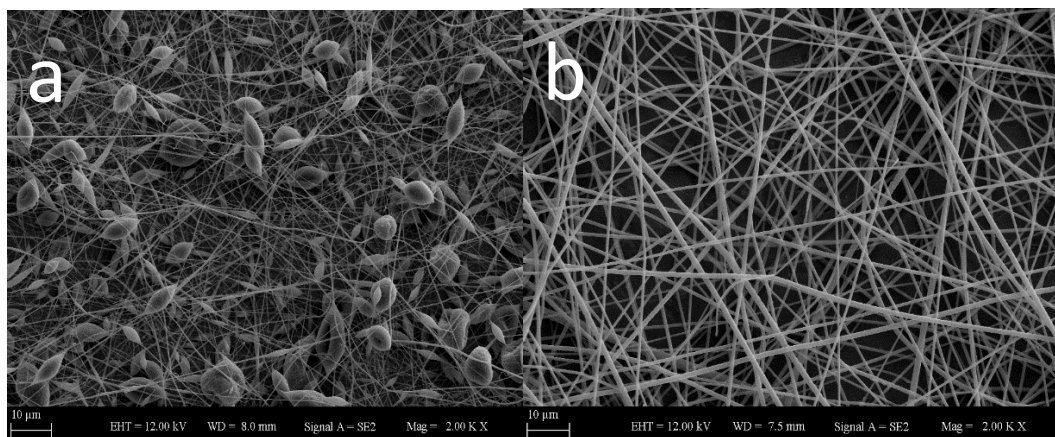


Figure 4.33 : General surface images of a) PLA b) PLA+PEO c) PLA/(PEO+SSD) (at X 2000 magnification).

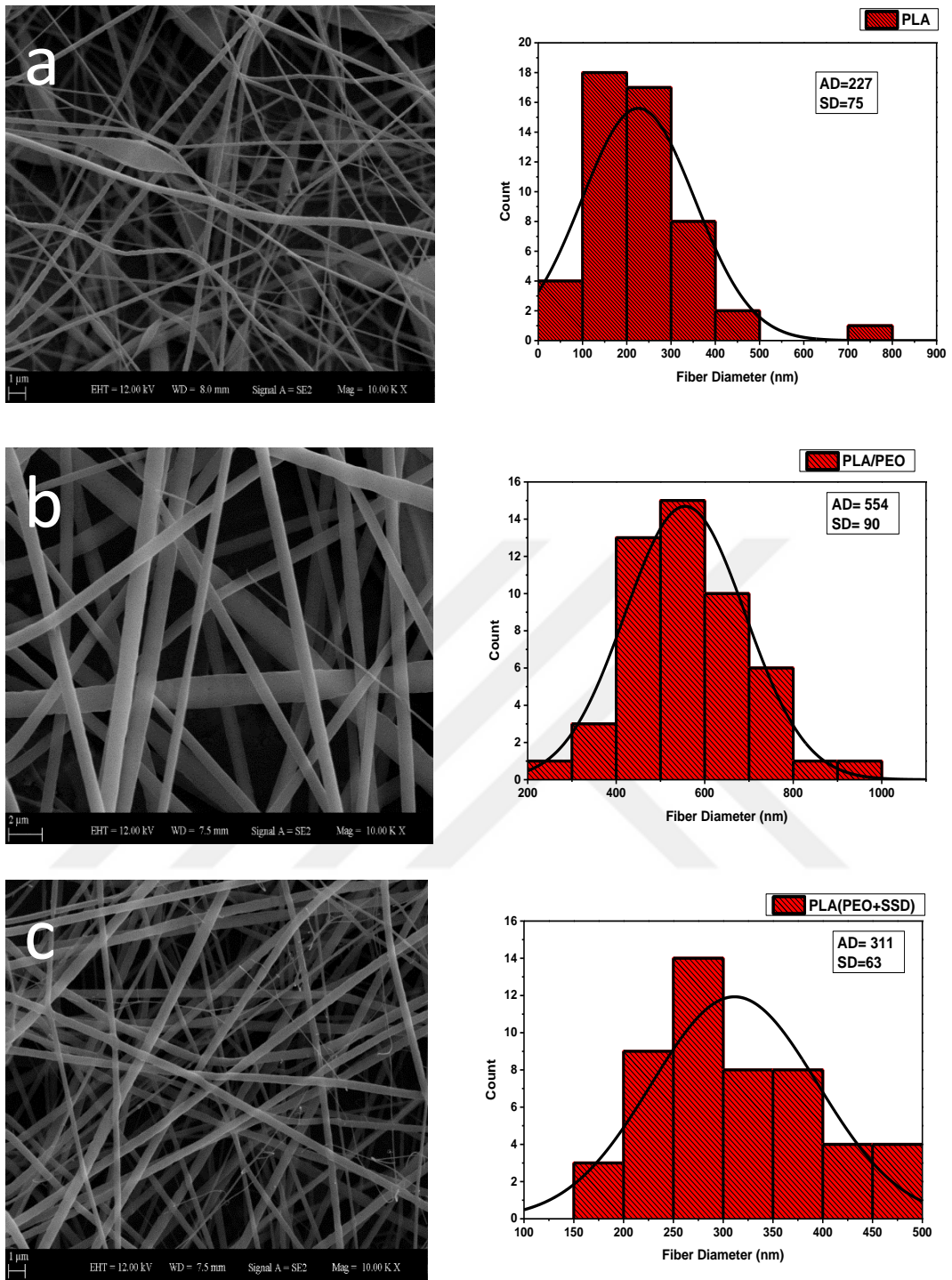


Figure 4.34 : SEM Images and corresponding diameter distribution histograms of a) Pure PLA b) Pure PEO c) PLA/PEO (7:3) and d) SSD loaded PLA/PEO composite nanofibers.

4.8.1.3 Effect of viscosity on nanofiber morphology

Viscosity has reverse effects on the fiber diameter (Zeng et al., 2003). PLA solution has a lower viscosity than the PLA/ PEO solution. In agreement with the literature, the increase of solution viscosity led to an increase in average fiber diameter from 227 nm (PCL) to 311 nm (PCL/PEO+SSD) and 554 nm (PCL/PEO). Furthermore, high viscosity solution promoted smooth fiber formation, for this reason, pure PLA nanofibers had bead defects whereas PLA/PEO had no beads (Souza et al., 2018; Dubey & Gopinath, 2016). However, while the viscosity of the PEO+SSD was higher than the PEO solution, the diameter of PEO+SSD (251 ±90 nm) was smaller than pure PEO (313±67 nm) nanofibers. It shows that increased conductivity with the SSD addition was more effective than viscosity on the fiber diameter. In other words, the conductivity factor was more effective than the viscosity factor on the fiber diameters. The addition of SSD causes increased conductivity and contributes to the generation of nanofibers with smaller diameters. Viscosity values of the prepared solutions were shown in Table 4.12.

Table 4.12 : Viscosity values of the electrospinning solutions.

| | PEO | PEO+SSD (2) | PLA | PLA/PEO (7:3) | PLA(PEO+SSD) (7:3) |
|-----------------------------|-----------|-------------|------------|---------------|--------------------|
| Viscosity (Pa.s) | 0.190 | 0.320 | 0.021 | 0.061 | 0.063 |
| Fiber Diameters (nm) | 313±67 nm | 251 ±90 nm | 227 ±75 nm | 554 ±90 nm | 311 ±63 nm |

4.8.1.4 Water uptake

The water uptake was evaluated by immersing electrospun patches in buffer solution at room temperature for 24 hours. The weight of the wet sample was measured after drying in incubator to remove the surface water. Swelling and surface destruction were investigated by SEM as shown in Figure 4.36. The water uptake percentage was calculated by *Equation 2* and was found as 40 % ±4 as mean value.

In the equation; W_d is dried weight of the patch and W_w is the wet weight of the patch. Three nanofiber patches were examined to calculate water uptake percentage and the average value was recorded.

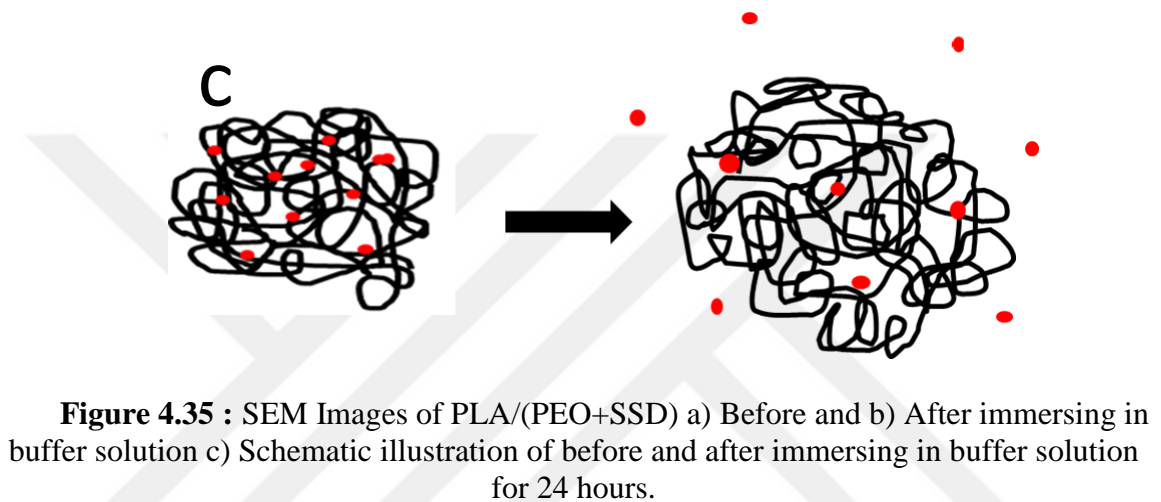
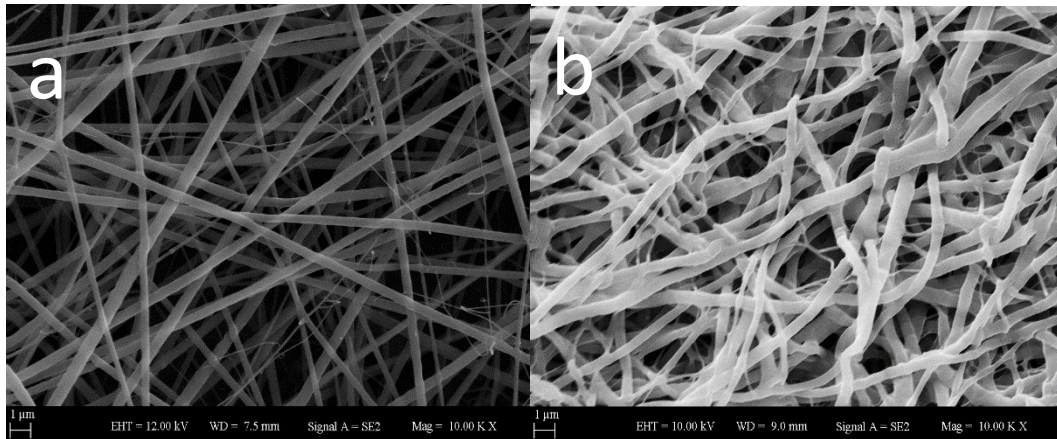


Figure 4.35 : SEM Images of PLA/(PEO+SSD) a) Before and b) After immersing in buffer solution c) Schematic illustration of before and after immersing in buffer solution for 24 hours.

SEM images demonstrate that diameter of nanofibers increase due to swelling of PLA and smoothness of nanofibers is damaged because of destruction and polymer erosion of the PLA/PEO matrix. Moreover, the nanofiber structure shifted from straight to the entangled state.

4.8.2 Elemental analyses of SSD loaded composite nanofibers

Energy dispersive spectra (EDS) analysis was performed to confirm that PCL/(PEO+SSD) nanofibers contain SSD, by detecting the Silver (Ag), Nitrogen (N), Sulphur (S) content of the nanofibers. Moreover, EDS-Mapping was carried out to show the distributions of these elements in composite nanofibers. SEM-EDS spectra and EDS-Mapping images of PLA/(PEO+SSD) composite nanofibers can be seen in Figure 4.37. The peaks of Ag, N, S within the EDS spectra show their presence in the fiber structure, indicating that the nanofiber mats are evenly loaded with SSD. The elemental distribution of S, N and Ag atoms of formulation was shown with SEM-EDS Mapping Image in Figure 4.38. The elemental distribution of the Ag, S, N is represented with their corresponding amount in Table 4.13. EDS-Mapping images

showed that SSD molecules were distributed homogeneously in the fiber structure without any aggregation.

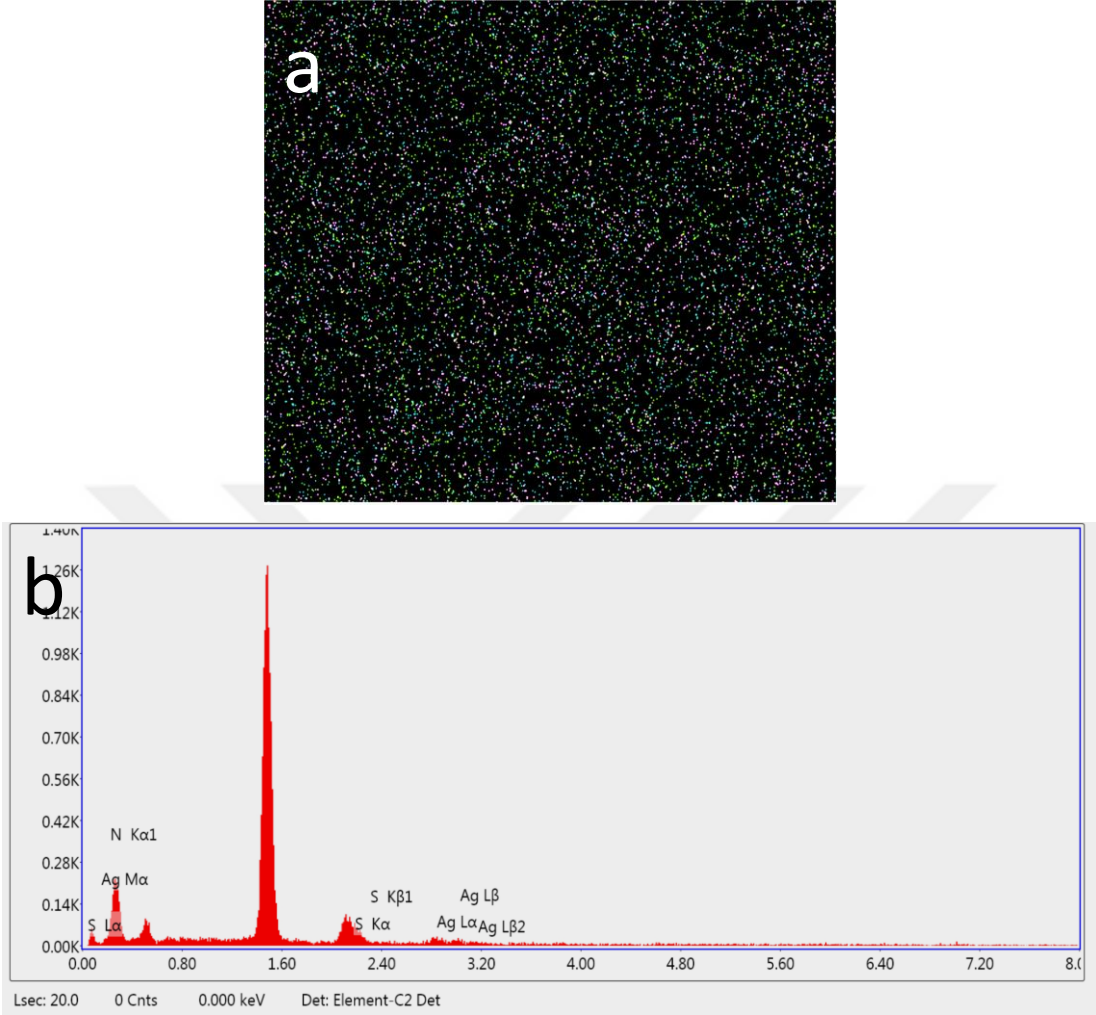


Figure 4.36 : EDS Mapping image (a) and spectra (b) of PLA(PEO+SSD).

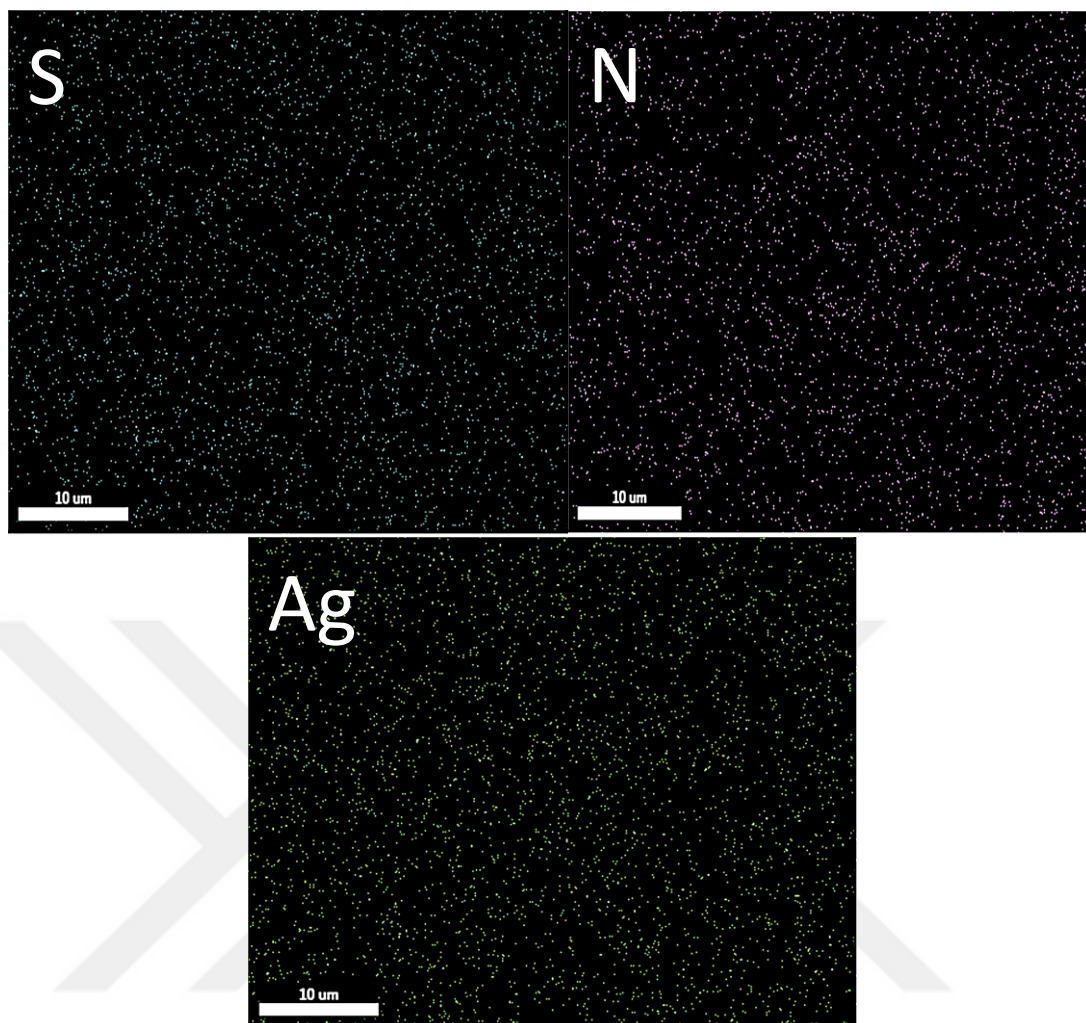


Figure 4.37 : Representation of elemental distribution of S, N and Ag atoms on formulation with SEM-EDS Mapping image.

Table 4.13 : Elemental distribution of Ag, S and N on EDS Mapping image.

| Elements | Ag | N | S |
|----------------|----|----|----|
| Distribution % | 36 | 29 | 36 |

4.8.3 Atomic Force Microscopy (AFM)

AFM was used to investigate the surface topography and to determine the surface roughness of the nanofibers. AFM Images of the drug-free PLA/PEO and the PLA/(PEO+SSD) were represented in Figure 4.39 and Figure 4.40 with 3D images.

Very few nanofibers were electrospun on the cover glass for 20 second and the specimens were analysed. AFM Images shows the roughness structure of nanofibers. Moreover, it is determined that the surface roughness of the drug loaded nanofibers was higher than pure PCL/PEO nanofibers (from 220 to 330 nm). This can be

attributed to the presence of SSD on the surface of the nanofibers as well as it presents inside the nanofibers.

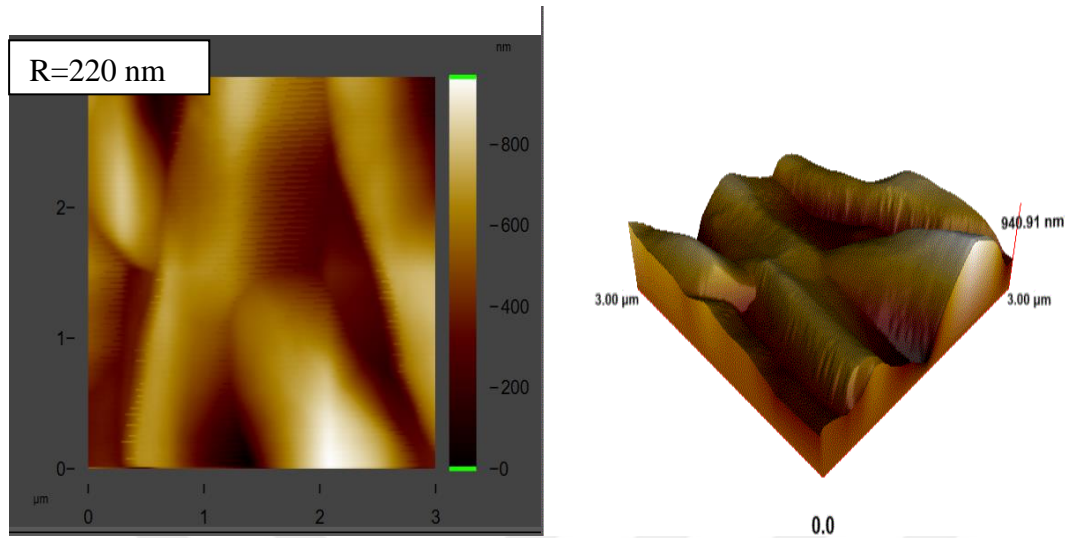


Figure 4.38 : AFM Images of pure PLA/ PEO nanofibers.

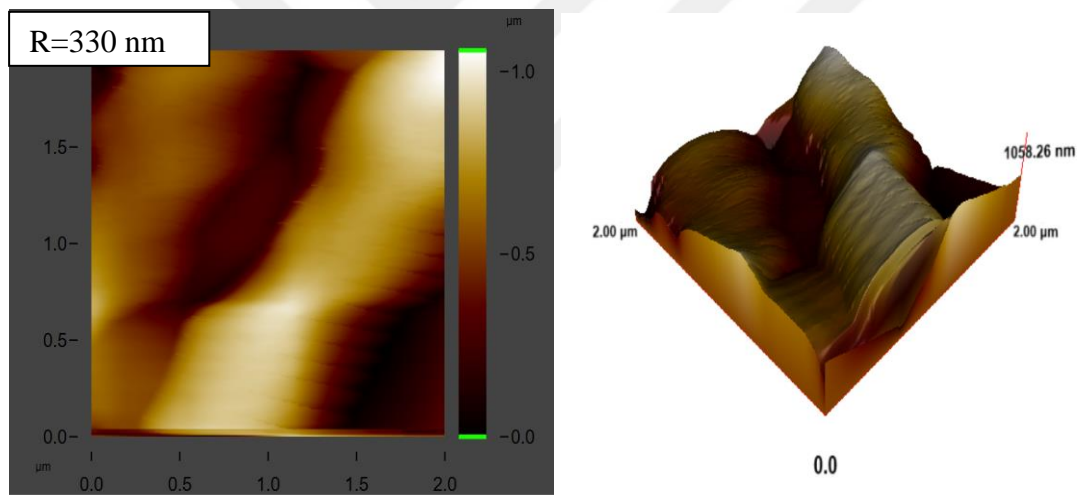


Figure 4.39 : AFM images of SSD loaded PLA/ PEO nanofibers.

4.8.4 Wettability-Contact angle measurements

In this work, due to the hydrophilic nature of the PEO polymer, there was a necessity to combine it with a hydrophobic polymer. For this reason, a well-known hydrophobic polymer PLA was added to PEO. Wettability of PLA, PEO, PLA/PEO, PLA/(PEO+SSD) nanofibers were evaluated with contact angle measurements. Contact angle test photographs were shown in Figure 4.41 and contact angle values were given as graph in Figure 4.42.

When PEO nanofiber patch contacts with water, because of its super hydrophilic nature, PEO patch is spread on the surface immediately. On the other hand, PLA is a

hydrophobic polymer and it has low wettability. Therefore, using PLA alone is a challenge in biomedical field because there is a necessity of contact with body fluids of the material. Stabilization of the polymer matrix was done by blending PEO with a hydrophobic PLA polymer. Otherwise, there is no important difference but the contact angle values of the drug-free composite nanofibers were lower than the SSD loaded composite nanofibers. This can be attributed to the hydrophobic characteristic of SSD, decreasing the surface hydrophilicity of the formulation.

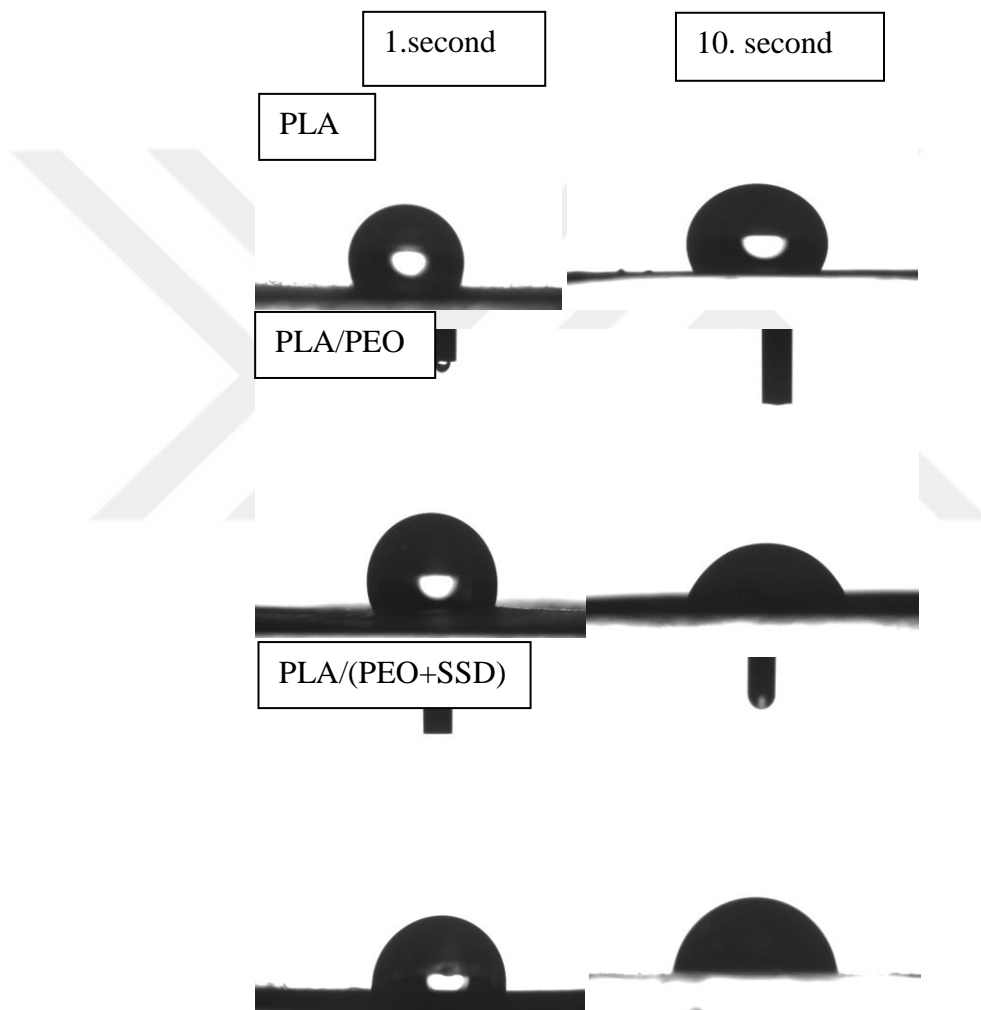


Figure 4.40 : Contact angle photographs of nanofibers.

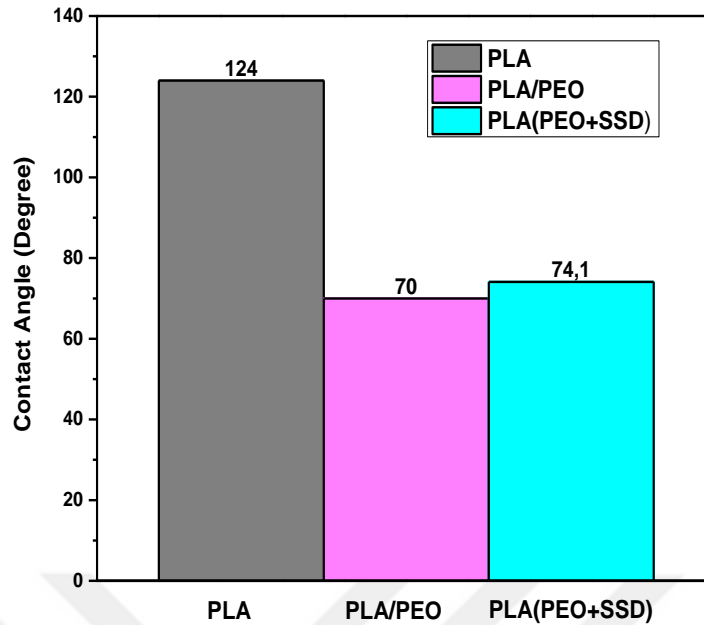


Figure 4.41 : Contact angle values of nanofibers.

Contact angle results of the PCL/(PEO+SSD) casting film, PCL/(PEO+SSD) composite nanofibers and PLA/(PEO+SSD) composite nanofibers were represented in Figure 4.43. Contact angle values of the PLA, PLA/PEO and PLA/(PEO+SSD) formulations are higher than the PCL, PCL/PEO and PCL/(PEO+SSD) formulations. Although nature of PCL polymer is more hydrophobic than PLA polymer, contact angle results of pure PLA and PLA blends are higher than the pure PCL and PCL blends (Yao et al, 2017; Patricio et al., 2014). This can be explained by the surface properties, surface roughness of PLA/PEO nanofibers (Ramazanoglu et al.,2019). AFM results showed that PLA/PEO (220 nm) nanofibers have more surface roughness value than PCL/PEO (150 nm) nanofibers. Because, as indicated in the literature, high roughness limits the wetting ability (wettability) and results increased hydrophobicity with high contact angle (Dubey et al., 2015). Moreover, polymer concentration of PLA (6 %) is higher than PCL (4 %). Also, it may affect the wettability properties of the material surface.

Contact angle values of the PCL, PCL/PEO and PCL/(PEO+SSD) casting films are higher than the PCL, PCL/PEO and PCL/(PEO+SSD) nanofibers. Because the films formed thicker surfaces than the PCL nanofibers.

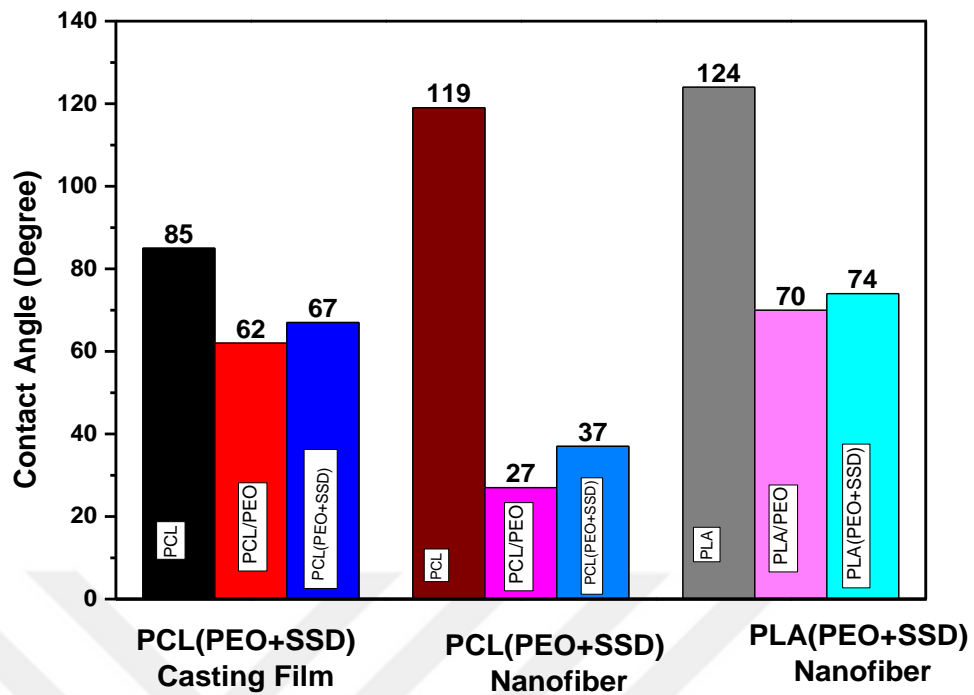


Figure 4.42 : Contact angle values of PCL/(PEO+SSD) casting film, PCL/(PEO+SSD) and PLA/(PEO+SSD) nanofiber formulations.

4.8.5 X-ray diffraction (XRD) study

X-ray diffraction (XRD) analysis was performed to examine the crystalline structure of the SSD loaded electrospun nanofibers. XRD pattern of silver sulfadiazine powder and PEO+SSD, PLA/PEO, PLA/(PEO+SSD) nanofiber patches were shown in Figure 4.44.

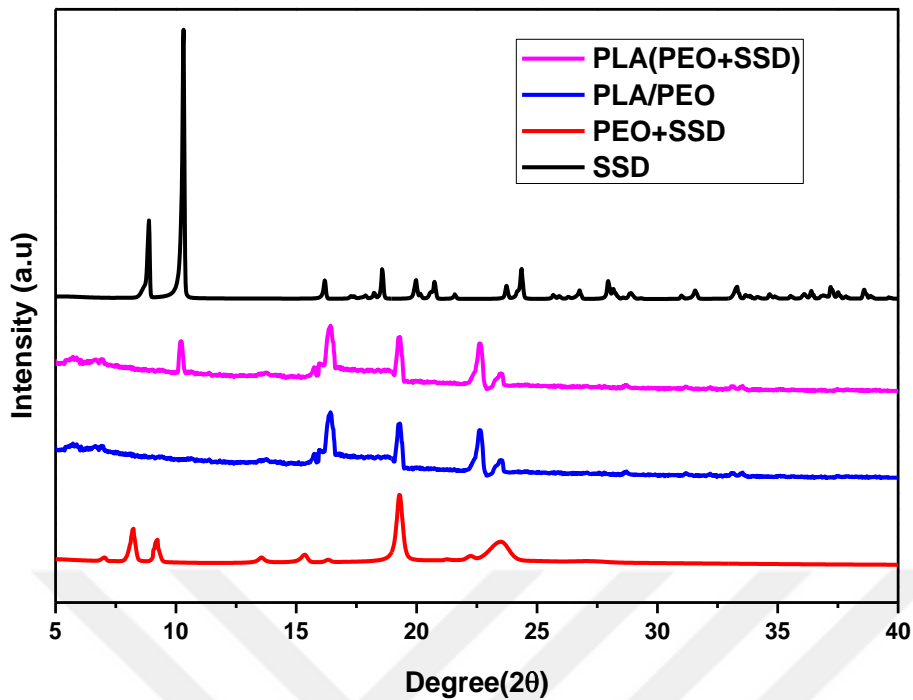


Figure 4.43 : XRD pattern of SSD, PEO+SSD, PEO+PLA and PLA/(PEO+SSD) nanofibers.

SSD showed its characteristic peaks at around $2\theta = 8.8^\circ$ and 10.2° corresponding to the (0 0 2), (0 1 1) planes as explained in literature (Aguzzi et al., 2014; Ghodekar et al., 2012; Luan et al., 2012). X-ray diffraction (XRD) pattern of PEO+SSD nanofibers showed diffraction peaks of semicrystalline PEO at $2\theta = 19^\circ$ interrelated to the (1 2 0) and (0 3 2) helical structure of the PEO crystal. Also, in the pattern of PEO+SSD, SSD was confirmed with its distinctive peaks which were shifted from 8.8° to 8.2° and 10.2° to 9.3° respectively.

In the XRD pattern of PLA/PEO nanofibers, the diffraction peaks of PLA were seen at $2\theta = 16.4$ and $2\theta = 22.6$ (Lu et al., 2016). With the addition of SSD into the PLA/PEO polymer matrix, microcrystalline structure of SSD was exhibited by the distinctive one single peak at 10.2° . However, the other distinctive peak of SSD at 8.8° did not appear in the diffraction pattern of PLA/(PEO+SSD) whereas it appears in PEO+SSD with shifting to 8.2° . This is related to the addition of PLA that decreases the percentage of SSD in the formulation. Moreover, the weak peak at $2\theta = 8.8^\circ$ totally disappeared while the stronger peak at $2\theta = 10.2^\circ$ was still observed in the XRD pattern. PLA/(PEO+SSD) formulation showed the characteristics peak of SSD at

10.2°. Loaded SSD into the nanofiber matrix was crystalline and it determines that structural stability of SSD was achieved during electrospinning process.

4.8.6 Attenuated Total Reflectance Infrared (FTIR-ATR) spectroscopy analysis

The stability of SSD in the fiber structure and the molecular interactions in the drug-free and drug loaded nanofibers were examined by Attenuated Total Reflectance Infrared (FTIR-ATR) Spectroscopy. FTIR-ATR spectra of silver sulfadiazine powder and PLA, PEO nanofibers and interaction between PLA, PEO, and Silver sulfadiazine were shown in Figure 4.45a; PEO+SSD, PLA/PEO, PLA/(PEO+SSD) nanofiber patches were shown in Figure 4.45b.



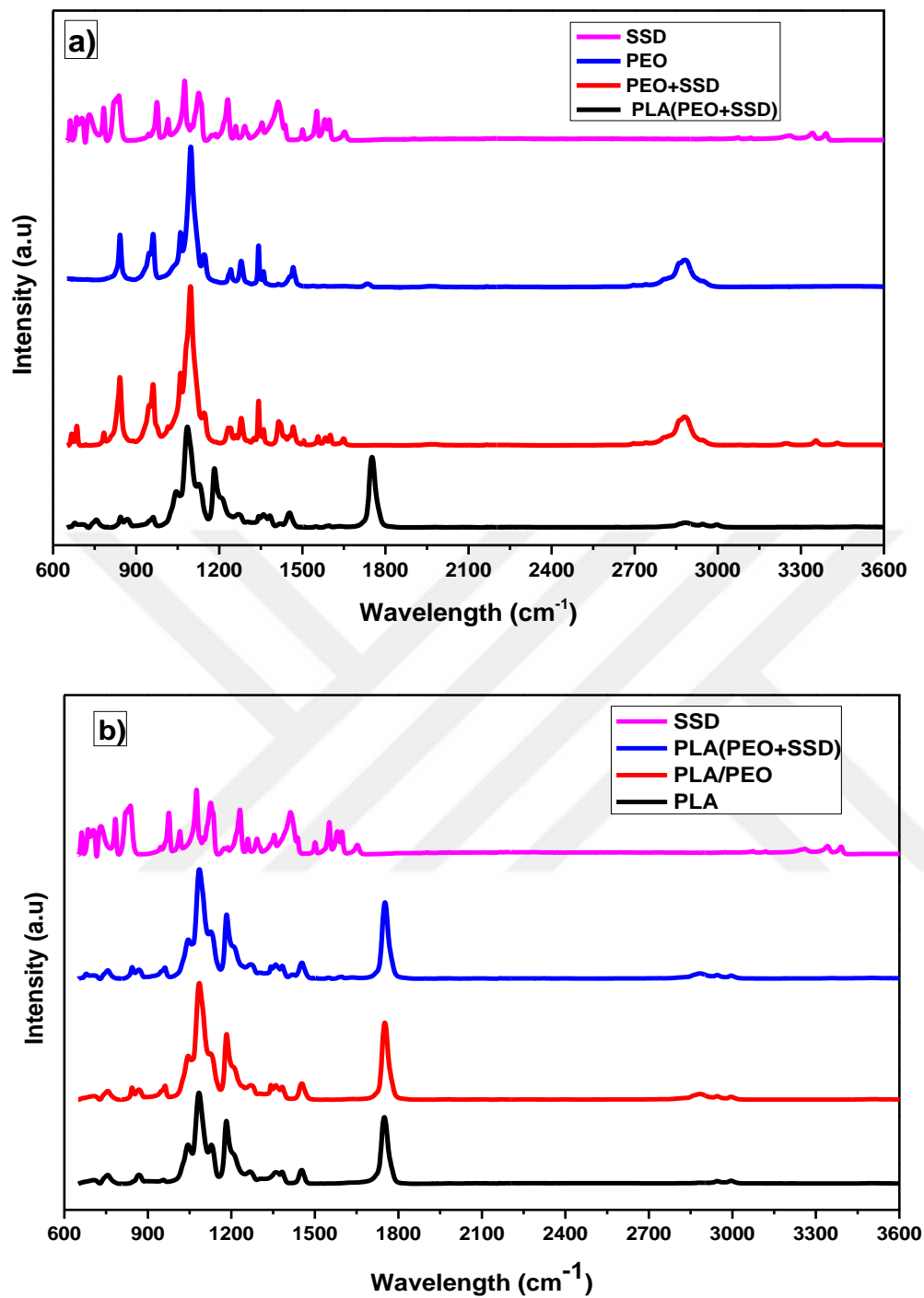


Figure 4.44 : FTIR -ATR spectra of a) SSD, PLA, PEO and b) PEO+SSD, PLA/PEO, PLA/(PEO+SSD) nanofibers.

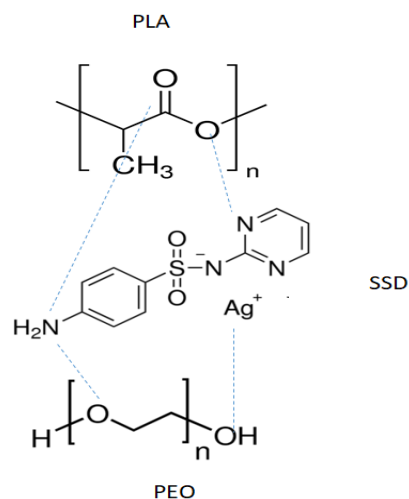


Figure 4.45 : Interaction between PLA, PEO and SSD.

SSD presented peaks at 3343 and 3393 cm^{-1} were due to the amine (NH_2) stretching mode. Exhibited peaks at 1651 cm^{-1} associated with NH_2 bending, at 1595, 1581, 1552 and 1500 cm^{-1} were attributed to the aromatic $\text{C}=\text{C}$ stretching, at 783, 1016, 1356 cm^{-1} due to the asymmetric and at 1124 cm^{-1} conjugated to the symmetric stretching of SO_2 (Ghodekar et al., 2012; Patel et al., 2019; Zepon et al., 2014). Finally, the peaks exhibited at around 1230 cm^{-1} conjugated to aromatic $\text{C}-\text{N}$ stretching and at 1075 cm^{-1} corresponding to aromatic vibrations.

All characteristic peaks of PEO appeared at around 2880-2885 cm^{-1} due to $\text{C}-\text{H}$ stretching vibration, at 1465 cm^{-1} attributed to CH_2 scissoring vibration, at 1360 and 1340 cm^{-1} associated with wagging vibration of CH_2 , at 1280 cm^{-1} due to CH_2 twisting vibration, at 840 cm^{-1} and 960 cm^{-1} belonging to CH_2 rocking vibrations. Also, the semicrystalline structure of PEO was observed by the triplet peak of $\text{C}-\text{O}-\text{C}$ stretching vibrations at 1147, 1100, and 1060 cm^{-1} (Aguzzi et al., 2014).

Typical peaks for the PLA were seen at 1751 cm^{-1} related to the $\text{C}=\text{O}$ stretching of carbonyl groups. The peaks at around 1181-1184 and 1082-1088 were conjugated to $\text{C}-\text{O}-\text{C}$ bending vibrations; the peak at 1042-1046 cm^{-1} was corresponding to $\text{C}-\text{CH}_3$ vibrations. The peaks were exhibited at around 1452-1454 and 1385-1388 cm^{-1} interrelated to the $\text{C}-\text{H}$ deformation from $-\text{CH}_2$. The peaks at 869 and 755 cm^{-1} are associated to $\text{C}-\text{C}$ stretching vibrations (Altan et al., 2018; Cosme et al., 2016).

SSD loaded PEO nanofibers represented the specific peaks of SSD at 784 cm^{-1} due to the asymmetric stretching of SO_2 , at 1583 and 1556 cm^{-1} attributed to aromatic $\text{C}=\text{C}$ stretching, 1649 cm^{-1} conjugated to NH_2 . Drug-free PLA/PEO nanofibers were not

influenced quietly by the addition of SSD in PLA/PEO nanofibers. This means, SSD bounded to polymer matrix physically and overall symmetry of the SSD molecule did not significantly change in the electrospun nanofiber matrix (Xue et al., 2014).

4.8.7 Loading efficiency, drug release profile and kinetics

The drug loading efficiency of nanofibers was calculated by *Equation 1* and was found as 80 % \pm 4 as mean value. In literature, SSD was loaded into different carriers which were reported with loading efficiency values in Table 4.14.

In comparison with the other studies, the optimized PLA/(PEO+SSD) and the PCL/(PEO+SSD) formulations showed high loading efficiency. It is indicated that the nanofiber formulation is a promising drug carrier for efficient drug loading thanks to the specific surface area and high porous structure of nanofibers (Morie et al., 2016).

Table 4.14 : Drug loading efficiencies (%) of SSD loaded formulations in the literature.

| Drug Carrier Matrix | Drug Loading Efficiency % | References |
|---|----------------------------------|-----------------------------|
| Silver sulfadiazine microsponges incorporated gel | 70 | (Kumar & Gosh, 2017) |
| SSD loaded chitosan nanogel | 62 | (El-Feky et al., 2017) |
| Aloevera based silver sulfadiazine cubogel | 76-90 | (Thakkar et al., 2016) |
| Chitosan nanoparticles | 60-89 | (El-Feky et al., 2017) |
| Alginate and gelatine based bio-polymeric wafers | 80-93 | (Boetang et al., 2015) |
| SSD Niosomal gel | 53-72 | (Dharashivkar et al., 2015) |
| PCL/(PEO+SSD) Nanofiber | 86 | |
| PCL/(PEO+SSD) Casting Film | 65 | |
| PLA/(PEO+SSD) Nanofiber | 80 | |

Percentage cumulative drug release was determined via the amount of SSD present in the composite nanofiber formulation and the plot was shown in Figure 4.47 for cumulative release % versus time. It was also observed that nanofiber formulations were stable in buffer media over 24 hours. PLA/PEO nanofibers were blended homogeneously so that smooth, continuous and uniform fiber morphology were obtained (Figure 4.35) and phase separation did not occur during electrospinning. In addition, the photograph of the homogenous mixture of PEO and PLA was shown in

Figure 4.2. Due to the good composition of PLA and PEO in the fiber matrix, composite nanofiber formulation exhibited one phase release kinetics, hence biphasic release kinetics were not observed in the drug release profile.

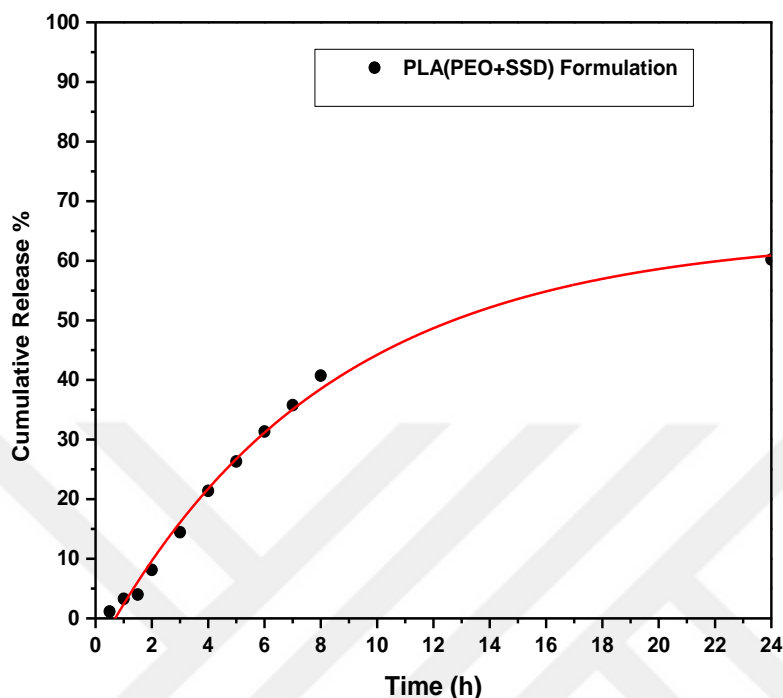


Figure 4.46 : Cumulative release % of SSD of PLA/(PEO+SSD) nanofibers.

The SSD showed an initial release of 12-13 %, which could be due to the adhered particles to the nanofiber surface and also the high dissolution rate of the PEO polymer (Dubey & Gopinath, 2016). The initial release was followed by sustained release of SSD which was around 45 % \pm 2 in 8 hours. Afterwards, the controlled release of SSD was proceeded up to 24 h and it was around 55 % \pm 3 exhibiting a retarded rate of release.

Cumulative SSD release profiles of PCL/(PEO+SSD) casting film, PCL/(PEO+SSD) nanofibers and PLA/(PEO+SSD) nanofibers are plotted in Figure 4.48. It is shown that cumulative release % of PCL/(PEO+SSD) casting film is lower than the nanofiber formulations with 50 % release in 24 hours. The PCL/(PEO+SSD) and PLA/(PEO+SSD) nanofiber formulations exhibited better release profile with 80 % and 60 % release in 24 hours, respect. This is conjugated to specific surface area and high pore interconnectivity of nanofibers. Therefore, the nanofiber formulations are better candidates than casting film for topical burn treatments. PCL/(PEO+SSD) nanofibers showed high release % in comparison to PLA/(PEO+SSD) nanofibers. This

can be explained by the more hydrophobicity of the PLA/(PEO+SSD) formulation that was demonstrated with contact angle measurements. Hydrophobicity of the material restrict the polymer degradation and drug dissolution resulting in slow and long release action. The PLA/(PEO+SSD) nanofibers can be utilize for prolonged topical drug delivery systems. For instance, it can be preferred for 2-3 daylong drug release while the PCL/(PEO+SSD) nanofibers are suitable for 24-hour drug release period. Additionally, it is known that 4 % SSD loaded into the PLA/(PEO+SSD) nanofibers while 3.2 % loaded into PCL/(PEO+SSD) nanofibers. When the release amount of SSD was evaluated it is shown that there is no important difference in release amount of SSD between PCL/(PEO+SSD) and PLA/(PEO+SSD) nanofiber formulations. The graphs of released amounts are plotted in Figure 4.49.

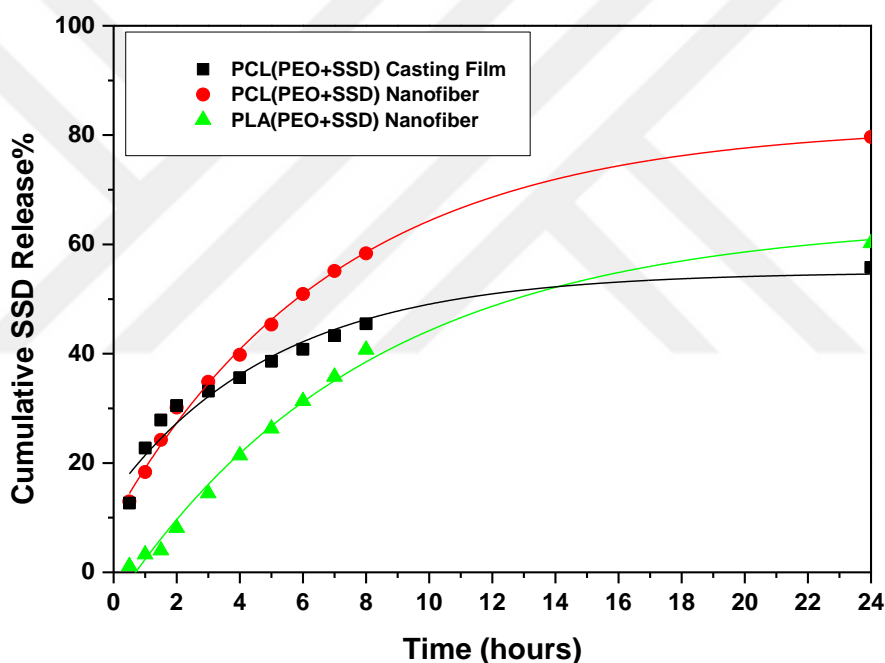


Figure 4.47 : Cumulative SSD release of PCL/(PEO+SSD) casting film, PCL/(PEO+SSD) nanofibers and PLA/(PEO+SSD) nanofibers.

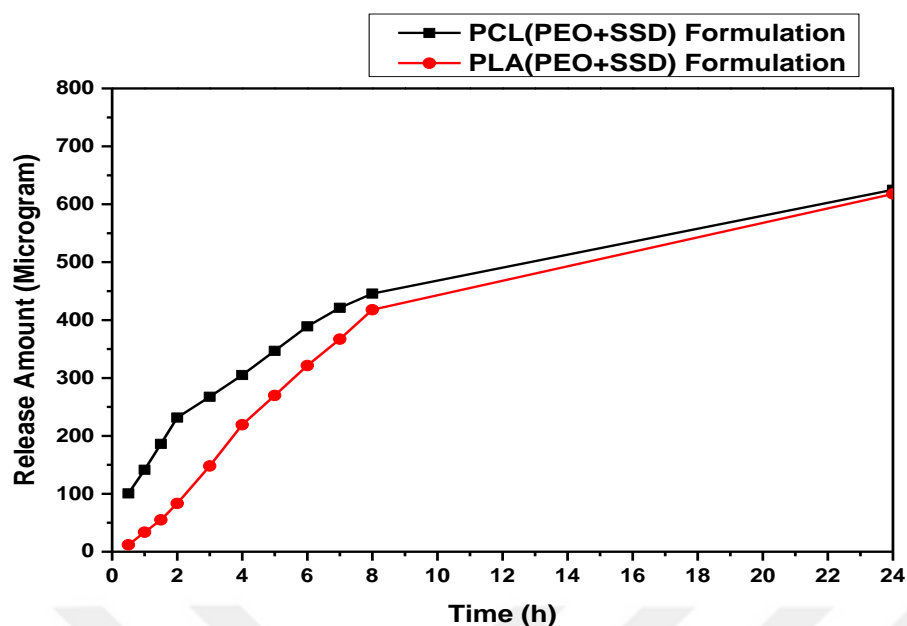


Figure 4.48 : Amount of SSD release from PCL/(PEO+SSD) and PLA/(PEO+SSD) formulations.

SSD release was significantly higher than the other nanofiber formulations found in the literature, as summarized in Table 4.15. The probable reason is improving the water solubility of SSD by loading it into a highly aqueous soluble PEO polymer. The enhanced solubility of SSD increased the release amount of SSD from nanofiber to buffer media. Moreover, the use of a new buffer media (Water/ Propylene Glycol/ Phosphoric Acid), which could entirely dissolve SSD, is an important parameter to simulate release behaviour.

Table 4.15 : Cumulative release of SSD loaded formulations in the literature.

| Nanofiber Matrix | Buffer | Cumulative Release | References |
|---|--|-----------------------|--------------------------|
| PVA/PCL | Deionized water and 5 % CO ₂ | 70 % in 7 days | (Mohseni et al., 2016) |
| PVP/Gelatine | Phosphate Buffer Saline 7 | 35-40 ppm in 30 hours | (Semnani et al., 2018) |
| PVA nanofibers containing Cyclo Dextrin | Deionized Water | 80 ppm in 7 hours | (Nalbandi & Amiri, 2019) |
| Gelatine /PU | Phosphate Buffer Saline 7.4 | 100 % in 48 hours | (Heo et al., 2013) |
| PCL/ β - Cyclo Dextrin | NH ₃ OH solution (30% v/v) | 66.4 % in 24 hours | (Souza et al., 2018) |
| PCL/PEO Nanofiber | Water/ Propylene Glycol/ Phosphoric Acid | 82 % in 24 hours | |
| PLA/PEO Nanofiber | Water/ Propylene Glycol/ Phosphoric Acid | 60 % in 24 hours | |
| PCL/PEO Casting Film | Water/ Propylene Glycol/ Phosphoric Acid | 55 % in 24 hours | |

Both diffusion and polymer degradation are key factors in controlling the drug release of SSD from the PLA/PEO nanofiber matrix. Highly soluble and degradable PEO rapidly induces the SSD release whereas hydrophobicity and slow degradation rate of PLA provide a gradual release of SSD (Yoo et al., 2009). Moreover, the high surface area of nanofibers enhances the drug dissolution. Basically, the micro-porous structure of PLA/PEO nanofibers enables the drug diffusion from the matrix in two steps: one is the buffer diffusion into the pores to dissolve the SSD drug and the second one is the diffusion of dissolved drug to the outer of the pores. Therefore, the controlled drug release from nanofiber is associated with its micro-porous structure which balances the free access of the buffer into the matrix and diffusion of SSD out of the matrix (Garg et al., 2014).

To explain the SSD drug release kinetics from SSD loaded composite nanofiber; Zero Order, First Order, Higuchi, Hixon Crowell and Korsmeyer-Peppas kinetics models were applied in the drug release profile. The regression coefficients (R^2) according to different kinetic models were given in Table 4.16.

Table 4.16 : Drug release kinetics models for PLA/(PEO+SSD) nanofibers with regression coefficient (R^2).

| Release Kinetic Models | R^2 |
|-------------------------|--------------------|
| Zero Order | 0.814888209 |
| First Order | 0.448341611 |
| Hixon Crowell | 0.584386233 |
| Higuchi | 0.95434973 |
| Korsmeyer-Peppas | 0.994252079 |

The result best fits with the Korsmeyer-Peppas model that indicates the regression coefficient $R^2 = 0.994$. This mathematical model describes the drug release with the following formula as:

$$M_t / M_\infty = k t^n \quad (3)$$

M_t/M_∞ is the released amount of drug at time (t), M_∞ is the total released amount of drug after time ∞ (total drug amount in the formulation), n is the drug release exponent which defines the release mechanism, k is the constant of the release rate. Hence, the exponent of n was found as 0.562. For the cylindrical-shaped matrices; $0.45 \leq n$ represents Fickian diffusion mechanism and non-Fickian or anomalous transport exhibits when $0.45 < n < 0.89$, $n = 0.89$ corresponding to Case II (relaxational) transport and $n > 0.89$ indicates super case II transport (Gouda et al., 2017). In this study, the release profile value of n is higher than 0.45, pointing clearly to the non-Fickian mass transport mechanism which means that diffusion and dissolution are the main factors of the drug release kinetics for SSD loaded composite nanofibers.

4.8.8 Controlling the drug release with conductivity

Drug release studies were also verified with conductivity measurements due to the conductive nature of SSD. At predetermined time intervals of 0.5, 1, 1.5, 2, 3, 4, 5, 6, 7, 8 and 24 hours, 1.5 mL aliquots were sampled. The conductivity of aliquots was measured using Multiparameter meter InoLabMulti 720 (WTW) at room temperature. Conductivity of aliquots versus time plot was represented in Figure 4.50. It is shown that the conductivity increased with time. The reason is related to the release of

conductive SSD particles from nanofiber matrix to the buffer solution. SSD is a silver salt and is conductive in nature. Therefore, when SSD is released to the buffer solution, the electrical conductivity of the solution increases with time.

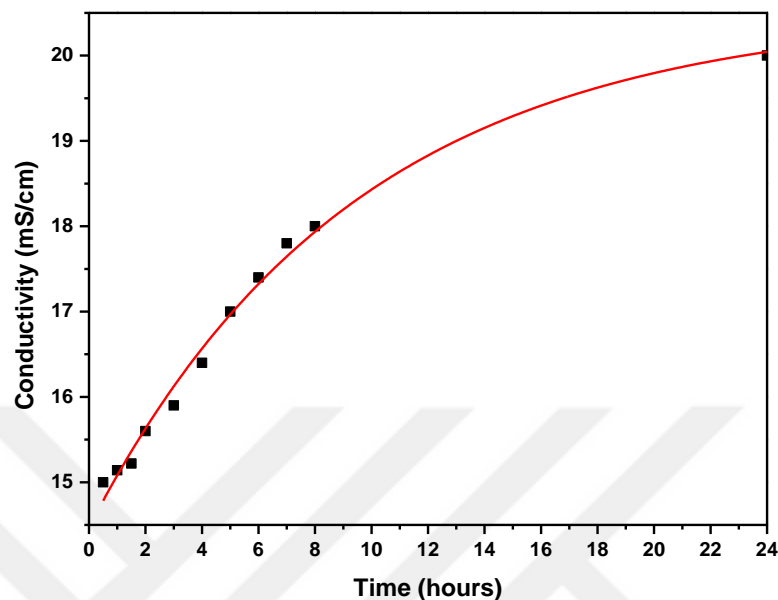


Figure 4.49 : Conductivity of released aliquots versus time.

4.9 Results of Antibacterial Activity Studies

4.9.1 Results of disc diffusion tests

Antibacterial activities of the composite nanofibers against gram negative *Pseudomonas aeruginosa* (*P. aeruginosa*), *Escherichia coli* (*E. coli*) and gram-positive *Staphylococcus aureus* (*S. aureus*) bacteria were performed for the period of 24, 48 and 72 hours.

For antibacterial tests, the PCL(PEO+SSD), PCL+PEO, PLA(PEO+SSD), PLA+PEO nanofiber mats were cut into 1.2 cm circular shaped pieces and the same weighted of the nanofiber samples were chosen to have same amount of SSD. SSD powder was weighed and SSD solution were prepared in the buffer for positive control. Drug-free PCL/PEO and PLA/PEO nanofibers were used as the negative control for antibacterial activity. The antibacterial activity of commercial SSD cream was also evaluated to compare with composite nanofiber patches. Hence, SSD cream was weighted in order to adjust SSD amount within the nanofiber formulations. Then the SSD cream was impregnated on to discs (d=6 mm).

The mortality of the bacteria was observed with formation of the clean zone around the samples. The diameters of the inhibition zone were measured and the results were represented in Table 4.17.

According to the results, SSD loaded composite nanofibers samples showed antibacterial activity against the tested bacteria and they showed controlled release behaviour due to increased zone diameter in three days. Moreover, PCL/(PEO+SSD) and PLA/(PEO+SSD) composite nanofibers were compared with commercial silver sulfadiazine cream and results show that SSD loaded composite nanofibers are more effective on bacteria than silver sulfadiazine cream. Furthermore, the nanofibers showed an increasing antibacterial effect during 3 days. It signs, continued and controlled release of SSD for 3 days period. The needing for change frequency of the nanofiber patch was reduced. At the same time, the antibacterial effects of PLA and PCL nanofibers were measured by the MIC and MBC method. Antibacterial activity test photographs of SSD loaded PCL/PEO composite nanofibers are represented in Figure 4.51.

Table 4.17 : Disc diffusion test results.

*diameters of the inhibition zones in terms of cm

| SAMPLES | <i>P. aeruginosa</i> | | | <i>E. coli</i> | | | <i>S. aureus</i> | | |
|--------------------------------------|----------------------|----------|----------|----------------|----------|----------|------------------|----------|----------|
| | 24 hours | 48 hours | 72 hours | 24 hours | 48 hours | 72 hours | 24 hours | 48 hours | 72 hours |
| PCL (PEO+SSD) | 0.9 | 1 | 1.1 | 0.9 | 0.9 | 1 | 1 | 1.1 | 1.2 |
| PLA(PEO+SSD) | 0.8 | 0.9 | 1.2 | 0.9 | 1 | 1.4 | 1 | 1.1 | 1.3 |
| SSD Cream | 0.7 | 0.75 | 0.75 | 1 | 1.1 | 0.7 | 1.1 | 1.1 | 1.1 |
| Positive Control (Pure SSD) | 1.1 | 1.2 | 1.2 | 1.2 | 1.25 | 1.3 | 1 | 1.1 | 1.1 |
| Negative Control (Drug-free PCL/PEO) | 0.6 | 0.6 | 0.6 | 0.6 | 0.6 | 0.6 | 0.6 | 0.7 | 0.7 |

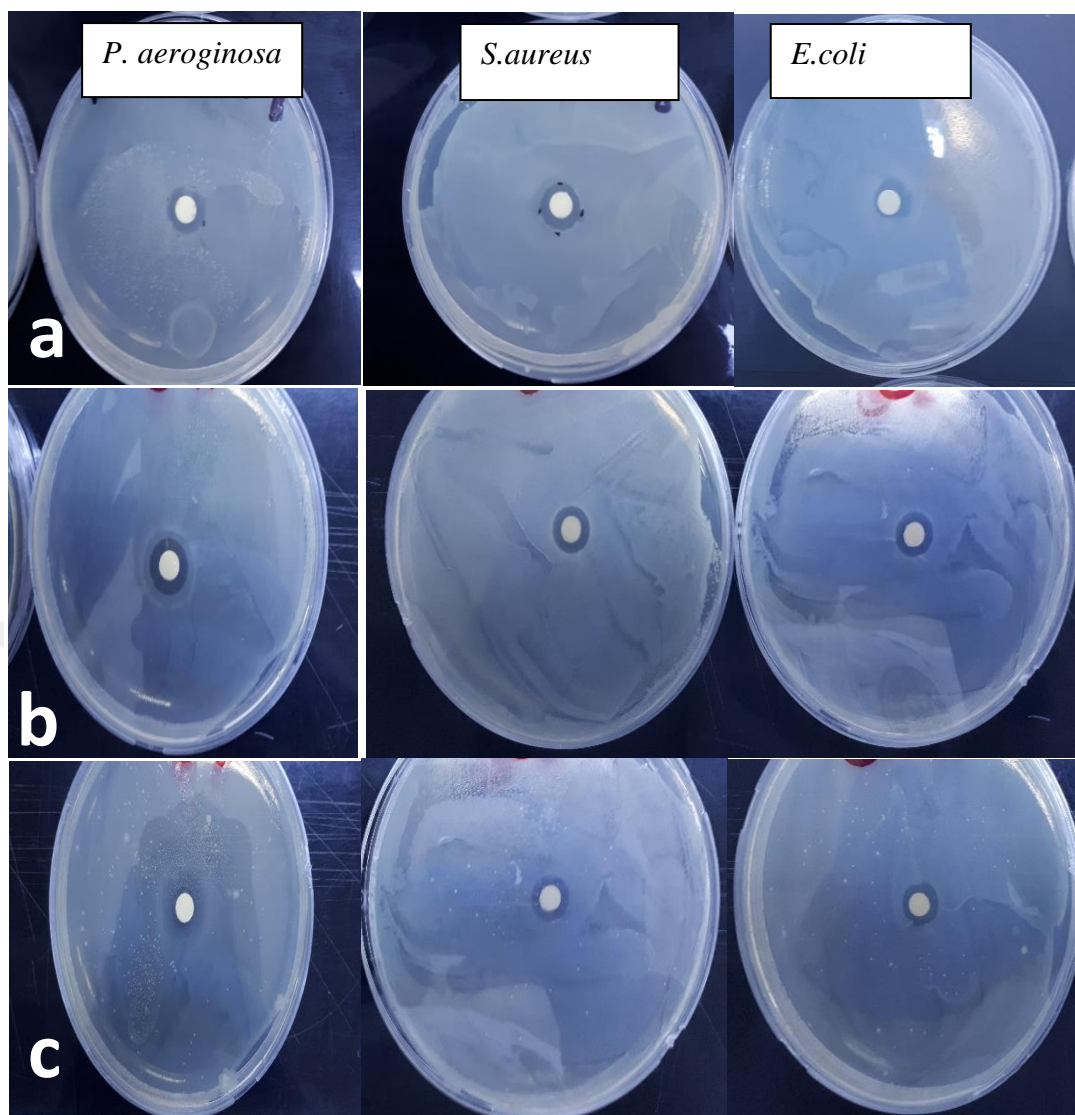


Figure 4.50 : Antibacterial activity photographs of SSD loaded a) PCL/PEO and b) PLA/PEO composite nanofiber mats c) Commercial SSD cream.

4.9.2 Results of Minimum Inhibition Concentration (MIC) and Minimum Bactericidal Concentration (MBC)

Antibacterial activity of the SSD loaded PCL/PEO and PLA/PEO nanofibers were examined against *Pseudomonas aeruginosa* (ATCC 27853) *Staphylococcus aureus* (ATCC 25023) and *E. coli* (ATCC 25922) with determining MIC and MBC values. These values were measured using broth dilution (micro dilution) method.

For the estimation of MIC (Minimum Inhibition Concentration) Series of sample solutions at concentrations of 2560, 1280, 640, 480, 320, 160, 80 ,40 $\mu\text{g/mL}$ were prepared and dispersed in 2 mL of broth media. Then, 20 μL of bacterial suspensions (10^8 CFU/mL) were added into the series of tubes. Therefore, the bacterial cultures were appropriately diluted to get 10^8 CFU/mL and used as primary inoculum. Growth

or no growth was determined by visual inspection. The amount of MIC was determined after overnight incubation on the basis of the lowest concentration of an anti-microbial agent that fully inhibits the growth of bacteria. The MBC quantity was calculated by subcultivating the last transparent agar MIC tube and assessing it for bacterial growth.

For the estimation of MBC (Minimum Bactericidal Concentration), the invisible bacterial suspension samples at different concentrations (2560, 1280, 640, 480, 320, 160, 80, 40 $\mu\text{g/mL}$) were prepared. They were cultured to the agar plates and incubated at 37 °C for 24 h. The surviving colonies were calculated to find the MBC values of the nanofiber specimens. MIC and MBC test results of PLA/(PEO+SSD) and PCL/(PEO+SSD) composite nanofibers were reported in Table 4.18. Also, a test photograph is shown in Figure 4.52.

Table 4.18 : MIC and MBC results of PLA/(PEO+SSD) and PCL/(PEO+SSD) formulations.

| | PLA/(PEO+SSD) | | PCL/(PEO+SSD) | |
|----------------------|--------------------------|--------------------------|--------------------------|--------------------------|
| | MIC ($\mu\text{g/ml}$) | MBC ($\mu\text{g/ml}$) | MIC ($\mu\text{g/ml}$) | MBC ($\mu\text{g/ml}$) |
| <i>P. aeruginosa</i> | 80 | 120 | 320 | 960 |
| <i>E. coli</i> | 160 | 220 | 320 | 480 |
| <i>S. aureus</i> | 80 | 160 | 160 | 480 |

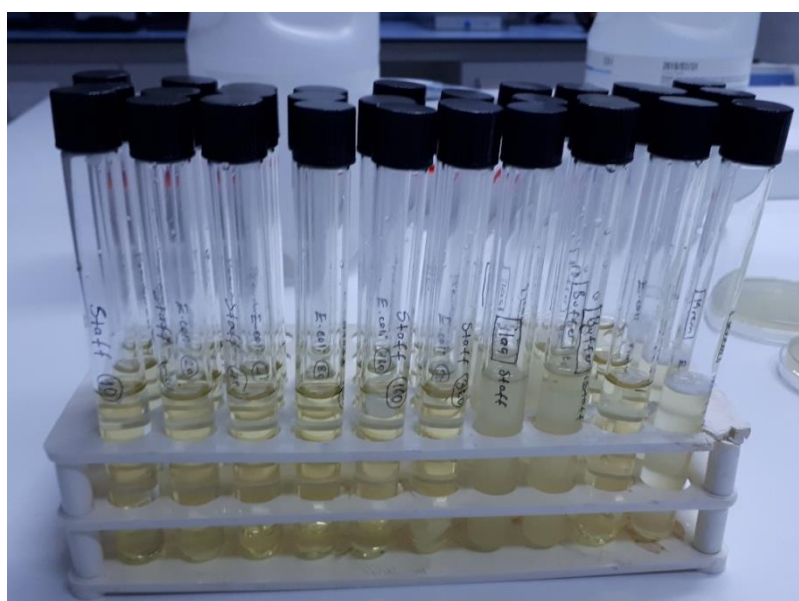


Figure 4.51 : Photograph from MIC and MBC tests.

The MIC and MBC test result verified the antibacterial activity of composite nanofibers. MIC and MBC values should be lower than 16 mg/mL for an effective antimicrobial activity. As seen in Table 4.18, in PLA/(PEO+SSD) nanofibers, the MIC for *P. aeruginosa* and *S. aureus* was found to be 80 µg / mL, while it was 160 µg / mL for *E. Coli*. For PCL/(PEO+SSD) nanofibers, it was found to be 320 µg / mL for *P. aeruginosa* and *E. coli*, and 160 µg / mL for *S. aureus*. In PLA/(PEO+SSD) nanofibers, the concentration to which they are sensitive for *E. Coli* (220 µg / mL) and *S. aureus* (160 µg / mL) in MBC analysis is much lower. For PCL/(PEO+SSD) nanofibers, the situation is the opposite and the concentration to which *P. aeruginosa* is sensitive is lower (960 µg / mL). It has been shown by MIC and MBC analyses that SSD loaded PLA/(PEO+SSD) and PCL/(PEO+SSD) nanofibers have antibacterial effects on *P. aeruginosa*, *S. aureus* and *E. coli* bacteria.

4.10 Results of Stability Studies

Stability studies of the composite nanofibers were done for 3- and 6-month periods. Nanofiber samples were both kept at refrigerator conditions (+4°C) and room conditions (25°C ±2 and 65 % ±2 relative humidity) to evaluate stability of nanofiber patches. Stability tests were performed with calculating drug loading amount, cumulative drug release by UV absorption measurements, analysing surface morphology by SEM analysis.

4.10.1 Results of stability testing with SEM analysis

Drug loaded and drug-free PCL/PEO and PLA/PEO nanofiber formulations were waited for 3 and 6 months at 20 ±2°C, 65 % relative humidity and +4°C refrigerator conditions. Surface morphologies and average fiber diameters of the formulations were examined by SEM. Then stability of the formulations was evaluated according to the SEM Images. SEM images and fiber diameter histograms of the PCL/PEO, PCL/(PEO+SSD), PLA/PEO and PLA/(PEO+SSD) formulations are represented in Figure 4.53, Figure 4.54, Figure 4.55 and Figure 4.56.

Figure 4.53 showed that, average fiber diameter of the PCL/PEO nanofiber decreases from 400 ±60 nm to 395 ±55 nm after storage under +4°C refrigerator conditions for 3 months. Besides, average fiber diameter of PCL/PEO nanofiber increases from 400 ±60 nm to 424 ±100 nm after storage under 25°C room conditions for 3 months.

Figure 4.54 showed that, average fiber diameter of the PCL/(PEO +SSD) nanofiber decreases from 340 ± 58 nm to 338 ± 100 nm after storage under $+4^{\circ}\text{C}$ refrigerator conditions for 3 months. Besides, average fiber diameter of PCL/PEO nanofiber increases from 340 ± 58 nm to 451 ± 110 nm after storage under $25 \pm 2^{\circ}\text{C}$ room conditions for 3 months.

Figure 4.55 showed that, average fiber diameter of the PLA/PEO nanofiber decreases from 554 ± 90 nm to 470 ± 80 nm after storage under $+4^{\circ}\text{C}$ refrigerator conditions and decreases from 554 ± 90 nm to 402 ± 60 nm after storage under $25 \pm 2^{\circ}\text{C}$ room conditions for 3 months.

Figure 4.56 showed that, average fiber diameter of the PLA/(PEO+SSD) nanofiber increases from 311 ± 63 nm to 314 ± 60 nm after storage under $+4^{\circ}\text{C}$ refrigerator conditions for 3 months. Besides, average fiber diameter of PLA/(PEO+SSD) nanofiber increases from 311 ± 63 nm to 460 ± 60 nm after storage under $25 \pm 2^{\circ}\text{C}$ room conditions for 3 months.

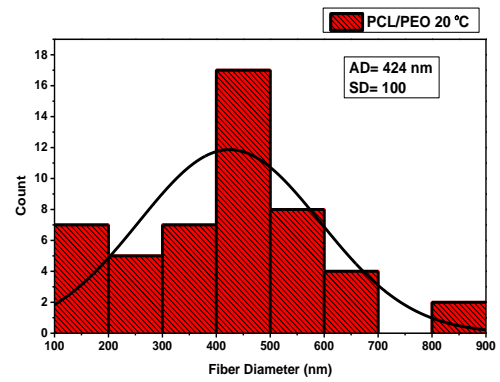
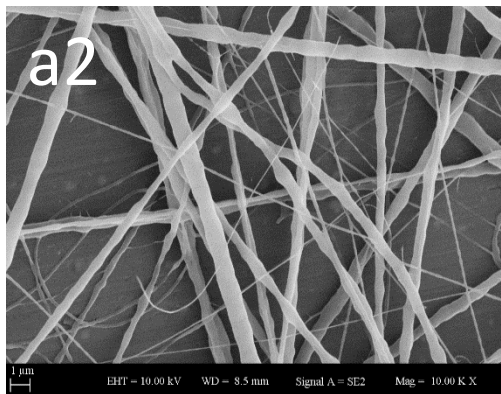
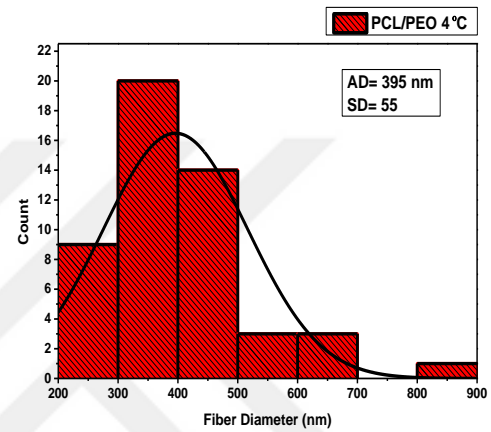
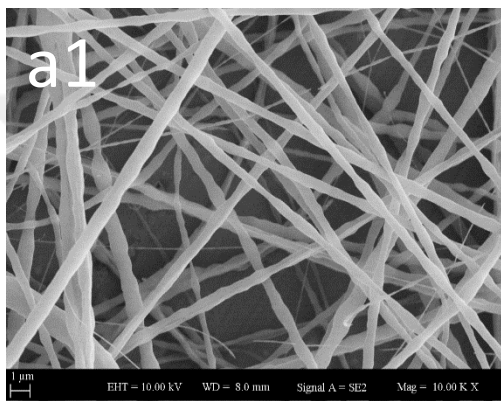
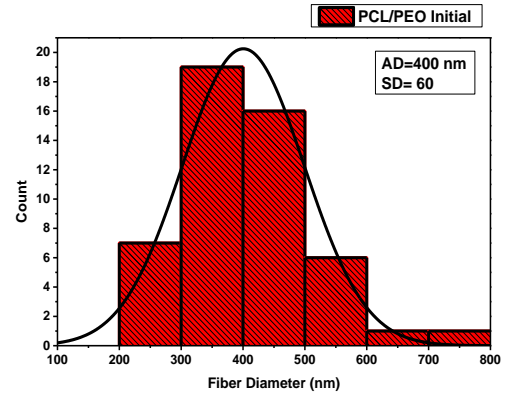
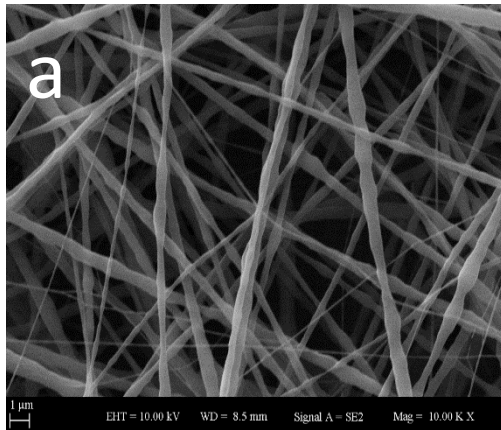


Figure 4.52 : SEM images of PCL/PEO a) Initial a1) Storage at +4°C; a2) Storage at 25°C after 3 months.

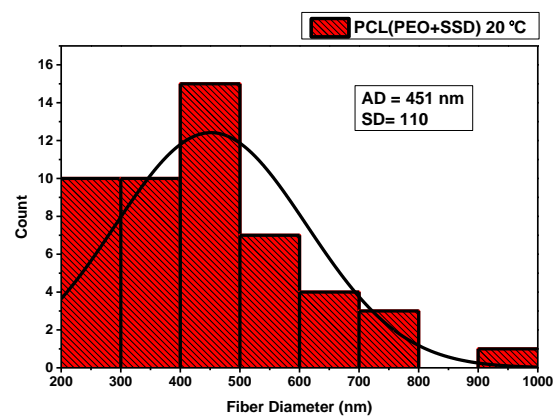
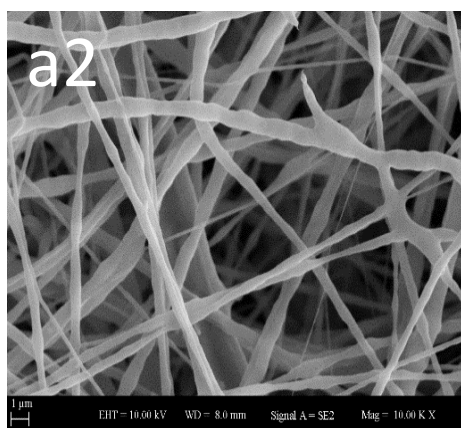
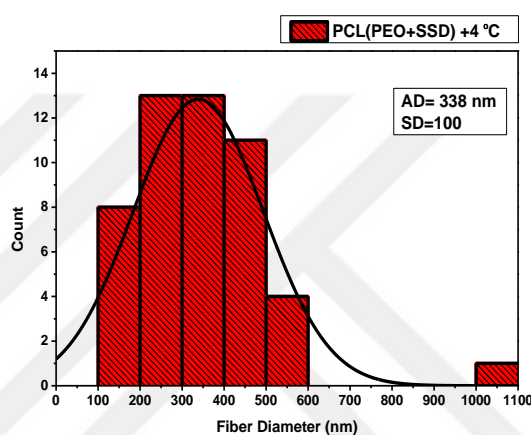
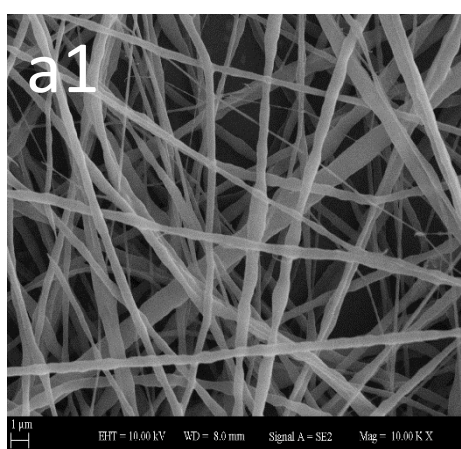
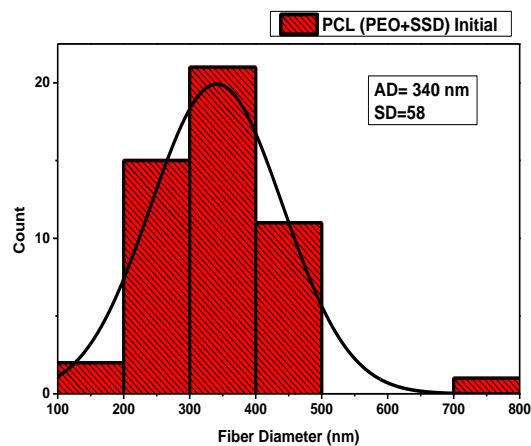
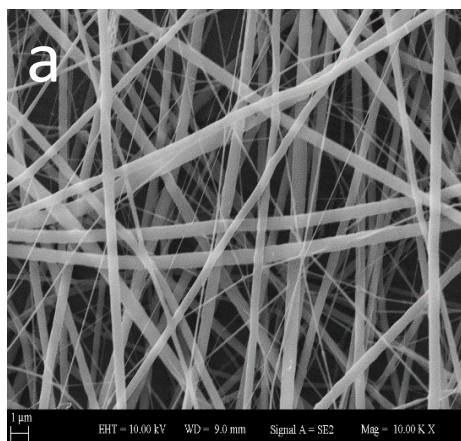


Figure 4.53 : SEM images of PCL/(PEO+SSD) composite nanofibers a) Initial, a1- Storage at +4°C after 3 months, a2) Storage at 25°C after 3 months.

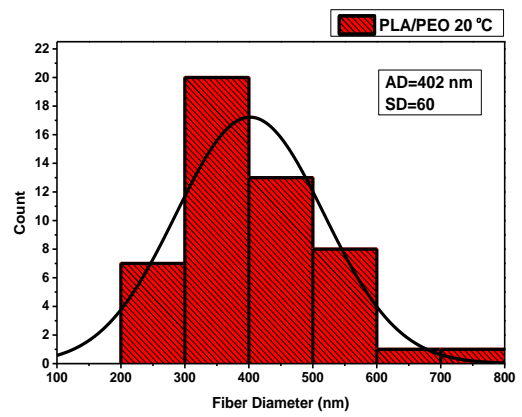
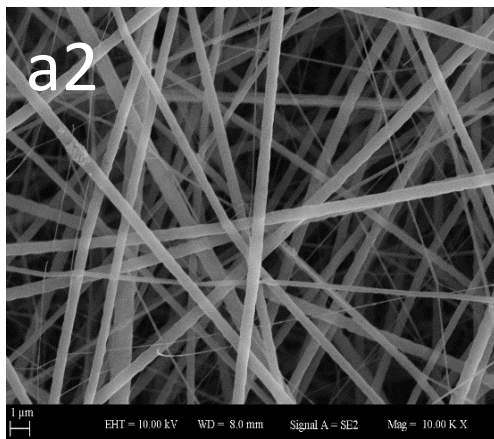
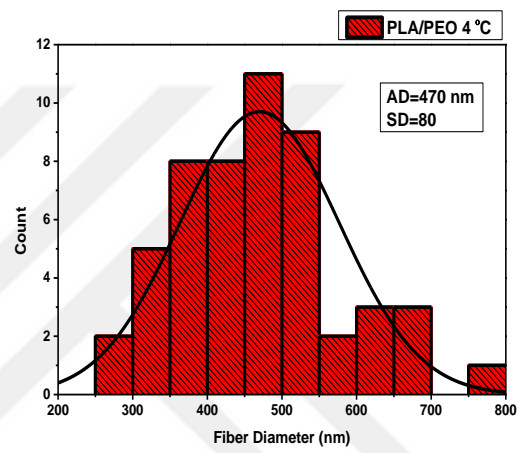
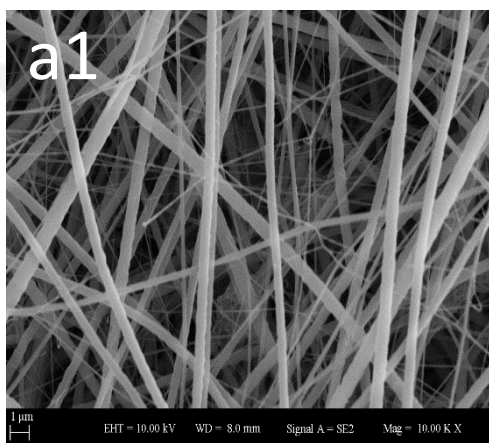
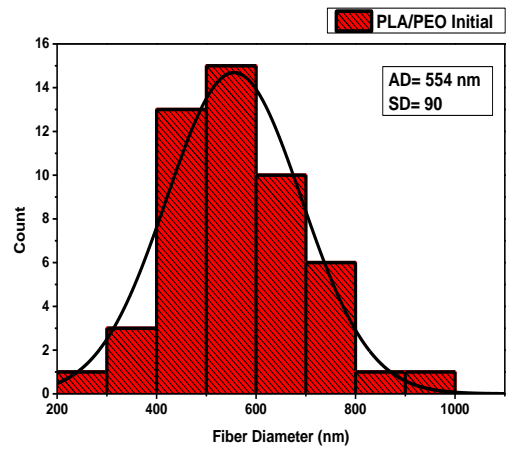
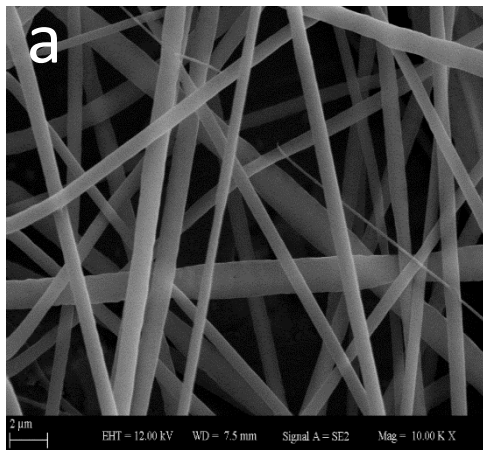


Figure 4.54 : SEM Images of a) PLA/PEO composite nanofibers a) Initial a1) Storage at +4°C; a2) storage at 25°C after 3 months.

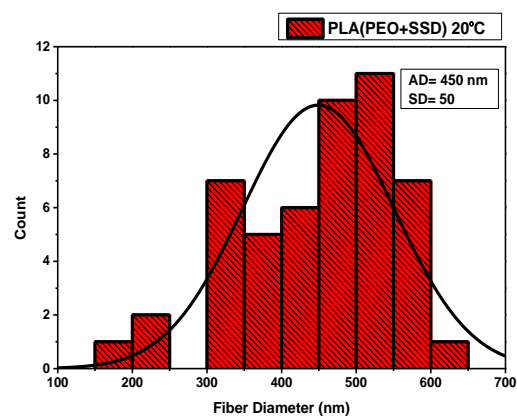
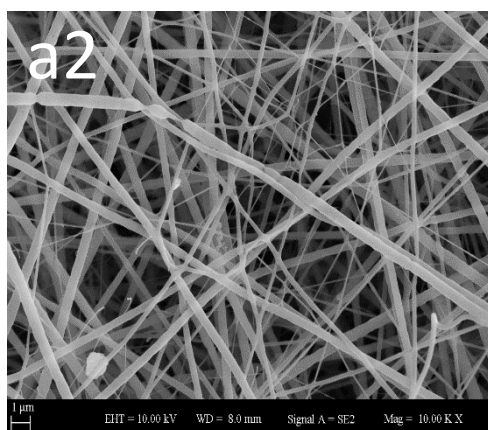
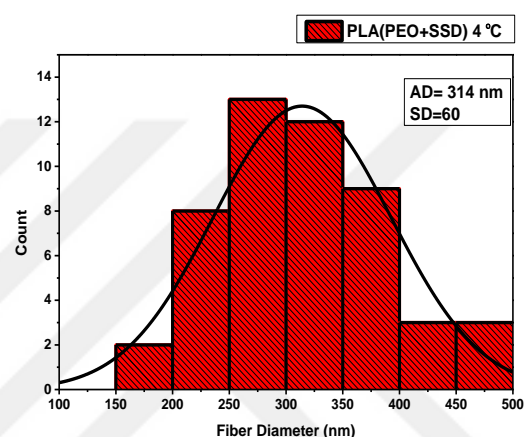
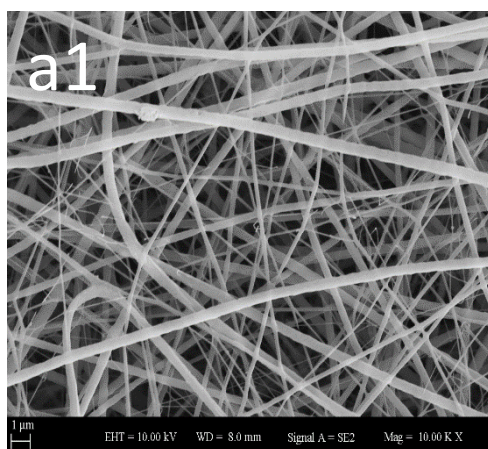
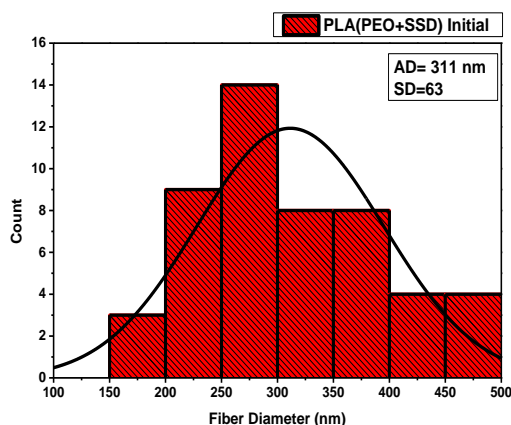
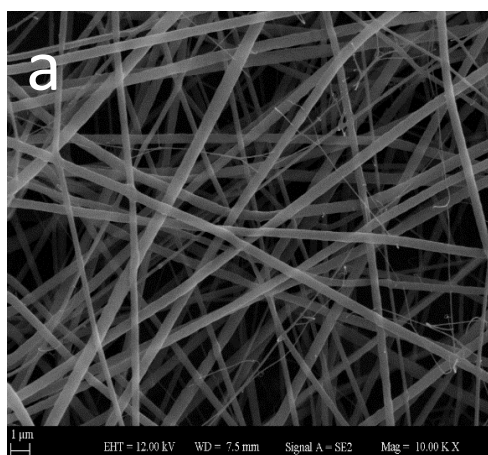


Figure 4.55 : SEM images of PLA/(PEO+SSD) composite nanofibers a) Initial a1) Storage at +4°C after 3 months; a2) Storage at 25°C after 3 months.

SEM images demonstrated that there was no sharp or marked distinction between general fiber morphologies of nanofiber formulations which were stored under refrigerator conditions and room conditions. It is shown that fibers are coarser and have less fiber uniformity under room conditions in comparison to initial state of formulations. This can be explained effect of temperature and relative humidity of the

room conditions. However, when the formulations stored at refrigerator conditions, fiber diameters were stable with high uniformity in comparison to initial state of the formulations. Moreover, when the fiber diameters of stored nanofibers are compared; it is seen that the fiber diameters of the nanofibers which are stored at room conditions have more diameters with higher SD than stored at refrigerator conditions. Therefore, SSD loaded composite PCL/PEO and PLA/PEO nanofibers should be kept in refrigerator until 3 months. These formulations can be utilized in topical drug delivery with complying the storage conditions.

4.10.2 Results of stability testing with calculating the drug loading amount

Drug loaded and drug-free nanofiber formulations were waited for 3 and 6 months at $20 \pm 2^\circ\text{C}$ and $+4^\circ\text{C}$ refrigerator conditions. Then loading drug amount of the formulations were estimated which method were explained in 3.7.7. Drug Loading Efficiency section. Test results were shown in Table 4.19.

Table 4.19 : Drug loading amount of SSD loaded and SSD free nanofiber formulations which were waited for 3 and 6 months at $25 \pm 2^\circ\text{C}$ and $+4^\circ\text{C}$ refrigerator conditions.

| Formulation | Initial % | Storage at $+4^\circ\text{C}$ | | Storage at $25 \pm 2^\circ\text{C}$ | |
|--------------|-----------|-------------------------------|------------|-------------------------------------|------------|
| | | 3 Months % | 6 Months % | 3 Months % | 6 Months % |
| PCL(PEO+SSD) | 86 | 83 | 79 | - | - |
| PLA(PEO+SSD) | 82 | 80 | 77 | - | - |

The results showed that, $25 \pm 2^\circ\text{C}$ (room temperature) is not a suitable storage condition for PCL/(PEO+SSD) and PLA/(PEO+SSD) formulations. Since, the drug loaded nanofiber patches were decomposed with changing the colour so drug loading efficiency could not be calculated. However, PCL/(PEO+SSD) and PLA/(PEO+SSD) formulations should be kept and storage in $+4^\circ\text{C}$ refrigerator conditions. Changing the patch color from white to yellowish, signs the oxidation of SSD (Cioroiu et al., 2013; Url-8). Since SSD active agent shows oxidation sensitivity with the effect of temperature, SSD loaded composite nanofibers could not maintain their stability at room temperature. However, this sensitivity was tolerated with the decrease in the temperature of the environment, that is, by keeping the formulations under refrigerator conditions instead of room conditions. SSD loaded composite nanofibers can be stored

in refrigerator conditions without the need for any antioxidant or pharmaceutical excipient.

4.10.3 Results of stability testing with cumulative drug release

Drug loaded and drug-free nanofiber formulations were waited for 3 and 6 months at $25 \pm 2^\circ\text{C}$ and $+4^\circ\text{C}$ refrigerator conditions. Then the cumulative drug release % versus time graph was plotted for initial, 3 months and 6 months stored samples. The graphs were represented in Figure 4.57.



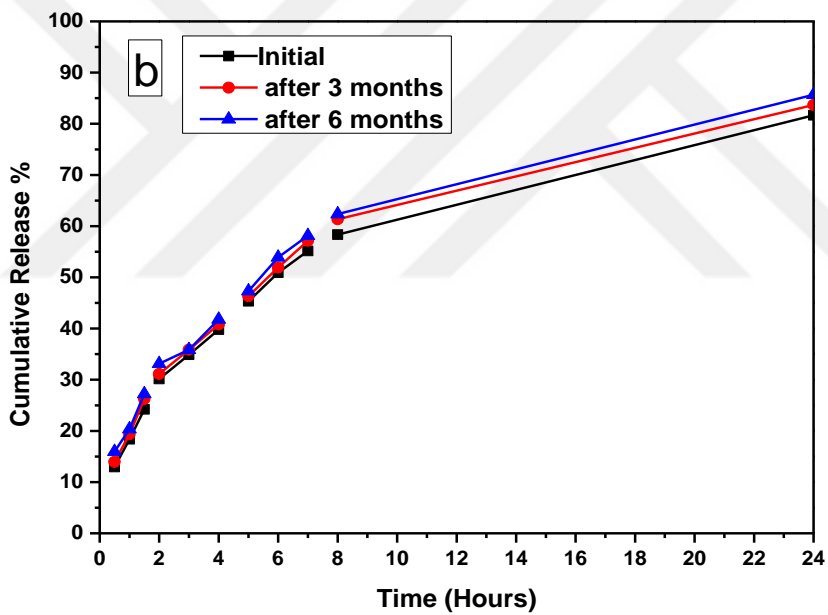
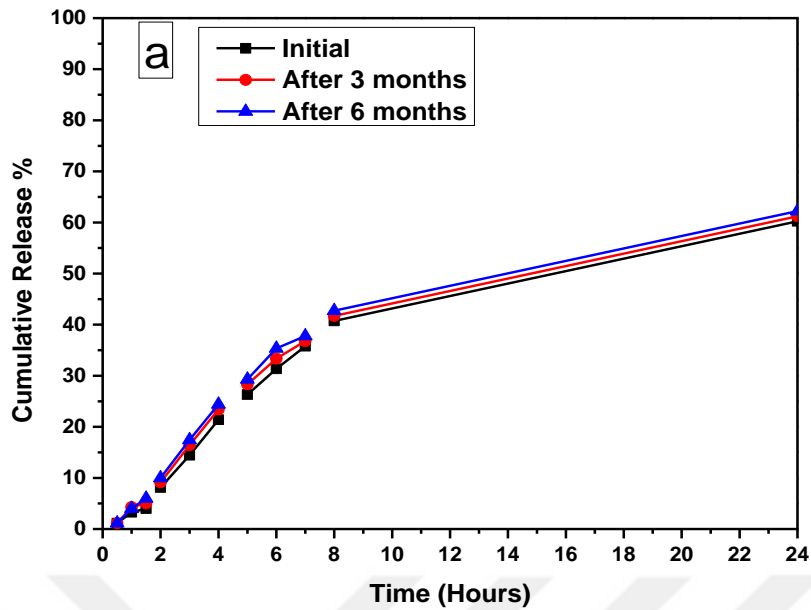


Figure 4.56 : *In vitro* drug release profiles for a) PLA(PEO+SSD) nanofibers b) PCL(PEO+SSD) after 3 and 6 months of storage, protecting from light at +4°C refrigerator conditions.

In vitro test results showed that after storage for 3 and 6 months, the release profile of the SSD loaded PCL/PEO and PLA/PEO nanofibers appeared to be much similar to that obtained at initial time. It indicated that SSD loaded PCL/PEO and PLA/PEO nanofibers were stable under the refrigerator storage conditions.

4.11 Results of Cytotoxicity Test

The cytotoxicity studies of the drug loaded and drug-free PCL/PEO and PLA/PEO nanofiber patches were made using the cell viability assay (MTT assay). Four samples were prepared for each composite nanofiber in a circular shape with 10 mm diameter. The samples were sterilized under UV light for 30 minutes to avoid contamination.

L929 mouse fibroblast cells were used for the experiment and they are seeded into 96-well cell culture plates. 100 µl DMEM medium was used as negative control and 1 % phenol solution was used as positive control. Nanofiber samples were placed wells and treated with cells. After 24 hours treatment, the cells were inoculated in 100 µl growth DMEM medium and 100 µl MTT medium. The well culture plate was kept in a dark environment for 4 h at 37°C. Then, MTT was removed, the cells were rinsed with glycine buffer and 100 µl DMSO was added to each well respectively. Finally, the absorbance at 570 nm was measured using a UV-visible spectrophotometer (Ozdemir et al., 2009). Cytotoxicity test values were represented in Table 4.20.

Table 4.20 : Cytotoxicity test results.

| SAMPLE | VIABILITY % | STANDARD DEVIATION |
|---|-------------|--------------------|
| PLA /PEO | 100.26 | 0.342 |
| PCL/PEO | 98.5 | 0.263 |
| PLA(PEO+SSD) | 3.9 | 0.002 |
| PCL(PEO+SSD) | 7.9 | 0.003 |
| Negative Control (100 µl DMEM medium) | 100 | 0.04 |
| Positive Control (1 % phenol solution) | 3.46 | 0.001 |

Cytotoxicity test results showed that PLA/PEO and PCL/PEO polymer matrices are suitable and safe materials for biomedical applications with 100 and 98 % viability values. However, with addition of SSD viability values decreased because of the antibacterial effect of SSD.

5. CONCLUSIONS

Drug delivery systems is an important field in biomedical applications, which facilitates the introduction of a drug in the body and increases the treatment efficiency, maintains sufficient drug content in the blood for a period of time, carries drug to target point in a safe way and reduces side effects of release within the body (Zamani et al., 2013) Possessing ideal surface properties, microstructure and polymer matrix plays a critical role for drug carriage and delivery.

Electrospun nanofibers have excellent properties such as high interconnected porosity, specific surface area, ability to imitate the Extra Cellular Matrix (ECM) and potential carrier for drug delivery. Due to these fascinating properties, nanofibers are attractive materials for drug delivery systems (Wen et al., 2005; Huang et al., 2003). Utilization of nanofibers in drug delivery systems is based on the principle that the high surface area of the nanofibrous formulation increases the dissolution rate of the drug. In comparison to other dosage forms major advantages of nanofibers are increment in drug loading efficiency and loading capacity, low systemic toxicity and excellent stability (Hu et al.,2014). Furthermore, several drugs can be carried within nanofibers with high local drug concentration due to their excellent targeting and drug transportation ability in a safe way (Morie et al.,2016). Electrospinning is one of the simplest among all methods to fabricate nanoscaled fibers and it offers the opportunity for direct loading of drug into the electrospun nanofibers (Taylor, 1964; Sarac, 2017). Many drugs and bioactive molecules are loaded into nanofibers which were explained in literature survey of the thesis.

Silver sulfadiazine (SSD) is a non-ionized, water-insoluble, topical antibacterial agent that is used extensively in the topical treatment of infected burns (White & Cooper, 2005). SSD is a poorly aqueous soluble drug (3.4 mg/ L at pH = 6.8). The low solubility restricts the drug efficiency, bioavailability and potential antibacterial activity of SSD thus its applications are limited. Drug solubility is an important issue since efficient drug release occurs just by decomposition of SSD to sulfadiazine and silver ions. Also, the solubility problem of SSD makes it difficult to be stabilized and incorporated into

the polymer matrix. Water insolubility is a challenge of SSD. Therefore, researchers have focused on the enhancement of its solubility and bioavailability. To this end, SSD was formed as nanoparticles, nanorods, nanosuspensions or incorporated into different polymeric carriers by formulating as film, semi-interpenetrating networks (Kao et al., 2009), hydrogel, composite and fiber-based drug delivery systems (Szegedi et al., 2014; Li et al., 2015). However, in the literature, there are a limited number of researches on SSD loading into electrospun nanofibers, its solubility and drug release behaviour. In this study, SSD was used as a drug for loading into the electrospun fibers.

Polymer blending is an efficient approach to prepare functional nanofibers by incorporating the favourable properties of the component polymers. Furthermore, polymer blending facilitates the manipulation of physical, mechanical or biochemical properties of nanofibers. Hydrophilic/hydrophobic polymer blends have been electrospun into nanofibers to fabricate controlled DDS. The hydrophobic polymer forms the backbone structure and it degrades slowly, creating a long term but steady-state drug release. On the other hand, the hydrophilic polymer degrades with a more rapid process, faster than hydrophobic, which accelerates the drug release (Heunis & Dicks, 2010; Hanumantharao et al., 2019). In this study, hydrophilic water-soluble PEO was selected for the polymer matrix to improve the solubility and bioavailability of insoluble SSD. The hydrophobic character of PCL and PLA offers a long period SSD release therefore hydrophilic PEO was blended with hydrophobic PCL. Thus, PCL/ PEO and PLA/PEO composite polymer matrix was used to provide both increased solubility and controlled release of SSD.

The aim of the thesis is to produce a novel SSD loaded topical drug delivery system by using advantages of electrospun nanofibers. For this purpose, three different formulations were fabricated; namely, PCL/(PEO+SSD) nanofibers, PCL/(PEO+SSD) casting films and PLA/(PEO+SSD) nanofibers.

PEO, PEO+SSD, PCL, PLA, PCL/PEO, PLA/PEO, PCL/(PEO+SSD) and PLA/(PEO+SSD) polymer solutions were prepared and then they were electrospun into nanofibers. Different electrospinning and solution parameters were tried to obtain smooth, bead free and uniform fiber morphology. Optimum parameters for PEO, PEO+SSD, PCL, PLA, PCL/PEO, PLA/PEO, PCL/(PEO+SSD) and PLA/(PEO+SSD) polymer solutions and nanofibers were given in experimental

section. PCL/PEO and PLA/PEO solutions were miscible and phase separation was not seen in the PCL/PEO and PLA/PEO blend solution.

PCL/(PEO+SSD) casting film was fabricated to compare with the nanofiber formulations. The prepared PCL, PEO, PCL/PEO and PCL/(PEO+SSD) solution was dropped on aluminium foil, then solution was sheared in a rapid by doctor blade micrometre. The solution formed as a film and the film samples were dried in oven at 40°C for 30 min. EDS Mapping images showed that SSD molecules distributed in the casting film structure with some agglomeration, not as homogeneously as in the nanofiber structures.

SEM method was used to enable the observations of fiber defects and irregularities in the nanofibers structures which have significance on behaviour of nanofibers in drug release. The fiber diameters were determined using the Image J Program from 50 different fiber sections of a scanning electron microscopy (SEM) image. SEM Images showed that successful production of the pure and SSD loaded PCL/PEO and PLA/PEO composite electrospun nanofibers were achieved by the electrospinning method. PCL/PEO and PLA/PEO blended homogeneously and phase separation did not occur during electrospinning. Additionally, blend of PCL-PEO-SSD and PLA-PEO-SSD molecules were bonded physically and have good interaction in the composite fiber structure. Thereby, continuous, uniform, homogenous, porous and bead free composite nanofibers with circular cross sections were obtained. Moreover, it was seen that the average fiber diameter decreased from 374 nm (PCL/PEO) to 254 nm PCL/(PEO+SSD) and from 554 nm PLA/PEO to 311 nm PLA/(PEO+SSD) due to the inclusion of the conductive SSD particles in nanofiber matrices. Electrospinning solution contains a high amount of charged silver and sulfadiazine ions by the addition of SSD into the PEO solution. It supplies more electric charges to the electrospinning jet in order to overcome the surface tension of the solution. The bead defects are formed on the fiber surface if the polymer jet is not fully stretched. Therefore, when SSD is added to the solution, the electrical conductivity of the solution increases, resulting in the stretching of the solution. Consequently, smooth fibers were formed and fiber diameter decreases with greater uniformity by cause of a high stretching force (Saquing et al., 2009). Thus, when compared to pure nanofibers, diameters of the SSD loaded composite nanofibers were smaller with less \pm SD.

Energy dispersive spectra (EDS) analysis was performed to confirm that PCL/(PEO+SSD) nanofibers contain SSD, by detecting the Silver (Ag), Nitrogen (N), Sulphur (S) content of the nanofibers. Moreover, EDS-Mapping was carried out to show the distributions of these elements in composite nanofibers. The peaks of Ag, N, S within the EDS spectra indicate their presence in the fiber structure, indicating that the nanofiber mats are evenly loaded with SSD. EDS-Mapping images demonstrated that SSD molecules were distributed homogeneously in the fiber structure without any aggregation. The smaller diameter of SSD containing nanofibers can be related to the uniform distribution of the SSD in the nanofiber matrix without aggregation.

The stability of SSD in the fiber structure and the molecular interactions in the drug-free and drug loaded nanofibers were examined by Attenuated Total Reflectance Infrared (FTIR-ATR) Spectroscopy. SSD loaded PEO nanofibers represented the specific peaks of SSD at 784 cm^{-1} due to the asymmetric stretching of SO_2 , at 1583 and 1556 cm^{-1} attributed to aromatic C=C stretching, 1649 cm^{-1} conjugated to NH_2 stretching. Drug-free PCL/PEO and PLA/PEO nanofibers were not influenced quietly with the addition of SSD in PCL/PEO nanofibers. This means, SSD bounded to polymer matrix physically and overall symmetry of the SSD molecule did not significantly change in the electrospun nanofiber matrix (Xue et al., 2014).

X-ray diffraction (XRD) analysis was performed to examine the crystalline structure of the SSD loaded composite electrospun nanofibers. The XRD pattern of SSD loaded PCL/PEO and PLA/PEO nanofibers exhibited microcrystalline nature of SSD, by the distinctive one single peak at 10.2° . However, the other distinctive peak of SSD at 8.8° did not appear in the diffraction pattern of PCL/(PEO+SSD) whereas it appears in PEO+SSD with shifting to 8.2° . This is related to the addition of PCL and PLA that decreases the percentage of SSD in the formulations. Moreover, the weak peak at $2\theta = 8.8^\circ$ totally disappeared while the stronger peak at $2\theta = 10.2^\circ$ was still observed in the XRD pattern. PCL/(PEO+SSD) and PLA/(PEO+SSD) formulations showed the characteristics peak of SSD at 10.2° with a low intensity that points out the loss in crystallinity. Moreover, loaded SSD into the nanofiber matrix was crystalline with reduced crystallinity determining that structural stability of SSD was achieved during electrospinning.

AFM was used to evaluate the surface roughness of the composite nanofibers. 3D AFM Images shows the roughness structure of nanofibers. Surface roughness values

increase with the addition of SSD. It is observed that the roughness values of the drug loaded PCL/PEO (200 nm) and PLA/PEO (330 nm) nanofibers were higher than pure PCL/PEO and PLA/PEO (220 nm) nanofibers (150 nm). The probable reason of that is not only the presence of SSD inside the fiber but also the presence of SSD on the surface of the nanofibers.

The wettability properties of the surfaces were examined with water contact angle measurement. Because of the inherent hydrophilic nature of the PEO polymer there was a need to blend it with hydrophobic polymers for this reason well-known hydrophobic PCL and PLA were added to the PEO. When PEO nanofibers patch contacts with water, due to its super hydrophilic nature, PEO patch is spread on the surface immediately and contact angle of the PEO patch could not measure. With the addition of PCL and PLA, individually, hydrophobicity of the PLA/PEO and PCL/PEO nanofibers increased. On the other hand, PCL and PLA are very hydrophobic polymers and they have low wettability. Therefore, using PCL and PLA alone is a challenge in biomedical field because there is a necessity of contact with body fluids of the material. Stabilization of the polymer matrix was done by combination of PEO with hydrophobic PCL and PLA polymers individually. Otherwise there is no significant difference but the contact angle values of the drug-free composite nanofibers were lower than the SSD loaded composite nanofibers. This can be attributed to the hydrophobic characteristic of SSD decreased the surface hydrophilicity of the formulation.

As it is stated in the thesis, SSD has limited and low solubility in aqueous solutions. Although SSD is usually utilized in burn treatment, there is limited number of researches on SSD loading into nanofibers. The solubility behaviour of SSD was examined in different buffers. Among them, an unused buffer Water/Propylene Glycol / Phosphoric Acid (82:16:2) was decided to use as release media owing to the better solubility and enabling sink condition for drug release study. Hydrophilic water-soluble PEO was selected for the polymer matrix to improve the solubility and bioavailability of insoluble SSD. The hydrophobic character of PCL and PLA offers a long period SSD release therefore hydrophilic PEO was blended with hydrophobic PCL and PLA. Thus, taking the advantages of nanofibers such as high interconnected porosity and high surface area SSD was loaded into PCL/PEO and PLA/PEO

nanofibers for the first time. PCL/ PEO and PLA/PEO composite polymer matrix was used to provide both increased solubility and controlled release of SSD.

In vitro drug release media and release conditions were optimized and the controlled drug release profile was obtained for 24 hours. It is shown that cumulative release % of PCL/(PEO+SSD) casting film is lower than the nanofiber formulations with 50 % release in 24 hours. The PCL/(PEO+SSD) and PLA/(PEO+SSD) nanofiber formulations exhibited better release profile with 80 % and 60 % release in 24 hours, respect. This is attributed to high surface are and high pore interconnectivity of nanofiber. Therefore, the nanofiber formulations are better candidates than casting film for topical drug delivery systems. PCL/(PEO+SSD) nanofibers showed high release % in comparison to PLA/(PEO+SSD) nanofibers. This can be explained the more hydrophobicity of PLA/(PEO+SSD) nanofibers which was demonstrated with contact angle studies. Hydrophobicity of the material restrict the polymer degradation and drug dissolution resulting in slow and long release action. The PLA/(PEO+SSD) nanofibers can be utilize for prolonged topical drug delivery systems. For instance, it can be preferred for 2-3 daylong drug release while the PCL/(PEO+SSD) nanofibers are suitable for 24-hour drug release period. Additionally, it is known that 4 % SSD loaded into the PLA/(PEO+SSD) nanofibers while 3.2 % loaded into PCL/(PEO+SSD) nanofibers. When the release amount of SSD was evaluated it is shown that there is not important difference in release amount of SSD between PCL/(PEO+SSD) and PLA/(PEO+SSD) nanofiber formulations.

Drug loading efficiency $86 \% \pm 4$ was achieved for PCL/(PEO+SSD) nanofibers, $65 \% \pm 2$ for PCL/(PEO+SSD) casting film and $80 \% \pm 4$ for PLA/(PEO+SSD) nanofibers. The casting film formulation showed lower loading efficiency than the PCL/(PEO+SSD) and PLA/(PEO+SSD) nanofiber formulations. It is indicated that the nanofiber formulations are better candidates than the PCL/(PEO+SSD) casting film formulation for topical drug delivery. In comparison with the other studies in the literature, the optimized PLA/(PEO+SSD) and PCL/(PEO+SSD) nanofibers formulations showed high loading efficiency. It is clearly pointed that the nanofiber formulations are promising drug carriers for efficient drug loading thanks to the specific surface area and high porous structure of nanofibers (Morie et al., 2016).

To understand the SSD drug release mechanisms from SSD loaded composite nanofiber; Zero Order, First Order, Higuchi, Hixon Crowell and Korsmeyer-Peppas

kinetics models were applied in the drug release profiles of the formulations. The regression coefficients (R^2) best fit with the Korsmeyer-Peppas model for all formulations. In this thesis, the release profile value of n is higher than 0.45 for nanofiber formulations, that is pointing clearly to the non-Fickian mass transport mechanism which means that diffusion and dissolution are the main factors of the drug release kinetics for SSD loaded composite nanofibers. Otherwise, the release profile value of n is lower than 0.45 for casting film, that is pointing clearly to the Fickian mass transport mechanism which means that only diffusion is the key factor for the drug release kinetics of SSD loaded composite nanofibers.

Drug release studies were also verified with conductivity measurement due to the conductive nature of SSD. It is shown that the conductivity increased with time. The reason is related to the release of conductive SSD particles from nanofiber matrix to the buffer solution. SSD is a conductive silver salt and when it is released to the buffer solution, the electrical conductivity of the solution increases with time.

Antibacterial activities of the composite nanofibers against gram negative *Pseudomonas aeruginosa* (*P. aeruginosa*), *Escherichia coli* (*E. Coli*) and gram-positive *Staphylococcus aureus* (*S. aureus*) bacteria were performed for the period of 24, 48 and 72 hours. The antibacterial activity of commercial SSD cream was also evaluated to compare with composite nanofiber patches. According to the results, SSD loaded composite nanofibers samples showed antibacterial activity against the tested bacteria and they showed controlled release behaviour due to increased zone diameter in three days. Moreover, PCL/(PEO+SSD) and PLA/(PEO+SSD) composite nanofibers were compared with commercial silver sulfadiazine cream and results show that SSD loaded composite nanofibers are more effective on bacteria than silver sulfadiazine cream. Furthermore, antibacterial activity of the SSD loaded PCL/PEO and PLA/PEO nanofibers were examined with determining MIC and MBC values. It has been shown by MIC and MBC analyses that SSD loaded PLA (PEO+SSD) and PCL/(PEO+SSD) nanofibers have antibacterial effects on *Pseudomonas aeruginosa*, *Escherichia coli* and *Staphylococcus aureus* bacteria.

Stability studies of the composite nanofibers were done for 3- and 6-month periods. Nanofiber samples were kept both at refrigerator conditions ($+4^{\circ}\text{C}$) and room conditions ($25^{\circ}\text{C} \pm 2$ and $65\% \pm 2^{\circ}\text{C}$ relative humidity) to evaluate stability of nanofiber patches. Stability tests were performed with calculating drug loading amount,

cumulative drug release by UV absorption measurements and analysing surface morphology by SEM analysis.

SEM images demonstrated that fibers are coarser and have less fiber uniformity under room conditions in comparison to initial state of formulations. However, when the formulations stored at refrigerator conditions, fiber diameters were stable with high uniformity in comparison to initial state of the formulations. Moreover, when the fiber diameters of stored nanofibers are compared; it is seen that the fiber diameters of the nanofibers which are stored at room conditions are coarser with higher \pm SD than stored at refrigerator conditions. Therefore, SSD loaded composite PCL/PEO and PLA/PEO nanofibers should be kept in refrigerator until 3 months. These formulations might be utilized for topical drug delivery with complying the storage conditions.

The results of drug loading efficiency studies showed that, $25 \pm 2^\circ\text{C}$ (room temperature) is not a suitable storage condition for PCL/(PEO+SSD) and PLA/(PEO+SSD) formulations. Since, the drug loaded nanofiber patches were decomposed with changing the color (from white to yellowish) so drug loading efficiency could not be calculated. However, PCL/(PEO+SSD) and PLA/(PEO+SSD) formulations should be kept and storage in $+4^\circ\text{C}$ refrigerator conditions. Changing the patch color from white to yellowish, signs the oxidation of SSD (Cioroiu et al., 2013; Uri-8). Since SSD active agent shows oxidation sensitivity with the effect of temperature, SSD loaded composite nanofibers could not maintain their stability at room temperature. However, this sensitivity was tolerated with the decrease in the temperature of the environment, that is, by keeping the formulations under refrigerator conditions instead of room conditions. SSD loaded composite nanofibers can be stored in refrigerator conditions without the need for any antioxidant or pharmaceutical excipient.

In vitro test results showed that after storage for 3 and 6 months, the release profile of the SSD loaded PCL/PEO and PLA/PEO nanofibers appeared to be much similar to that obtained at initial time. It indicated that SSD loaded PCL/PEO and PLA/PEO nanofibers were stable under the refrigerator storage conditions.

The cytotoxicity studies of the drug loaded and drug-free PCL/PEO and PLA/PEO nanofiber patches were carried with using the cell viability assay (MTT assay). Cytotoxicity test results showed that PLA/PEO and PCL/PEO polymer matrices are suitable and safe materials for biomedical applications with 100 and 98 % viability

values. Overall, these findings suggest that the electrospun nanofibers can be applied on the skin as topically without any irritation.

As a result, the solubility and release of SSD were enhanced by its dissolution in the highly aqueous soluble PEO polymer. In this thesis, it is shown that the electrospun nanofibers provided a better surface area for effective antibacterial activity, controlled drug delivery, high drug loading efficiency, adequate drug dissolution, drug stabilization and perfect drug carriage. Furthermore, the utilization of a new buffer media is an important parameter for perfect SSD release from the fiber matrix to the buffer. Thus, the buffer media simulated release behaviour of the body successfully. It was concluded that SSD loaded PCL/PEO and PLA/PEO composite nanofibers possess a great potential to be used in topical drug delivery application.

As a potential future research, different hydrophobic biopolymers can be blended with PEO instead of PLA and PCL to release SSD. Furthermore, to measure the size of loaded SSD particles in the nanofiber structure, TEM analysis of the SSD loaded composite nanofibers can be examined. As it is stated in the literature PCL and PLA polymers have good mechanical properties. Thus, the mechanical properties of the composite PCL/PEO and PLA/PEO nanofibers can be investigated with DMA instrument. In this work, the release of SSD followed with *in vitro* drug release studies (dialysis bag method). In addition, the permeation of SSD from the pig skin can be determined with *in vitro* skin permeation studies in a modified Franz's diffusion cell. Moreover, online electrical conductivity measurement -during the period of release- might be an alternative method for evaluation the drug release from formulation to buffer media.



REFERENCES

- Aegerter, M. A., & Mennig, M.** (Eds.). (2013). *Sol-gel technologies for glass producers and users*. Springer Science & Business Media.
- Aguzzi, C., Sandri, G., Bonferoni, C., Cerezo, P., Rossi, S., Ferrari, F., ... & Viseras, C.** (2014). Solid state characterisation of silver sulfadiazine loaded on montmorillonite/chitosan nanocomposite for wound healing. *Colloids and Surfaces B: Biointerfaces*, *113*, 152-157.
- Altan, A., Aytac, Z., & Uyar, T.** (2018). Carvacrol loaded electrospun fibrous films from zein and poly (lactic acid) for active food packaging. *Food Hydrocolloids*, *81*, 48-59.
- Aravamudhan, A., Ramos, D. M., Nada, A. A., & Kumbar, S. G.** (2014). Natural polymers: polysaccharides and their derivatives for biomedical applications. In *Natural and synthetic biomedical polymers* (pp. 67-89). Elsevier.
- Awad, N. K., Niu, H., Ali, U., Morsi, Y. S., & Lin, T.** (2018). Electrospun fibrous scaffolds for small-diameter blood vessels: a review. *Membranes*, *8*(1), 15.
- Aytac Z., Sen H.S., Durgun E., Uyar T.** (2015). Sulfisoxazole/cyclodextrin inclusion complex incorporated in electrospun hydroxypropyl cellulose nanofibers as drug delivery system, *Colloids and Surfaces B: Biointerfaces* *128*, 331–338
- Azevedo, E. P., Saldanha, T. D., Navarro, M. V., Medeiros, A. C., Ginani, M. F., & Raffin, F. N.** (2006). Mechanical properties and release studies of chitosan films impregnated with silver sulfadiazine. *Journal of applied polymer science*, *102*(4), 3462-3470.
- Behera, S., Ghanty, S., Ahmad, F., Santra, S., & Banerjee, S.** (2012). UV-visible spectrophotometric method development and validation of assay of paracetamol tablet formulation. *J Anal Bioanal Techniques*, *3*(6), 151-7.
- Berni A., Mennig M., Schmidt H.** (2004). Doctor Blade. In: Aegerter M.A., Mennig M. (eds) *Sol-Gel Technologies for Glass Producers and Users*. Springer, Boston, MA
- Boateng, J., Burgos-Amador, R., Okeke, O., & Pawar, H.** (2015). Composite alginate and gelatin based bio-polymeric wafers containing silver sulfadiazine for wound healing. *International journal of biological macromolecules*, *79*, 63-71.
- Catoira, M. C., Fusaro, L., Di Francesco, D., Ramella, M., & Boccafoschi, F.** (2019). Overview of natural hydrogels for regenerative medicine applications. *Journal of Materials Science: Materials in Medicine*, *30*(10), 115.

- Cheng, F., Gao, J., Wang, L., & Hu, X.** (2015). Composite chitosan/poly (ethylene oxide) electrospun nanofibrous mats as novel wound dressing matrixes for the controlled release of drugs. *Journal of Applied Polymer Science*, 132(24).
- Chew, S. Y., Mi, R., Hoke, A., and Leong, K. W.** (2007). Aligned protein-polymer composite fibers enhance nerve regeneration: a potential tissue-engineering platform, *Advanced Functional Materials*, 17, 8, 1288–1296.
- Chew, S. Y., Wen, J., Yim, E. K. F., and Leong, K.W.** (2005). Sustained release of proteins from electrospun biodegradable fibers, *Biomacromolecules*, 6, 4, 2017–2024.
- Cioroiu, B. I., Lazar, M. I., Bello-López, M. A., & Fernandez-Torres, R.** (2013). Identification of the specified impurities of silver sulfadiazine using a screening of degradation products in different stress physico-chemical media. *Talanta*, 116, 653-662.
- Cosme, J. G., Silva, V. M., Nunes, R. R., & Picciani, P. H.** (2016). Development of biobased poly (lactic acid)/epoxidized natural rubber blends processed by electrospinning: Morphological, structural and thermal properties. *Materials Sciences and Applications*, 7(4), 210-219.
- Dash, T. K., & Konkimalla, V. B.** (2012). Poly-ε-caprolactone based formulations for drug delivery and tissue engineering: A review. *Journal of Controlled Release*, 158(1), 15-33.
- Dharashivkar, S. S., Sahasrabuddhe, S. H., & Saoji, A. N.** (2015). Niosomally encapsulated silver sulfadiazine gel for burn treatment. *Journal of microencapsulation*, 32(2), 137-142.
- Doğan, Z.** (2013). *Nanolif Yara Örtücü Yüzeylerin Geliştirilmesi Ve Karakterizasyonu* (Master dissertation, Fen Bilimleri Enstitüsü).
- Duan, Y., Jia J., Wang, S. H., Yan, W., Jin, L., and Wang, Z. Y.** (2007). Preparation of antimicrobial poly(ε-caprolactone) electrospun nanofibers containing silver-loaded zirconium phosphate nanoparticles, *Journal of Applied Polymer Science*, 106, 2, 1208–1214.
- Dubey P., Bhushan B., Sachdev A., Matai I., Kumar S.U., Gopinath P.** (2015). Silver-Nanoparticle- Incorporated Composite Nanofibers for Potential Wound Dressing Applications, *J. Appl. Polym. Sci.*, 42473,2-12
- Dubey P. and Gopinath P.** (2016). Fabrication of electrospun poly(ethylene oxide)–poly(capro lactone) composite nanofibers for co-delivery of niclosamide and silver nanoparticles exhibits enhanced anti-cancer effects in vitro, *Journal of Materials Chemistry B*,4, 726-742
- Ebrahimi-Hosseinzadeh, B., Pedram, M., Hatamian-Zarmi, A., Salahshour-Kordestani, S., Rasti, M., Mokhtari-Hosseini, Z. B., & Mir-Derikvand, M.** (2016). In vivo evaluation of gelatin/hyaluronic acid nanofiber as Burn-wound healing and its comparison with ChitoHeal gel. *Fibers and Polymers*, 17(6), 820-826.

- El-Feky, G. S., El-Banna, S. T., El-Bahy, G. S., Abdelrazek, E. M., & Kamal, M.** (2017). Alginate coated chitosan nanogel for the controlled topical delivery of Silver sulfadiazine. *Carbohydrate polymers*, 177, 194-202.
- El-Feky, G. S., Sharaf, S. S., El Shafei, A., & Hegazy, A. A.** (2017). Using chitosan nanoparticles as drug carriers for the development of a silver sulfadiazine wound dressing. *Carbohydrate polymers*, 158, 11-19.
- Eshraghi, S., & Das, S.** (2010). Mechanical and microstructural properties of polycaprolactone scaffolds with one-dimensional, two-dimensional, and three-dimensional orthogonally oriented porous architectures produced by selective laser sintering. *Acta biomaterialia*, 6(7), 2467-2476.
- Esentürk, İ., Erdal, M. S., & Güngör, S.** (2016). Electrospinning method to produce drug-loaded nanofibers for topical/transdermal drug delivery applications. *İstanbul Üniversitesi Eczacılık Fakültesi Dergisi*, 46(1), 49-69.
- Fox, C. L., & Modak, S. M.** (1974). Mechanism of silver sulfadiazine action on burn wound infections. *Antimicrobial agents and chemotherapy*, 5(6), 582-588.
- Garg, T., Malik, B., Rath, G., & Goyal, A. K.** (2014). Development and characterization of nano-fiber patch for the treatment of glaucoma. *European Journal of Pharmaceutical Sciences*, 53, 10-16.
- Gencturk, A., Kahraman, E., Güngör, S., Özhan, G., Özsoy, Y., & Sarac, A. S.** (2017). Polyurethane/hydroxypropyl cellulose electrospun nanofiber mats as potential transdermal drug delivery system: characterization studies and in vitro assays. *Artificial cells, nanomedicine, and biotechnology*, 45(3), 655-664.
- Ghedini, E., Pizzolitto, C., Albore, G., Menegazzo, F., Signoretto, M., Operti, L., & Cerrato, G.** (2017). Sulfadiazine-based drug delivery systems prepared by an effective sol-gel process. *Journal of Sol-Gel Science and Technology*, 83(3), 618-626.
- Ghodekar, S. V., Chaudhari, S. P., & Ratnaparakhi, M. P.** (2012). Development and characterization of silver sulfadiazine emulgel for topical drug delivery. *Int J Pharm Pharm Sci*, 4(4), 305-316.
- Gibson, P., Schreuder-Gibson, H., & Rivin, D.** (2001). Transport properties of porous membranes based on electrospun nanofibers. *Colloids and Surfaces A: Physicochemical and Engineering Aspects*, 187, 469-481.
- Greiner, A., & Wendorff, J. H.** (2007). Electrospinning: a fascinating method for the preparation of ultrathin fibers. *Angewandte Chemie International Edition*, 46(30), 5670-5703.
- Guler, Z., Silva, J. C., & Sezai Sarac, A.** (2017). RGD functionalized poly (ϵ -caprolactone)/poly (m-anthranilic acid) electrospun nanofibers as high-performing scaffolds for bone tissue engineering RGD functionalized PCL/P3ANA nanofibers. *International Journal of Polymeric Materials and Polymeric Biomaterials*, 66(3), 139-148.

- Gunn, J., & Zhang, M.** (2010). Polyblend nanofibers for biomedical applications: perspectives and challenges. *Trends in biotechnology*, 28(4), 189-197.
- Goyal, R., Macri, L. K., Kaplan, H. M., & Kohn, J.** (2016). Nanoparticles and nanofibers for topical drug delivery. *Journal of Controlled Release*, 240, 77-92.
- Gouda, R., Baishya, H., & Qing, Z.** (2017). Application of mathematical models in drug release kinetics of carbidopa and levodopa ER tablets. *J. Dev. Drugs*, 6(02).
- Hajjali, F., Tajbakhsh, S., & Shojaei, A.** (2018). Fabrication and properties of polycaprolactone composites containing calcium phosphate-based ceramics and bioactive glasses in bone tissue engineering: a review. *Polymer reviews*, 58(1), 164-207.
- Hassan, M., Chong, L., & Sultana, N.** (2006). Wettability and water uptake properties of pla and pcl/gelatin-based electrospun scaffolds. *ARPN J. Eng. Appl. Sci*, 11, 13604-13607.
- Heo, M., Lee, S. J., Heo, D. N., Lee, D., Lim, H. N., Moon, J. H., & Kwon, I. K.** (2018). Multilayered co-electrospun scaffold containing silver sulfadiazine as a prophylactic against osteomyelitis: Characterization and biological in vitro evaluations. *Applied Surface Science*, 432, 308-316.
- Heo, D. N., Yang, D. H., Lee, J. B., Bae, M. S., Kim, J. H., Moon, S. H., ... & Kwon, I. K.** (2013). Burn-wound healing effect of gelatin/polyurethane nanofiber scaffold containing silver-sulfadiazine. *Journal of biomedical nanotechnology*, 9(3), 511-515.
- Heunis, T. D. J., & Dicks, L. M. T.** (2010). Nanofibers offer alternative ways to the treatment of skin infections. *Journal of Biomedicine and Biotechnology*, 2010.
- Huang, Z. M., Zhang, Y. Z., Kotaki, M., & Ramakrishna, S.** (2003). A review on polymer nanofibers by electrospinning and their applications in nanocomposites. *Composites science and technology*, 63(15), 2223-2253.
- Hu, W. W., Wu, Y. C., & Hu, Z. C.** (2018). The development of an alginate/polycaprolactone composite scaffold for in situ transfection application. *Carbohydrate polymers*, 183, 29-36.
- Hu, X., Liu, S., Zhou, G., Huang, Y., Xie, Z., & Jing, X.** (2014). Electrospinning of polymeric nanofibers for drug delivery applications. *Journal of controlled release*, 185, 12-21.
- Ito, K., Saito, A., Fujie, T., Nishiwaki, K., Miyazaki, H., Kinoshita, M., ... & Takeoka, S.** (2015). Sustainable antimicrobial effect of silver sulfadiazine-loaded nanosheets on infection in a mouse model of partial-thickness burn injury. *Acta Biomaterialia*, 24, 87-95.
- Jain, K. K. (Ed.)**. (2008). *Drug delivery systems* (Vol. 2). Totowa, NJ: Humana press.
- Jeong, L., Kim, M. H., Jung, J. Y., Min, B. M., & Park, W. H.** (2014). Effect of silk fibroin nanofibers containing silver sulfadiazine on wound healing. *International journal of nanomedicine*, 9, 5277.

- Kanmaz, D., Toprakci, H. A. K., Olmez, H., & Toprakci, O.** (2018). Electrospun polylactic acid based nanofibers for biomedical applications. *Material Science Research India*, 15(3), 224-240.
- Kashmola, T. O., & Kamil, E. S.** (2014). Structure rheology of polyethylene oxide solution. *Iraqi journal of chemical and petroleum engineering*, 15(1), 23-32.
- Kim, T. G., Lee, D. S., & Park, T. G.** (2007). Controlled protein release from electrospun biodegradable fiber mesh composed of poly (ϵ -caprolactone) and poly (ethylene oxide). *International journal of pharmaceutics*, 338(1-2), 276-283.
- Kim, K., Luu, Y. K., Chang, C., Fang, D., Hsiao, S. B., Chu, B. and Hadjiargyrou M.** (2004). Incorporation and controlled release of a hydrophilic antibiotic using poly(lactide-co-glycolide)-based electrospun nanofibrous scaffolds, *Journal of Controlled Release*, 98, 1, 47–56.
- Kleinbeck K.R., Bader R. A., Kao W. J.** (2009). Concurrent in Vitro Release of SSD and Bupivacaine from Semi-Interpenetrating Networks for Wound Management, *J Burn Care Res.*, 30(1): 98–104
- Kohsari, I., Shariatinia, Z., & Pourmortazavi, S. M.** (2016). Antibacterial electrospun chitosan–polyethylene oxide nanocomposite mats containing bioactive silver nanoparticles. *Carbohydrate polymers*, 140, 287-298.
- Kowalczyk, T., Nowicka, A., Elbaum, D., and Kowalewski, T. A.** (2008). Electrospinning of bovine serum albumin optimization and the use for production of biosensors, *Biomacromolecules*, 9, 7, 2087–2090.
- Kumar, P. M., & Ghosh, A.** (2017). Development and evaluation of silver sulfadiazine loaded microspunge based gel for partial thickness (second degree) burn wounds. *European journal of pharmaceutical sciences*, 96, 243-254.
- Kumbar, S. G., James, R., Nukavarapu, S. P., & Laurencin, C. T.** (2008). Electrospun nanofiber scaffolds: engineering soft tissues. *Biomedical materials*, 3(3), 034002.
- Larsen, S. W., & Larsen, C.** (2009). Critical factors influencing the in vivo performance of long-acting lipophilic solutions—impact on in vitro release method design. *The AAPS journal*, 11(4), 762-770.
- Laurencin, C., & Deng, M.** (Eds.). (2014). *Natural and synthetic biomedical polymers*. Newnes.
- Lee, S. J., Park, S. A., Heo, D. N., Lee, D., Jang, H. J., Kim, K. S., ... & Kwon, I. K.** (2016). Preparation of electrospun fibrous scaffold containing silver sulfadiazine for biomedical applications. *Journal of Nanoscience and Nanotechnology*, 16(8), 8554-8558.
- Li, Y., Jiang, H., & Zhu, K.** (2008). Encapsulation and controlled release of lysozyme from electrospun poly (ϵ -caprolactone)/poly (ethylene glycol) non-woven membranes by formation of lysozyme–oleate complexes. *Journal of Materials Science: Materials in Medicine*, 19(2), 827-832

- Li, P., Xu, X., Wu, L., Li, B., & Zhao, Y.** (2015). Synthesis of silver nanoparticle-loaded sulfadiazine/polyvinyl alcohol nanorods and their antibacterial activities. *MedChemComm*, 6(12), 2204-2208.
- Li, Y. F., Rubert, M., Aslan, H., Yu, Y., Howard, K. A., Dong, M., ... & Chen, M.** (2014). Ultraporous interweaving electrospun microfibers from PCL–PEO binary blends and their inflammatory responses. *Nanoscale*, 6(6), 3392-3402.
- Lim, C. T.** (2017). Nanofiber technology: current status and emerging developments. *Progress in Polymer Science*, 70, 1-17.
- Liu, G., Gu, Z., Hong, Y., Cheng, L., & Li, C.** (2017). Electrospun starch nanofibers: Recent advances, challenges, and strategies for potential pharmaceutical applications. *Journal of Controlled Release*, 252, 95-107.
- Liu, X., Gan, H., Hu, C., Sun, W., Zhu, X., Meng, Z., ... & Dou, G.** (2019). Silver sulfadiazine nanosuspension-loaded thermosensitive hydrogel as a topical antibacterial agent. *International Journal of Nanomedicine*, 14, 289.
- Lu, Y., Chen, Y. C., & Zhang, P. H.** (2016). Preparation and characterisation of polylactic acid (PLA)/polycaprolactone (PCL) composite microfibre membranes. *Fibres & Textiles in Eastern Europe*.
- Luu, Y. K., Kim, K., Hsiao, B. S., Chu, B., and Hadjiargyrou, M.** (2003). Development of a nanostructured DNA delivery scaffold via electrospinning of PLGA and PLA-PEG block copolymers, *Journal of Controlled Release*, 89, 2, 341–353.
- Luan, J., Wu, J., Zheng, Y., Song, W., Wang, G., Guo, J., & Ding, X.** (2012). Impregnation of silver sulfadiazine into bacterial cellulose for antimicrobial and biocompatible wound dressing. *Biomedical Materials*, 7(6), 065006.
- Madhaiyana K., Sridhar R., Sundarrajan S., Venugopala J. R., Ramakrishna S.** (2013). Vitamin B₁₂ loaded polycaprolactone nanofibers: A novel transdermal route for the water soluble energy supplement delivery, *International Journal of Pharmaceutics* 444 70– 76
- Malikmammadov, E., Tanir, T. E., Kiziltay, A., Hasirci, V., & Hasirci, N.** (2018). PCL and PCL-based materials in biomedical applications. *Journal of Biomaterials science, Polymer edition*, 29(7-9), 863-893.
- McLaughlin, A. R., & Thomas, N. L.** (2012). Biodegradable polymer nanocomposites. In *Advances in Polymer Nanocomposites* (pp. 398-430). Woodhead Publishing.
- Merrell, J. G., McLaughlin, S. W., Tie, L., Laurencin, C. T., Chen, A. F., & Nair, L. S.** (2009). Curcumin loaded poly (ϵ -caprolactone) nanofibers: diabetic wound dressing with antioxidant and anti-inflammatory properties. *Clinical and experimental pharmacology & physiology*, 36(12), 1149.

- Morie, A., Garg, T., Goyal, A. K., & Rath, G.** (2016). Nanofibers as novel drug carrier—an overview. *Artificial cells, nanomedicine, and biotechnology*, 44(1), 135-143.
- Mohseni, M., Shamloo, A., Aghababaei, Z., Vossoughi, M., & Moravvej, H.** (2016). Antimicrobial wound dressing containing silver sulfadiazine with high biocompatibility: in vitro study. *Artificial organs*, 40(8), 765-773.
- Morie, A., Garg, T., Goyal, A. K., & Rath, G.** (2016). Nanofibers as novel drug carrier—an overview. *Artificial cells, nanomedicine, and biotechnology*, 44(1), 135-143.
- Muslim, N. B., Hamzah, A. F., & Al-kawaz, A. E.** (2018). Study of mechanical properties of wollastonite filled epoxy functionally graded composite. *Int. J. Mech. Eng. Technol*, 9, 669-677.
- Nalbandi, B., & Amiri, S.** (2019). Antibacterial activity of PVA-based nanofibers loaded with silver sulfadiazine/cyclodextrin nanocapsules. *International Journal of Polymeric Materials and Polymeric Biomaterials*, 68(11), 647-659.
- Nagam Hanumantharao, S., & Rao, S.** (2019). Multi-functional electrospun nanofibers from polymer blends for scaffold tissue engineering. *Fibers*, 7(7), 66.
- Narayanan, G., Gupta, B. S., & Tonelli, A. E.** (2015). Enhanced mechanical properties of poly (ϵ -caprolactone) nanofibers produced by the addition of non-stoichiometric inclusion complexes of poly (ϵ -caprolactone) and α -cyclodextrin. *Polymer*, 76, 321-330.
- Nayon, M. A. U., Nesa, J. U., Uddin, M. N., Amran, M. S., & Bushra, U.** (2013). Development and validation of UV Spectrometric Method for the Determination of Cefixime trihydrate in Bulk and Pharmaceutical Formulation. *Asian Journal of Biomedical and Pharmaceutical Sciences*, 3(2), 1-5.
- Nottelet, B., Pektok, E., Mandracchia, D., Tille, J. C., Walpoth, B., Gurny, R., & Moeller, M.** (2009). Factorial design optimization and in vivo feasibility of poly (ϵ -caprolactone)-micro-and nanofiber-based small diameter vascular grafts. *Journal of Biomedical Materials Research Part A: An Official Journal of The Society for Biomaterials, The Japanese Society for Biomaterials, and The Australian Society for Biomaterials and the Korean Society for Biomaterials*, 89(4), 865-875.
- Oliveira, J. E., Mattoso, L. H., Orts, W. J., & Medeiros, E. S.** (2013). Structural and morphological characterization of micro and nanofibers produced by electrospinning and solution blow spinning: a comparative study. *Advances in Materials Science and Engineering*, 2013.
- Osathanon, T., Chanjavanakul, P., Kongdecha, P., Clayhan, P., & Huynh, N. C. N.** (2017). Polycaprolactone-Based Biomaterials for Guided Tissue Regeneration Membrane. *Periodontitis-A Useful Reference successful. InTech*, 171-188.

- Ozdemir, K. G., Yılmaz, H., & Yılmaz, S.** (2009). In vitro evaluation of cytotoxicity of soft lining materials on L929 cells by MTT assay. *Journal of Biomedical Materials Research Part B: Applied Biomaterials*, 90(1), 82-86.
- Pasquarelli, R. M., Ginley, D. S., & O'Hayre, R.** (2011). Solution processing of transparent conductors: from flask to film. *Chemical Society Reviews*, 40(11), 5406-5441.
- Patel, K. K., Surekha, D. B., Tripathi, M., Anjum, M. M., Muthu, M. S., Tilak, R., ... & Singh, S.** (2019). Antibiofilm potential of silver sulfadiazine-loaded nanoparticle formulations: a study on the effect of DNase-I on microbial biofilm and wound healing activity. *Molecular pharmaceutics*, 16(9), 3916-3925.
- Patrício, T., Domingos, M., Gloria, A., D'Amora, U., Coelho, J. F., & Bártolo, P. J.** (2014). Fabrication and characterisation of PCL and PCL/PLA scaffolds for tissue engineering. *Rapid Prototyping Journal*.
- Peijs, T.** (2018). 6.7 Electrospun Polymer Nanofibers and Their Composites.
- Piyush, M., Deepak, S., Ashok, D., Deepak, S., Kumar, G. R., Piyush, A., & Deepak, K.** (2013). Design, development and evaluation of lipid based topical formulations of silver sulfadiazine for treatment of burns and wounds. *Innov. J. Life Sci*, 1, 38-44.
- Polaskova, M., Peer, P., Cermak, R., & Ponizil, P.** (2019). Effect of thermal treatment on crystallinity of poly (ethylene oxide) electrospun fibers. *Polymers*, 11(9), 1384.
- Ramalingam, M., & Ramakrishna, S.** (2017). Introduction to nanofiber composites. In *Nanofiber Composites for Biomedical Applications* (pp. 3-29). Woodhead Publishing.
- Ramazanoglu, M., Özönder, Ş., & Salcı, R.** (2019). Bulk-boundary correspondence in soft matter. *Physical Review E*, 100(2), 020702.
- Rana, D., Kumar, T. S., & Ramalingam, M.** (2014). Cell-laden hydrogels for tissue engineering. *J Biomater Tissue Eng*, 4(7), 507-535.
- Rao, N. R., Bn, A. K., & Laxmi, A.** (2011). Method validation of metaxalone drug by using UV spectroscopy. *Int. J. Pharm. Bio. Sci*, 1(3), 284-302.
- Rath, G., Hussain, T., Chauhan, G., Garg, T., & Goyal, A. K.** (2016). Collagen nanofiber containing silver nanoparticles for improved wound-healing applications. *Journal of drug targeting*, 24(6), 520-529.
- Safdari, F., Carreau, P. J., Heuzey, M. C., Kamal, M. R., & Sain, M. M.** (2017). Enhanced properties of poly (ethylene oxide)/cellulose nanofiber biocomposites. *Cellulose*, 24(2), 755-767.
- Saquinig C. D., Manasco J. L., Khan S.A.** (2009). Electrospun Nanoparticle–Nanofiber Composites via a One-Step Synthesis, *Small*, 5, No. 8, 944–951
- Sarac, A. S.** (2017). *Nanofibers of conjugated polymers*. CRC Press.

- Selcan Gungor-Ozkerim, P., Balkan, T., Kose, G. T., Sezai Sarac, A., & Kok, F. N.** (2014). Incorporation of growth factor loaded microspheres into polymeric electrospun nanofibers for tissue engineering applications. *Journal of Biomedical Materials Research Part A*, 102(6), 1897-1908.
- Shao, W., Liu, H., Wu, J., Wang, S., Liu, X., Huang, M., & Xu, P.** (2016). Preparation, antibacterial activity and pH-responsive release behavior of silver sulfadiazine loaded bacterial cellulose for wound dressing applications. *Journal of the Taiwan Institute of Chemical Engineers*, 63, 404-410.
- Shelke, N. B., Lee, P., Anderson, M., Mistry, N., Nagarale, R. K., Ma, X. M., ... & Kumbar, S. G.** (2016). Neural tissue engineering: nanofiber-hydrogel based composite scaffolds. *Polymers for Advanced Technologies*, 27(1), 42-51.
- Sill T.J., Recum H.A.,** (2008). Electrospinning: applications in drug delivery and tissue engineering. *Biomaterials*, 29 (13):1989-2006.
- Smith, R. (Ed.)**. (2005). *Biodegradable polymers for industrial applications*. CRC Press.
- Souza, S. O. L., Cotrim, M. A. P., Oréface, R. L., Carvalho, S. G., Dutra, J. A. P., de Paula Careta, F., ... & Villanova, J. C. O.** (2018). Electrospun poly (ϵ -caprolactone) matrices containing silver sulfadiazine complexed with β -cyclodextrin as a new pharmaceutical dosage form to wound healing: preliminary physicochemical and biological evaluation. *Journal of Materials Science: Materials in Medicine*, 29(5), 67.
- Stout, D. A., Basu, B., & Webster, T. J.** (2011). Poly (lactic-co-glycolic acid): carbon nanofiber composites for myocardial tissue engineering applications. *Acta biomaterialia*, 7(8), 3101-3112.
- Sun, Y., Cheng, S., Lu, W., Wang, Y., Zhang, P., & Yao, Q.** (2019). Electrospun fibers and their application in drug controlled release, biological dressings, tissue repair, and enzyme immobilization. *RSC advances*, 9(44), 25712-25729.
- Szegedi, Á., Popova, M., Yoncheva, K., Makk, J., Mihály, J., & Shestakova, P.** (2014). Silver-and sulfadiazine-loaded nanostructured silica materials as potential replacement of silver sulfadiazine. *Journal of Materials Chemistry B*, 2(37), 6283-6292.
- Taylor, G. I.** (1964). Disintegration of water drops in an electric field. *Proceedings of the Royal Society of London. Series A. Mathematical and Physical Sciences*, 280(1382), 383-397.
- Thakkar, V., Korat, V., Baldaniya, L., Gohel, M., Gandhi, T., & Patel, N.** (2016). Development and characterization of novel hydrogel containing antimicrobial drug for treatment of burns. *International journal of pharmaceutical investigation*, 6(3), 158.

- Timofeeva, L., & Kleshcheva, N.** (2011). Antimicrobial polymers: mechanism of action, factors of activity, and applications. *Applied microbiology and biotechnology*, 89(3), 475-492.
- Tonglairoum, P., Ngawhirunpat, T., Rojanarata, T., Kaomongkolgit, R., & Opanasopit, P.** (2014). Fast-acting clotrimazole composited PVP/HP β CD nanofibers for oral candidiasis application. *Pharmaceutical research*, 31(8), 1893-1906.
- Tyler, B., Gullotti, D., Mangraviti, A., Utsuki, T., & Brem, H.** (2016). Polylactic acid (PLA) controlled delivery carriers for biomedical applications. *Advanced Drug Delivery Reviews*, 107, 163-175.
- Ullah, S., Hashmi, M., Khan, M. Q., Kharaghani, D., Saito, Y., Yamamoto, T., & Kim, I. S.** (2019). Silver sulfadiazine loaded zein nanofiber mats as a novel wound dressing. *RSC advances*, 9(1), 268-277.
- Ullah, S., Hashmi, M., Kharaghani, D., Khan, M. Q., Saito, Y., Yamamoto, T., ... & Kim, I. S.** (2019). Antibacterial properties of in situ and surface functionalized impregnation of silver sulfadiazine in polyacrylonitrile nanofiber mats. *International journal of nanomedicine*, 14, 2693.
- Url-1**<https://microbewiki.kenyon.edu/index.php/Silver_as_an_Antimicrobial_Agent#Silver_sulfadiazine>, date retrieved 25.02.2021.
- Url-2**<<https://pubchem.ncbi.nlm.nih.gov/compound/Silversulfadiazine#section=Pharmacology-and-Biochemistry>>, date retrieved 25.02.2021.
- Url-3**< <https://www.drugbank.ca/drugs/DB05245>>, date retrieved 25.02.2021.
- Url-4**<<https://www.cannify.us/education/faq-cannabis-education/what-is-the-difference-between-topical-and-transdermal/>>, date retrieved 25.02.2021.
- Url-5**<<https://www.americanpharmaceuticalreview.com/Featured-Articles/170872-Lipids-in-Transdermal-and-Topical-Drug-Delivery/>>, date retrieved 25.02.2021.
- Url-6**<<https://www.qlaboratories.com/minimum-inhibitory-mic-and-minimum-bactericidal-concentration-mbc-evaluations-as-rd-tools/>>, date retrieved 25.02.2021.
- Url-7**<https://www.softschools.com/formulas/chemistry/cellulose_formula/464/>, date retrieved 25.02.2021.
- Url-8**<<https://www.mayoclinic.org/drugs-supplements/silver-sulfadiazine-topical-route/precautions/drg-20068819?p=1>>, date retrieved 25.02.2021.
- Vert, M.** (2001). Biopolymers and artificial biopolymers in biomedical applications, an overview. *Biorelated Polymers*, 63-79. https://doi.org/10.1007/978-1-4757-3374-7_6
- Verma, A., Singh, S., Kaur, R., & Jain, U. K.** (2013). Topical gels as drug delivery systems: A review. *Int. J. Pharm. Sci. Rev. Res*, 23(2), 374-382.

- Wang, B., Li, H., Yao, Q., Zhang, Y., Zhu, X., Xia, T., ... & Ni, S.** (2016). Local in vitro delivery of rapamycin from electrospun PEO/PDLLA nanofibers for glioblastoma treatment. *Biomedicine & Pharmacotherapy*, *83*, 1345-1352.
- Wen, X. T., Fan, H. S., Tan, Y. F., Cao, H. D., Li, H., Cai, B., & Zhang, X. D.** (2005). Preparation of electrospun PLA nanofiber scaffold and the evaluation in vitro. In *Key Engineering Materials* (Vol. 288, pp. 139-142). Trans Tech Publications Ltd.
- White, R., & Cooper, R.** (2005). Silver sulphadiazine: a review of the evidence. *Wounds uk*, *1*(2), 51.
- Xue, J., He, M., Liu, H., Niu, Y., Crawford, A., Coates, P. D., ... & Zhang, L.** (2014). Drug loaded homogeneous electrospun PCL/gelatin hybrid nanofiber structures for anti-infective tissue regeneration membranes. *Biomaterials*, *35*(34), 9395-9405.
- Yao, Q., Cosme, J. G., Xu, T., Miszuk, J. M., Picciani, P. H., Fong, H., & Sun, H.** (2017). Three dimensional electrospun PCL/PLA blend nanofibrous scaffolds with significantly improved stem cells osteogenic differentiation and cranial bone formation. *Biomaterials*, *115*, 115-127.
- Yao, Y., Wei, H., Wang, J., Lu, H., Leng, J., & Hui, D.** (2015). Fabrication of hybrid membrane of electrospun polycaprolactone and polyethylene oxide with shape memory property. *Composites Part B: Engineering*, *83*, 264-269.
- Yoo, H. S., Kim, T. G., & Park, T. G.** (2009). Surface-functionalized electrospun nanofibers for tissue engineering and drug delivery. *Advanced drug delivery reviews*, *61*(12), 1033-1042.
- Zander, N. E., Orlicki, J. A., Rawlett, A. M., & Beebe, T. P.** (2013). Electrospun polycaprolactone scaffolds with tailored porosity using two approaches for enhanced cellular infiltration. *Journal of Materials Science: Materials in Medicine*, *24*(1), 179-187.
- Zamani, M., Prabhakaran, M. P., & Ramakrishna, S.** (2013). Advances in drug delivery via electrospun and electrospayed nanomaterials. *International journal of nanomedicine*, *8*, 2997.
- Zeng, J., Haoqing, H., Schaper, A., Wendorff, J. H., & Greiner, A.** (2003). Poly-L-lactide nanofibers by electrospinning—Influence of solution viscosity and electrical conductivity on fiber diameter and fiber morphology. *e-Polymers*, *3*(1).
- Zeng, J., Xu, X., Chen, X., Liang, Q., Bian, X., Yang, L. And Jing, X.** (2003). Biodegradable electrospun fibers for drug delivery, *Journal of Controlled Release*, *92*, 3, 227–231.
- Zepon, K. M., Petronilho, F., Soldi, V., Salmoria, G. V., & Kanis, L. A.** (2014). Production and characterization of cornstarch/cellulose acetate/silver sulfadiazine extrudate matrices. *Materials Science and Engineering: C*, *44*, 225-233.
- Zhang, Y., Ouyang, H., Lim, C. T., Ramakrishna, S., & Huang, Z. M.** (2005). Electrospinning of gelatin fibers and gelatin/PCL composite fibrous

scaffolds. *Journal of Biomedical Materials Research Part B: Applied Biomaterials: An Official Journal of the Society for Biomaterials, The Japanese Society for Biomaterials, and The Australian Society for Biomaterials and the Korean Society for Biomaterials*, 72(1), 156-165.

Zia, F., Anjum, M. N., Saif, M. J., Jamil, T., Malik, K., Anjum, S., ... & Zia, M. A. (2017). Alginate-poly (ethylene) glycol and poly (ethylene) oxide blend materials. In *Algae Based Polymers, Blends, and Composites* (pp. 581-601). Elsevier.



CURRICULUM VITAE

Name Surname : Zarife BARBAK

EDUCATION :

- **B.Sc.** : 2009, Suleyman Demirel University, Faculty of Engineering, Textile Engineering Department
- **M.Sc.** : 2012, Istanbul Technical University, Textile Engineering Department

PROFESSIONAL EXPERIENCE AND REWARDS:

- 2009-2010 Research Assistant, Bartın University
- 2010-2021 Research Assistant, Istanbul Technical University
- **Doğan Z., Kıyak Y.E., Öznergiz E., Demir A.,** “Elektro-Üretim Yöntemiyle Nanolif Yara Örtücü Üretimi”, 3. Uluslararası Ar-Ge Proje Pazarı, Bursa, 2011, s. 104-105. (This work won the second prize in “R&D Project Bazaar Competition” among publications on technical textile subject.)
- **04/2016- Continue:** ITU BAP Project Nr. 36905 “Nanofiber Production and Characterization for Topical Drug Delivery”, Researcher
- **04/2012-09/2012:** ITU BAP Project Nr. 36536 “In Vivo Studies of Nanofiber Wound Dressings”, Researcher
- **04/2010 – 01/2012:** TUBITAK Project Nr: 108M045 “Design of a Mobile Prototype System that Manufactures Nanofibers via Electrospinning”, Researcher

PUBLICATIONS, PRESENTATIONS AND PATENTS ON THE THESIS:

- **Barbak, Z., Karakas, H., Esenturk, I., Erdal, M. S., & Sarac, A. S.** (2020). Silver sulfadiazine Loaded Poly (ϵ -Caprolactone)/Poly (Ethylene Oxide) Composite Nanofibers for Topical Drug Delivery. *Nano*, 2050073.
- **Barbak Z., Karakas H., Sarac S.,** “Characterization Study of Drug Loaded PLA Electrospun Nanofibers”, VI. International Fiber and Polymer Symposium, 24-25 January 2020, Bursa
- **Barbak Z., Karakas H., Sarac S., Karakas Y., Yılmaz A.,** “Fabrication and Antibacterial Activity of Composite PEO/PCL Electrospun Nanofibers”, 2. ICONTEX, 17-18 April 2019, Tekirdag

- **Barbak Z.**, Karakas H., Sarac S., Fabrication and Characterization of Drug Loaded Casting Films, V. International Fiber and Polymer Symposium, 2-3 May 2019, Istanbul
- **Barbak Z.**, Karakas H., Sarac S. “Characterization Study of Drug Incorporated Electrospun Nanofiber Formulations”, III. International Fiber and Polymer Symposium, 8-9 March 2018, Bursa
- **Barbak Z.**, Karakas H., Sarac S., “Composite Nanofibers for Drug Delivery Systems” 18th Autex World Textile Conference, June 20-22, 2018, Istanbul, Turkey

OTHER PUBLICATIONS, PRESENTATIONS AND PATENTS:

- **Barbak Z.**, Esentürk İ., Saraç S. A., Erdal S. M., Karakaş H., “Electrospun Composite Nanofibers and Their Characterization in order to Produce a Sport Corset”, IX. International R&D Brokerage Event in Turkish Textile and Clothing Sector, 27-28 April 2017, Bursa
- **Barbak Z.**, Esentürk İ., Saraç S. A., Erdal S. M., Karakaş H., “Ayak Mantarı Tedavisine Yönelik Fonksiyonel Bir Çorap Tasarımı”, 8. Uluslararası Ar-Ge Proje Pazarı, Bursa, Mayıs 2016